Theoretical high-resolution spectroscopy for reactive molecules in astrochemistry and combustion processes

Dissertation
for the award of the degree
"Doctor rerum naturalium" (Dr.rer.nat.)
of the Georg-August-Universität Göttingen

within the doctoral program Chemistry
of the Georg-August University School of Science (GAUSS)

submitted by
Benjamin Schröder
from Sömmerda

Göttingen, 2019

Thesis Committee

Prof. Dr. Ricardo A. Mata
Institute for Physical Chemistry
Georg-August-University Göttingen

Prof. Dr. Thomas Zeuch
Institute for Physical Chemistry
Georg-August-University Göttingen

Members of the Examination Board

Reviewer:
Prof. Dr. Ricardo A. Mata
Institute for Physical Chemistry
Georg-August-University Göttingen

Second Reviewer:
Prof. Dr. Thomas Zeuch
Institute for Physical Chemistry
Georg-August-University Göttingen

Further members of the Examination Board

Prof. Dr. Götz Eckold
Institute for Physical Chemistry
Georg-August-University Göttingen

Prof. Dr. Alec M. Wodtke
Institute for Physical Chemistry
Georg-August-University Göttingen

Prof. Dr. Burkhard Geil
Institute for Physical Chemistry
Georg-August-University Göttingen

Prof. Dr. Konrad Koszinowski
Institute for Organic and Biomolecular Chemistry
Georg-August-University Göttingen

Date of the oral examination: 15.08.2019

Danksagung

Mein tief empfundener Dank gilt Allen, die mich während meiner Promotion unterstützt und aufgebaut haben. Zweifelsohne ist eine Promotion eine große Herausforderung, welche ohne gebührende Unterstützung und Führung nicht zu bewältigen ist.

Zu aller erst möchte ich mich bei meinen Betreuern bedanken, Prof. Dr. Ricardo Mata und PD Dr. Thomas Zeuch. Der Beginn meiner Promotion war gelinde gesagt turbulent. Aber dank ihrer Unterstützung konnten wir gemeinsam dieses Projekt wieder in geordnete Bahnen lenken. Ich bin beiden für ihr Vertrauen während der 5 Jahre meiner Promotion unendlich dankbar.

Zwei Personen bin ich zu Dank verpflichtet für ihren Beitrag zu meiner wissenschaftlichen Entwicklung und den Weg den diese Arbeit genommen hat. Zu erst ist da Dr. Peter Sebald, dessen Erfahrung im Bereich der theoretischen Spektroskopie eine große Hilfe war. Nicht selten ergaben sich in unseren langen Gesprächen neue Ideen und wertvolle Anregungen für das weitere Vorgehen in einem der Projekte. Auch die moralische Unterstützung, wenn es mal nicht so richtig voranging, war von unschätzbarem Wert für mich. Die zweite Person is Prof. Dr. Peter Botschwina. Er war es, der mein Interesse für theoretische Molekülspektroskopie und die theoretische Chemie im Allgemeinen geweckt hat. Ich war überglücklich nachdem ich von ihm die Zusage erhalten habe eine Promotion bei ihm durchführen zu dürfen. Sein überraschender und tragischer Tod im Dezember 2014 war ein Schock. Nichtsdestotrotz ist diese Arbeit inspiriert von seinem wissenschaflichen Schaffen und ich widme sie ihm in Gedenken an einen großartigen Lehrer und Wissenschaftler.

Weiterhin möchte ich allen ehemaligen und gegenwärtigen Mitgliedern der Arbeitsgruppe "Computational Chemistry and Biochemistry" danken. Es war und ist mir eine Freude Teil dieser Gruppe zu sein. Die vielfältigen Diskussionen und Gespräche zu den unterschiedlichsten Themen bereicherten den Arbeitsalltag auch jenseits der theoretischen Chemie. Ein besonderer Dank geht an Karin Schoppe, die immer ein offenes Ohr bei Problemen hatte und eine unschätzbare Hilfe vor allem bei organisatorischen Dingen war. Auch Dr. Rainer Oswald möchte ich danken für die Unterstüzung in Bezug auf technische Probleme.

Ich würde nun nicht an diesem Punkt stehen ohne die Liebe und Unterstützung meiner Familie. Es war ein langer Weg, gepflastert mit verschiedensten Problemen. Nicht selten bin ich ins Straucheln geraten aber ihr wart immer zur Stelle um mich wieder aufzurichten. Mir bleibt nicht viel mehr zu sagen als einfach nur: "Danke für alles!" Eine Person fehlt nun noch, welcher ich zu danken habe. Sie ist vor allen Anderen die wohl Wichtigste. Meiner Freundin Jenni kann ich gar nicht genug danken für all das, was sie für mich getan hat in den letzten Jahren. Besonders die letzten Wochen waren eine Herausforderung für uns beide, aber gemeinsam haben wir sie gemeistert. Dabei war vor allem ihre Liebe und Treue sowie ihr unerschütterliches Vertrauen in mich ein Rettungsanker und ein schützendes Schild. Ich kann nicht in Worte fassen wie dankbar ich bin dich zu haben. Nun ist es vollbracht und das hätte ich ohne dich niemals geschafft. Danke.

Abstract

Rovibrational spectroscopy is a prime tool for the indirect investigation of molecular potential energy surfaces (PES). Naturally, theoretical predictions of molecular spectra have been the focus of numerous works since the early days of quantum chemistry. With the formulation of modern *ab initio* methods and ever increasing computing power of modern high-performance computing facilities it has become possible to calculate the PES with unprecedented accuracy. On the other hand, such a high-level PES requires also an accurate treatment of the rovibrational problem. For molecules with up to 3 atoms such methods have been know for quite some time and are available in different formulations but going beyond that still poses a challenge. In this thesis, methods for calculating rovibrational spectra of linear molecules with up to four atoms are presented, rivaling with experimental lab accuracy.

As a first step towards a general procedure for high-level theoretical spectroscopy of linear molecules a composite *ab initio* approach to the construction of a PES is presented. The method is tested on two experimentally well known triatomic linear molecules hydrogen cyanide (HCN) and tricarbon (C_3). For HCN, the composite PES reproduces the experimental results with standard deviations of 0.33 cm^{-1} and 0.00009 cm^{-1} in the vibrational term energies and rotational constants, respectively, considering all 113 vibrational states up to about 6500 cm^{-1} above the ground state. A new electric dipole moment function, which has been constructed also in a composite manner, yields accurate rovibrational intensities for a large variety of HCN transitions ranging form the strong CH stretching and bending fundamentals to very weak $\Delta\ell > 1$ overtone transitions. The intensity of the peculiar CN stretching fundamental of HCN is in much better agreement with experiment than previous theoretical results.

For the very flexible C_3 molecule the presented composite PES yields fundamental vibrational transition frequencies which are within 1 cm^{-1} compared to experiment. The rovibrational calculations on C_3 highlight the necessity of an accurate rovibrational treatment. Common perturbational approaches based on contact transformation of the Hamiltonian fail to describe the strong rovibrational couplings in C_3. Employing the variational ground state rotational constants a mixed experimental/theoretical equilibrium geometry is determined and shown to be superior to results obtained from experimental results only. In cooperation with the Linnartz group for laboratory astrophysics a joint experimental/theoretical investigation of highly excited stretching state is presented.

In order to increase the size of linear molecules which can be studied by such composite approaches a new method (C8v4) has been developed. C8v4 is based on the exact kinetic energy operator formulated in normal coordinates and the rovibrational term energies and wave functions of linear tetra atomic molecules are calculated by a variational *ansatz*. Products of harmonic oscillator and rigid-rotor functions are used to expand the rovibrational wave function. Intricacies related to the vibrational angular momentum in linear molecules require a careful study of symmetry properties

to set up a symmetry adapted basis set. Kinetic energy matrix elements can be evaluated in a fast mixed numerical/analytical fashion. The main computational bottlenecks are the integration of the potential energy matrix and the diagonalisation of the Hamiltonian. These can be overcome by exploiting the block structure of the Hamiltonian. Benchmark calculations on acetylene (HCCH) and boranimine (HBNH) are presented which perfectly reproduce previous variational calculations based on a different Hamiltonian formulated in internal coordinates.
Using the C8v4 program and a composite quartic force field obtained earlier, variational rovibrational calculations for the interesting astromolecule propynylidynium (l-C_3H^+) are carried out. The results of these calculations rectify long standing discrepancies between theory and experiment. The need for high-order correlation contributions to the composite force field is clearly highlighted. The new composite PES yields a ground state rotational constant based on C8v4 variational term energies which is within 5 MHz of the experimental result and a quartic centrifugal distortion constant in virtual agreement with experiment. Spectroscopic parameters for low-lying excited vibrational states are presented which should provide a starting point in forthcoming experimental studies on l-C_3H^+. A close relationship can be established by comparing the properties of the l-C_3H^+ composite PES with the composite PES of C_3. An analysis of differences in rotational parameters calculated variationally and by perturbation theory confirms the assumption that l-C_3H^+ behaves like a "protonated", albeit more rigid, C_3.

Contents

Chapter 1

Introduction

Theoretical spectroscopy is among the core competences of quantum chemistry. It aims at the accurate calculation of spectroscopic properties like transition frequencies between molecular energy levels and/or the intensities of such transitions. This requires a detailed knowledge of the potential energy surface (PES) of the molecule under study. The development of new theoretical techniques and subsequent implementation in software for numerical calculations coupled with the advancement in computing hardware nowadays allows the determination of the molecular PES to unprecedented accuracy. For small polyatomic molecules the transition frequencies obtained from such *ab initio* calculations can routinely reach what is called "spectroscopic accuracy" of ~ 1 cm^{-1} when comparing to known experimental results.

While calculations for experimentally well studied systems provide a consistent way to assess and benchmark the accuracy of an *ab initio* approach, the real power of theoretical spectroscopy lays in its ability to produce such data for any molecular system without prior knowledge of laboratory data. In a similar vein, the intensities of spectroscopic transitions can be obtained *ab initio* by studying the electronic properties of a molecule which govern its interaction with electromagnetic radiation. Within the dipole approximation, which is usually well-satisfied, the intensities of, e.g., rovibrational transitions are determined from the electric dipole moment surface (EDMS). Here the situation is more in favour of theory since accurate experimental determination of intensities can be a formidable undertaking due to the requirement of well defined and precise experimental conditions like the temperature and the concentration of the absorbing molecules. On the other hand, for a theoretician it is relatively easy to calculate the intensity of such transitions once the rovibrational problem is solved. Depending on the employed PES and EDMS the accuracy of theoretical results can rival those obtained in experiment. Of course, this neglects the possible effort needed to develop such an approach. However, modern theoretical spectroscopy can provide reliable data which leads to a fruitful interplay between theory and experiment.

A general procedure for obtaining theoretical rovibrational spectroscopic parameters of molecular systems can be divided into two sections and Figure 1.1 summarizes the individual steps in a flowchart diagram. The underlying assumption for almost all theoretical spectroscopic investigations is the validity of the Born-Oppenheimer-Approximation [1, 2] by which the electronic motion is separated from the nuclear motion. This defines the first phase wherein the electronic Schrödinger equation is solved for a set of nuclear arrangements to scan the PES of the molecule. Additionally, the dipole moments of the molecule can be obtained in a similar fashion. From this set of data points a functional relationship has to be derived between a suitable set of coordinates that correspond to the nuclear arrangement and the electronic energy and dipole moments of the system. Such a relation is usually called a potential energy function (PEF) $V(\mathbf{R})$ or electric dipole moment function (EDMF) $\mu(\mathbf{R})$. The second phase is the solution of the nuclear Schrödinger equation to obtain the rovibrational wavefunctions Ψ_{VR} and term energies $T_v(J)$. The former, when combined with the EDMF, gives access to squared transition dipole moments μ_{if}^2 between rovibrational states which determine the intensities A_{if} of rovibrational transitions. The term en-

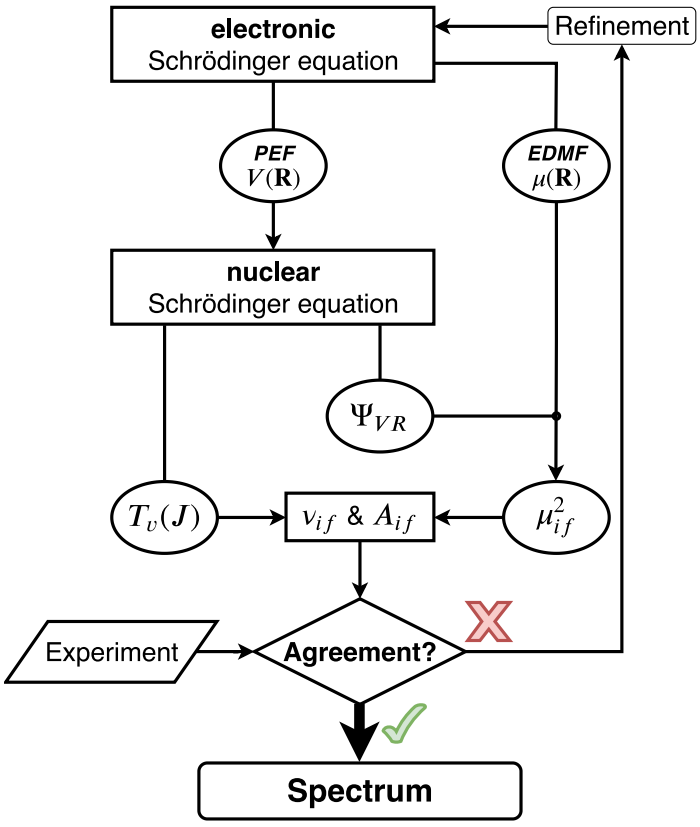

Figure 1.1: Workflow of a theoretical rovibrational spectroscopic investigation showing the different steps involved in obtaining accurate theoretical spectra.

ergies or transition frequencies ν_{if} between rovibrational states as well as the intensities can then be compared to available experimental data. A direct line-by-line comparison is only occasionally done. Instead, one resorts to comparing spectroscopic parameters which are derived from the line frequencies or term energies. This allows to judge the quality of the underlying PEF and EDMF.

In case a disagreement between theory and experiment is found, a critical assessment of the possible cause is required. This can originate on both ends either the theoretical treatment or the experimental analysis. From the theoretical point of view, the main sources of error can be divided further into those from an insufficient treatment of the electronic structure problem yielding a poor PEF/EDMF and those arising from an inadequate treatment of the nuclear motion. The former can be remedied by improving the *ab initio* description of the PES. Modern quantum chemistry offers a plethora of methods each with their individual strengths and weaknesses. The task thus is to find a general procedure to produce reliable PEFs and EDMFs for a variety of molecular systems by combining different levels of sophistication. Errors arising from an inappropriate treatment of the rovibrational problem usually indicate a distinctive feature of the molecule under study. For example, a simplistic harmonic treatment of vibration in polyatomic molecules can not be expected to reach spectroscopic accuracy when comparing to experimental results which are inherently anharmonic. Yet, inclusion of anharmonic effects also poses the risk of producing erroneous theoretical results since the treatment of anharmonicity is in many cases done under the assumption that the latter is a small effect compared to the harmonic solution. Once an accurate theoretical PEF and rovibrational treatment is employed, it becomes possible to point out errors or misinterpretations of experimental results. But theory and experiment should not be viewed as mutually opposing fields of research. They are meant to complement each other with on the one hand experiment providing definite reliable data for benchmarking the theoretical approaches and on the other hand theory providing further insight into aspects of a molecule which are not or only very difficult to access with experiment. Theoretical spectroscopy can further provide guidance for new experimental studies regarding the spectral range where a molecular transition might occur.

Many of the ca. 200 molecules which have been detected in the interstellar medium or circumstellar shells [3–5] are highly reactive species such as radicals, carbenes or molecular ions. These may be very diffcult to study spectroscopically in the laboratory since the obtainable concentrations are often too low for conventional absorption spectroscopy. Therefore, highly accurate predictions of spectroscopic parameters based on theory are desirable [6]. Unidentified features in interstellar spectra have persisted almost from the beginning of the field of astrospectroscopy. A famous example is the fortuitous detection of the formyl cation HCO^+ by Buhl and Snyder [7] in 1970. The spectral features detected towards different galactic sources were attributed to what they called the X-ogen molecule because of its unknown extraterrestrial origin. Klemperer [8] immediately speculated that the signal at 89.190 GHz could be due to protonated carbon monoxide on the basis of theoretical considerations. Only five years later, Woods and coworkers [9] confirmed Klemperers initial suggestion by recording the first laboratory rotational spectrum of HCO^+. More recent

examples are the detection of C_6H^- [10] and C_5N^- [11] in the evolved carbon star IRC+10216. In 1995 Kawaguchi *et al.* [10] detected a series of unidentified lines (B1377) in the microwave region with a rotational constant B of 1377 MHz. As a possible carrier of B1377 the cyanobutadiynyl radical C_5N was investigated by Botschwina [12]. On the basis of *ab initio* calculations a rotational constant of $B_0 = 1397 \pm 3$ MHz was obtained, thereby ruling out C_5N as a candidate for B1377. But these results were not in vain, because they served as excellent guides for Kasai and coworkers [13] who detected the rotational transitions of C_5N using a Fourier transform (FT) microwave spectrometer equipped with a pulsed-discharge-nozzle. The experimental data subsequently enabled the detection of C_5N in the Taurus molecular cloud TMC-1 by Guélin *et al.* [14] using the 30-m and the 100-m radiotelescopes situated at IRAM and Effelsberg, respectively. The matter of the unassigned B1377 lines was ultimately resolved by McCarthy and coworkers [15] who recorded the centimeter- and millimeter-wave spectrum of C_6H^- which reproduced the lines observed by Kawaguchi *et al.*. Finally, the assignment of C_5N^- to the B1389 series of lines detected toward IRC+10216 [11] is exclusively based on comparison with theoretical data. The latter were again provided by the Botschwina group [16] who obtained *ab initio* values of $B_0 = 1389 \pm 1$ MHz and $D_e = 30$ Hz for the ground state rotational constant and the equilibrium quartic centrifugal distortion constant, respectively. The latter value is expected to be slightly too small compared to the vibrationally averaged D_0 which is determined experimentally. Botschwina and Oswald [16] estimated a value of $D_0 = 33.8$ Hz (uncertainty $\sim 2\%$) by comparison to D_0/D_e ratios for the $HC_{2n+1}N$ cyanopolyynes. These theoretical values for B_0 and D_0 are in excellent agreement with their astronomical counterparts of 1388.860(2) MHz and 33(1) Hz [11] with the uncertainty with respect to the last significant digit given in parentheses.

Clearly, theoretical spectroscopy can be a major asset in the understanding of the internal dynamics of molecular systems and the prediction of yet unobserved rovibrational transitions. The purpose of this thesis therefore is the application of modern *ab initio* quantum chemistry to study the rovibrational spectrum of small polyatomic linear molecules. The theoretical groundwork is presented in Chapter 2. Wave function based methods will be presented which are required to obtain highly accurate representations of the molecular PES. Additivity based composite schemes are highlighted for this purpose. Theoretical methods to obtain spectroscopic parameters for molecular rovibrational transitions are presented. Such methods are either based on a perturbational expansion of the rovibrational Hamiltonian or employ a variational description of the nuclear wave function and their merits are reviewed.

Chapter 3 presents the application of composite approaches to triatomic systems. The benchmark molecule hydrogen cyanide (HCN) provides an excellent test case since experimental information on a large number of rovibrational states [17] and the intensities of transitions between the energy levels is available [18–24]. It will be shown that an accurate description of the dominant spectral features as well as the more subtle rovibrational interactions governing the weaker bands requires converged descriptions of both the PEF and EDMF. In a second part, the very flexible tricarbon molecule

C_3 is investigated. This system has always attracted the interest of both theoreticians [25, 26] and experimentalists [27] because of the strong rovibrational coupling. The theoretical study of the C_3 rovibrational spectrum illustrates the necessity of an accurate description of the molecular motion since simple approaches like perturbation theory are bound to fail when strong interactions are present [28]. In a combined experimental/theoretical study together with the Linnartz group for laboratory astrophysics at the University of Leiden on stretch-stretch combination bands in C_3 [29] the fruitful interplay between theory and experiment will be highlighted.

In order to extend the established composite approach tetraatomic molecular species the development of a new variational program (C8V4) is outlined in Chapter 4. Starting from the definition of the rovibrational wave function *ansatz* and the constituent basis functions, the additional theoretical groundwork for variational calculations on linear molecules with more than three atoms are presented. A detailed study of symmetry aspects and the non-vanishing matrix elements of the Hamiltonian in the chosen harmonic oscillator and rigid rotor product basis helps to establish the basic structure of the Hamiltonian matrix. The latter is important in the implementation of an efficient program to carry out actual numerical calculations. One faces the common "curse of dimensionality" in quantum chemistry, i.e., the size of the problem grows exponentially with the system size. While for triatomic systems converged variational rovibrational calculations can be carried out with basis sets of about 1000 to 4000 primitive functions for tetraatomic molecules this number grows by at least an order of magnitude. A key feature of C8V4 therefore is the use of a hybrid parallelisation making use of Message Passing Interface (MPI) and Open Multi-Processing (OMP) standards which exploits the block structure of the Hamiltonian for the computational bottleneck of Gaussian integration of the matrix representation. The program is tested on two systems where results of variational calculations using a different formulation based on an internal coordinate Hamiltonian are available.

Chapter 5 combines the results and conclusions of the previous chapters and presents rovibrational calculations on the tetraatomic linear propynylidynium molecular ion l-C_3H^+, a species of interest to astrochemistry. Previous theoretical calculations [30] on l-C_3H^+ have provided somewhat doubtful results concerning certain rotational spectroscopic parameters. Using C8V4 variational calculations it will be conclusively shown that the previous results are in error. Additionally, a new full dimensional composite PEF is presented that allows variational calculations for low-lying rovibrational states. The derived spectroscopic parameters should provide valuable information for forthcoming experimental studies.

Chapter 2

Theoretical Background

In this chapter the theoretical groundwork of this thesis is reviewed. Starting from the fundamental Born-Oppenheimer approximation (Section 2.1) methods for solving the electronic Schrödinger equation are presented in Section 2.2. State-of-the-art *ab initio* theory for both single-reference (Section 2.2.1) and multi-reference (Section 2.2.2) approaches is introduced. Explicit correlation as a mean to speed up electronic structure calculations is discussed in Section 2.2.3. Special attention is given to the convergence of the one- and N-particle functions (Section 2.2.5) and the calculation of molecular properties (Section 2.2.4). The nuclear Schrödinger equation is considered in Section 2.3. Focusing on the rovibrational problem formulated in normal coordinates (Section 2.3.1) perturbational (Section 2.3.2) and variational (Section 2.3.3) methods for obtaining rovibrational spectra (Section 2.3.4) from first principles are presented.

2.1 The Born-Oppenheimer Approximation

The notion of a PES arises under the Born-Oppenheimer (BO) approximation [1,2] that separates the motion of the electrons from that of the nuclei. Then, the PES $E_n(\mathbf{R})$ is obtained from the solution of the time-independent electronic Schrödinger equation

$$\hat{\mathrm{H}}_\mathrm{e} \left|\Psi_n(\mathbf{r};\mathbf{R})\right\rangle = E_n(\mathbf{R}) \left|\Psi_n(\mathbf{r};\mathbf{R})\right\rangle , \tag{2.1}$$

where $\mathbf{R}$ and $\mathbf{r}$ are the coordinates of the nuclei and electrons, respectively, relative to the center of mass (CoM) of the molecule. The index n signifies the electronic state of the molecule with $n = 0$ being the so called electronic ground state. The electronic Hamilton operator for a system composed of n_e electrons and N_at nuclei represented as point charges $\{Z_\mathrm{I}\}$ in the *clamped nuclei* approximation is given by

$$\hat{\mathrm{H}}_\mathrm{e} = \underbrace{-\frac{1}{2}\sum_i^{n_\mathrm{e}} \nabla^2_{\mathbf{r}_i}}_{\hat{\mathrm{T}}_\mathrm{e}} \underbrace{-\sum_i^{n_\mathrm{e}}\sum_\mathrm{I}^{N_\mathrm{at}} \frac{Z_\mathrm{I}}{|\mathbf{R}_\mathrm{I}-\mathbf{r}_i|}}_{\hat{\mathrm{V}}_\mathrm{eN}} + \underbrace{\sum_i^{n_\mathrm{e}}\sum_{j>i}^{n_\mathrm{e}} \frac{1}{|\mathbf{r}_i-\mathbf{r}_j|}}_{\hat{\mathrm{V}}_\mathrm{ee}} + \underbrace{\sum_\mathrm{I}^{N_\mathrm{at}}\sum_{\mathrm{J}>\mathrm{I}}^{N_\mathrm{at}} \frac{Z_\mathrm{I}Z_\mathrm{J}}{|\mathbf{R}_\mathrm{I}-\mathbf{R}_\mathrm{J}|}}_{\hat{\mathrm{V}}_\mathrm{NN}} . \tag{2.2}$$

Operators $\hat{\mathrm{T}}_\mathrm{e}$, $\hat{\mathrm{V}}_\mathrm{NN}$, $\hat{\mathrm{V}}_\mathrm{eN}$ and $\hat{\mathrm{V}}_\mathrm{ee}$ occuring in Equation (2.2) are the kinetic energy operator (KEO) of the electrons and the three Coulomb potential terms for nuclei-nuclei, nuclei-electron and electron-electron interaction, respectively. Although $\hat{\mathrm{V}}_\mathrm{NN}$ only depends on nuclear coordinates it is usually added to the electronic solution, since it constitutes a contribution to the potential energy in which the nuclei move.
The time-independent Schrödinger equation for the nuclear motion in the electronic ground state is given by

$$\overbrace{\left[\underbrace{-\sum_\mathrm{I}^{N_\mathrm{at}} \frac{1}{2M_\mathrm{I}}\nabla^2_{\mathbf{R}_\mathrm{I}}}_{\hat{\mathrm{T}}_\mathrm{N}} + \underbrace{E_0(\mathbf{R})}_{V}\right]}^{\hat{\mathrm{H}}_\mathrm{N}} \left|\Psi_\mathrm{VR}(\mathbf{R})\right\rangle = T_v(J) \left|\Psi_\mathrm{VR}(\mathbf{R})\right\rangle \tag{2.3}$$

with the nuclear KEO $\hat{\mathrm{T}}_\mathrm{N}$ and $E_0(\mathbf{R})$ acting as the potential energy (also denoted as V in the following) for the internal movement of the nuclei. Since the separation of translational (external) CoM movement and internal (rotational and vibrational) degrees of freedom is always possible and exact, the eigenfunctions and -values of the nuclear Hamiltonian are the rovibrational wave function $\left|\Psi_\mathrm{VR}(\mathbf{R})\right\rangle$ and term energies $T_v(J)$, respectively.

2.2 *Ab initio* electronic structure methods

Analytic solution of the electronic Schrödinger equation Equation (2.1) for all but the simplest systems of interest to chemistry is not possible. Therefore, approximations have to be introduced which can be separated into two classes:

1. The one-particle basis which corresponds to the use of atom centered basis functions termed atomic orbitals (AOs). Molecular wave functions are then built up from molecular orbitals (MOs) as one-electron functions obtained by linear combinations of the AOs. This is commonly referred to as *linear combination of atomic orbitals* (LCAO).

2. The N-particle space which describes the extension of the wave function beyond that of a single *Slater determinant* (anti-symmetric product of spin MOs). Using the formalism of Configuration Interaction (CI) methods [31] the electronic wave function can be expanded in the following way:

$$|\Psi\rangle = |\Phi_0\rangle + \sum_{i,a} C_i^a \, |\Phi_i^a\rangle + \sum_{i>j} \sum_{a>b} C_{ij}^{ab} \, |\Phi_{ij}^{ab}\rangle + \ldots, \tag{2.4}$$

   where $|\Phi_0\rangle$ is the reference determinant, $|\Phi_i^a\rangle$ and $\left|\Phi_{ij}^{ab}\right\rangle$ are singly and doubly excited determinants, respectively, in which an electron (or multiple) has been excited from an *occupied* spin orbital labeled with letters $i,\ j,\ k,\ \ldots$ to an unoccupied (*virtual*) spin orbital labeled with letters $a,\ b,\ c,\ \ldots$ The coefficients $C_{\text{occ}}^{\text{virt}}$ then give the weight of the individual determinants to the wave function.

Both, the one-particle and N-particle space have well defined, albeit impractical, limiting cases. In the former case this is called the *complete basis set* (CBS) limit and in the latter case the *full configuration interaction* (FCI) limit. The exact solution of the electronic Schrödinger equation is thus given by the Full Configuration Interaction (FCI)/complete basis set (CBS) wavefuncion/energy.

The simplest method for obtaining a solution of the electronic Schrödinger equation is the Hartree-Fock (HF) method [32–36]. In HF theory the wave functions is given by a single Slater determinant built up from MOs. The motion of an electron is described in an averaged field of all other electrons (*mean field theory*). HF is able to recover about 99 % of the total electronic energy. The remaining 1 % is commonly referred to as *correlation energy* as it results from the instantaneous reaction of the motion of an electron to that of another electron which is not covered by the mean field approach of HF.

One way of recovering the *correlation energy* is by the use of the CI method outlined above. In practical calculations the expansion has to be truncated at a certain order of excitation. Due to the Brillouin Theorem [37, 38] at least double excitations are required to obtain a contribution to the electronic ground state energy since matrix elements of the Hamilton operator between single excitations and the reference configuration vanish. This leads to the CISD (Configuration Interac-

tion with Single and Double excitations) method [39,40]. While in general improving upon the HF solution, this truncated form of CI has the major drawback of not being *size consistent*. This error relates to the electronic energy calculated for a supersystem A+B consisting of the non-interacting subsystems A and B (for example achieved by sufficiently large distance) being different to the sum of the electronic energies of the individual subsystems.

Although CI offers a systematic way of improving the wave function and energy by inclusion of higher than double excitations, more powerful methods have emerged over the years to treat electron-electron correlation. Among those, Coupled-Cluster (CC) theory [41, 42] is probably the most successful one based on a single HF reference Slater determinant. Through the use of a non-linear *ansatz* for the wave function a larger part of the *correlation energy* can be recovered by CC methods of a certain order compared to a CI expansion of that same order. CC methods therefore offer a cost-efficient and accurate way of treating molecular problems.

The use of a single reference determinant somewhat limits the range of a PES that can be sampled since effects like bond dissociation can not be described by a single determinant. Additionally, in regions away from the minimum of the PES the influence of excited states of the molecule on the ground state electronic wave function might become very large thereby making a single reference *ansatz* questionable. In order to treat such effects of non-dynamical or *static* correlation one has to resort to approaches which account for the *multi-reference* nature of the problem. The Multireference Configuration Interaction (MRCI) method is the most prominent method that aims at incorporating both *static* and *dynamic* correlation effects.

On the other side of the coin, the extension of the one-particle basis plays an important role in accurate *ab initio* calculations. A particularly noteworthy breakthrough was the introduction of the correlations-consistent basis sets cc-pVnZ (correlation-consistent polarized valence n-tuple ζ) by Dunning and coworkers [43] which systematically converge the electronic energy towards the CBS limit. This has lead to the development of extrapolation protocols which approximate the CBS limit from a small number of calculations [44–50]. A second approach is the inclusion of terms in the wave function which explicitly depend on the interelectronic distance. Such methods, called R12 or F12 *explicitly correlated* depending on the formulation [51, 52], have become very successful in recent years.

In addition to the energy of a molecular system its physical properties pertaining to a perturbation by an external field (e.g. a magnetic or an electric field) are of interest to theoretical spectroscopy and quantum chemistry in general (see e.g. [53] for a review). *First-order properties* like the *dipole moment* or higher moments are key in understanding various spectroscopic techniques since they determine the coupling between the electromagnetic radiation and the molecular system. Further spectroscopically relevant properties include the spin densities at the nuclei for electron-spin resonance (ESR) spectroscopy or the field grandient at the nucleus for nuclear quadrupole couplings (NQC). Such properties can be calculated following different procedures, these include perturbation theory and response theory [54]. The latter approach is especially suited in the study of *time-dependent* properties. Here, the perturbational approach will be the main focus since the

interest is on *static* properties and the latter is well suited to evaluate molecular dipole moments that determine the intensity of rovibrational transitions.

A quantitative description of the rovibrational spectrum of a molecule requires precise knowledge of the molecular PES. *Ab initio* methods like CCSD(T) can routinely achieve an accuracy of 5-10 cm^{-1} in the calculation of fundamental vibrational transitions [55–58]. However, modern IR spectroscopy can easily reach an accuracy of 0.0001 cm^{-1} in determining rovibrational transition frequencies [17] which corresponds to an energy on the order of $10^{-10}\ E_\mathrm{h}$. Reaching such a level of agreement *ab initio* would be rather ambitious. Then again, the separations between adjacent rovibrational transitions for small polyatomic molecules are on the order of $2B \sim 1\ \mathrm{cm}^{-1}$ where B is the rotational constant. This suggests that in order to provide useful quantitative spectroscopic information for the assignment of lines, a target accuracy of $\sim 1\ \mathrm{cm}^{-1}$ (*spectroscopic accuracy*) is desirable. Composite *ab initio* methods [50, 59] aim at converging the PES description to this level of agreement by inclusion of various contributions that account for typical sources of error of standard frozen core CCSD(T) (coupled-cluster with singles, doubles and a perturbative treatment of triple excitations). These encompass but are not limited to core-valence correlation effects, relativistic corrections and higher-order correlation beyond CCSD(T). The inclusion of corrections beyond the BO approximation [60] can also be important especially for molecules containing hydrogen atoms.

The following sections give a more detailed account of the *ab initio* methods that are relevant for this work. Section 2.2.1 and Section 2.2.2 summarize the coupled-cluster and multi-reference methods for correlated *ab initio* calculations. Explicit correlation mainly in the F12 formulation of Werner and coworkers [52, 61] is covered in Section 2.2.3. Details on the calculation of electric molecular dipole moments are given in Section 2.2.4 and composite approaches to the construction of highly accurate potential energy and property surfaces in Section 2.2.5.

2.2.1 Coupled-cluster theory

The main problems of truncated CI methods can be linked to the linear parametrization of the CI wave function according to the expansion Equation (2.4). The CI expansion can be rewritten by introducing the excitation (cluster) operator $\hat{\mathrm{T}}$ according to

$$\hat{\mathrm{T}} = \sum_{i}^{n_\mathrm{e}} \hat{\mathrm{T}}_i \,, \tag{2.5}$$

where the $\hat{\mathrm{T}}_i$ are excitation operators which generate all i-fold excitations from the reference wave function. For example the effect of $\hat{\mathrm{T}}_2$ on $|\Phi_0\rangle$ is

$$\hat{\mathrm{T}}_2 \,|\Phi_0\rangle = \sum_{i>j} \sum_{a>b} t_{ij}^{ab} \,|\Phi_{ij}^{ab}\rangle \ , \tag{2.6}$$

where the coefficients $t_{\mathrm{occ}}^{\mathrm{virt}}$ are called *amplitudes* within CC theory. In CI expansions the latter are usually denoted as $C_{\mathrm{occ}}^{\mathrm{virt}}$. The CISD expansion ($\hat{\mathrm{T}} = \hat{\mathrm{T}}_1 + \hat{\mathrm{T}}_2$) is then given by

$$\begin{aligned} |\Psi_{\mathrm{CI}}\rangle &= \left(1 + \hat{\mathrm{T}}\right) |\Psi_0\rangle \\ &= |\Psi_0\rangle + \hat{\mathrm{T}}_1 |\Psi_0\rangle + \hat{\mathrm{T}}_2 |\Psi_0\rangle \\ &= |\Phi_0\rangle + \sum_{i,a} C_i^a |\Phi_i^a\rangle + \sum_{i>j} \sum_{a>b} C_{ij}^{ab} |\Phi_{ij}^{ab}\rangle \ . \end{aligned} \tag{2.7}$$

A more efficient parameterization can be achieved by using a non-linear *ansatz* for the generation of the excited determinants. This idea leads to the Coupled-Cluster wave function which is given in the following form

$$|\Psi_{\mathrm{CC}}\rangle = \mathrm{e}^{\hat{\mathrm{T}}} |\Phi_0\rangle \ . \tag{2.8}$$

The power of this approach can be realized from the Taylor expansion of the exponential function:

$$\mathrm{e}^{\hat{\mathrm{T}}} = 1 + \hat{\mathrm{T}} + \frac{\hat{\mathrm{T}}^2}{2} + \frac{\hat{\mathrm{T}}^3}{6} + \ldots = \sum_{k=0} \frac{\hat{\mathrm{T}}^k}{k!} \, , \tag{2.9}$$

showing that upon truncation of the cluster operator (Equation (2.5)) at an order $i < n_{\mathrm{e}}$ the wave function still contains contributions from higher substitutions. Taking $\hat{\mathrm{T}} = \hat{\mathrm{T}}_2$ (Coupled-Cluster Doubles, CCD) as an example, the exponential expansion contains the term $\frac{1}{2}\hat{\mathrm{T}}^2$ that, when acting on $|\Phi_0\rangle$, yields

$$\frac{1}{2}\hat{\mathrm{T}}_2^2 |\Phi_0\rangle = \frac{1}{2} \sum_{i>j} \sum_{a>b} \sum_{k>l} \sum_{c>d} t_{ij}^{ab} t_{kl}^{cd} |\Phi_{ijkl}^{abcd}\rangle \, . \tag{2.10}$$

The operator $\hat{\mathrm{T}}_2^2$ thus generates a so called disconnected fourfold excitation $\left|\Phi_{ijkl}^{abcd}\right\rangle$. With this a direct comparison of CI and CC methods is possible. For example the CCSD (Coupled-Cluster with singles and doubles) and CISD wave functions with $\hat{\mathrm{T}} = \hat{\mathrm{T}}_1 + \hat{\mathrm{T}}_2$ are:

$$\begin{aligned} |\Psi_{\mathrm{CC}}\rangle &= |\Psi_0\rangle + \sum_{i,a} t_i^a |\Phi_i^a\rangle + \sum_{i>j} \sum_{a>b} (t_{ij}^{ab} + \frac{1}{2} t_i^a t_j^b) |\Phi_{ij}^{ab}\rangle + \ldots \, , \\ |\Psi_{\mathrm{CI}}\rangle &= |\Psi_0\rangle + \sum_{i,a} C_i^a |\Phi_i^a\rangle + \sum_{i>j} \sum_{a>b} C_{ij}^{ab} |\Phi_{ij}^{ab}\rangle \ . \end{aligned}$$

showing the connection between the cluster amplitudes $t_{\mathrm{occ}}^{\mathrm{virt}}$ and the CI coefficients $C_{\mathrm{occ}}^{\mathrm{virt}}$. The disconneted higher-order terms in the CCSD expansion (not shown) ensure the size consistency of the CC approach. In fact, a CCSD wave functions includes all excited determinants which are present in an FCI expansion.

The determination of the cluster amplitudes $t_{\mathrm{occ}}^{\mathrm{virt}}$ proceeds via the electronic Schrödinger equation

$$\hat{\mathrm{H}}_{\mathrm{e}} \mathrm{e}^{\hat{\mathrm{T}}} |\Phi_0\rangle = E_0 \mathrm{e}^{\hat{\mathrm{T}}} |\Phi_0\rangle \, , \tag{2.11}$$

which upon multiplication with $e^{-\hat{T}}$ yields

$$e^{-\hat{T}}\hat{H}_e e^{\hat{T}} |\Phi_0\rangle = E_0 |\Phi_0\rangle . \tag{2.12}$$

Using the Baker-Campbell-Hausdorff formula [62] for the similarity transformed Hamilton operator in the right hand side of Equation (2.12) one obtains [63]

$$\left(\hat{H}_e + \left[\hat{H}_e, \hat{T}\right] + \frac{1}{2!}\left[\left[\hat{H}_e, \hat{T}\right], \hat{T}\right] + \frac{1}{3!}\left[\left[\left[\hat{H}_e, \hat{T}\right], \hat{T}\right], \hat{T}\right] + \frac{1}{4!}\left[\left[\left[\left[\hat{H}_e, \hat{T}\right], \hat{T}\right], \hat{T}\right], \hat{T}\right]\right) |\Phi_0\rangle = E_0 |\Phi_0\rangle . \tag{2.13}$$

Multiplying this equation from the left with $\langle\Phi_0|$, $\langle\Phi_i^a|$, $\langle\Phi_{ij}^{ab}|$, ... and requiring orthonormality of the configurations yields a set of coupled non-linear equations that determine the energy E and cluster amplitudes $t_{\text{occ}}^{\text{virt}}$. This formulation of CC theory is not variational and the equations have to be solved in an iterative fashion. However, since the wave function includes all higher excitations due to the exponential *ansatz* the method is *size consistent*. In an actual calculation one usually restricts the space of occupied orbitals from which electrons can be excited to the valence electrons leading to the so called *frozen-core* (fc) approximation.
Coupled-Cluster approaches are classified according to the order at which the cluster operator $\hat{T}$ is truncated. The most common approach includes $\hat{T} = \hat{T}_1 + \hat{T}_2$ the coupled cluster singles and doubles method (CCSD) [64, 65]. Further adding $\hat{T}_3$ yields CCSDT (coupled cluster with singles, doubles and triples) [66, 67]. This series can be continued including ever higher levels of excitation up till $\hat{T}_n$, where n is the number of electrons, which is equivalent to FCI as outlined above. The CCSD(T) method introduced by Raghavachari *et al.* [68] includes a perturbative treatment of $\hat{T}_3$ on top of a converged CCSD calculation. This method has been shown to provide excellent results for a large range of systems [16, 26, 50, 55–58, 69–71], leading to it being referred to as the "gold standard" of quantum chemistry [70]. Of course, this is partially due to a fortuitous cancellation of errors arising from the perturbative treatment of the triples, the incomplete basis set, the neglect of core electrons and higher-order correlation effects. The advancement in computing power has enabled the implementation and application of CC methods of high order such as CCSDTQ [72] or its non-iterative perturbational counterpart CCSDT(Q) [73] for example in the MRCC program by Kállay [74, 75]. With this a systematic way of accounting for missing correlation effects is possible going well beyond fc-CCSD(T) and will be further addressed in Section 2.2.5.

2.2.2 Multi-reference methods

The wave functions presented so far have been based on *single reference* methods that construct the excited configurations from a single determinant (in most cases the HF ground state). By virtue of this approach the orbitals or more precisely the linear combinations of AO basis functions that make up the substitutions are the same as in the HF reference determinant. For electronic

wave functions dominated by more than one electronic configuration such an *ansatz* is of course inappropriate even when applying a CI or CC calculation on top of the HF solution since the orbitals generated by HF might not be suitable for the excited configuration. Examples for chemical problems that are inherently multi-configurational are the dissociation of molecules [76–78], low lying excited electronic states [79] or conical intersections which are regions of a PES where two or more electronic states of a molecule are nearly degenerate [80–85].
A better solution to such *multi reference* problems is provided by constructing the wave function in a CI fashion and at the same time variationally optimizing the MOs of each configuration. This approach is called the *multi-configurational self-consistent field* (MCSCF) method. A rather compact formulation of the MCSCF wave function is [63]

$$|\Psi_{\mathrm{MCSCF}}\rangle = \mathrm{e}^{-\hat{\kappa}} \sum_i C_i \, |\Phi_i\rangle \,, \tag{2.14}$$

where $\mathrm{e}^{-\hat{\kappa}}$ is the orbital-rotation operator that performs unitary transformations of the orbitals and C_i are CI coefficients. The wave function is then obtained by minimizing the expectation value of the energy

$$E_0 = \min_{\boldsymbol{\kappa},\boldsymbol{C}} \frac{\left\langle \Psi_{\mathrm{MCSCF}} \middle| \hat{\mathrm{H}}_e \middle| \Psi_{\mathrm{MCSCF}} \right\rangle}{\langle \Psi_{\mathrm{MCSCF}} \,|\, \Psi_{\mathrm{MCSCF}} \rangle}, \tag{2.15}$$

with respect to the parameters given above.
Different schemes exist for the selection of the configurations $|\Phi_i\rangle$ that are included in a MCSCF calculation. The *complete active space* (CASSCF) method [86–90] partitions the orbital space into a set of *inactive* orbitals which are doubly occupied in all configurations, *active* orbitals with no restriction of the occupation of these orbitals and *external* orbitals which are unoccupied in all configurations. For a given molecular system the available electrons are then distributed into the *occupied* orbitals consisting of the *inactive* and *active* orbitals. In the space spanned by the *active* orbitals the CASSCF wave function corresponds to a FCI wave function with all possible configurations included. This latter feature already shows that CASSCF is a *size consistent* method. Besides the CASSCF method more intricate methods exist like the *restricted active space* (RAS) scheme [91] which further divides the active space based on certain restrictions. MCSCF methods already include some *dynamical correlation* compared to a HF calculation through the underlying CI approach. Using the MCSCF solution as reference in a, e.g., 2^{nd} order perturbational treatment (CASPT2) [92–101] or in a variational CI calculation (MRCI) allows to recover an even larger fraction. Besides that, there are also some non-variational MRCI variants like the *multi-reference averaged coupled pair functional* (MR-ACPF) method [102] which is size consistent by construction. Attempts at the formulation of *multi-reference* versions of CC theory [103–109] are still rather scarce and not widely applicable and suffer from technical complications [110, 111]. In the following the focus will be on the MRCI and Multireference Averaged Coupled-Pair Functional (MR-ACPF) method since these will be used for the construction of PEFs in this work.
MRCI calculations are basically an extension of the CI method to a reference that consists of more

than one configuration. The CI expansion is usually truncated after the double excitations and the wave function can then be written [31, 112–114]

$$|\Psi_{\mathrm{MRCI}}\rangle = \sum_I C_I |\Phi_I\rangle + \sum_S \sum_a C_S^a |\Phi_S^a\rangle + \sum_P \sum_{ab} C_P^{ab} |\Phi_P^{ab}\rangle . \tag{2.16}$$

In Equation (2.16) the $|\Phi_I\rangle$ are the configurations that can be constructed from the *occupied* orbitals in the reference wave function. Therefore, the first term can be identical to the reference wave function and will be so when employing a full valence CASSCF reference. The *singly external* configuration state functions (CSFs) $|\Phi_S^a\rangle$ are the single substitutions obtained by placing one electron in an *external* orbital a. Analogously the $\left|\Phi_P^{ab}\right\rangle$ are *doubly external* CSFs. The index P designates an orbital pair $P = (i, j, p)$ with p characterizing the spin state of the CSF($p = 1 - 2S$, i.e. $p = 1$ for singlet and $p = -1$ for triplet).

Considering all single and double excitations from the reference $|\Phi_0\rangle$ can lead to a huge number of configurations which makes the calculations very demanding with large AO basis sets. A more efficient formulation is obtained by applying the double excitation operator to the total reference wave function. This approach is known as *internally contracted* (ic-)MRCI and was developed by Meyer [115] as well as Werner and Reinsch [116]. The doubly excited configurations are then given by

$$|\Phi_{ij}^{ab}\rangle = \hat{\mathrm{T}}_2 \sum_R C_R |\Phi_R\rangle = \sum_R C_R |\Phi_{ijR}^{ab}\rangle , \tag{2.17}$$

where R runs over the number of configurations in the reference function. Contracted configurations contain the same external orbitals a, b but differ in the internal (active) orbitals. With this the number of double substitutions in the CI expansion is independent of the number of reference configurations. The introduction of the contraction introduces a small loss of about 0.3-0.5 % on the recovered correlation energy [117] but this is significantly smaller than the difference of MRCISD with respect to a FCI treatment.

In analogy to truncated single reference CI , MRCISD is not size consistent. This can lead to problems in describing dissociation curves or molecular clusters. A cheap *a posteriori* method to obtain approximate size consistency is called the "Davidson correction" following Davidson and Silver [118]. The correction term ΔE_Q to the correlation energy E_{corr} is then given by

$$\Delta E_{\mathrm{Q}} = E_{\mathrm{corr}} \frac{1 - C_0^2}{C_0^2}, \tag{2.18}$$

where C_0 is the coefficient of the reference wave function in the converged MRCI wave function $C_0 = \sum_R C_R$. Applications that employ the Davidson method are usually termed MRCI+Q since the correction mainly accounts for neglected quadruple excitation which are important for achieving (approximate) size consistency.

A multi-reference approach that is size-consistent by construction is the ACPF method first introduced by Gdanitz and Ahlrichs [102]. The n_{e} electrons in the molecule are divided into $\frac{1}{2}n_{\mathrm{e}}$

non-interacting pairs and the energy of the system is then obtained by minimizing the functional

$$E = E_0 + \frac{\left\langle \Phi_0 + \Phi_c \left| \hat{\mathrm{H}}_e - E_0 \right| \Phi_0 + \Phi_c \right\rangle}{1 + g_a \left\langle \Phi_a \,|\, \Phi_a \right\rangle + g_e \left\langle \Phi_e \,|\, \Phi_e \right\rangle}. \tag{2.19}$$

In Equation (2.19) $|\Phi_0\rangle$ and $|\Phi_c\rangle$ are the normalized reference and the correlation functions, respectively. The latter are the functions created by the single and double excitation operators acting on the reference. Wave functions $|\Phi_a\rangle$ occuring in the denominator of Equation (2.19) are CSFs in the set $|\Phi_c\rangle$ that have, outside of the active orbitals, the same occupation as the reference and $|\Phi_e\rangle$ are all the remaining external CSFs contributing to $|\Phi_c\rangle$. The parameters $g_a = 1$ and $g_e = 2/n_\mathrm{e}$ then provides the ACPF method. The choice $g_a = g_e = 1$ will yield the MRCI solution.

2.2.3 Explicitly correlated methods

The electron-electron interaction potential V_{ee} in Equation (2.1) is singular when the electron-electron distance r_{12} of an electron pair tends towards zero. This is called the *Coulomb cusp* and the condition imposed on the wave function have been worked out by Kato [119]

$$\left(\frac{\partial \Psi}{\partial r_{12}}\right)_{r_{12}=0} = \frac{1}{2}\Psi(r_{12} = 0)\,. \tag{2.20}$$

A wave function expanded in terms of MOs constructed from contracted Gaussian-type orbitals (cGTOs) requires a large number of those basis functions to describe the shape of the *Coulomb cusp*. This is of course due to the basis set not depending on the interelectronic distance r_{12}. Already in 1929 Hylleraas [120] in his seminal paper on the ground state of the Helium atom included the interelectronic distance r_{12} (geminals) directly into his basis functions. This idea was later picked up by Kutzelnigg and coworkers [51, 121, 122] leading to the developement of the so called R12 methods. A different approach termed F12 was introduced by Werner and coworkers [52, 61] employing Slater-type geminals

$$f(r_{12}) = -\frac{1}{\beta}\mathrm{e}^{-\beta r_{12}}\,, \tag{2.21}$$

follwing Ten-no's suggestion [123]. The parameter β in Equation (2.21) has the dimension of an inverse length and common recommended values are in the range 0.9-1.5 Å^{-1} depending on the employed basis set [124]. A complication arising in explicitly correlated methods is that computationally demanding three- and four-electron integrals have to be evaluated. This can be circumvented by introducing the resolution-of-the-identity (RI) approximation [51], which reduces the many-electron integrals to products of no more than two-electron integrals. The RI approximation requires a complementary auxilliary basis set (ABS) which together with the AO basis forms the complementary auxilliary basis set (CABS) and together with density fitting (DF) techniques the CCSD(T)-F12 methods [52, 61] as implemented in Molpro [125] provide efficient explicitly correlated coupled-cluster approaches. Explicitly correlated MRCI-F12 and MR-ACPF-F12 meth-

ods [83, 126, 127] have also been introduced by the group of Werner employing approximations similar to CCSD(T)-F12.
The perturbative (T) contribution is treated in the standard manner in CCSD(T)-F12 and to approximate a fully explicit correlation treatment a triples scaling scheme has been proposed by Werner *et al.* [61,128]. In the so called (T*) approach the contribution of triples to the correlation energy $\Delta E^{\mathrm{corr}}_{(\mathrm{T}^*)}$ is calculated according to

$$\Delta E^{\mathrm{corr}}_{(\mathrm{T}^*)} = \Delta E^{\mathrm{corr}}_{(\mathrm{T})} \frac{E^{\mathrm{corr}}_{\mathrm{MP2\text{-}F12}}}{E^{\mathrm{corr}}_{\mathrm{MP2}}} \,. \tag{2.22}$$

In Equation (2.22) $\Delta E^{\mathrm{corr}}_{(\mathrm{T})}$ is the triples energy which is scaled by the ratio of the correlation energy obtained from 2$^{\mathrm{nd}}$ order Møller-Plesset perturbation theory (MP2) [129] employing explicit correlation $E^{\mathrm{corr}}_{\mathrm{MP2\text{-}F12}}$ [130–132] and in the standard MP2 formulation $E^{\mathrm{corr}}_{\mathrm{MP2}}$.
The various approximations that are involved in CCSD(T)-F12 calculations demand a careful assessment of the method with respect to canonical CCSD(T) calculations with large AO basis sets. For example, the recent extensive study by Feller [133] indicated that the use of the (T*) scheme can lead to poorer results especially for larger AO basis sets. He suggested that, until a complete explicitly correlated treatment of the connected triples in the spirit of (T) is available, the use of the $E^{\mathrm{corr}}_{\mathrm{CCSD\text{-}F12}}/E^{\mathrm{corr}}_{\mathrm{CCSD}}$ ratio to scale triples energies might provide a more robust estimate to explicitly correlated triples contributions.

2.2.4 The electric dipole moment

The dipole moment can be interpreted as the response of a molecular system to an external field acting as a perturbation [134]. Using a Taylor expansion of the energy with respect to a static electric field $\mathbf{F}$ expanded around the field-free case one obtains

$$E(\mathbf{F}) = E_0 + \sum_{\alpha} \left(\frac{\partial E}{\partial F_\alpha} \right)_0 F_\alpha + \frac{1}{2} \sum_{\alpha\beta} \left(\frac{\partial^2 E}{\partial F_\alpha \partial F_\beta} \right)_0 F_\alpha F_\beta + \ldots \,, \tag{2.23}$$

where the summations are carried out over the cartesian components $\{\alpha, \beta\} = \{x, y, z\}$. The multipole expansion of the interaction energy of a charge distribution with a uniform electric field is given by

$$E = q_{\mathrm{tot}} V_{\mathrm{el}} - \boldsymbol{\mu}\mathbf{F} - \frac{1}{2}\boldsymbol{\Theta}\mathbf{F}^{'} - \ldots \,, \tag{2.24}$$

where q_{tot} is the total charge of the molecule and V_{el} the electric potential. The symbols $\boldsymbol{\mu}$ and $\boldsymbol{\Theta}$ designate the electric dipole and quadrupole moment, respectively, and the electric field gradient is $\mathbf{F}^{'}$. The presence of an electric field further induces a dipole moment which can be approximated by a Taylor expansion of $\boldsymbol{\mu}$

$$\boldsymbol{\mu} = \boldsymbol{\mu}_0 + \boldsymbol{\alpha}\mathbf{F} + \frac{1}{2}\boldsymbol{\beta}\mathbf{F}^2 + \ldots \tag{2.25}$$

Equation (2.25) defines the permanent dipole moment $\boldsymbol{\mu}_0$, the dipole polarizability $\boldsymbol{\alpha}$ and the first hyperpolarizability $\boldsymbol{\beta}$. In a homogenous electric field the term $\mathbf{F}^{'}$ in Equation (2.24) and all higher derivatives vanish. Then, one can identify the derivatives in Equation (2.23) with the derivatives of the dipole moment:

$$\mu_{0\alpha} = -\left(\frac{\partial E}{\partial F_\alpha}\right)_0 , \tag{2.26}$$

$$\alpha_{\alpha\beta} = -\left(\frac{\partial^2 E}{\partial F_\alpha \partial F_\beta}\right)_0 . \tag{2.27}$$

In the context of molecular rovibrational spectroscopy both these quantities are important. The permanent dipole moment and its variation with the molecular geometry (electric dipole moment function, EDMF) determines the intensity of rotational and rovibrational spectra in the microwave and infrared and the polarizability tensor $\boldsymbol{\alpha}$ determines the intensities in Raman spectroscopy.
Determination of μ_α via *ab initio* methods is predominantly performed by simple numerical differentiation

$$\mu_\alpha \approx \frac{E(f_\alpha) - E(-f_\alpha)}{2f_\alpha} . \tag{2.28}$$

This is termed *finite field approach*, since it involves including a finite electric field as an operator $f_\alpha \hat{\alpha}$ in determining the *ab initio* energies $E(\pm f_\alpha)$. The numerical approach requires a field that is sufficiently small to approximate the differential ∂F_α and still large enough for the calculated fraction to be numerically stable. A typical value employed in this thesis is $f_\alpha = \pm 0.0003$ in atomic units.
The dipole moment is a vector in cartesian space and per convention the individual components are assigned a positive sign if the dipole points from the negative end to the positive end in the direction of the cartesian axis. This is important in understanding the signs of the dipole moments given in this thesis. They are given with respect to the molecule being aligned along the z-axis in their equilibrium configuration according to the molecular formula. As an example, for hydrogen cyanide HCN a negative sign of the permanent dipole moment μ_z corresponds to a polarity +HCN−. For the application in variational rovibrational calculations the *ab initio* dipole moment vectors is transformed locally to the Eckart frame [135]. Then, the dipole vector of linear molecules $\boldsymbol{\mu} = \begin{pmatrix} \mu_\parallel \\ \mu_\perp \end{pmatrix}$ has the two components $\mu_\parallel$ along the molecular symmetry axis (z) and $\mu_\perp$ perpendicular to the molecular axis.

2.2.5 Composite approaches

A comprehensive review of composite approaches is beyond the scope of this work and the reader is refered to the reviews by Feller, Peterson and Dixon [136] and Karton [59]. The schemes which have become quite popular in recent years are the *Gaussian-n* (Gn) methods [137–144] originally introduced by Pople and coworkers, the *highly accurate extrapolated ab initio thermochemistry* (HEAT) methods of Stanton and coworkers [69, 145, 146], the *Weizmann-n* (Wn) family of meth-

ods by Martin *et al.* [48, 147, 148], the work of Allen and coworkers on the *Focal-Point-Analysis* (FPA) [149–153] or the *correlation consistent composite approach* (ccCA) developed by the Wilson group [154–158]. The method probably closest related to the present composite approach is the *Feller-Peterson-Dixion* (FPD) approach [50,136,159–162]. Starting from coupled-cluster CCSD(T) calculations with large Gaussian basis sets (including up to aug-cc-pV8Z) the method accounts for effects due to core-core and core-valence correlation, scalar relativistic effects and higher-order correlation beyond CCSD(T). When necessary even smaller effects like spin-orbit coupling or adiabatic corrections are also taken into account. Especially designed for high accuracy atomization energies the FPD method is able to achieve root-mean-square (RMS) deviations of about 0.30 kcal/mol compared to experiment. As a by product the FPD approach yields molecular equilibrium geometries and harmonic vibrational frequencies that are within 0.002-0.003 Å and 1-2 cm^{-1} of their experimental counterparts. This level of agreement makes FPD a promising approach for the construction of potential energy functions.
As with all composite methods the basic idea of the present *ansatz* is based on the assumption of additivity for the various corrections that enter the PEF. That implies that the PEF can be represented as a simple sum according to

$$V = \sum_{(\alpha)} V^{(\alpha)} = V^{(\mathrm{F12b})} + V^{(\mathrm{CV})} + V^{(\mathrm{SR})} + V^{(\mathrm{HC})} + V^{(\mathrm{DBOC})} \,, \tag{2.29}$$

where the contributions are designated by (α) (for an explanation of the used abbreviations see below). In addition to composite PEFs, the scheme can be applied to any molecular property and will be used to construct composite EDMFs

$$\boldsymbol{\mu} = \sum_{(\alpha)} \boldsymbol{\mu}^{(\alpha)} = \boldsymbol{\mu}^{(\mathrm{F12b})} + \boldsymbol{\mu}^{(\mathrm{CV})} + \boldsymbol{\mu}^{(\mathrm{SR})} + \boldsymbol{\mu}^{(\mathrm{HC})} \,. \tag{2.30}$$

The basic contribution to the PEF and EDMF is chosen such that it already incorporates a large fraction of the correlation contribution at or very close to CBS limit. Therefore, the explicitly correlated fc-CCSD(T)-F12b method (abbreviated F12b) will be employed to provide such results. The individual corrections which are added to this term are discussed in the following.

Core-valence correlation

Core-core and core-valence correlation (CV) are among the most important contributions to the composite scheme. The influence on bond lengths and harmonic vibrational frequencies is on the order of 0.001 Å and up to 10 cm^{-1}, respectively, depending on the molecule under study. Conventional coupled-cluster CCSD(T) calculations are employed to correct the PEF for CV effects and the contribution is obtained as the energy difference of CCSD(T) with all electrons correlated and fc-CCSD(T). This requires large AO basis sets of the (aug-)cc-pCVnZ family [163–165] that are specifically designed to recover CV effects. In order to reach near CBS quality at least quintuple

ζ ($n = 5$) basis sets are required. This makes the CV contribution rather expensive especially for regions of low symmetry on the PES of a linear molecule. The recent development by Peterson and coworkers [166] of specialized cc-pCVnZ-F12 basis sets for all electrons explicitly correlated calculations will help to mitigate this cost in the future. For example, a ae-CCSD(T)-F12b/CVQZ-F12 calculation offers CBS quality electronic energies for the combined F12b+CV contribution at a fraction of the cost required when combining e.g. a F12b/VQZ-F12 basic contribution with CV calculated with a large CV6Z basis set [167].

Scalar relativistic effects

The electronic Hamiltonian of Equation (2.2) is strictly non-relativistic. The neglect of scalar relativisitc (SR) effects introduces a comparably small error on the spectroscopic parameters of molecules consisting of light first- and second-row elements. However, to reach spectroscopic accuracy it is still necessary to account for this contribution. To this end CCSD(T) calculations employing the 2$^{\text{nd}}$ order Douglas-Kroll-Hess (DKH) Hamiltonian [168, 169] are performed. Again, the SR contribution is obtained as the energy difference of two calculations at the DKH2 fc-CCSD(T) and standard fc-CCSD(T) level of theory. The former employ the recontracted (aug-)cc-pVnZ-DK basis sets [170] designed for DKH applications and the latter utilize standard Dunning type basis sets.

Higher-order correlation

Higher-order correlation (HC) of the valence electrons beyond the basic contribution fc-CCSD(T) is incorporated in a series of calculations. The employed decomposition of the CC correlation energy corresponds to

$$E_{\text{corr}} = \Delta E_{\text{SD}} + \Delta E_{(\text{T})} + \overbrace{\underbrace{\left[\Delta E_{\text{T}} - \Delta E_{(\text{T})}\right] + \Delta E_{(\text{Q})}}_{\text{(Q)-(T)}} + \underbrace{\left[\Delta E_{\text{Q}} - \Delta E_{(\text{Q})}\right]}_{\text{Q-(Q)}} + \underbrace{\Delta E_{\text{P}}}_{\text{P-Q}} + \underbrace{\Delta E_{\text{S}}}_{\text{S-P}} + \ldots}^{\text{HC}}, \quad (2.31)$$

where each term corresponds to the contribution of a different excitation operator $\hat{\text{T}}_i$. The first two terms correspond to the CCSD(T) correlation energy. The first HC contribution termed (Q)-(T) in fact incorporates two effects. It corrects the perturbative triples to the full CCSDT result and adds the quadruples effect via (Q) calculated with the converged CCSDT amplitudes [73]. The (Q)-(T) contribution is therefore obtained from the difference CCSDT(Q)-CCSD(T) and constitutes the largest HC effect. From the energy difference CCSDTQ-CCSDT(Q) the corrections to the full iterative quadruples is obtained (termed Q-(Q)). The influences of $\hat{\text{T}}_5$ and $\hat{\text{T}}_6$ are calculated from CCSDTQP-CCSDTQ (P-Q) and CCSDTQPS-CCSDTQP (S-P) [72].
The first HC contribution (Q)-(T) usually has an opposite effect compared to the CV contribution and a at least partial compensation has been observed for a number of systems [48,50,159,171–173]. An important factor supporting the success of composite methods is the finding that HC effects

show much faster convergence with respect to the AO basis as shown by Karton and coworkers [48,174]. This enables the inclusion of computationally demanding contributions like P-Q and S-P evaluated with small cc-pVDZ basis sets, yet still providing reasonably converged results.

Diagonal Born-Oppenheimer correction

The first correction for effects beyond the Born-Oppenheimer approximation can be calculated from the electronic ground state wave function $|\Psi_0(\mathbf{r};\mathbf{R})\rangle$ (*diagonal Born-Oppenheimer correction* DBOC) and is given by [60,175]

$$\Delta E_{\mathrm{DBOC}}(\mathbf{R}) = -\sum_{\mathrm{I}}\sum_{\alpha}\frac{1}{2M_{\mathrm{I}}}\left\langle \Psi_0(\mathbf{r};\mathbf{R}) \,\middle|\, \nabla^2_{R_{\mathrm{I}\alpha}} \,\middle|\, \Psi_0(\mathbf{r};\mathbf{R})\right\rangle . \tag{2.32}$$

The summations in Equation (2.32) run over all atoms I with nuclear mass M_{I} in the molecule and the cartesian coordinates $\alpha = \{x, y, z\}$. The operator $\nabla^2_{R_{\mathrm{A}\alpha}}$ is the second derivative with respect to the nuclear coordinates acting on $|\Psi_0(\mathrm{r};\mathrm{R}\rangle$. Due to the parametric dependence of the wave function on the nuclear coordinates, ΔE_{DBOC} also depends slightly on the internal coordinates of the molecule resulting in small changes of the equilibrium geometry and the shape of the potential energy. Evaluation of the DBOC is enabled by analytic gradient techniques and has been implemented in CFOUR [176] for CCSD wave functions [177].
The DBOC constitutes a mass-dependent contribution to the PEF. Due to the nuclear mass entering as a denominator it is most important for light nuclei especially hydrogen. Converting the DBOC between isotopologues of a molecule presents no challenge once the integrals in Equation (2.32) are evaluated. Potential energy surfaces incorporating DBOC effects are also referred to as *adiabatic* surfaces since they still preserve the concept of a single *adiabatic* potential for a molecule. Higher-order effects beyond DBOC are therefore often called non-Born-Oppenheimer (NBO) or non-adiabatic effects that require integrals of the ground state with excited electronic states coupled through derivatives with respect to the nuclear coordinates [178,179].

2.3 Nuclear motion calculations

The nuclear Hamiltonian $\hat{\mathrm{H}}_{\mathrm{N}}$ in Equation (2.3) is given with respect to cartesian coordinates of the atoms in a *space fixed* (SF) coordinate system. This choice of coordinates is inconvenient for the study of rovibrational energy levels because of the huge degree of coupling between rotational and vibrational motion in SF-coordinates. Therefore, a new set of coordinates is introduced termed *normal coordinates* by invoking the Eckart conditions [135]. This then relates normal coordinates to the cartesian coordinates of the atoms in a *molecule fixed* (MF) coordinate system that rotates (and translates) with the molecular inertial frame. The complete separation of vibrational and rotational motion is not possible but the Eckart frame minimizes the coupling between these coordinates. Wilson and Howard [180] were the first to derive the general rovibrational Hamiltonian

for polyatomic molecules in terms of normal coordinates which was later refined by Darling and Dennison [181]. Todays commonly accepted form is that due to Watson [182]. By use of commutation relations and sum rules for molecular parameters he greatly simplified the Darling-Dennison Hamiltonian. A more detailed discussion of the specific form of the Watson Hamiltonian for linear molecules will be given in Section 2.3.1.

Analogous to the electronic Schrödinger equation, a general analytic solution of Equation (2.3) is not possible and one has to resort to approximate solutions of the rovibrational problems. The two most common approaches are the *perturbational* and the *variational* approach. The former is based on a perturbation expansion of the rovibrational Hamiltonian [183–187] and at least second order vibrational perturbation theory is required to obtain anharmonic corrections to the zeroth order (harmonic) vibrational energies. Employing a *contact transformation* of the Hamiltonian and evaluating matrix elements with respect to the zeroth order wave functions yields *spectroscopic parameters* which depend on the molecular geometry as well as the (an)harmonic PES. These parameters can therefore be calculated *ab initio* or, in a reverse process, extracted from molecular spectra. The standard perturbational approach is based on the assumption of *small amplitude* vibrations. This is not always valid and VPT is therefore prone to failure in case of e.g. "*floppy*" molecules with large amplitude motions.

The second approach is based on variational theory [188–190] employing the exact KEO for the rovibrational problem. In case of linear variational calculations the nuclear wave function $|\Psi_{\mathrm{VR}}(\mathbf{R})\rangle$ is approximated as a linear combination of basis functions whose coefficients are varied in order to minimize the expectation value over the rovibrational Hamiltonian. By increasing the size of the basis set, the latter value will approach $T_v(J)$ from above. Once convergence up to a desired accuracy with respect to the basis set size is reached all differences that remain compared to experiment must originate from the PES and thus from the method used for its calculation (either *ab initio* or from fitting to spectroscopic data). The variational calculation of rovibrational properties therefore provides a means to accurately assess the performance of an *ab initio* method.

In the following sections a more detailed discussion of linear-molecule nuclear motion calculations is presented. First, Section 2.3.1 introduces the rovibrational Hamiltonian for linear molecules in Watson's formulation. Then, Section 2.3.2 and Section 2.3.3 review the basic aspects of the perturbational and variational solution of the nuclear Schrödinger equation. Finally, Section 2.3.4 gives a general overview of rovibrational transitions, the determination of spectroscopic parameters and the calculation of rovibrational intensities.

2.3.1 Watson's isomorphic Hamiltonian

The rovibrational Hamiltonian for linear molecules as given by Watson [191] following the initial simplification of the Darling-Dennison Hamiltonian by the same author for non-linear molecules

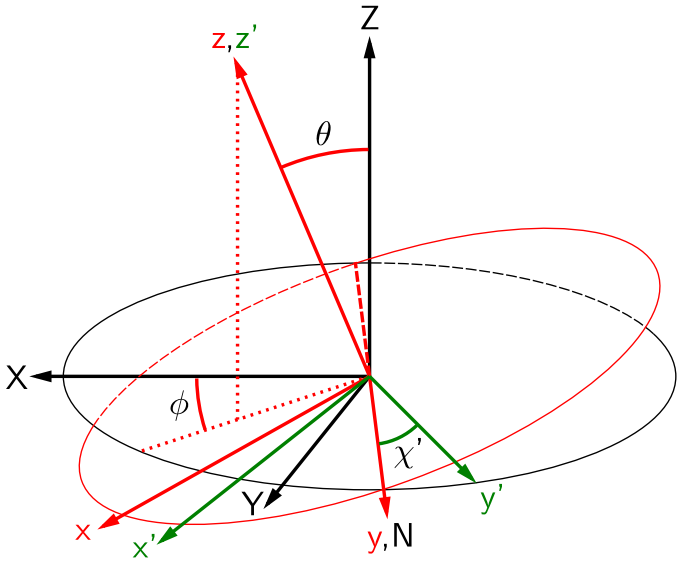

Figure 2.1: Definition of the molecule fixed axes system (x', y', z') and the Euler angles that relate it to the space fixed axes (X, Y, Z) via an intermediate system (x, y, z) with Euler angles $(\theta, \phi, 0)$.

[182] is:

$$\hat{\mathrm{H}}_{\mathrm{W}} = \underbrace{\frac{1}{2}\sum_i \hat{\mathrm{P}}_i^2 + \frac{1}{2}\mu\left(\hat{\pi}_x^2 + \hat{\pi}_y^2\right)}_{\hat{\mathrm{T}}_{\mathrm{V}}} + \underbrace{\frac{1}{2}\mu\left(\hat{\Pi}_x'^2 + \hat{\Pi}_y'^2\right)}_{\hat{\mathrm{T}}_{\mathrm{R}}} \underbrace{- \mu\left(\hat{\Pi}_x'\hat{\pi}_x + \hat{\Pi}_y'\hat{\pi}_y\right)}_{\hat{\mathrm{T}}_{\mathrm{VR}}} + V\,, \tag{2.33}$$

where the summation i runs over all $3N_{\mathrm{at}} - 5$ vibrations of a linear molecule. For linear molecules the first $N_{\mathrm{at}} - 1$ vibrations are stretching vibrations labeled by index s. The remaining $2N - 4$ are doubly degenerate bending vibrations labeled t_α ($\alpha = \{x, y\}$) or where appropriate without α designating the individual components.

Individual terms in the Hamiltonian Equation (2.33) can be identified with different contributions to the rovibrational term energy $T_v(J)$ of the molecule. The first two terms are the vibrational KEO $\hat{\mathrm{T}}_{\mathrm{V}}$ and together with the potential energy V constitute the vibrational Hamiltonian. The third term is the rotational KEO $\hat{\mathrm{T}}_{\mathrm{R}}$ and the operator $\hat{\mathrm{T}}_{\mathrm{VR}}$ couples rotation and vibration and is commonly referred to as the Coriolis coupling operator.

The Hamiltonian in Equation (2.33) is formulated in normal coordinates Q_i and their conjugate linear momenta $\hat{\mathrm{P}}_i = -\mathrm{i}\hbar\frac{\partial}{\partial Q_i}$. Normal coordinates are defined with respect to a molecule fixed coordinate system whose origin is the CoM and its orientation with respect to the space fixed coordinate system (X, Y, Z) is defined by Euler angles (θ, ϕ, χ). A molecule fixed coordinate system

(x, y, z) is required to fullfil the Eckart conditions [135]:

$$\sum_{\mathrm{I}} M_{\mathrm{I}} \mathbf{R}_{\mathrm{I}} = \mathbf{0}\,, \tag{2.34}$$

$$\sum_{\mathrm{I}} M_{\mathrm{I}} (\mathbf{R}_{\mathrm{I}}^{\mathrm{e}} \times \mathbf{R}_{\mathrm{I}}) = \mathbf{0}\,. \tag{2.35}$$

In Equation (2.34) and (2.35) the vectors $\mathbf{R}_{\mathrm{I}}^{\mathrm{e}}$ and $\mathbf{R}_{\mathrm{I}}$ are the equilibrium and the instantaneous cartesian coordinate vector in the molecule fixed axes system, respectively. By setting up the axis system in this way, the (x, y, z) axes coincide with the principal inertia axes of the molecule. For linear molecules the symmetry axis is commonly chosen to be along the z axis. This results in one of the Euler angles (χ) which describes the rotation of the x- and y-axis around z being undefined. This problem is rectified by introducing a new axis system (x', y', z') which is obtained by the following procedure. First one sets $\chi = 0°$ and then introduces a new angle χ' that rotates the (x', y', z') axes from the (x, y, z) axes about $z(= z')$. The actual value of the angle χ' is arbitrary. It is the (x', y', z') axis system in which the normal coordinates are defined. In the following the primes will be omitted for clarity except for cases where explicit relations between the two axes systems are described by the angle χ'. The three discussed axis systems together with the Euler angles (θ, ϕ, χ') that relate them to each other are graphically displayed in Figure 2.1.
The vibrational KEO $\hat{\mathrm{T}}_{\mathrm{V}}$ in Equation (2.33) can be separated into two terms, one for the squared linear momenta of the vibrations $\hat{\mathrm{T}}_{\mathrm{P}}$ and the second term $\hat{\mathrm{T}}_{\pi}$ which accounts for the vibrational angular momentum

$$\begin{aligned} \hat{\mathrm{T}}_{\mathrm{V}} &= \hat{\mathrm{T}}_{\mathrm{P}} + \hat{\mathrm{T}}_{\pi} \\ &= \frac{1}{2} \sum_{i} \hat{\mathrm{P}}_i^2 + \frac{1}{2} \mu \left(\hat{\pi}_x^2 + \hat{\pi}_y^2 \right). \end{aligned} \tag{2.36}$$

The quantity μ can be interpreted as the inverse effective moment of inertia of the molecule and is given by [191]

$$\mu = \frac{\mathrm{I_e}}{\left(\mathrm{I_e} + \sum_{\mathrm{I},i} \sqrt{M_{\mathrm{I}}} r_{\mathrm{Iz}}^{\mathrm{e}} l_{\mathrm{I}z,i} Q_i \right)^2}\,, \tag{2.37}$$

where $\mathrm{I_e}$ is the equilibrium moment of inertia and $l_{\mathrm{I}z,i}$ is an element of the $3N_{\mathrm{at}} \times 3N_{\mathrm{at}} - 5$ matrix $\mathscr{L}$ that transforms the normal coordinate vector $\mathbf{Q}$ to mass weighted cartesian displacement coordinates $u_{\mathrm{I}\alpha} = \sqrt{M_{\mathrm{I}}}(R_{\mathrm{I}\alpha} - R_{\mathrm{I}\alpha}^{\mathrm{e}})$ according to

$$\mathbf{u} = \mathscr{L} \mathbf{Q}\,. \tag{2.38}$$

By introducing the coefficients $a_k = 2\sum_{\mathrm{I}} \sqrt{M_{\mathrm{I}}} R^{\mathrm{e}}_{\mathrm{I}z} l_{\mathrm{I}z,i}$ and recognizing that the latter are only non-zero for stretching vibrations [192] on can rewrite Equation (2.37) yielding

$$\mu = \frac{\mathrm{I_e}}{\left(\mathrm{I_e} + \frac{1}{2}\sum_s a_s Q_s\right)^2} \ . \tag{2.39}$$

The operators $\hat{\pi}_\alpha$ occuring in Equation (2.36) are the vibrational angular momentum operators defined as

$$\hat{\pi}_\alpha = \sum_{ij} \zeta^\alpha_{ij} Q_i \hat{\mathrm{P}}_j \ , \tag{2.40}$$

where ζ^α_{ij} is an element of the Coriolis coupling matrix $\boldsymbol{\zeta}^\alpha$ that represents the coupling of the vibrations i and j via rotation about the α-axis. The elements of these matrices are defined according to

$$\zeta^\alpha_{ij} = \sum_{\mathrm{I}} l_{\mathrm{I}\beta,i} l_{\mathrm{I}\gamma,j} - l_{\mathrm{I}\gamma,i} l_{\mathrm{I}\beta,j} \ , \tag{2.41}$$

where (α, β, γ) are cyclic permutations of (x, y, z). The matrices $\boldsymbol{\zeta}^\alpha$ are skew symmetric and the following relations hold:

$$\zeta^\alpha_{ij} = -\zeta^\beta_{ij} = \zeta^\beta_{ji} = -\zeta^\alpha_{ji} \ . \tag{2.42}$$

Furthermore, the ζ^α_{ij} are only non-vanishing when the direct product of the symmetry species for normal coordinate Q_i and Q_j contains the symmetry species for rotation about the α-axis [192]. Therefore, for a linear molecule the non-zero ζ^α_{ij} are those with $\{i, j\} = \{s, t_y\}$ and $\{i, j\} = \{s, t_x\}$ for $\alpha = x$ and $\alpha = y$, respectively.

The operators $\hat{\Pi}'_\alpha$ occuring in $\hat{\mathrm{T}}_{\mathrm{R}}$ and $\hat{\mathrm{T}}_{\mathrm{VR}}$ of Equation (2.33) are components of the total angular momentum operator $\hat{\Pi}'$ with associated quantum number J. They are obtained by the above mentioned change of coordinates from (ϕ, θ, χ) to (ϕ, θ, χ') [191]. Another effect of this change of coordinates is that the operators $\hat{\mathrm{H}}_{\mathrm{W}}$ and $(\hat{\Pi}'_z - \hat{\pi}_z)$ commute and thus have a common set of eigenfunctions. In order to obtain physical meaningful eigenvalues of $\hat{\mathrm{H}}_{\mathrm{W}}$ one requires the eigenfunctions to have eigenvalue 0 for the operator $(\hat{\Pi}'_z - \hat{\pi}_z)$. Therefore, basis functions employed in calculations have to obey the Sayvetz relation [193]

$$k = \ell = \sum_t \ell_t \ , \tag{2.43}$$

where k and ℓ are the quantum numbers of the operators $\hat{\Pi}'_z$ and $\hat{\pi}_z$, respectively. For a given value of J the quantum number k can take values of $k = 0, \pm 1, \ldots, \pm J$. The Sayvetz relation Equation (2.43) is tantamount to stating that in linear molecules the angular momentum around the z-axis with operator $\hat{\Pi}'_z$ is carried by the vibrations alone with operator $\hat{\pi}_z$.

2.3.2 (Ro-)Vibrational perturbation theory

The perturbational treatment of the rovibrational problem has been discussed by numerous authors. Following the seminal work of Nielsen [183, 184] the formulas of vibrational perturbation theory (VPT) have been worked out for example by Aliev & Watson [187] or in the monograph by Papoušek & Aliev [186]. Probably the most complete (although rather complicated to follow) account of VPT up to 4^{th} order was given by Amat, Nielsen and Tarrago [185]. In the following a short summary of VPT2 will be given as this is the common approach to the anharmonic treatment of rovibrational spectra used by both theoreticians and experimentalists. The formulation closely follows that given by Allen *et al.* [194] as it gives rather compact formulas.
Using the usual perturbational expansion of the Hamiltonian in orders of magnitude one obtains

$$\hat{\mathrm{H}}_{\mathrm{N}} = \hat{\mathrm{H}}_0 + \lambda\hat{\mathrm{H}}_1 + \lambda^2\hat{\mathrm{H}}_2 + \lambda^3\hat{\mathrm{H}}_3 + \dots \tag{2.44}$$

The individual operators $\hat{\mathrm{H}}_0$, $\hat{\mathrm{H}}_1$, ... collect terms in the expanded Hamiltonian containing increasing potencies and/or combinations of vibrational and rotational operators. For example, quartic terms in the potential energy $\phi_{ijkl}q_iq_jq_kq_l$ will contribute to $\hat{\mathrm{H}}_2$. Evaluating matrix elements of this operator up to 2^{nd} order with respect to the (harmonic) eigenfunctions of $\hat{\mathrm{H}}_0$ shows that $\hat{\mathrm{H}}_1$ results in a large number of off-diagonal matrix elements. In order to diagonalize the Hamiltonian a contact transformation up to 2^{nd} order is employed

$$\mathrm{e}^{i\lambda S}\hat{\mathrm{H}}\mathrm{e}^{-i\lambda S} = \hat{\mathrm{H}}' = \hat{\mathrm{H}}_0 + \lambda\hat{\mathrm{H}}_1^{'} + \lambda^2\hat{\mathrm{H}}_2^{'} \ . \tag{2.45}$$

The transformation function S is chosen such that $\hat{\mathrm{H}}_0 + \lambda\hat{\mathrm{H}}_1^{'}$ only has diagonal matrix elements yielding

$$\hat{\mathrm{H}}_1 = \mathrm{i}\left(\hat{\mathrm{H}}_0 S - S\hat{\mathrm{H}}_0\right) \tag{2.46}$$

and the exact form of S has been derived by Herman and Shaffer [195]. Finally, the contact transformed second order Hamiltonian is given by

$$\hat{\mathrm{H}}_2^{'} = \hat{\mathrm{H}}_2 + \left[iS, \hat{\mathrm{H}}_1^{''}\right]_{\mathrm{V}} + \left[iS, \hat{\mathrm{H}}_0\right]_{\mathrm{R}} , \tag{2.47}$$

where the indices V and R refer to vibrational and rotational contributions. Evaluating the matrix elements of $\hat{\mathrm{H}}'$ with respect to the harmonic eigenfunctions and collecting terms of like powers in the v_i, ℓ_t and J one arrives at the term formula for linear molecules:

$$T_v(J) = G_v + F_v(J) \ , \tag{2.48}$$

where G_v is the vibrational term energy

$$G_v = E_0 + \sum_i \omega_i \left(v_i + \frac{d_i}{2}\right) + \sum_{i\le j} x_{ij}\left(v_i + \frac{d_i}{2}\right)\left(v_j + \frac{d_j}{2}\right) + \sum_{t\le t'} x_{\ell_t\ell_{t'}}\ell_t\ell_{t'} \tag{2.49}$$

and $F_v(J)$ the rotational term energy

$$F_v(J) = B_v \left[J(J+1) - \ell^2\right] - D_\mathrm{e} \left[J(J+1) - \ell^2\right]^2 + H_\mathrm{e} \left[J(J+1) - \ell^2\right]^3 . \tag{2.50}$$

In Equation (2.49) ω_i are the harmonic vibrational frequencies, x_{ij} and $x_{\ell_t \ell_{t'}}$ are anharmonicity constants and d_i the degeneracy of i^{th} normal mode. Term E_0 is usually neglected in anharmonic calculations since it does not contribute to rovibrational transition frequencies but is important when absolute energies are of interest. B_v, D_e and H_e in Equation (2.50) are the rotational parameter, the equilibrium quartic and equilibrium sextic centrifugal distortion parameters, respectively. Although the latter parameter arises only in VPT4 it contains only contributions of second order importance.

Using the quartic expansion of the potential energy with respect to the dimensionless normal coordinates q_i given by Allen *et al.* [194]

$$V = \frac{1}{2} \sum_i \omega_i q_i^2 + \frac{1}{6} \sum_{ijk} \phi_{ijk} q_i q_j q_k + \frac{1}{24} \sum_{ijkl} \phi_{ijkl} q_i q_j q_k q_l \tag{2.51}$$

the spectroscopic parameters can be expressed with respect to the potential parameters and the equilibrium rotational constant B_e

$$B_\mathrm{e} = \frac{\hbar^2}{2hc\mathrm{I}_\mathrm{e}} . \tag{2.52}$$

In Equation (2.52) I_e is the the equilibrium moment of inertia

$$\mathrm{I}_\mathrm{e} = \sum_\mathrm{I} M_\mathrm{I} R^\mathrm{e}_{\mathrm{I}z} . \tag{2.53}$$

For the constant term in G_v one finds

$$\begin{aligned} E_0 = {} & \frac{1}{64} \sum_i \sigma_i \phi_{iiii} - \frac{7}{576} \sum_i \phi_{iii}^2 \frac{1}{\omega_i} + \frac{3}{64} \sum_{i \neq j} \sigma_i \phi_{iij}^2 \frac{\omega_j}{4\omega_i^2 - \omega_j^2} \\ & - \frac{1}{4} \sum_{i<j<k} d_j \phi_{ijk}^2 \frac{\omega_i \omega_j \omega_k}{\Delta_{ijk}} - B_\mathrm{e} \sum_{st} \zeta_{st}^2 , \end{aligned} \tag{2.54}$$

with a constant factor σ_i that is 1 for $i = s$ and 4/3 for $i = t$ and the usual degeneracy factor d_j for mode j. The denominator Δ_{ijk} is qiven below in Equation (2.59). It is important to note that the summations in Equation (2.54) run only over stretching indeces s and one component of the degenerate bending vibration t_y (using the definition of the ζ_{st} given in Equation (2.42)). The fourth term in Equation (2.54) vanishes for triatomic molecules. A similar formula has been given by Stanton and coworkers [196] for a general non-linear molecule in which case the factors σ_i and d_j do not appear in E_0. The Coriolis contribution (second to last term in eq. (26) of [196]) for non-linear molecules is written slightly different compared to the last term in Equation (2.54). However, when realizing that for linear molecules $B^x_\mathrm{e} = B^y_\mathrm{e} = B_\mathrm{e}$ ($B^z_\mathrm{e} = 0$) and the restrictions on

the ζ_{ij}^{α} introduced in Section 2.3.1 both formulations are found to yield the same result. The last term in Equation (26) of Ref. [196] is due to the so called Watson pseudo-potential term in the Hamiltonian [182] which vanishes for linear molecules.
The diagonal anharmonicity constants x_{ss}, x_{tt} and $x_{\ell_t\ell_t}$ are given by

$$x_{ss} = \frac{1}{16}\phi_{ssss} - \frac{1}{16}\sum_{s'}\phi_{sss'}^2\frac{8\omega_s^2 - 3\omega_{s'}^2}{\omega_{s'}(4\omega_s^2 - \omega_{s'}^2)} \ , \tag{2.55}$$

$$x_{tt} = \frac{1}{16}\phi_{tttt} - \frac{1}{16}\sum_{s}\phi_{stt}^2\frac{8\omega_t^2 - 3\omega_s^2}{\omega_s(4\omega_t^2 - \omega_s^2)} \tag{2.56}$$

and

$$x_{\ell_t\ell_t} = -\frac{1}{48}\phi_{tttt} - \frac{1}{16}\sum_{s}\phi_{stt}^2\frac{\omega_s}{4\omega_t^2 - \omega_s^2} \ . \tag{2.57}$$

The off-diagonal contribution $x_{ss'}$ is calculated according to

$$x_{ss'} = \frac{1}{4}\phi_{sss's'} - \frac{1}{4}\sum_{s''}\phi_{sss''}\phi_{s''s's'}\frac{1}{\omega_{s''}} - \frac{1}{2}\sum_{s''}\phi_{ss's''}^2\frac{\omega_{s''}(\omega_{s''}^2 - \omega_s^2 - \omega_{s'}^2)}{\Delta_{ss's''}} \ , \tag{2.58}$$

where the denominator Δ_{ijk} is defined as

$$\Delta_{ijk} = (\omega_i + \omega_j + \omega_k)(\omega_i + \omega_j - \omega_k)(\omega_i - \omega_j + \omega_k)(\omega_i - \omega_j - \omega_k). \tag{2.59}$$

Stretch-bend coupling through the anharmonicity constant x_{st} is obtained via

$$x_{st} = \frac{1}{4}\phi_{sstt} - \frac{1}{4}\sum_{s'}\phi_{sss'}\phi_{s'tt}\frac{1}{\omega_{s'}} - \frac{1}{2}\sum_{t'}\phi_{stt'}^2\frac{\omega_{t'}(\omega_{t'}^2 - \omega_s^2 - \omega_t^2)}{\Delta_{stt'}} + B_e\zeta_{st}^2\left(\frac{\omega_s}{\omega_t} + \frac{\omega_t}{\omega_s}\right). \tag{2.60}$$

For linear molecules with more than 3 atoms two additional types of anharmonicity constants contribute to G_v. The off-diagonal bend-bend coupling $x_{tt'}$ is given by

$$x_{tt'} = \frac{1}{4}\phi_{ttt't'}^{(+)} - \frac{1}{4}\sum_{s}\phi_{stt}\phi_{st't'}\frac{1}{\omega_{s'}} - \frac{1}{4}\sum_{s}\phi_{stt'}^2\frac{\omega_s(\omega_s^2 - \omega_t^2 - \omega_{t'}^2)}{\Delta_{stt'}}, \tag{2.61}$$

where the semi-diagonal force constant in $x_{tt'}$ is calculated from two force constant contributions $\phi_{ttt't'}^{(+)} = 1/2\left(\phi_{t_xt_xt'_xt'_x} + \phi_{t_xt_xt'_yt'_y}\right)$. Off-diagonal vibrational angular momentum anharmonicity can be calculated according to

$$x_{\ell_t\ell_{t'}} = \frac{1}{2}\sum_{s}\phi_{stt'}^2\frac{\omega_s\omega_t\omega_{t'}}{\Delta_{stt'}}. \tag{2.62}$$

The summations in all the formulae given above and in the following are unrestricted in the specified space of stretching s and bending t vibrations unless otherwise noted.
The anharmonic zero-point vibrational energy (ZPE) of a linear molecule up to 2^{nd} order in VPT

can be obtained by setting the $\{v_i, \ell_t\} = 0$ in Equation (2.49) and inserting the above formulae for E_0 and the anharmonicity constants. After sorting terms one obtains

$$\left.\begin{aligned} \mathrm{ZPE} = &\sum_i \omega_i \frac{d_i}{2} \\ &+ \frac{1}{32}\sum_{ij}\phi_{iijj} - \frac{1}{48}\sum_{ijk}\phi_{ijk}^2 \frac{1}{\omega_i+\omega_j+\omega_k} - \frac{1}{32}\sum_{ijk}\phi_{iik}\phi_{kjj}\frac{1}{\omega_k} \\ &+ \frac{1}{2}B_\mathrm{e}\sum_{st}\zeta_{st}^2\frac{(\omega_s-\omega_t)^2}{\omega_s\omega_t} \end{aligned}\right\} \begin{aligned} &\mathrm{ZPE_h} \\ &\mathrm{ZPE_a} \\ &\mathrm{ZPE_k}\ . \end{aligned} \qquad (2.63)$$

In Equation (2.63) $\mathrm{ZPE_h}$ is the harmonic ZPE, $\mathrm{ZPE_a}$ the VPT2 anharmonic contribution and $\mathrm{ZPE_k}$ the VPT2 kinetic (Coriolis) contribution. The summations in $\mathrm{ZPE_a}$ run over *all* $3N_\mathrm{at} - 5$ normal coordinates.

Formulae for the parameters entering the rotational term energy in Equation (2.50) are defined using the derivatives of the equilibrium moment of inertia $a_s = (\partial \mathrm{I_e}/\partial Q_s)_\mathrm{e}$ defined in Section 2.3.1 and the rotational derivatives

$$B_s = -\frac{\hbar^3}{2h^{3/2}c^{3/2}\omega_s^{1/2}}\frac{a_s}{\mathrm{I_e^2}}. \qquad (2.64)$$

Within VPT2 the rotational constant in a vibrational state v is calculated according to

$$B_v = B_\mathrm{e} - \sum_i \alpha_i \left(v_i + \frac{d_i}{2}\right) , \qquad (2.65)$$

where α_i are the vibration-rotatioan interaction constants. The latter are given by

$$\alpha_s = -\frac{2B_\mathrm{e}^2}{\omega_s}\left[\frac{3a_s^2}{4I_\mathrm{e}} + \sum_t \zeta_{st}^2\frac{3\omega_s^2+\omega_t^2}{\omega_s^2-\omega_t^2} + \pi\sqrt{\frac{c}{h}}\sum_s \phi_{sss'}a_{s'}\frac{\omega_s}{\omega_{s'}^{3/2}}\right] \qquad (2.66)$$

and

$$\alpha_t = -\frac{2B_\mathrm{e}^2}{\omega_t}\left[\frac{1}{2}\sum_s \zeta_{st}^2\frac{3\omega_t^2+\omega_s^2}{\omega_t^2-\omega_s^2} + \pi\sqrt{\frac{c}{h}}\sum_s \phi_{stt}a_s\frac{\omega_t}{\omega_s^{3/2}}\right] \ . \qquad (2.67)$$

Following Herzberg [197], the three terms in α_s can be characterized as a harmonic, a Coriolis and an anharmonic contribution, respectively. The bending vibration-rotation interaction constants α_t contain only Coriolis and anharmonic contributions. Centrifugal distortion constants D_e, H_e and terms of higher order have been worked out by Aliev and Watson [187]. According to these authors D_e is given by

$$D_\mathrm{e} = \frac{1}{2}\sum_s \frac{B_s^2}{\omega_s} \ , \qquad (2.68)$$

and the VPT4 formula for the sextic centrifugal distortion constant is

$$H_{\mathrm{e}} = \frac{4D_{\mathrm{e}}^2}{B_{\mathrm{e}}} - 2B_{\mathrm{e}}^2 \sum_s \frac{B_s^2}{\omega_s^3} - \frac{1}{6} \sum_{ss's''} \phi_{ss's''} \frac{B_s B_{s'} B_{s''}}{\omega_s \omega_{s'} \omega_{s''}} \,, \tag{2.69}$$

where only totally symmetric normal modes contribute. Close inspection of these equations show that the perturbational treatment of quartic and sextic centrifugal effects only accounts for the influence of stretching vibrations. In fact, the effect of bending normal modes on these parameters can be rather drastic and such effects will be discussed in more detail in the following chapters. The effect of ℓ-type doubling caused by the coupling of the degenerate bending and the stretching vibrations through the Coriolis operator is represented by parameters q_t in VPT2 [198]. Following the work of Watson [199] the splitting of the e/f-parity [200] states in the fundamental bending states is given by $q_t J(J+1)$ and

$$q_t \approx q_t^{\mathrm{e}} + q_t^J J(J+1) \,. \tag{2.70}$$

The equilibrium ℓ-type doubling parameter q_t^{e} is given by

$$q_t^{\mathrm{e}} = -\frac{2B_{\mathrm{e}}^2}{\omega_t} \sum_s \zeta_{st}^2 \frac{3\omega_t^2 + \omega_s^2}{\omega_t^2 - \omega_s^2} \tag{2.71}$$

and is on the order of a vibration-rotation interaction constant α_i. Centrifugal distortion results in the l-type doubling parameter termed q_t^J which upon introducing $C_s = -B_s/\omega_s$ can be calculated as

$$\begin{aligned} q_t^J = &- \frac{4D_{\mathrm{e}} q_t^{\mathrm{e}}}{B_{\mathrm{e}}} + \frac{2B_{\mathrm{e}}^4}{\omega_t^3} + \frac{B_{\mathrm{e}}^2(2\alpha_t - q_t^{\mathrm{e}})}{\omega_t^2} - 4B_{\mathrm{e}}^2(2\alpha_t + q_t^{\mathrm{e}}) \sum_s \zeta_{st}^2 \frac{\omega_s^2 + \omega_t^2}{(\omega_s^2 - \omega_t^2)^2} \\ &- 12B_{\mathrm{e}}\omega_t \left(\sum_s C_s \zeta_{st} \frac{\omega_s^{3/2}}{\omega_s^2 - \omega_t^2} \right)^2 - 8B_{\mathrm{e}}\omega_t \left(\sum_s C_s \zeta_{st} \frac{\omega_s^{3/2}}{\omega_s^2 - \omega_t^2} \right) \left(\sum_{s'} C_{s'} \zeta_{s't} \frac{1}{\omega_{s'}^{1/2}} \right) \\ &- 8B_{\mathrm{e}}^2 \omega_t \sum_{ss's''} C_s \phi_{ss's''} \zeta_{s't} \zeta_{s''t} \frac{(\omega_{s'}\omega_{s''})^{1/2}}{(\omega_{s'}^2 - \omega_t^2)(\omega_{s''}^2 - \omega_t^2)} - 32B_{\mathrm{e}}^4 \omega_t \sum_{t' \neq t} \left(\frac{3\omega_t^2 + \omega_{t'}^2}{\omega_t^2 - \omega_{t'}^2} \right) \\ &\times \left(\sum_s \zeta_{st} \zeta_{st'} \frac{1}{\omega_s^2 - \omega_t^2} \right)^2 - 16B_{\mathrm{e}}^2 \sum_{t' \neq t} \left(\frac{(\omega_t^3 \omega_{t'})^{1/2}}{\omega_t^2 - \omega_{t'}^2} \right) \left(\sum_s \zeta_{st} \zeta_{st'} \frac{1}{\omega_s^2 - \omega_t^2} \right) \left(\sum_{s'} C_{s'} \phi_{s'tt'} \right) . \end{aligned} \tag{2.72}$$

For linear molecules with at least two bending vibrations the effect of vibrational ℓ-type doubling has to be considered. Vibrational states where two bending vibrations are excited $(v_t^{\ell_t}, v_{t'}^{\ell_{t'}}) = (1^{\pm 1}, 1^{\pm 1})$ can be classified according to the sum $\ell = \sum_t \ell_t$ and the symmetry species: two Δ states with $\ell = \pm 2$ which will be further split by rotational ℓ-type resonance and two Σ states with $\ell = 0$ which are degenerate when neglecting vibrational ℓ-type doubling. The latter will cause a

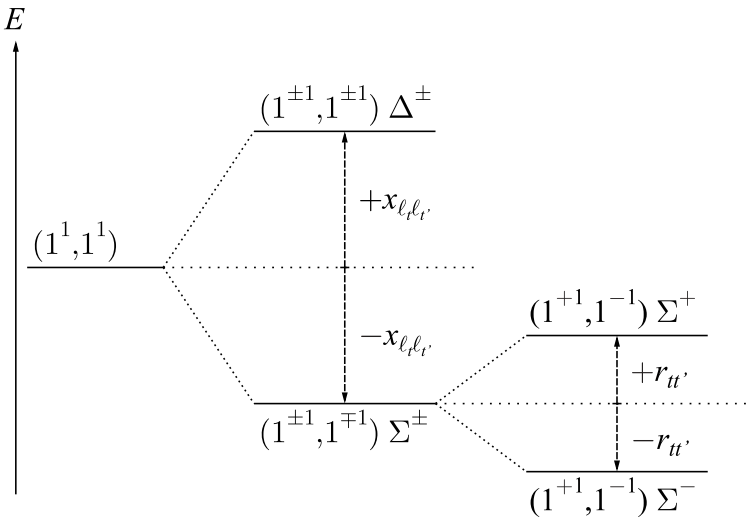

Figure 2.2: Influence of vibrational anharmonicity on bend-bend combination states according to 2^{nd} order vibrational perturbation theory. The scheme assumes positive values for the anharmonicity constants $x_{\ell_t\ell_{t'}}$ and $r_{tt'}$.

splitting of the Σ^+ and Σ^- states proportional to

$$r^{\text{e}}_{tt'} = \frac{1}{2}\phi^{(-)}_{ttt't'} - \frac{1}{2}\sum_s \phi^2_{stt'}\frac{\omega_s(\omega_s^2-\omega_t^2-\omega_{t'}^2)}{\Delta_{stt'}}\,. \tag{2.73}$$

In Equation (2.73) the off-diagonal quartic coupling force constant is calculated according to $\phi^{(-)}_{ttt't'} = 1/2\left(\phi_{t_xt_xt'_xt'_x} - \phi_{t_xt_xt'_yt'_y}\right)$. As an example Figure 2.2 depicts the energetic relationships for a $(1^{\pm1},1^{\pm1})$ vibrational state.

VPT2 and perturbation theory in general is prone to failure in cases where 0^{th} order vibrational states are energetically close to each other. There are 2 types of such so called *Fermi-resonances* in VPT2 which occur if the following conditions are fulfilled:

$$\text{Type-I:} \qquad \omega_i \approx 2\omega_j \qquad \text{and} \qquad \phi_{ijj} \neq 0 \qquad , \tag{2.74}$$

$$\text{Type-II:} \qquad \omega_i \approx \omega_j + \omega_k \qquad \text{and} \qquad \phi_{ijk} \neq 0 \qquad . \tag{2.75}$$

As a consequence of these accidental degeneracies the *resonance denominators* in the anharmonicity constants that involve harmonic vibrational frequency differences of the resonant modes become very large leading to unphysical values of the x_{ij}. The origin of these resonance denominators is the transformation function S and in order to remove these a modification of the latter to a new function S^* is required [185]. This leads to so called *deperturbed* parameters which are commonly marked with an asterisk. The first order transformed Hamiltonian $\hat{\text{H}}'_1$ then has off-diagonal matrix elements due to the use of the S^* function and to obtain the VPT2 term energies

Table 2.1: Quantum number dependence and spectroscopic parameters for linear molecules derived from diagonal matrix elements of the twice contact transformed rovibrational Hamiltonian up to 4^{th} order (VPT4).[a]

Term	Dependence	$\hat{\mathrm{h}}_0^\dagger$	$\hat{\mathrm{h}}_2^\dagger$	$\hat{\mathrm{h}}_3^\dagger$	$\hat{\mathrm{h}}_4^\dagger$
G_v	$\left(v_i+\frac{d_i}{2}\right)$	ω_i	–	–	$\Delta\omega_i$
	$\left(v_i+\frac{d_i}{2}\right)\left(v_j+\frac{d_j}{2}\right)$	–	x_{ij}	–	–
	$\ell_t\ell_{t'}$	–	$x_{\ell_t\ell_{t'}}$	–	–
	$\left(v_i+\frac{d_i}{2}\right)\left(v_j+\frac{d_j}{2}\right)\left(v_k+\frac{d_k}{2}\right)$	–	–	–	y_{ijk}
	$\left(v_i+\frac{d_i}{2}\right)\ell_t\ell_{t'}$	–	–	$y^{(3)}_{s\ell_t\ell_{t'}}$	$y^{(4)}_{s\ell_t\ell_{t'}}+y_{t\ell_t\ell_{t'}}$
B_v	$\left[J(J+1)-\ell^2\right]$	B_e	–	–	ΔB_e
	$\left[J(J+1)-\ell^2\right]\left(v_i+\frac{d_i}{2}\right)$	–	α_i	–	$\Delta\alpha_i$
	$\left[J(J+1)-\ell^2\right]\left(v_i+\frac{d_i}{2}\right)\left(v_i+\frac{d_i}{2}\right)$	–	–	–	γ_{ij}
	$\left[J(J+1)-\ell^2\right]\ell_t\ell_{t'}$	–	–	–	$\gamma_{\ell_t\ell_{t'}}$
D_v	$\left[J(J+1)-\ell^2\right]^2$	–	D_e	–	ΔD_e
	$\left[J(J+1)-\ell^2\right]^2\left(v_i+\frac{d_i}{2}\right)$	–	–	–	β_i
H_v	$\left[J(J+1)-\ell^2\right]^3$	–	–	–	H_e

[a] Diagonal matrix elements of VPT2 are obtained by neglecting $\hat{\mathrm{h}}_3^\dagger+\hat{\mathrm{h}}_4^\dagger$

matrix representations for interacting states with the new $\hat{\mathrm{H}}'$ have to be diagonalized.
As an example related to this thesis, the following will outline the treatment required for l-C_3H^+ where a resonance between the fundamental stretching vibration ν_1 (i) and the stretch-stretch combination band $\nu_2+\nu_3$ (j & k) occurs (cf. Chapter 5). For this Type-I Fermi-resonance the anharmonicity constants x_{ij}, x_{ik} and x_{jk} are affected. The deperturbation of the latter can be formulated with respect to the perturbed values $x_{ss'}$ according to

$$x^*_{ss'} = x_{ss'} \pm \frac{1}{8}\frac{\phi^2_{ijk}}{\omega_i-\omega_j-\omega_k} \qquad \{s,s'\}=\{i,j,k\}\,. \tag{2.76}$$

In Equation (2.76) the positive sign refers to the case $(s,s')=(j,k)$ and the negative sign to the other two cases. The constant factor E_0 is also affected by resonances and in this particular example the deperturbation is achieved by

$$E^*_0 = E_0 + \frac{1}{32}\frac{\phi^2_{ijk}}{\omega_i-\omega_j-\omega_k}\,. \tag{2.77}$$

The deperturbation of E^*_0 ensures that absolute term energies for states not involved in resonances are unchanged by the unitary transformation from S to S^*. The off-diagonal matrix element of

the operator $\hat{\mathrm{H}}_1^{'} = \phi_{ijk} q_i q_j q_k$ is given by

$$\left\langle v_i, v_j, v_k \left| \hat{\mathrm{H}}_1^{'} \right| v_i \pm 1, v_j \mp 1, v_k \mp 1 \right\rangle = \frac{1}{\sqrt{8}} \phi_{ijk} \,. \tag{2.78}$$

For the so called dyad $\nu_i // \nu_j + \nu_k$ the effective Hamiltonian to be diagonalized corresponds to the 2×2 matrix

$$\mathbf{H}_{\mathrm{F-I}} = \begin{pmatrix} G_i^* & \frac{1}{\sqrt{8}} \phi_{ijk} \\ \frac{1}{\sqrt{8}} \phi_{ijk} & G_{j+k}^* \end{pmatrix} , \tag{2.79}$$

where G_v^* are the vibrational term energies of the interacting states evaluated using the deperturbed spectroscopic parameters.

The presented formulae comprise the 2^{nd} order contribution to the rovibrational energy. This approach however is only valid up to a certain degree of excitation in the v_i and J. This has been discussed in some detail by Aliev & Watson [187] and Amat, Nielsen and Tarrago [185]. Extending the treatment up to the full 4^{th} order requires a much greater computational effort, since a second contact transformation is required. The complete fourth order twice contact transformed Hamiltonian has been obtained by Amat, Nielsen and Tarrago [185] and the diagonal matrix elements with their dependence on the linear molecule quantum numbers as given by the latter authors are summarized in Table 2.1. An important conclusion to be drawn from Table 2.1 is that an analysis of rovibrational spectra based on VPT4 will yield harmonic frequencies $\omega_i' = \omega_i + \Delta\omega_i$ and an equilibrium rotational constant $B_{\mathrm{e}}' = B_{\mathrm{e}} + \Delta B_{\mathrm{e}}$ which are different from the respective parameter obtained from the harmonic potential and the equilibrium geometry.

2.3.3 Variational rovibrational calculations

The basic idea of variational rovibrational calculations is to expand the unknown eigenfunctions of the nuclear Hamiltonian $|\Psi_{\mathrm{VR}}\rangle$ as a linear combination of a suitable set of basis functions $\left\{ \left| \phi_i^{(J)} \right\rangle \right\}$. Since the total angular momentum quantum number J is strictly conserved the eigenfunctions for each value of J can be determined individually (cf. also Section 4.1.4). The approximate wave function $\left|\psi_v^J\right\rangle$ for rovibrational state (v, J) is then

$$\left| \psi_v^{(J)} \right\rangle = \sum_i c_i^{(v,J)} \left| \phi_i^{(J)} \right\rangle \,. \tag{2.80}$$

In general rovibrational basis functions for linear molecule are formulated as a product of a vibrational and a rotational basis function $\left| \phi_i^{(J)} \right\rangle = |\phi_{\mathbf{v}_i}\rangle \left| \phi_{\mathrm{R}}^{Jkm} \right\rangle$ depending on a set of vibrational quantum numbers $\{v_k\}$ and vibrational angular momentum quantum numbers $\{\ell_t\}$ summarized in the vector $\mathbf{v}_i$ as well as the rigid rotor (RR) quantum numbers J, k and m (for further details on rovibrational basis functions cf. Section 4.1.1). The product basis functions, when employing

e.g. harmonic oscillator vibrational functions, form an orthonormal system of functions

$$\left\langle \phi_i^{(J)} \,\middle|\, \phi_j^{(J)} \right\rangle = \left\langle \phi_{\mathbf{v}_i} \,\middle|\, \phi_{\mathbf{v}_j} \right\rangle \left\langle \phi_{\mathrm{R}}^{Jkm} \,\middle|\, \phi_{\mathrm{R}}^{Jkm} \right\rangle = \delta_{ij} \,. \tag{2.81}$$

The coefficients $c_i^{(v,J)}$ are determined by minimizing the expectation value of the nuclear Hamiltonian $\hat{\mathrm{H}}_{\mathrm{N}}$ with the approximate wave function

$$\left\langle \hat{\mathrm{H}}_{\mathrm{N}} \right\rangle_{v,J} = \left\langle \psi_v^{(J)} \,\middle|\, \hat{\mathrm{H}}_{\mathrm{N}} \,\middle|\, \psi_v^{(J)} \right\rangle = \sum_{ij} c_i^{(v,J)} c_j^{(v,J)} \underbrace{\left\langle \phi_i^{(J)} \,\middle|\, \hat{\mathrm{H}}_{\mathrm{N}} \,\middle|\, \phi_j^{(J)} \right\rangle}_{\mathrm{H}_{ij}^{(J)}} , \tag{2.82}$$

where the shorthand notation for matrix elements of the nuclear Hamiltonian in the chosen basis $H_{ij}^{(J)}$ is introduced. The eigenfunctions $\left|\psi_v^{(J)}\right\rangle$ are required to be orthonormal

$$\begin{aligned} \left\langle \psi_v^{(J)} \,\middle|\, \psi_{v'}^{(J)} \right\rangle &= \sum_{ij} c_i^{(v,J)} c_j^{(v',J)} \left\langle \phi_i^{(J)} \,\middle|\, \phi_j^{(J)} \right\rangle \\ &= \sum_{ij} c_i^{(v,J)} c_j^{(v',J)} \delta_{ij} = \sum_i c_i^{(v,J)} c_i^{(v',J)} = \delta_{vv'} \,. \end{aligned} \tag{2.83}$$

In order to obtain energy optimized wave functions $\left|\psi_v^{(J)}\right\rangle$ and simultaneously keeping the wave function orthonormal with respect to all eigenfunctions of the Hamiltonian, Lagrange multiplier $\lambda_v^{(J)}$ for each rovibrational state are introduced. The Lagrangian for state (v, J) is then given by

$$\mathcal{L}(\{c_k^{(v,J)}\}, \lambda_v^{(J)}) = \sum_{ij} c_i^{(v,J)} c_j^{(v,J)} \mathrm{H}_{ij}^{(J)} - \sum_{v'} \sum_i \lambda_{v'}^{(J)} (c_i^{(v,J)} c_i^{(v',J)} - \delta_{vv'}) \,. \tag{2.84}$$

The necessary conditions for the coefficients are

$$\frac{\partial \mathcal{L}}{\partial c_k^{(v,J)}} = 0 \quad \forall \quad k \,. \tag{2.85}$$

Carrying out the differentiation yields

$$\begin{aligned} \frac{\partial \mathcal{L}}{\partial c_k^{(v,J)}} = 0 &= \sum_{i \neq k} c_i^{(v,J)} \mathrm{H}_{ik}^{(J)} + \sum_{j \neq k} c_j^{(v,J)} \mathrm{H}_{kj}^{(J)} + 2 c_k^{(v,J)} \mathrm{H}_{kk}^{(J)} - 2 \sum_{i \neq k} c_i^{(v,J)} \lambda_v^{(J)} - 2 c_k^{(v,J)} \lambda_v^{(J)} \\ &= \sum_j \mathrm{H}_{kj}^{(J)} c_j^{(v,J)} - \sum_j c_j^{(v,J)} \lambda_v^{(J)} \,, \end{aligned} \tag{2.86}$$

where the hermitian property of the Hamiltonian $\mathrm{H}_{ij}^{(J)} = \mathrm{H}_{ji}^{(J)}$ is used. One thus arrives at a set of k linear equations

$$\sum_j \left[\mathrm{H}_{kj}^{(J)} - \lambda_v^{(J)} \right] c_j^{(v,J)} = 0 \,, \tag{2.87}$$

which when written in matrix-vector form reads

$$\mathbf{H}^{(J)}\mathbf{c}^{(v,J)} = \mathbf{c}^{(v,J)}\lambda_v^{(J)} \tag{2.88}$$

and constitutes an eigenvalue equation of the hermitian matrix $\mathbf{H}^{(J)}$ with eigenvector $\mathbf{c}^{(v,J)}$ and eigenvalue $\lambda_v^{(J)}$. The Lagrange multiplier thus is the (approximate) rovibrational term energy for state (v, J). Formulating the Lagrangian Equation (2.84) for each vibrational state, collecting the resulting eigenvectors in a matrix $\mathbf{X}^{(J)}$ such that they are the columns of this matrix $\left(\mathbf{X}^{(J)}\right)_{iv} = \mathbf{c}_i^{(v,J)}$ and the eigenvalues in the diagonal matrix $(\mathbf{\Lambda}^{(J)})_{vv'} = \lambda_v^{(J)}\delta_{vv'}$ the final form of the variational formulation is obtained

$$\mathbf{H}^{(J)}\mathbf{X}^{(J)} = \mathbf{X}^{(J)}\mathbf{\Lambda}^{(J)}\,. \tag{2.89}$$

The solution of the rovibrational problem thus reduces to finding the matrix $\mathbf{X}^{(J)}$ which diagonalizes $\mathbf{H}^{(J)}$.

The introduced basis set $\left\{\left|\phi_v^{(J)}\right\rangle\right\}$ forms a complete set which is unpractical in a numerical calculation. Therefore, the set is truncated at a certain number $N_{\mathrm{VR}}^{(J)}$ of rovibrational basis functions. By monitoring the convergence of the $\lambda_v^{(J)}$ with respect to $N_{\mathrm{VR}}^{(J)}$ one obtains upper bounds to the rovibrational term energies $T_v(J)$ (Hylleraas-Undheim-MacDonald theorem [201, 202]). This approach is also commonly referred to as *finite basis set representation* (FBR). The details of variational rovibrational calculations depends on the form of $\hat{\mathrm{H}}_{\mathrm{N}}$ and the basis functions. Over the years different formulations of variational rovibrational calculations have been presented for linear molecules of which some will be shortly reviewed in the following.

For general (bent and linear) triatomic molecules Carter and Handy introduced the Rvib3 program based on a Hamiltonian formulated in internal coordinates [203, 204]. The wave function is expanded in harmonic oscillator (HO) or Morse-oscillator functions for stretching coordinates, Legendre polynomials for the bond angle coordinate and RR functions for the the rotational motion. A similar programm called Triatom was introduced by Tennyson *et al.* [205–208] based on a Hamiltonian formulated in Jacobi coordinates [205]. For a triatomic molecule A-B-C the latter can be defined as the vector $\mathbf{r}_{\mathrm{BC}}$ between atom B and C, the vector $\mathbf{R}_{\text{A-BC}}$ between the atom A and the CoM of the BC subsystem and the angle θ between these two vectors. The basis functions are are constructed from Morse-oscillator or spherical oscillator functions for radial degrees of freedom, Legendre polynomials for the bending angle and RR functions. Following the pioneering work by Whitehead and Handy [209] Sebald [210] developed a variational program for rovibrational energies and wave functions of triatomic linear molecules based on the Watson Hamiltonian (C8vpro). The Hamiltonian is diagonalized in a (symmetrized) basis of products of 1D (stretch) and 2D (bending) HO basis functions for vibrational degrees of freedom as well as rigid rotor functions.

Bramley and Handy [211] developed the Vista program, a variational approach which is based on a KEO for sequentially bonded tetra-atomic molecules expressed in internal coordinates and product basis functions of HO stretching basis functions, Legendre polynomials for the two bond

angle coordinates, Fourier components $e^{i\omega\phi}$ for the torsion and rigid rotor functions. The method was later extended by the former authors in collaboration with Stuart Carter [212] resulting in the RVIB4 program, that additionally allows for least squares refinement of potential energy surfaces based on experimental results. The most recent FBR variational method developed for tetraatomic linear molecules [213] is bases on the *Theoretical ROVibrational Energies* (TROVE) approach by Yurchenko, Thiel and Jensen [214]. The key feature of TROVE is a numerical representation of the KEO in terms of internal coordinates which requires no analytic pre-derivation of the Hamiltonian. While TROVE is generally applicable to any molecule, extensive symmetrisation of the primitive rovibrational (1D HO and RR) basis is required for calculating rovibrational eigenenergies [213, 215, 216].

Besides the FBR approach, discrete variable representation (DVR) methods [217–221] have become quite successful for rovibrational calculations. In DVR the representation of the basis functions is changed from the spectral form $\{\phi_i^{\mathrm{FBR}}\} = \{|\phi_i\rangle\}$ of FBR to a point-wise discrete form $\{\phi_\alpha^{\mathrm{DVR}}\} = \{\frac{1}{\sqrt{N_\alpha}}\phi_i(x_\alpha)\}$. Both approaches are related since on the one hand the DVR grid points x_α in a certain vibrational degree of freedom q are chosen as zeros of a suitable orthogonal polynomial $p_n(q)$ and on the other hand the $|\phi_i\rangle$ can be expressed as the product of that same polynomial and a suitable weight function $W(q)$. A very general approach has been worked out by Mladenović [222–224]. Employing an internal coordinate Hamiltonian [225–227], a combination of DVR with a FBR solution for certain degrees of freedom is used to solve the eigenvalue problem. Tennyson and coworkers [228] developed the Wide Amplitude Vibration-Rotation 4-atomic (WAVR4) method, which is also capable of treating tetraatomic linear molecules [229, 230] using a Hamiltonian based on polyspherical coordinates [225]. A DVR approach to calculate vibrational term energies based on the Watson Hamiltonian for both linear and non-linear molecules (called DEWE) was introduced by the group of Császár [231]. The DVR grids are constructed from 1D HO functions for *all* $3N_{\mathrm{at}} - 5$ vibrational coordinates in case of linear molecules. The approach thus does not take full account of the degeneracy of the bending vibrations and the Sayvetz condition (cf. Equation (2.43)) is not fulfilled. This results in unphysical $k \neq 0$ states which are obtained from a $J = 0$ calculation.

2.3.4 Calculation of spectroscopic parameters and rovibrational intensities

The rovibrational spectra of linear molecules consist of *bands* corresponding to transitions between different vibrational states. *Fundamental* transitions ν_i originating from from the vibrational ground state have singly excited final states with $\Delta v_i = 1$. *Overtones* $n\nu_i$ are bands with $\Delta v_i \geq 2$ and *combination bands* $\nu_i + \nu_j$ occur when more than one vibrational mode is excited. Rovibrational transitions between excited vibrational states are usually referred to as *hot band* transition (e.g. $\nu_i + \nu_j - \nu_j$). The individual bands show a rotational fine structure with so called P-, R- and Q-branches according to the rotational selection rules $\Delta J = -1, +1$ and 0, respectively. Furthermore,

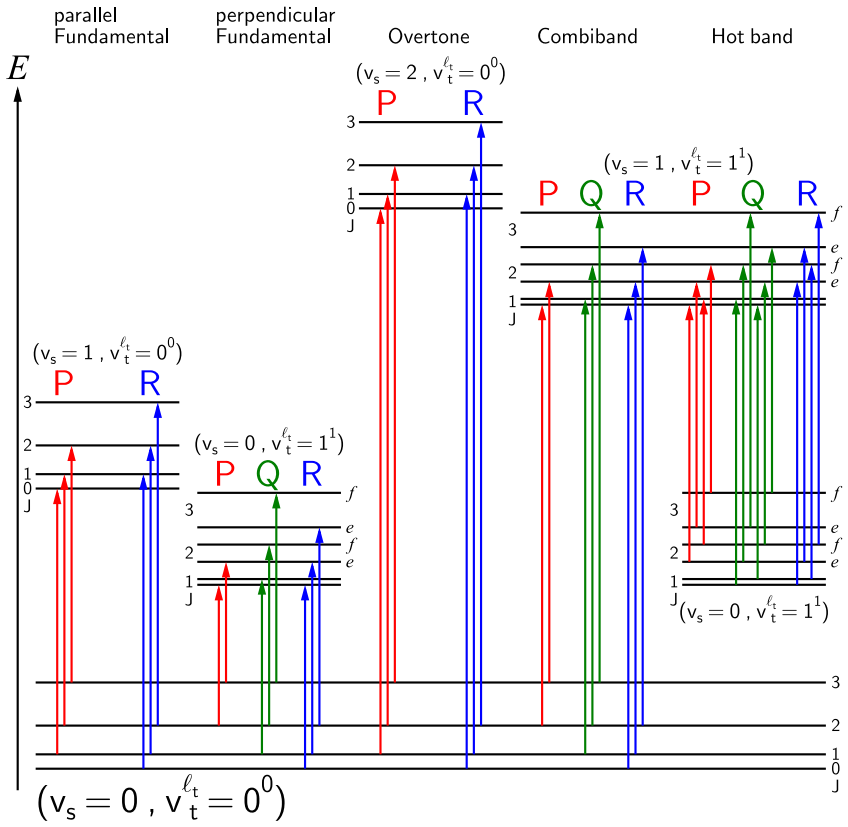

Figure 2.3: Schematical representation of various types of rovibrational transitions and the associated selection rules observed for linear molecules. Effects due to ℓ-type doubling are greatly exaggerated for clarity.

the selection rules for parity components of the involved states are for P- and R-branches $e \leftrightarrow e$ and $f \leftrightarrow f$. Q-branches with $\Delta J = 0$ occur for *perpendicular* bands that involve a change in K between initial and final state (angular momentum conservation) and follow the parity selection rule $e \leftarrow f$. Weak Q-branches due to Coriolis coupling can also occur for $\Delta K = 0$ bands in case of hot bands involving $K \neq 0$ states. A summary of rovibrational transitions in linear molecules is depicted in Figure 2.3.

The line frequencies are the differences of the rovibrational term energy in the upper state (v', J') and the lower state (v'', J'')

$$\nu = T_{v'}(J') - T_{v''}(J'') \,. \tag{2.90}$$

The experimental analysis of rovibrational spectra generally proceeds via assuming the expansion of $T_v(J)$ according to VPT (cf. Section 2.3.2) yielding

$$T_v(J) = G_v + B_v \left[J(J+1) - \ell^2\right] - D_v \left[J(J+1) - \ell^2\right]^2 + H_v \left[J(J+1) - \ell^2\right]^3 + \ldots \tag{2.91}$$

Spectroscopic parameters G_v, B_v, D_v, ... are then determined by least-squares fitting of the observed line frequencies. In case observed bands share an initial or final state these are usually fitted simultaneously.
For bands that involve only $K = 0$ states the presented procedure is rather straightforward. The analysis of $K \neq 0$ states is more involved and is performed by setting up effective Hamiltonian matrices for the involved states to describe the effects of rovibrational ℓ-type doubling and resonance. Following the work of Papoušek and Aliev [186] the diagonal matrix elements are given by

$$\left\langle v, J, K \left| \hat{\mathrm{H}}_{\mathrm{eff}} \right| v, J, K \right\rangle = G_v + B_v \left[J(J+1) - K^2\right] - D_v \left[J(J+1) - K^2\right]^2 + H_v \left[J(J+1) - K^2\right]^3 + \ldots \tag{2.92}$$

and off-diagonal matrix elements by

$$\begin{aligned}\left\langle v_t^{\ell_t}, J, K \left| \hat{\mathrm{H}}_{\mathrm{eff}} \right| v_t^{\ell_t \pm 2}, J, K \pm 2 \right\rangle = \frac{1}{4} &\left[q_v + q_v^J J(J+1) + q_v^{JJ} J^2 (J+1)^2 + \ldots\right] \\ &\times \left\{ \left[(v_t^2+1)^2 - (\ell_t \pm 1)^2\right] \left[J(J+1) - K(K \pm 1)\right] \right. \\ &\left. \times \left[J(J+1) - (K \pm 1)(K \pm 2)\right] \right\}^{1/2} .\end{aligned} \tag{2.93}$$

The determination of the parameters of such effective Hamiltonians then involves diagonalization of $\mathbf{H}_{\mathrm{eff}}$ and least-squares fitting.
The outlined techniques for determining rovibrational parameters rely on the validity of the perturbational expansions presented in Section 2.3.2. In case the requirements of VPT of any order are not fulfilled for a certain molecule, discrepancies in spectroscopic parameters determined from experiment and by theoretical methods will arise. These errors will persist even for highly accurate variational rovibrational calculations employing composite potential energy surfaces that provide the line frequencies ν of rovibrational transitions with an accuracy of 1 cm^{-1} or better. Examples for such deviations from the usual behaviour will be presented in Section 3.2 and Section 5.2.
The intensity of a rovibrational transition between initial state i and final state f is given by

$$\begin{aligned} A_{if} &= \frac{1}{p \cdot l} \int \ln \frac{I_0}{I} \mathrm{d}\nu \\ &= \frac{8\pi^3 \nu_{if} g}{3hcZRT} \left[1 - \exp\left(-\frac{\nu_{if}}{k_{\mathrm{B}} T}\right)\right] \exp\left(-\frac{E_i}{k_{\mathrm{B}} T}\right) \mu_{if}^2 \ , \end{aligned} \tag{2.94}$$

where the integration of the absorption coefficient $k(\nu) = \ln(I_0/I)$ is performed over the entire absorption line. In Equation (2.94) p is the partial pressure of the absorbing species and l the optical pathlength of the absorption cell. The frequency of the transition is given by ν_{if} and the energy of the lower state by E_i. Z designates the total internal partition sum at the temperature T and g is the statistical weight factor that accounts for nuclear spin statistics and isotopic abundance. Natural constants occuring in Equation (2.94), whose values are taken from [232], are Planck's constant h, the speed of light in vacuum c, the universal gas constant R and Boltzmann's constant

k_{B}.
Within the dipole approximation the squared transition dipole moment μ_{if}^2 is defined as (see e.g. [233] for a derivation)

$$\mu_{if}^2 = |\langle \Psi_{\mathrm{VR}i} | \mu(\mathbf{R}) | \Psi_{\mathrm{VR}f} \rangle|^2 \,, \tag{2.95}$$

where $|\Psi_{\mathrm{VR}i}\rangle$ and $|\Psi_{\mathrm{VR}f}\rangle$ are the rovibrational wave functions of the initial and final state, respectively and $\mu(\mathbf{R})$ is the electric dipole moment function (EDMF) with respect to the SF-coordinate system (X, Y, Z) (cf. the definition of the Euler angles in Section 2.3.1). In the absence of an external field each rotational level is $2J+1$ times degenerate and (2.95) can be rewritten:

$$\mu_{if}^2 = 3 \sum_m \sum_{m'} \left| \left\langle \Psi_{\mathrm{VR}i}^{(Jm)} \,\middle|\, \mu_Z(\mathbf{R}) \,\middle|\, \Psi_{\mathrm{VR}f}^{(J'm')} \right\rangle \right|^2 , \tag{2.96}$$

where the explicit m dependence of the rovibrational wave function is recovered. The components of the dipole moment in the MF-axes system μ_α $(\alpha = x, y, z)$ can be written as the elements of a first rank spherical tensor [186]

$$\mu(1,1) = -\frac{1}{\sqrt{2}} \left(\mu_x + \mathrm{i}\mu_y\right) \,, \tag{2.97}$$

$$\mu(1,0) = \mu_z \,, \tag{2.98}$$

$$\mu(1,-1) = \frac{1}{\sqrt{2}} \left(\mu_x - \mathrm{i}\mu_y\right) \,. \tag{2.99}$$

A short sketch of the subsequent steps will then be as follows: first the relation between the SF dipole moment μ_Z and the MF dipole moment components in tensor formulation $\mu(1,\mathrm{q})$ $(\mathrm{q} = \{-1,0,1\})$ are established through rotation matrices $\mathrm{D}_{mk}^J(\phi,\theta,\chi')$ [234] and the Eckart conditions that define the (x,y,z) MF coordinate system. Then, the (symmetrized) variational expansion is inserted (cf. (4.85)). The resulting multiple sum over vibrational basis functions and K in the initial and final state then involves two types of integrals:

- integrals of the tensor components $\mu(1,\mathrm{q})$ over vibrational basis functions

$$\left\langle \phi_{\mathbf{v}_j} \,\middle|\, \mu(1,\mathrm{q}) \,\middle|\, \phi_{\mathbf{v}_j} \right\rangle$$

- integrals over rotational basis functions and the rotation matrices D_{mk}^J

$$\left\langle \phi_{\mathrm{R}}^{Jkm} \,\middle|\, D_{0\mathrm{q}}^1 \,\middle|\, \phi_{\mathrm{R}}^{J'k'm'} \right\rangle$$

The latter can be evaluated via the 3j-symbols [234] for RR rotational basis functions and will fix the selection rules $\Delta J = 0, \pm 1$. Furthermore, only those 3j-symbols for which $k - k' = \mathrm{q}$ are non-zero and thus only matrix elements $\left\langle \phi_{\mathbf{v}_j} \,\middle|\, \mu(1,\mathrm{q}) \,\middle|\, \phi_{\mathbf{v}_j} \right\rangle$ with $\Delta k = 0, \pm 1$ need to be calculated. This approach has been implemented for triatomic molecules into the C8VPRO program [210] and

will be used for intensity calculations.
The squared dipole transition dipole moments can be approximated according to

$$\mu_{if}^2 \approx \mu_v^2 F_{\mathrm{HL}} F_{\mathrm{HW}} \,, \tag{2.100}$$

where μ_v is the vibrational transition dipole moment, F_{HL} the rotational contribution to the intensity known as Hönl-London factor [235, 236] and F_{HW} the Herman-Wallis factor [237] which is due to rovibrational coupling. Following the work of Watson [238] the latter can be expanded as

$$F_{\mathrm{HW}}^{\mathrm{PR}} = \left[1 + A_1 m + A_2^{\mathrm{PR}} m^2\right]^2 \tag{2.101}$$

for P- and R-branch transitions and

$$F_{\mathrm{HW}}^{\mathrm{Q}} = \left[1 + A_2^{\mathrm{Q}} J^{''}(J^{''}+1)\right]^2 \tag{2.102}$$

for Q-branch transitions. In Equation (2.101) m is the usual running number of rovibrational transitions within a band (P-branches: $m = -J^{''}$; R-branches $m = J^{''} + 1$). Watson [239] also developed the necessary formulae needed to analyze $|\Delta K| = 2$ transition intensities which have been observed for e.g. in hydrogen cyanide [20] and nitrous oxide [240]. For such bands $\mu_v = 0$ and the intensity is caused by rovibrational interactions only.

Chapter 3

High accuracy composite potential energy functions for triatomic molecules

This chapter presents the application of the outlined composite approach to triatomic linear molecules. In Section 3.1 near-equilibrium PEFs for the electronic ground state of hydrogen cyanide (HCN) are constructed from both single and multi reference based composite approaches. A highly accurate EDMF obtained from a CC based composite approach is also developed. Comparisons of large-scale variational rovibrational calculations to experimental results demonstrate the accuracy of the composite approach for obtaining rovibrational term energies and transition intensities. Recent theoretical results [241,242] are compared to the present ones and commented on. Section 3.2 covers the development of a highly-accurate PEF for the challenging tricarbon (C_3) molecule in its electronic ground state. This section highlights the necessity of a proper treatment of both the electronic structure calculations and the rovibrational treatment to obtain the desired accuracy of 1 cm^{-1} in the vibrational term energies. The interplay of theory and experiment is illustrated in a combined study on the 3 μm spectrum of C_3 produced in a propyne plasma.

3.1 Hydrogen Cyanide - HCN

3.1.1 Introduction

Hydrogen cyanide (HCN, $\tilde{X}^1\Sigma^+$) is one of the best studied linear triatomic species. The 2016 version of the high-resolution transmission molecular absorption database (HITRAN) [243] includes about 58000 rovibrational transitions up to transition frequencies of 18000 cm^{-1}. HCN also serves as a key tracer molecule in astrophysical studies (cf. e.g. [244] and references therein). Following its first detection by Snyder and Buhl [245], HCN has been detected toward numerous sources like molecular clouds [246–248], comets [249, 250], carbon stars [251, 252], protoplanetary disks [253, 254] and very recently in the atmosphere of the exoplanet 55 Cancri E [255]. Owing to the large dipole moment in the vibrational ground state $\mu_0 = -2.98519(1)$ D [256] HCN is mainly observed in emission of the $J = 0 \leftarrow 1$ transition [257]. Nevertheless, the importance of its rovibrational spectrum in modeling cool carbon star atmospheres has been demonstrated by Jørgensen and coworkers [258, 259]. Lab based spectroscopic studies on HCN can be traced back to 1913 and the work of Burmeister [260] who recorded the first IR spectrum using a prism spectrometer. He detected the three fundamental transtions ν_1 (CH stretch), ν_2 (bending) and ν_3 (CN stretch) at wavelengths around 3, 14 and 5 μm, respectively. Since then, the invention of modern high-resolution spectroscopic techniques has provided a very detailed picture of the HCN rovibrational spectrum [17]. Enabled by the huge amount of experimental data HCN clearly is one of the benchmark systems of quantum chemistry that is used to test modern *ab initio* approaches [145,261,262]. There is also considerable interest in the isomerisation process to hydrogen isocyanide HNC [263, 264]. The work of Mellau and coworkers [264] showed that in the vicinity of the transition state the rovibrational wave functions of HCN and HNC would coalesce into a saddle point localized wave function.

An exhaustive review of both the experimental high-resolution and *ab initio* theoretical spectroscopy studies on hydrogen cyanide is beyond the scope of the present work. Therefore, the following paragraphs will focus on the most relevant studies in the context of this thesis. The most extensive experimental spectroscopic characterisation of HCN has been provided by Mellau [17]. His work compiles data on HCN spanning more than 30 years of research from rotational, infrared absorption, *hot gas molecular emission* (HOTGAME) spectroscopy and laser photoacoustic measurements (cf. [17] and references therein). From this vast amount of precise line frequencies spectroscopic parameters for the lowest 71 vibrational states of HCN up to $(0, 10^0, 0)$ at 6855.44 cm^{-1} including vibrational term energies, rotational parameters as well as l-type doubling and resonance parameters were determined. Furthermore, the work provides a complete list of rovibrational term energies relative to the experimentally not determinable zero-point energy up to 6880 cm^{-1}. This corresponds to slightly more than 3800 rovibrational states which are assigned an upper limit of uncertainty in the $T_v(J)$ typically on the order of 10^{-4} to 10^{-3} cm^{-1}.

Intensity measurements have been performed on quite a large number of rovibrational transitions

in HCN. The intensities of individual bands in the HCN spectrum were first studied by Hyde and Horning [265] in 1952 who determined an integrated intensity of 222.40, 188.15 and 0.59 $cm^{-2}atm^{-1}$ for the fundamental bands ν_1, ν_2 and ν_3, respectively. In the following years the intensity of the ν_1 band was remeasured by several authors resulting in integrated band intensities that spread a quite large range between 219 and 256 $cm^{-2}atm^{-1}$ [18,19,21,265–269]. Probably the most accurate analysis was provided by Devi *et al.* [21] using a multispectrum fitting technique employing 40 different high-resolution spectra with various experimental conditions. The integrated band intensity was determined to be 225.73 $cm^{-2}atm^{-1}$. Devi and coworkers also provided a precise intensity investigation of the bending fundamental and the corresponding overtone [22–24]. Similar to ν_1, measurements of the ν_2 intensity show a broad distribution of 188 to 266 $cm^{-2}atm^{-1}$ in the value of the band intensity [19, 23, 24, 265, 266]. Again using a multispectrum fitting approach Smith *et al.* [24] obtained the most reliable band intensity of 266.15±0.15 $cm^{-2}atm^{-1}$ for ν_2. The unusual intensity of the ν_3 CN stretch fundamental of hydrogen cyanide has attracted quite some interest by experimentalists [18, 265, 266]. Hyde and Horning [265] showed that this band is exceptionally weak and the excellent work of Maki and coworkers [18] established that the combination of the small transition dipole moment and the large permanent dipole moment causes a minimum in the R-branch of the ν_3 band at the R(7) transition. The selection rule $\Delta\ell = 0, \pm 1$ for rovibrational transitions of linear molecules can be lifted by rovibrational interactions that mix states with different ℓ. This results in transitions e.g. from the vibrational ground state to the $\ell = 2$ component of the excited bending state $(0, 2^\ell, 0)$ to be observable, albeit rather weak. Such transitions have been measured in HCN by Maki *et al.* [20] who linked the intensity of the P- and R-branch to ℓ-type resonance in the $(0, 2^\ell, 0)$ manifold and the occurrence of an even weaker Q-branch to Coriolis-type interactions with the fundamental bending transition ν_2 and the 2^{nd} overtone $3\nu_2^1$. Watson later provided a theoretical analysis of the intensities of such transitions [239].

PEFs for the electronic ground state of HCN have been determined by various authors employing *ab initio* calculations [58, 241, 270–273], by fitting to experimental term energies in rovibrational calculations [274, 275] or by a combination of both [242, 276]. Carter, Handy and Mills [275] developed a PEF for HCN based on variational rovibrational calculations. By fitting term energies of $J = 0$, 1 and 2 rovibrational states up to about 19000 cm^{-1} 53 expansion coefficients of a PEF expressed in Morse coordinates for the stretches and the deviation from linearity for the bending were determined. The experimental vibrational energies are reproduced with an accuracy of about 0.5 cm^{-1} and rotational parameters B_v with ~ 0.0001 cm^{-1}. In 1997 Botschwina and coworkers presented a thorough analysis of HCN based on large-scale *ab initio* calculations. The PEF was obtained from least-squares fits to ae-CCSD(T)/CVQZ calculations and expanded with respect to the simple internal bond-stretching coordinates Δr (CH-stretch), ΔR (CN-stretch) and θ (deviation from linearity). The fundamental transition frequencies, as obtained from variational rovibrational calculations using Sebalds program [210], were 3313.6, 713.3 and 2102.6 cm^{-1} for ν_1, ν_2 and ν_3, respectively. These values are too large by 2.1, 1.3 and 5.8 cm^{-1} compared with experimental results [17]. Additionally, Botschwina *et al.* [58] developed the bending and stretch-bend coupling

part of an EDMF for HCN based on fc-CCSD(T) calculations with a basis set of 110 cGTOs which extends earlier work [277] on the stretch-only dependence of the EDMF. In combination with the fitted PEF of Carter, Handy and Mills [278] this EDMF reproduced the transition dipole moment of the ν_3 band to within experimental accuracy in variational calculations. However, due to a too large first Herman-Wallis coefficient A_1 the R-branch minimum occurs at a too low $J'' = 4$. A global HCN/HNC potential energy surface has been presented by van Mourik *et al.* [272] on the basis of ae-CCSD(T)/CVQZ calculations that also incorporate the results by Bowman *et al.* [271] obtained with a smaller basis set. The PEF further includes corrections for scalar relativistic effects and the DBOC. Vibrational term energies for the 16 $\ell = 0$ states up to $(2, 0^0, 0)$ obtained with Tennysons Dvr3d progam reproduced the experimental values with a standard deviation of 7.2 cm^{-1}. Transition dipole moments for the fundamental bands of 0.0853, 0.1996 and 0.0018 D were calculated from the PEF and EDMF to be compared with the experimental values [18, 19] of 0.0824(5), 0.189(1) and 0.00136(1) D. Harris *et al.* [279] later extended the rovibrational calculations to compute a line list for HCN and obtained the ν_3 R-branch minimum at R(8).

Recently Makhnev *et al.* [241] reinvestigated the HCN system. They developed a local HCN PEF as well as a global HCN/HNC surface from ic-MRCI calculations with a large ACV6Z basis set and all electrons correlated. The reference for the MRCI calculations and the size consitency correction were chosen in an *ad hoc* manner by extending the full-valence CASSCF active space by an additional a' orbital and including the relaxed reference Pople size-consistency correction [39] such that the resulting PES reproduces the experimental term energies best. Furthermore, the *ab initio* surface is augmented by the inclusion of scalar relativistic and adiabatic corrections. For vibrational states up to 15600 cm^{-1} a standard deviation of $\sigma = 2.1$ cm^{-1} is obtained. Calculations with the local HCN PEF included opportune so called non-Born-Oppenheimer (NBO) terms in the Hamiltonian (cf. eq. (8) and (9) in [241]) which were empirically adjusted using two parameters to best reproduce low lying $J = 0$ rovibrational states. From these calculations a standard deviation of $\sigma = 0.3$ cm^{-1} was obtained for all vibrational states with $J = 0$ and the lowest bending states with $\ell = J$ up to $J = 9$. In a second study by the same authors [242] the *ab initio* data was refit to a PEF expansion for HCN only in terms of the simple internal stretching coordinates Δr, ΔR and the cosine transformed bond angle coordinate. This PEF was adjusted by least-squares fitting to the experimental data of Mellau [17] which resulted in a standard deviation of $\sigma = 0.0373$ cm^{-1} for rovibrational levels with $J = 0$, 2, 5, 9 and 10. A new HCN dipole moment surface was developed by Makhnev and coworkers on the basis of ic-MRCI/ACV5Z calculations (CASSCF reference as employed in [241]). Absolute intensities calculated the fundamental transitions up to $J = 20$ show relative errors of 1.24, 1.48 and 16.58 % for ν_1, ν_2 and ν_3 (P-branch only). In terms of the ν_3 R-branch minimum the spectroscopically determined PEF and *ab initio* EMDF fail in reproducing the observed intensity minimum instead predicting the minimum for the R(6) line.

Despite considerable computational effort dipole surfaces presented until now fail to accurately describe the intensity of both the strong fundamental bands and the weak ν_3 band in a balanced matter. Calculations of PEFs for HCN have been somewhat more successful with the recent study

by Makhnev and coworkers [241] surpassing the accuracy mark of < 1 cm^{-1} in the fundamental transition frequency. The latter study suggested that in order to reach such a level of agreement with experiment NBO effects have to be considered. As has been shown previously [173], employing a composite approach for PEFs and EDMFs alike can yield highly accurate spectroscopic parameters *and* absolute rovibrational intensities close to experimental accuracy without the need to include NBO effects. Therefore it seems only logical to apply that same approach to HCN. Section 3.1.2 presents the details of the composite approach and the employed *ab initio* methods. The construction of the PEF and EDMF is described in Section 3.1.3 also highlighting the importance of the individual contributions. In Section 3.1.4 results of large-scale variational rovibrational calculations are given that demonstrate the capability of the underlying composite approach in obtaining highly accurate PEFs and EDMFs.

3.1.2 Composite *ansatz*

The composite *ansatz* chosen for HCN follows the one used by Schröder *et al.* [173] for the N_2O molecule. Both the PEF and the EDMF are constructed by combining different levels of theory. The detailed components of the former (termed Comp I) are:

- The basic F12b contribution is calculated at the fc-CCSD(T)-F12b level of theory with a F12-optimized VQZ-F12 basis set. The CABS and DF basis sets correspond to the default choice of Molpro: VQZ-F12/OPTRI, VQZ/JKFIT, AVQZ/MP2FIT [280–282]. The geminal β is set to the recommended value of 1.0 Å^{-1} [124].
- The CV is accounted for by conventional CCSD(T) with a CV6Z basis set. The energy difference of calculations with all electron correlated and frozen core calculations provides this contribution to the composite PEF.
- SR effects are obtained from CCSD(T) calculations with a recontracted VQZ-DK basis [170] corresponding to the energy difference of DKH2 fc-CCSD(T)/VQZ-DK and fc-CCSD(T)/VQZ.
- HC effects of the valence electrons are included via four contributions with up to sextuple excitations (CCSDTQPS in coupled-cluster nomenclature):
  - Effects up to perturbative quadruples are incorporated by the (Q)-(T) contribution, which is calculated as the difference CCSDT(Q) – CCSD(T) using a VTZ basis set
  - Correction to the full iterative quadruples is achieved via the difference CCSDTQ – CCSDT(Q) and a VDZ basis set is used for this contribution termed Q-(Q)
  - Contributions due to iterative pentuple excitations (P-Q) employ a VDZ basis set and are calculated as the difference CCSDTQP – CCSDTQ.
  - The S-P contribution, which accounts for sextuple substitutions, is obtained from the

CCSDTQPS – CCSDTQP difference calculated with a VDZ basis set

- The adiabatic DBOC correction for the individual HCN isotopologues is calculated at the ae-CCSD/CVQZ level of theory.

Additionally two MR based PEFs are constructed for comparison. The PEF Comp II uses explicitly correlated fc-MRCI-F12+Q (abbreviated MR-F12) as basic contribution, where as a reminder +Q signifies the inclusion of the *a posteriori* Davidson correction [118]. MR-F12 is calculated using a VQZ-F12 basis set. The basic contribution to the Comp III PEF is provided by fc-ACPF-F12/cc-pVQZ-F12 (AC-F12) calculations. Both multi-reference approaches employ a full-valence CASSCF reference wave function and the same β, CABS and DF basis sets as the F12b contribution. Corrections due to CV, SR and DBOC are taken from the contributions detailed above for the Comp I PEF.
The EDMF of HCN is calculated using the approach for the Comp I PEF but excludes the DBOC correction. Due to the dipole operator sampling mainly the outer valence region of the molecule, the basis sets for the individual contributions include additional diffuse basis functions. In detail the contribution to the Comp EDMF are:

F12b	fc-CCSD(T)-F12b/AV5Z β = 1.5 Å^{-1} as recommended by Peterson and coworkers [124] for AV5Z basis sets CABS: AV5Z/OPTRI, AV5Z/JKFIT, AV5Z/MP2FIT [281–283]
CV	[ae-CCSD(T) – fc-CCSD(T)]/ACV6Z
SR	DKH2 fc-CCSD(T)/AVQZ-DK – fc-CCSD(T)/AVQZ
(Q)-(T)	[CCSDT(Q) – CCSD(T)]/AVTZ
Q-(Q)	[CCSDTQ – CCSDT(Q)]/VTZ(H: *sp*; C,N: *spd*) VTZ(H: *sp*; C,N: *spd*): standard VTZ basis without *d*-functions on hydrogen and without *f*-functions on carbon and nitrogen
P-Q	[CCSDTQP – CCSDTQ]/VDZ
S-P	[CCSDTQPS – CCSDTQP]/VDZ

3.1.3 Construction of an accurate PES and EDMF for HCN

Within the present composite methodology the basic contribution to the PEF is chosen to provide near CBS results at the respective level of theory. Performance of the explicitly correlated fc-CCSD(T)-F12b variant in providing such results is studied in Table 3.1 (obvious shorthand notations are used for describing the employed basis sets). Results of conventional fc-CCSD(T) calculations with basis sets up to AV8Z (1000 cGTOs) are given for comparison. The latter calculations should provide equilibrium bond lengths converged to within 10^{-4} Å and harmonic vibrational frequencies to within 1 cm^{-1}. The equilibrium bond lengths obtained with fc-CCSD(T)-F12b and

Table 3.1: Frozen core CCSD(T) and CCSD(T)-F12b equilibrium bond lengths (in Å) and harmonic vibratonal frequencies (in cm^{-1}) of HCN.

Method	Basis	r_e	R_e	ω_1	ω_2	ω_3
CCSD(T)	AVTZ	1.06711	1.16010	3433.3	716.8	2107.9
	AVQZ	1.06707	1.15673	3435.5	721.3	2121.0
	AV5Z	1.06669	1.15573	3436.6	725.9	2124.5
	AV6Z	1.06665	1.15543	3437.1	727.2	2125.6
	AV7Z	1.06652	1.15527	3437.5	727.6	2126.5
	AV8Z	1.06656	1.15519	3437.7	728.0	2126.8
CCSD(T)-F12b	VDZ-F12	1.06698	1.15605	3438.7	724.2	2125.0
	VTZ-F12	1.06672	1.15540	3437.2	727.4	2126.6
	VQZ-F12	1.06660	1.15508	3438.2	728.0	2127.8
CCSD(T*)-F12b	VQZ-F12	1.06664	1.15522	3437.5	727.5	2126.7

a VQZ-F12 basis show a close agreement with the AV8Z results. Triples scaling according to the recipe of Werner and coworkers [61, 128] leads to equilibrium bond lengths which are slightly to long especially for the CN-bond (R_e). The convergence of the harmonic vibrational frequencies given in Table 3.1 is graphically displayed in Figure 3.1. From the trend of the CCSD(T)/AVnZ results it is clear that the F12b/VQZ-F12 ω_i provide excellent near CBS results. Again, triples scaling with VnZ-F12 basis sets appears to slightly underestimate the CBS-limit.

The variation of the spectroscopic parameters r_e, R_e and ω_i upon inclusion of the smaller contributions to the composite PEFs is presented in Table 3.2. The dominant corrections are provided by the CV and the first HC contribution (Q)-(T). The former leads to a contraction of the bond lengths by -0.00140 and -0.00259 Å for r_e and R_e, respectively. In case of the R_e this effect is somewhat compensated by HC effect with a combined contribution of $+0.00094$ Å. Conversely, while the CV contribution increase the harmonic vibrational frequencies HC effects lead too larger values of the ω_i. Interestingly, for ω_3 a near cancelation of contributions is observed, such that F12b/VQZ-F12 and Comp I agree to within 0.3 cm^{-1}.

The trends described in the preceding discussion can also be inferred from Figure 3.2 where the dependence of the relative contributions on the three internal coordinates Δr (CH-stretch), ΔR (CN-stretch) and θ (deviation from linearity) is shown. For the Δr coordinate only CV contributes significantly to the energy. HC effects are much more pronounced for the CN-stretching coordinate and are of opposite sign to the strong CV contribution. Except for (Q)-(T) the smaller contributions vary only slightly by about ± 10 cm^{-1} with θ up to 80°. Perturbative quadruples via the (Q)-(T) contribution show a strong non-linear dependence on θ and appear to approach a maximum at around 80-90°. However, due to the steep bending potential of HCN the $\sim$ 67 cm^{-1} (Q)-(T) contribution to the bending potential correspond to only 0.5 % at 80°.

The final composite results of the three PEFs (cf. Table 3.2) can be compared to literature results. Carter, Mills and Handy [284] used variationally determined differences $B_0 - B_e$, based

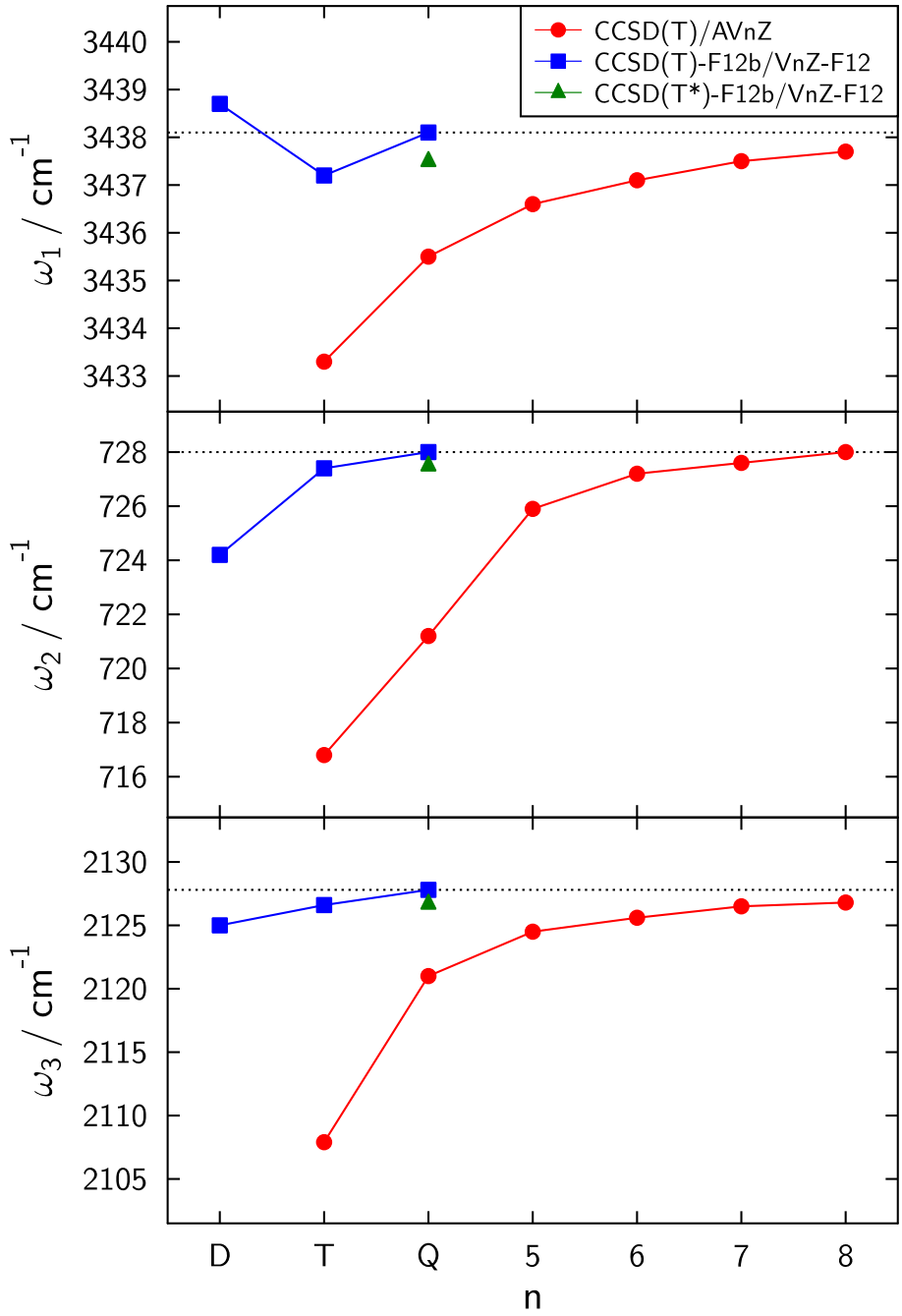

Figure 3.1: Dependence of the HCN harmonic vibrational frequencies on the size of the basis set for standard and explicitly correlated CC calculations. The horizontal line corresponds to the CCSD(T)-F12b/VQZ-F12 result.

on a PEF fitted to reproduce experimental results [275], to correct the accurate experimental B_0 values for vibrational effects yielding mixed experimental/theoretical B_e. These B_e values calculated for eight different isotopologues of HCN were then used to determine $r_e = 1.06501(8)$ Å and $R_e = 1.15324(2)$ Å. The latter results are in good agreement with the equilibrium geometry of the $H^{12}C^{14}N$ Comp I PEF $r_e = 1.06518$ Å and $R_e = 1.15325$ Å. The agreement becomes almost perfect when one considers the Born-Oppenheimer result $r_e = 1.06502$ Å and $R_e = 1.15324$ Å obtained upon neglecting the adiabatic correction in the present composite PEF. Maki and coworkers performed extensive studies of HCN isotopologues in the infrared [285, 286]. Based on the determined rotational parameters B_v for a large number of vibrationally excited states, fits according to the expansion (2.65) were performed to determine equilibrium rotational constants B_e for eight HCN isotopologues. From these an equilibrium geometry of $r_e = 1.06511(5)$ and $R_e = 1.15328(1)$ Å was determined. Finally, using the spectroscopically determined PEF by Makhnev *et al.* [242] adiabatic equilibrium bond lengths of $r_e = 1.06513$ and $R_e = 1.15333$ Å are obtained for $H^{12}C^{14}N$. These bond lengths appear to be slightly too short in case of r_e and slightly too long in case of R_e compared with the Comp I adiabatic results.

Table 3.2: Influence of smaller contributions to the composite PEFs on the equilibrium bond lengths (in Å) and harmonic vibrational frequencies (in cm^{-1}) for HCN.

PEF	Contribution	r_e	R_e	ω_1	ω_2	ω_3
Comp I	F12b	1.06660	1.15508	3438.1	728.0	2127.8
	CV	−0.00140	−0.00259	+7.2	+3.2	+9.5
	SR	−0.00014	−0.00019	+0.1	−0.1	−0.4
	(Q)-(T)	+0.00001	+0.00101	−2.1	−4.4	−10.7
	Q-(Q)	−0.00006	−0.00030	+1.0	+0.6	4.0
	P-Q	+0.00001	+0.00021	−0.4	−0.6	−2.5
	S-P	±0.00000	+0.00002	±0.0	−0.1	−0.3
	DBOC[a]	+0.00016	+0.00001	−0.6	+0.1	+0.1
	Total	1.06518	1.15325	3443.3	726.7	2127.5
Comp II	MR-F12	1.06445	1.15772	3460.1	708.2	2109.6
	CV	−0.00142	−0.00261	+7.4	+3.2	+9.6
	SR	−0.00014	−0.00019	+0.1	−0.1	−0.4
	DBOC[a]	+0.00015	+0.00001	−0.6	+0.1	+0.1
	Total	1.06304	1.15493	3467.0	711.4	2118.9
Comp III	AC-F12	1.06416	1.15761	3463.1	709.5	2110.6
	CV	−0.00140	−0.00259	+7.4	+3.2	+9.6
	SR	−0.00014	−0.00019	+0.1	−0.1	−0.4
	DBOC[a]	+0.00016	+0.00001	−0.6	+0.1	+0.1
	Total	1.06275	1.15482	3470.1	712.6	2119.8

[a] Diagonal Born-Oppenheimer correction for the $H^{12}C^{14}N$ isotopologue.

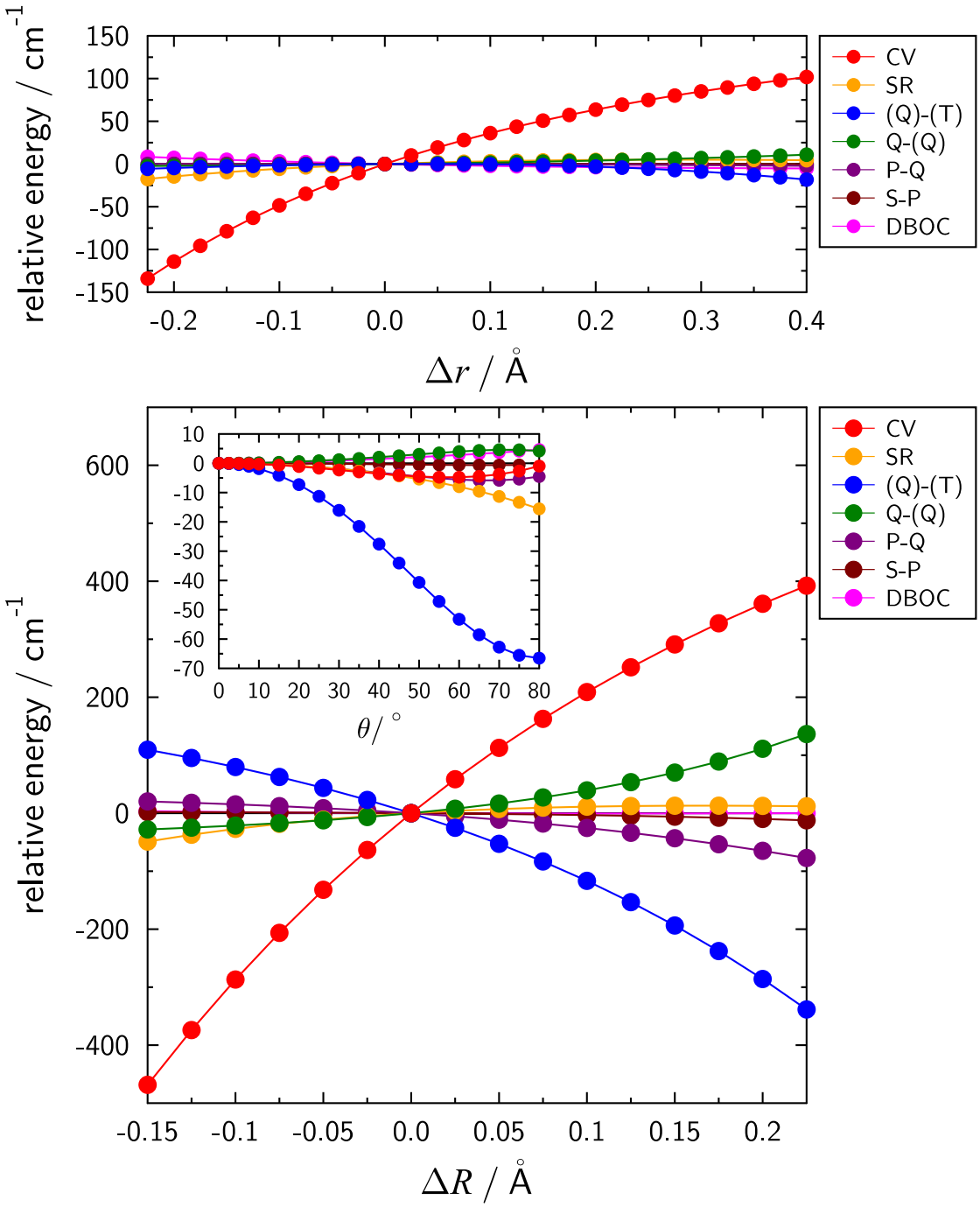

Figure 3.2: Dependence of smaller contributions to the HCN Comp I PEF on the internal coordinates Δr (CH-stretch, upper panel), ΔR (CN-stretch, lower panel) and θ (deviation from linearity, inset to lower panel). The DBOC contribution corresponds to the $H^{12}C^{14}N$ isotopologue.

Considering the harmonic vibrational frequencies, values of 3443.3, 726.7 and 2127.5 cm^{-1} are obtained for ω_1, ω_2 and ω_3, respectively, from the Comp I *ansatz*. These can be compared to the values derived from the PEF of Carter *et al.* [278]: 3441.2, 727.0 and 2127.0 cm^{-1} and the experimental values due to Maki and coworkers [286]: 3443.1, 727.0 and 2127.4 cm^{-1}. All ω_i are in close agreement between theory and experiment, with the larger spread in the CH stretching frequency due to anharmonicity effect in this mode. The PEF of Makhnev *et al.* [242] yields harmonic vibrational frequencies of 3443.8, 726.8 and 2127.1 cm^{-1}, with a somewhat surprisingly large ω_1 considering that the PEF is fitted to reproduce experimental rovibrational term energies below 6880 cm^{-1} with a standard deviation of 0.0373 cm^{-1}.

Up until this point comparisons have only been made with the Comp I PEF. The two multi-reference based PEFs Comp II and Comp III yield CH bond lengths of 1.06304 and 1.06275 Å, respectively, and CN bond lengths of 1.15493 and 1.15482 Å, respectively. Compared to the probably most accurate results of Carter *et al.* [284] the CH bond lenghts are clearly to short by about 0.002 Å and the CN bond lengths to long by about 0.0015 Å. These errors in the bond lengths transfer to the harmonic vibrational frequencies with large differences of almost 27 cm^{-1} (Comp III) observed for the CH stretching frequency compared to the Comp I result which almost coincides with the result of 3443.1 cm^{-1} determined experimentally by Maki *et al.* [286]. Differences in the bending and CN stretching harmonic frequencies with respect to experimental results are only slightly less pronounced. For ω_2 differences of -15.6 and -14.4 cm^{-1} are calculated and for ω_3 -8.5 and -7.6 cm^{-1} from Comp II and Comp III, respectively, compared to Maki *et al.* [286]. These large differences are well beyond the accuracy of 1 cm^{-1} typically achieved in single-reference based composite approaches and are even larger than those obtained for MR based composite approaches [173, 287]. For example in the case of N_2O maximum deviations of 2-4 cm^{-1} were calculated in Ref. [173] based on the same MR approach as adopted here. The main source of errors appears to be the basic contributions provided by explicitly correlated MRCI-F12 and ACPF-F12. Makhnev *et al.* [241] in their study of the HCN/HNC system already noted the deficiencies of MRCI calculations with a full valence CASSCF reference, resulting in differences of up to 26 cm^{-1} for the second overtone of the anharmonic CH-stretching vibration $2\nu_1$.

Individual contributions (α) to the composite PEFs are represented by polynomials according to

$$V^{(\alpha)} - V^{(\alpha)}_{\mathrm{ref}} = \sum_{ijk} C^{(\alpha)}_{ijk} \Delta r^i \Delta R^j \theta^k \quad (k\text{: even}) \,, \tag{3.1}$$

where the coefficients $C^{(\alpha)}_{ijk}$ are determined by least-squares fitting. The adopted reference geometry is $r_{\mathrm{ref}} = 1.0650$ and $R_{\mathrm{ref}} = 1.1532$ Å close to the final equilibrium BO geometry given above. In order to provide an accurate local PEF valid up to energies ≈ 10000 cm^{-1} above the minimum, the contributions are calculated in the following coordinate ranges: -0.225 Å $\leq \Delta r \leq 0.4$ Å, -0.15 Å $\leq \Delta R \leq 0.225$ Å and $0° \leq \theta \leq 80°$. After carrying out the individual least-squares fits which yield standard deviations on the order of 0.001 cm^{-1} the resulting polynomials (cf. Table A.1 and Table A.2 in Section A) are combined according to Equation (2.29). Residual gradient terms

are removed by transforming the polynomials to their respective minimum. This finally yields the composite PEFs Comp I, II, and III which are summarized in Table A.4.
The fc-CCSD(T) and fc-CCSD(T)-F12b basis set dependence of spectroscopic properties related to the EDMF are investigated in Table 3.3. Equilibrium dipole moments μ_e and intensities of fundamental vibrational transitions $I(\omega_i)$ evaluated in double-harmonic approximation (DHA)

$$I(\omega_i) = \frac{4\pi^3 N_\mathrm{A} d_i}{3hc} \omega_i \mu_i^2 \tag{3.2}$$

are calculated from dipole moment functions expanded around the Comp I adiabatic equilibrium geometry. In Equation (3.2), N_A is the Avogadro constant and $\mu_i = \left(\frac{\partial \boldsymbol{\mu}}{\partial q_i}\right)_\mathrm{e}$ the derivatives of the dipole moment vector with respect to the dimensionless normal coordinates. The Comp I PEF also provides the **L**-matrix elements necessary to transform the dipole derivatives from internal to normal coordinates and the harmonic frequencies. Standard CCSD(T) equilibrium dipole moments obtained with the AV6Z basis set appear to be converged to within 0.001 D. While the band intensity of the bending vibration converges rather fast in DHA, convergence of the stretching intensities is slower especially for the weak ν_3 fundamental. Following the scheme of Halkier *et al.* [288] a CBS extrapolation of the AV5Z and AV6Z dipole moments is carried out. The resulting equilibrium dipole moment are expected to be accurate to within 10^{-3} D and DHA intensities

Table 3.3: Frozen core CCSD(T) and CCSD(T)-F12b HCN equilibrium dipole moments (in D) and intensities of the fundamental bands (in $\mathrm{km \cdot mol^{-1}}$) obtained in double harmonic approximation[a].

Method	Basis	μ_e[b]	$I(\omega_1)$	$I(\omega_2)$	$I(\omega_3)$
CCSD(T)	AVTZ	−3.0079	64.16	69.97	0.1223
	AVQZ	−3.0159	64.72	69.61	0.1537
	AV5Z	−3.0189	65.17	69.34	0.1742
	AV6Z	−3.0205	65.36	69.38	0.1823
	AV[56]Z[c]	−3.0227	65.60	69.34	0.1938
CCSD(T)-F12b	VDZ-F12	−3.0162	64.75	71.39	0.1496
	VTZ-F12	−3.0195	65.32	70.16	0.1789
	VQZ-F12	−3.0223	65.64	70.16	0.1909
CCSD(T*)-F12b	VQZ-F12	−3.0216	65.57	70.16	0.1901
CCSD(T)-F12b	AVTZ	−3.0223	65.56	69.82	0.1755
	AVQZ	−3.0235	65.61	69.42	0.1954
	AV5Z	−3.0234	65.62	69.34	0.1975
CCSD(T*)-F12b	AV5Z	−3.0230	65.62	69.34	0.1972

[a] Using the Comp I PEF and expanding dipole moment around the adiabtic Comp I equilibrium geometry for $H^{12}C^{14}N$.
[b] Equilibrium dipole moments are quoted with the present sign convention corresponding to a polarity +HCN−.
[c] Results obtained from CBS extrapolation of AV5Z and AV6Z results.

are expected to be accurate to within 10^{-2} km·mol^{-1}. Explicitly correlated fc-CCSD(T)-F12b with a VQZ-F12 shows a good agreement for μ_e, $I(\omega_1)$ and $I(\omega_3)$ compared to the CBS values. Triples scaling has nearly no influence on the obtained results. However, the DHA intensity of the bending fundamental 70.16 km·mol^{-1} is larger by 1.2 % compared to CCSD(T)/AV[56]Z. This difference is rectified by the use of AVnZ type basis functions which are more diffuse than the VnZ-F12 type basis sets. The triples unscaled fc-CCSD(T)-F12b/AV5Z method yields the over all best performance in providing near CBS quality dipole moments and therefore is used as basic contribution to the composite EDMF.

Figure 3.3 depicts the dependence of the smaller contributions to dipole moment components $\mu^{\parallel}$ and $\mu^{\perp}$ on the internal coordinates. The CV and SR contributions show a slight linear dependence with respect to the stretching coordinates. In contrast, the dominant HC contribution (Q)-(T) provides the largest contribution to the dipole moment and varies non-linear as a function of the internal coordinates. Numerical values for the influence of the individual contributions on μ_e and the DHA intensities $I(\omega_i)$ are given in Table 3.4. The equilibrium dipole moment changes by only 0.35 % upon inclusion of the smaller effects. The magnitudes of the individual contributions are comparable to those calculated for N_2O [173] but due to the larger permanent dipole moment their relative importance is lower for HCN. The final composite equilibrium value of $\mu_e = -3.0127$ D is given with a negative sign which corresponds to a polarity of +HCN−. This is in agreement with the experimental results of Muenter and coworkers [256, 289]. The value of $\mu_e = -3.016(2)$ D (adjusted for the present sign convention, one standard deviation in the last significant digit in parentheses) obtained by DeLeon and Muenter [289] agrees to within 0.1 % with the composite result and the mixed experimental/theoretical result of Botschwina *et al.* [58] $\mu_e = -3.0146(5)$ D

Table 3.4: Influence of smaller contributions to the HCN EDMF on the equilibrium dipole moment (in D) and intensities of the fundamental bands (in km · mol^{-1}) obtained in double harmonic approximation[a].

Contribution	μ_e[b]	$I(\omega_1)$	$I(\omega_2)$	$I(\omega_3)$
F12b	−3.0234	65.62	69.34	0.1975
CV	−0.0014	+0.96	+0.06	0.0280
SR	+0.0030	−0.05	+0.36	−0.0146
(Q)-(T)	+0.0080	−0.54	+0.43	−0.0802
Q-(Q)	−0.0005	+0.26	+0.07	0.0160
P-Q	+0.0014	+0.05	+0.03	−0.0190
S-P	+0.0002	+0.02	±0.00	−0.0028
Total	−3.0127	66.32	70.29	0.1249

[a] Using the Comp I PEF and expanding dipole moment around the adiabatic Comp I equilibrium geometry for $H^{12}C^{14}N$.
[b] Equilibrium dipole moments are quoted with the present sign convention corresponding to a polarity +HCN−.

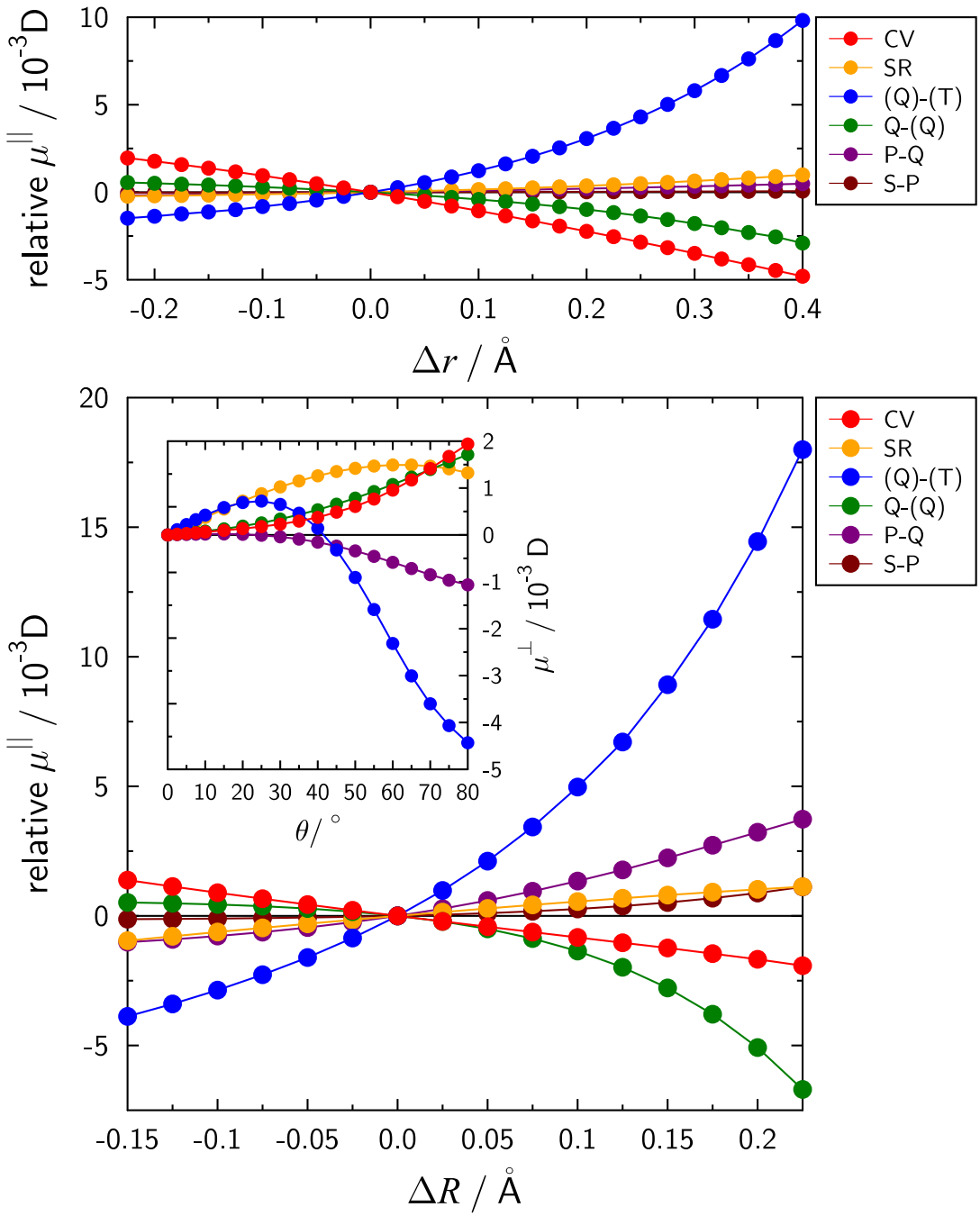

Figure 3.3: Dependence of smaller contributions to the HCN composite EDMF on the internal coordinates Δr (CH-stretch, upper panel) and ΔR (CN-stretch, lower panel) for the parallel component $\mu^{\parallel}$ and θ (deviation from linearity, inset to lower panel) for the perpendicular component $\mu^{\perp}$.

to within 0.6 ‰.
With respect to the DHA intensities, CV effects provide the dominant contribution to $I(\omega_1)$ and are slightly counterbalanced by HC effects. The overall modification of $I(\omega_1)$ due to the composite approach is only +1.1 %. A similar correction of +1.4 % is calculated for the bending fundamental $I(\omega_2)$ and in accordance with the inset of Figure 3.3 all effects provide a positive contribution in DHA. The CN-stretching fundamental is heavily influenced by the inclusion of CV, SR and HC with relative contributions of +14.2 %, −7.4 % and -43.5 %, respectively, compared to the F12b reference intensity of $I(\omega_3) = 0.1975$ km·mol^{-1}. Further taking the non-linear shape of the HC contributions into account (cf. Figure 3.3), it is clear that the inclusion of effect beyond CCSD(T) is of utmost importance to accurately describe the intensity of the ν_3 band.
The polynomial representations of the contributions (α) to the composite PEFs are

$$\mu_{\parallel}^{(\alpha)} = \sum_{ijk} D_{ijk}^{(\alpha)} \Delta r^i \Delta R^j \theta^k \quad (k\text{: even}) \tag{3.3}$$

and

$$\mu_{\perp}^{(\alpha)} = \sum_{ijk} D_{ijk}^{(\alpha)} \Delta r^i \Delta R^j \theta^k \quad (k\text{: odd}). \tag{3.4}$$

Coefficients $D_{ijk}^{(\alpha)}$ are determined by least-squares fitting of dipole moments in the same coordinate ranges as employed for the PEF fits: -0.225 Å $\leq \Delta r \leq 0.4$ Å, -0.15 Å $\leq \Delta R \leq 0.225$ Å and $0° \leq \theta \leq 80°$. The $H^{12}C^{14}N$ adiabatic Comp I equilibrium geometry $r_e = 1.06518$ Å and $R_e = 1.15325$ Å is used as a reference in these calculations. The specific coefficients $D_{ijk}^{(\alpha)}$ coefficients included in the fits are carefully chosen to yield standard deviations on the order of 10^{-5} D. They are given in Section A in Table A.5 - A.8. Summation of the polynomials according to Equation (2.30) gives the final composite EDMF (Table A.9 in Section A).

3.1.4 Variational rovibrational calculations on HCN

The PEFs of Table A.4 and EDMF of Table A.9 are employed in variational rovibrational calculations using Sebalds C8VPRO program [210]. The vibrational basis set consists of 1925 HO/RR product functions and provides all vibrational term energies up to the first overtone of the CH-stretching vibration $(2, 0^0, 0)$ converged to within 10^{-2} cm^{-1} or better. Calculations are carried out up to a total angular momentum quantum number of $J_{max} = 50$ and the vibrational angular momentum quantum number was restricted to $\ell = K \leq 17$.

Rovibrational term energies

The calculated rovibrational term energies $T_v(J)$ were least-squares fit according to Equation (2.91) employing term energies up to $J = 20$. This restriction to low J values allows to safely neglect higher-order terms in Equation (2.91) like the sextic centrifugal distortion constant H_v. For states with $\ell > 0$ effective spectroscopic parameters were determined by setting $\ell = 0$ in Equation (2.91)

Table 3.5: Experimental[a] and calculated spectroscopic parameters (in cm^{-1}) for HCN.

State	Method	G_v [b]	B_v	$10^6 D_v$
$(0,0^0,0)$	exp.	–	1.47822	2.909
	Comp I	3476.6	1.47825	2.907
	Comp II	3468.4	1.47570	2.918
	Comp III	3471.7	1.47606	2.917
$(0,1^1,0)e$	exp.	711.9	1.47803	2.932
	Comp I	711.9	1.47807	2.930
	Comp II	696.6	1.47575	2.942
	Comp III	697.8	1.47610	2.941
$(0,1^1,0)f$	exp.	711.9	1.48552	3.019
	Comp I	711.9	1.48556	3.018
	Comp II	696.6	1.48331	3.035
	Comp III	697.8	1.48364	3.033
$(0,0^0,1)$	exp.	2096.8	1.46814	2.916
	Comp I	2097.1	1.46817	2.912
	Comp II	2088.7	1.46564	2.923
	Comp III	2089.7	1.46600	2.922
$(1,0^0,0)$	exp.	3311.5	1.46780	2.884
	Comp I	3311.8	1.46783	2.882
	Comp II	3333.6	1.46516	2.899
	Comp III	3336.6	1.46552	2.898

[a] Obtained by effective fits of the experimental rovibrational term energies by Mellau [17] up to $J_{max} = 20$.
[b] For the vibrational ground state the quoted G_v corresponds to the zero-point energy (ZPE).

and performing individual fits of the e- and f-parity components. This avoids complications due to the non-linear fitting required to account for l-type doubling and l-type resonance, as outline in Section 2.3.4. A detailed listing of calculated spectroscopic parameters is given in Table A.10 of Section A. In case of HCN one is in the rather unique situation that an extensive database of experimental rovibrational term energies is available from the excellent work by Mellau [17]. All experimental reference $T_v(J)$ employed in the following were taken from that work and the quoted spectroscopic parameters were obtained by fitting the experimental term values analogous to the theoretical results. This provides an almost one-to-one comparison between theory and experiment.

Table 3.5 compares spectroscopic parameters for the vibrational ground state and singly excited vibrational states obtained with the three Comp PEFs. The vibrational term energies obtained with Comp I show almost perfect agreement with experiment [17], errors not exceeding 0.3 cm^{-1}. Given this accuracy the for the fundamental transitions the zero-point energy (ZPE) of 3476.6 cm^{-1}

should be accurate to within 0.1 cm^{-1}. Using the VPT2 formula for the ZPE (given in Equation (2.63)) and the Comp I PEF transformed via numerical differentiation to an expansion in dimensionless normal coordinates yields a value 3476.5 cm^{-1} in close agreement with the variational calculations. The latter value includes the $E_0 = -2.9$ cm^{-1} term. Rotational parameters obtained with the Comp I PEF agree to within 0.03 ‰ and 0.1 % for B_v and D_v, respectively. Performance of the MR based PEFs Comp II and III is far worse. Vibrational term energies for the $(0, 1^1, 0)$, $(0, 0^0, 1)$ and $(1, 0^0, 0)$ differ from experiment [17] by -15.3, -8.1 and $+22.1$ cm^{-1}, respectively, for the Comp II PEF and -14.1, -7.1 and $+25.1$ cm^{-1}, respectively, for Comp III. These differences closely mirror the errors obtained for the harmonic frequencies in Table 3.2. This suggests that, while the anharmonic part of the Comp II and Comp II PEFs gives a reasonable description of the true HCN potential, the main source of error lies in the description of the harmonic potential. While the 0.3-0.5 % deviation from experiment [17] of the Comp II and Comp III quartic centrifugal distortion constants is somewhat acceptable, the rotational parameters B_v are far to small by as much as 0.2 %, two orders of magnitude larger than the error of the Comp I PEF. A closer look at the differences of the rotational parameters helps to elucidate these deficiencies. From the experimental results [17] $\Delta B_v = B_v - B_0$ values of -0.01042, $+0.00730$ and -0.01008 cm^{-1} can be calculated for the $(1, 0^0, 0)$, $(0, 1^1, 0)f$ and $(0, 0^0, 1)$ state, respectively. The results for Comp II are in that same order: -0.01054, $+0.00763$, -0.01006 cm^{-1} and that for Comp III: -0.01054, $+0.00758$, -0.01006 cm^{-1}. From the perturbational expansion of B_v (cf. Equation (2.65)) one finds that these differences are effective values for the rotation-vibration interaction constants $\Delta B_v \approx -\alpha_v$. The acceptable agreement between the MR based composite approaches and the experimental values again shows that the shortcomings of the former are within the description of the harmonic problem, in this case the equilibrium rotational constant B_e and thus the molecular geometry. For comparison Comp I yields the ΔB_v values of -0.01042, $+0.00731$ and -0.01008 cm^{-1} in virtually perfect agreement with experiment. The preceding paragraphs show that the MR based approaches relying on a full valence CASSCF reference do not result in HCN PEFs that provide the desired accuracy of 1 cm^{-1}. Therefore, the following discussion will focus exclusively on results obtained with the Comp I PEF.

Figure 3.4 compares the differences with respect to experiment [17] in the lowest possible rovibrational term energy for all 63 HCN vibrational states up to $(2, 0^0, 0)$ obtained with the Comp I PEF and those obtained by Makhnev *et al.* [241]. For states with $\ell \neq 0$ these are rotationally excited states with $J = \ell$. In the upper part of Figure 3.4 the whole covered energetic range and all 63 states are shown. The errors obtained with the Comp I PEF are all within 1 cm^{-1} and from them a standard deviation of $\sigma = 0.34$ cm^{-1}. Results by Maknev *et al.* [241] show a similar agreement with $\sigma = 0.26$ cm^{-1}. However, the latter values include a so called non-Born-Oppenheimer contribution in the Hamiltonian (cf. eq. (8) and (9) in Ref. [241]). The parameters a and b in these additional Hamiltonian terms were fitted to experimental results. Therefore, the results termed BO+rel+ad+NBO by Makhnev *et al.* [241] do not constitute purely *ab initio* results. Without the NBO correction the errors of the Makhnev *et al.* [241] results are much worse compared to the

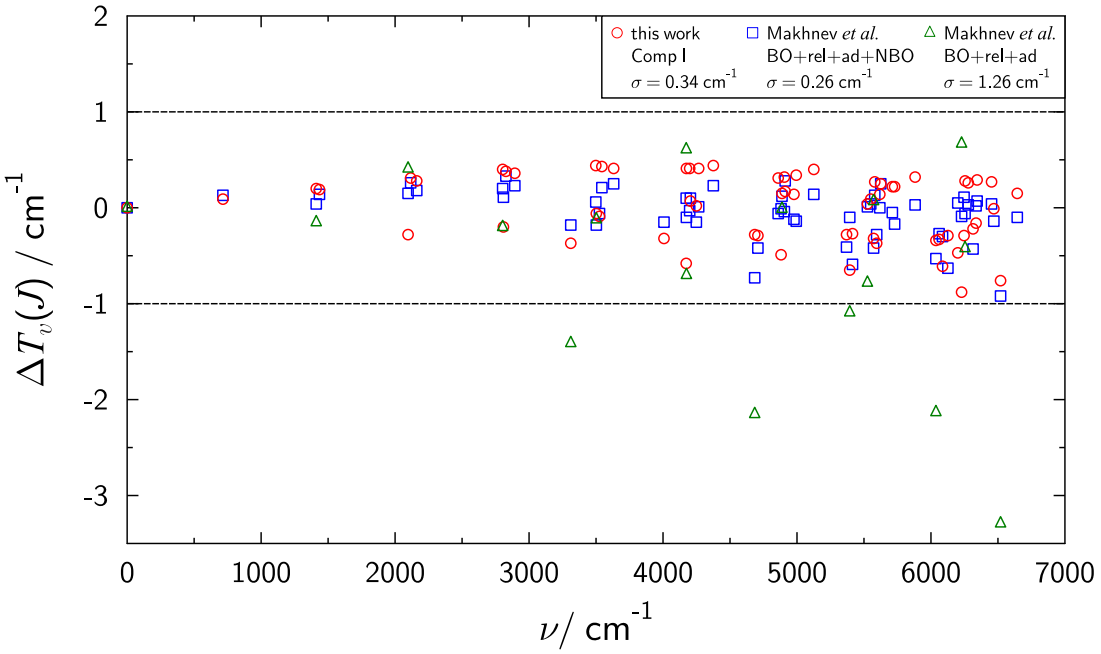

Figure 3.4: Comparison of errors in rovibrational term energies with respect to the experimental results by Mellau [17] calculated with the Comp I PEF and the those reported by Makhnev *et al.* [241].

(purely *ab initio*) Comp I results. For the 17 $J = 0$ states given in Ref. [241] $\sigma = 1.26$ cm^{-1} is obtained, whereas Comp I yields $\sigma = 0.44$ cm^{-1}. The main source of error in the former results stems from states with excited stretching vibrations. For example, the $(1, 0^0, 0)$ state is calculated 1.41 cm^{-1} too high compared to experiment [17]. This error reduces to $obs - calc = -0.18$ cm^{-1} upon inclusion of the so called NBO effects, yielding a NBO correction of -1.23 cm^{-1} on the calculated term energy. This is a surprisingly large value considering that Comp I places the $(1, 0^0, 0)$ state at 3311.84 cm^{-1} above the ground vibrational state, only 0.36 cm^{-1} too large.

In Figure 3.5 the v_i quantum number dependence of the calculated errors for the $(0, v_2^\ell, 0)$, $(v_1, 0^0, 0^0)$ and $(0, 0^0, v_3)$ series of states is depicted. The value of ℓ for the bending states corresponds to the lowest possible value so that either $\ell = 0$ or $\ell = 1$ for even or odd v_2, respectively. For a semi-rigid molecule one would expect the errors obtained from variational calculations to be a linear function of the quantum number as long as the employed potential describes the anharmonic shape of the "true" potential correctly. This can formally be realized by considering the VPT2 expansion of the vibrational term energy given in Equation (2.49). Subtracting ZPE $= E_0 + G_0$ and setting all other quantum numbers $v_j = 0$ yields the vibrational term energies $G_{v_i,\ell}$ for states

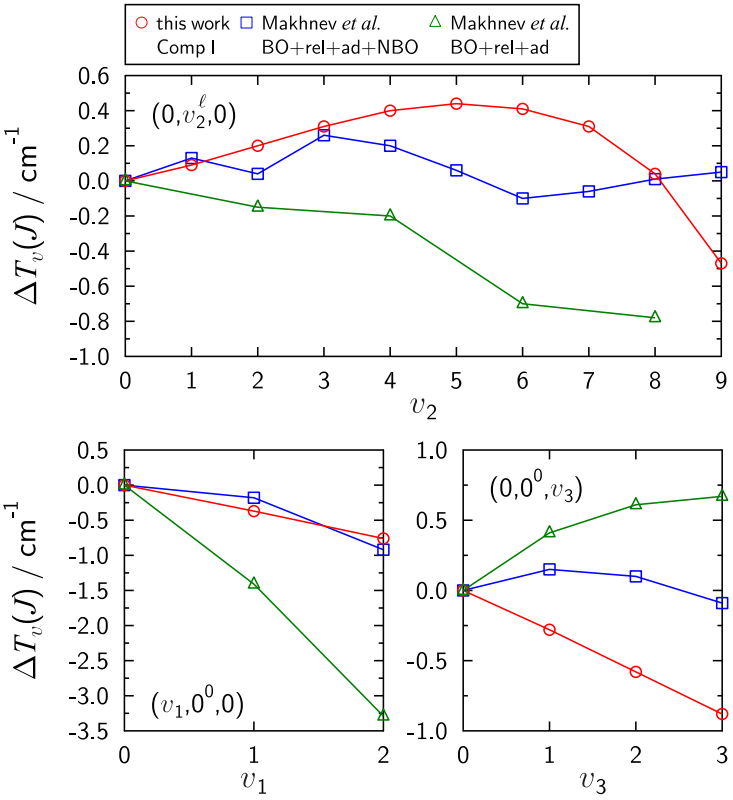

Figure 3.5: Quantum number dependence of errors in rovibrational term energies with respect to the experimental results by Mellau [17] calculated with the Comp I PEF and the those reported by Makhnev *et al.* [241].

with excitation only in v_i according to

$$G_{v_i,\ell} = \omega_i v_i + x_{ii} v_i \left(v_i + d_i\right) + \frac{1}{2} \sum_{j \neq i} x_{ij} v_i d_j + x_{\ell\ell} \ell^2 \,. \tag{3.5}$$

Terms in Equation (3.5) depending on anharmonicity parameters x_{ij} are mainly determined by the anharmonic shape of the potential. The error in the calculated vibrational term energies $\Delta G_{v_i,\ell}$ is then given by

$$\Delta G_{v_i,\ell} = \left(\Delta\omega_i + \Delta x_{ii} d_i + \frac{1}{2} \sum_{j \neq i} \Delta x_{ij} \right) v_i + \Delta x_{ii} v_i^2 + \Delta x_{\ell\ell} \ell^2 \,, \tag{3.6}$$

where the Δ signifies the error in the respective spectroscopic parameter. Since differences in rotational parameters are only on the order of the error in B_e and the α_i which both are much smaller than the $\Delta\omega_i$ it is safe to set the error in the total rovibrational term energies $\Delta T_{v_i}(J)$ to $\Delta G_{v_i,\ell}$.

Now, if the PEF describes the anharmonicity correctly one has $\Delta x_{ij} \ll \Delta\omega_i$ in Equation (3.6) and $\Delta G_{v_i,\ell} \approx \Delta\omega_i v_i + \Delta x_{ii} v_i^2$. The slope of the error $\Delta T_v(J)$ for the three series of states mentioned above is thus given by the error in the harmonic vibrational frequency for low values of v_i. Only for higher values of v_i deviations are to be expected due to the errors in the anharmonicity parameters and also higher order terms neglected in the expansion given in Equation (3.5).
The linear dependence can clearly be observed for the stretching states calculated with the Comp I PEF. For the bending states deviations from this linear relationship emerge for states with $v_2 > 4$. From the form of this curve some conclusions can be drawn on the bending potential of the Comp I PEF which mainly determines these errors. In the low energy region the potential is too steep, resulting in term energies that are too large compared to experiment [17]. With increasing energy the potential becomes wider leading to the decrease in the errors and beyond $v_2 = 8$ it is too wide compared to the "true" bending potential of HCN. In contrast, the errors for $(0, v_2^\ell, 0)$ states of

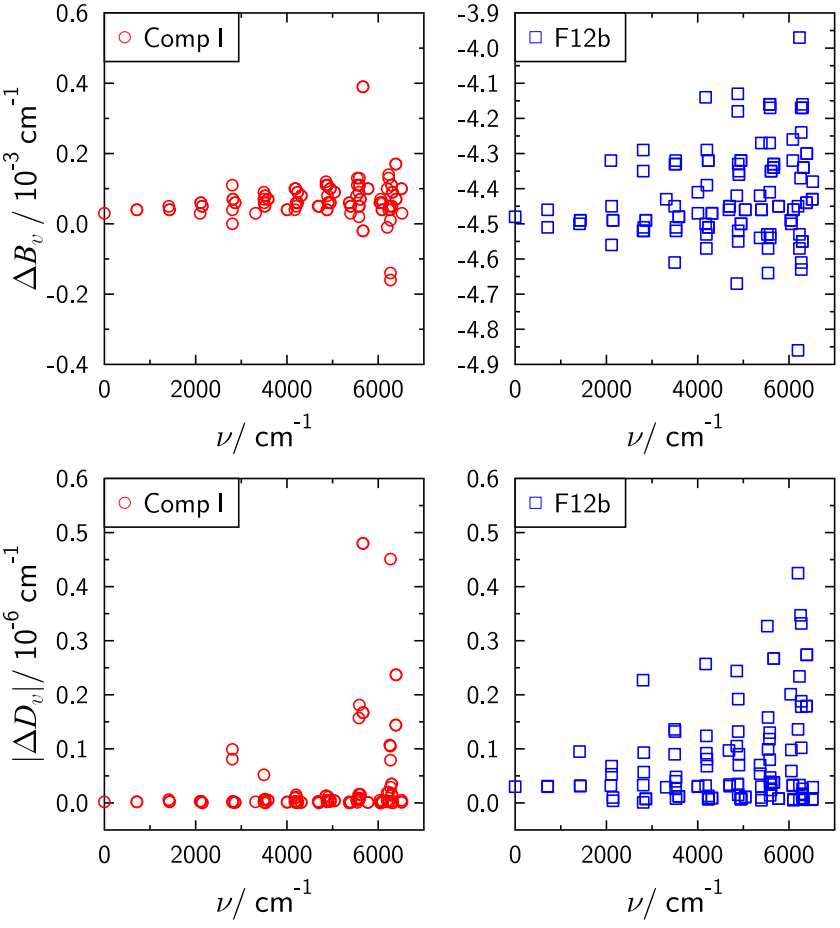

Figure 3.6: Errors in rotational parameters B_v and D_v calculated with the Comp I (left) and the F12b (right) PEF compared to results derived from the experimental results by Mellau [17].

Makhnev *et al.*show a rather unsystematic behaviour, this suggests problems in the form of the *ab initio* PEF of Makhnev *et al.* [241]. Similarly, the error for stretching term energies calculated by Makhnev *et al.* [241] show a non-linear dependence on v_1 and v_3 already for low excitations.
Calculated rotational parameters B_v and D_v for vibrational states up to $(2, 0^0, 0)$ are compared to values derived from the experimental term energies reported by Mellau (Figure 3.6). This encompasses the analysis of 1960 individual rovibrational states. The upper two panels depict $B_v^{\text{exp}} - B_v^{\text{calc}}$ for the Comp I and the F12b PEF. The latter results show an error of -0.00448 cm^{-1} in the ground state rotational parameter B_0. This is almost equal to the difference of -0.00459 cm^{-1} in the equilibrium rotational constants for the Comp I and F12b PEF. The error of the F12b rotational parameters show a larger spread compared to the Comp I results, which is due to the differences/errors in the vibration-rotation interaction parameters. The Comp I results produce somewhat outlying errors for the e and f components of $(0, 8^6, 0)$. This state shows an experimentally observed local resonance with the $(0, 5^5, 1)$ state. Mellau [17] places the avoided crossing at $J = 8$. The crossing point is reproduced by the Comp I PEF but the perturbed separation is slightly larger when comparing to experiment. This slight mismatch in the energy for low J values causes the B_v for the $(0, 8^6, 0)$ to show the largest error of the calculated values. In the lower

Table 3.6: Comparison of experimental[a] and calculated $J = 0$ vibrational term energies (in cm^{-1}) for higher lying states in HCN up to 15600 cm^{-1}.

		obs-calc				obs-calc	
State	G_v	this work[b]	Ref. [241]	State	G_v	this work[b]	Ref. [241]
$(1, 2^0, 1)$	6761.33	0.09	−1.24	$(2, 0^0, 2)$	10631.40	−1.24	−2.16
$(0, 10^0, 0)$	6855.53	−0.71	−2.89	$(0, 4^0, 4)$	11015.90	1.21	−0.78
$(0, 4^0, 2)$	6951.68	0.04	1.58	$(1, 0^0, 4)$	11516.60	−1.42	−0.70
$(1, 0^0, 2)$	7455.42	−0.93	−0.49	$(0, 2^0, 5)$	11654.59	0.11	
$(0, 2^0, 3)$	7620.22	−0.53	0.09	$(3, 0^0, 1)$	11674.50	−1.30	−3.13
$(2, 2^0, 0)$	7853.51	−0.74	−4.25	$(0, 6^0, 4)$	12364.42	1.14	3.51
$(1, 4^0, 1)$	8107.97	−0.52	−0.40	$(4, 0^0, 0)$	12635.89	−1.94	−2.84
$(0, 0^0, 4)$	8263.12	−1.44	1.24	$(2, 0^0, 3)$	12657.88	−1.38	−2.36
$(0, 6^0, 2)$	8313.53	1.27	2.33	$(0, 4^0, 5)$	13014.80	0.80	4.23
$(2, 0^0, 1)$	8585.58	−1.00	−2.17	$(0, 2^0, 6)$	13638.03	−1.50	0.86
$(1, 2^0, 2)$	8816.00	−0.78	−1.93	$(0, 8^0, 4)$	13693.87	0.23	
$(0, 4^0, 3)$	8995.22	1.30	3.39	$(3, 0^0, 2)$	13702.25	−1.31	−3.23
$(2, 4^0, 0)$	9166.62	−1.64	−1.98	$(0, 6^0, 5)$	14357.05	0.64	3.88
$(1, 0^0, 3)$	9496.44	−1.20	−0.54	$(2, 0^0, 4)$	14653.66	−1.53	−2.63
$(0, 2^0, 4)$	9648.65	0.41		$(4, 0^0, 1)$	14670.45	−1.68	−3.14
$(3, 0^0, 0)$	9627.09	−1.27	−3.30	$(3, 2^0, 2)$	14988.20	−0.18	1.10
$(2, 2^0, 1)$	9914.40	−1.01	−4.07	$(0, 4^0, 6)$	14992.06	−0.61	−1.81
$(0, 2^0, 4)$	10350.11	1.49		$(5, 0^0, 0)$	15551.94	−3.24	−1.11

[a] Experimental values from Yang *et al.* [290] and Smith *et al.* [291].
[b] Obtained from $J = 0$ variational calculations with the Comp I PEF using 3641 vibrational basis function.

panels of Figure 3.6 the absolute errors $|D_v^{\rm exp} - D_v^{\rm calc}|$ are given. Again, the overall agreement with experiment is improved by the inclusion of the smaller contributions in the Comp I PEF compared to F12b. Standard deviations calculated for the B_v and D_v with the F12b PEF compared to experiment amount to 0.00442 and $0.118 \cdot 10^{-6}$ cm^{-1}, respectively. An analogous analysis for the Comp I results yields 0.00009 cm^{-1} and $0.093 \cdot 10^{-6}$ cm^{-1}.
The coordinate range employed in the construction of the composite PEFs covers energies up to about 10000 cm^{-1} above the minimum. To test the reliability of the Comp I PEF above the $(2, 0^0, 0)$ state and its extrapolating capabilities beyond the aforementioned energy range $J = 0$ variational calculations are performed. The high degree of excitation in the vibrational modes (up to $v_1 = 5$, $v_2 = 10$ and $v_3 = 6$) requires a larger vibrational basis set to achieve convergence. A carefully selected basis comprising 3641 HO product functions gives the term energies converged to within 0.01 cm^{-1}. Results of these calculations for states up to $(5, 0^0, 0)$ at about 15600 cm^{-1} are compared in Table 3.6 to the experimental results of Smith *et al.* [291] from Fourier transform absorption spectroscopy and those obtained by Wodtke and coworkers [290] using stimulated emission pumping spectroscopy in the $\mathrm{A} - \tilde{\mathrm{X}}$ electronic band system of HCN. The observed absolute differences are in the range of up to 2 cm^{-1} with the exception of the highest lying state $(5, 0^0, 0)$ which deviates from experiment by as much as -3.24 cm^{-1}. The total standard deviation over the 36 states given in Table 3.6 is 1.24 cm^{-1} which is a factor of two better than the results obtained by Makhnev *et al.* [241] with their global HCN/HNC PES ($\sigma = 2.48$ cm^{-1}; results given in Table 3.6). In summary, the developed Comp I PEF is shown to provide highly accurate spectroscopic parameters for a large number of rovibrational states in HCN. In the energetic range up to the second overtone $2\nu_1$ of the CH stretching vibration, spectroscopic accuracy < 1 cm^{-1} is obtained for vibrational term energies and rotational paramters B_v are calculated that are within a few tenth of a percent of their experimental counterparts. In higher energetic regimes up to about 15600 cm^{-1} deviations in the vibrational terms increase to about 1-3 cm^{-1} which is still good considering that the PEF is designed for near-equilibrium applications up to ~ 10000 cm^{-1}.

Rovibrational intensities

A first test of the quality of the composite EDMF is achieved by comparing calculated dipole moments in the ground vibrational state and excited vibrational states to experimental measurements. Table 3.7 presents results obtained for low lying vibrational states of $\mathrm{H^{12}C^{14}N}$ from analysis using different numbers of rovibrational states. A vibrationally averaged ground state dipole moment of -2.9834 D is obtained which can be compared to the experimental value of $-2.98519(1)$ D determined by Ebenstein & Muenter [256]. The corresponding relative error amounts to only 0.6 %. The vibrational dependence of the dipole moment $\Delta\mu_v = \mu_v - \mu_0$ shows almost perfect agreement with the available experimental values with a maximum absolute deviation of 0.0007 D or 0.8 % obtained for the $(0, 2^2, 0)$ state. The latter value is comparable to the experimental uncertainty of 0.6 %. This level of agreement should allow a rather precise mixed experimental/theoretical estimate of the equilibrium dipole moment of HCN. Using the composite results for μ_e and μ_0 a

Table 3.7: Calculated[a] and experimental dependence of HCN electric dipole moments on vibrational excitation $\Delta\mu_v = \mu_v - \mu_0$ (in D).

	$\Delta\mu_v$			
State	$J_{\max} = 5$	$J_{\max} = 15$	$J_{\max} = 30$	exp.[b]
$(0, 0^0, 0)$[c]	−2.9834	−2.9834	−2.9834	−2.98519(1)
$(0, 1^1, 0)$	0.0437	0.0437	0.0437	0.0432(0)
$(0, 2^0, 0)$	0.0860	0.0860	0.0859	0.0862(1)
$(0, 2^2, 0)$	0.0875	0.0875	0.0874	0.0867(5)
$(0, 0^0, 1)$	0.0048	0.0048	0.0048	0.0047(1)
$(0, 1^1, 1)e$	0.0492	−0.2169	0.0362	
$(0, 1^1, 1)f$	0.0492	0.0492	0.0492	
$(0, 2^0, 1)$	0.0919	0.0919	0.1263	
$(0, 2^2, 1)e$	0.0937	0.0937	0.0936	
$(0, 2^2, 1)f$	0.0937	0.0937	0.0991	
$(1, 0^0, 0)$	−0.0321	−0.0321	−0.0321	−0.0322(0)
$(1, 1^1, 0)$	0.0122	0.0122	0.0122	
$(1, 2^0, 0)$	0.0553	0.0553	0.0551	
$(1, 2^2, 0)$	0.0566	0.0566	0.0565	

[a] Obtained from squared transition dipoles for rotational transitions (cf. Equation (2.100) and Equation (2.101)) up to the quoted $J_{\max}$.
[b] Experimental values from [256, 289].
[c] For the $(0, 0^0, 0)$ the quoted values correspond to the dipole moment in the vibrational ground state μ_0.

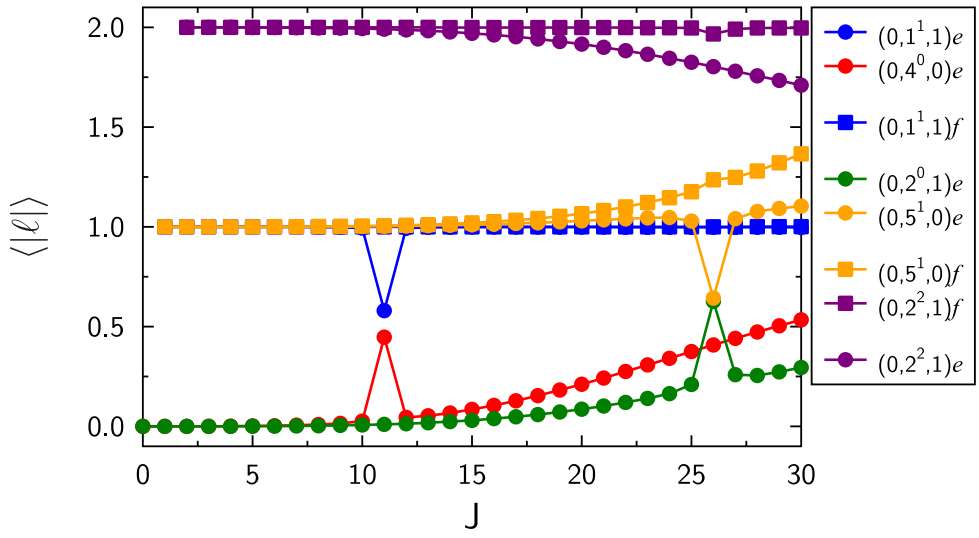

Figure 3.7: J dependence of the expectation value $\langle|\ell|\rangle$ for HCN rovibrational states involved in local Coriolis resonances (v_1, v_2^ℓ, v_3) // $(v_1, (v_2 + 3)^{\ell\pm1}, v_3 - 1)$.

theoretical vibrational correction of $\Delta\mu_0 = \mu_e - \mu_0 = -0.0293$ D is obtained. By adding the latter value to the experimental vibrational ground state dipole moment an equilibrium dipole moment of $-3.0145(3)$ D can be derived, where the error in parentheses is obtained by assuming a conservative error of 1 % in $\Delta\mu_0$. This value is slightly larger than the Comp I equilibrium dipole moment of -3.0127 D but agrees perfectly with the value of $-3.0146(5)$ D derived by Botschwina *et al.* [58]. The latter was obtained in a similar mixed experimental/theoretical approach by calculating $\Delta\mu_0$ based on the fitted PEF of Carter, Mills and Handy and an EDMF calculated using fc-CCSD(T) and a basis set of quadruple-zeta quality.

The calculated dipole moments of the $(0, v_2^\ell, 1)$ states with $v_2 > 0$ show signs of local anharmonic resonances through a strong dependence of the obtained $\Delta\mu_v$ on the number of analysed rotational transitions which differs between the e and f components. This can be understood from Figure 3.7. There, expectation values of the vibrational angular momentum quantum number $\langle|\ell|\rangle$ are depicted which have been shown [292,293] to provide a good indicator of the strength of Coriolis interactions. For the $(0, v_2^\ell, 1)$ states in question and the perturber states $(0, (v_2+3)^{\ell\pm1}, 0)$ $\langle|\ell|\rangle$ is given in Figure 3.7 up to $J = 30$. The $(0, 1^1, 1)e$ state shows a local and pronounced anharmonic interaction with the $(0, 4^0, 0)$ state between $J = 10$ and 12 which results in the drastic change of the fitted dipole moment difference in the former state from 0.0492 to -0.2169 D. The crossing point has also been determined by Mellau [17] to occur at $J = 10$ which agrees with the present results. Similarly, local resonances are predicted for the $(0, 2^0, 1)$ and $(0, 2^2, 1)f$ which interact with the e and f component of $(0, 5^1, 0)$, respectively, at $J = 26$ (experimentally determined avoided crossing [17] at $J = 25$ and $J = 26$, respectively). The remaining variation of $\langle|\ell|\rangle$ with J observed in Figure 3.7 can be attributed to normal ℓ-type resonance which mixes rovibrational states with the same vibrational quantum numbers v_i but different ℓ.

Turning toward absolute rovibrational line intensities, in Table 3.8 the results obtained with the present composite EDMF are compared to experiment [18, 19, 21–24] and the recent calculations of Makhnev *et al.* [242] (columns 2-3 in Table 3.8). The latter study is based on a PEF fitted to experimental results and an EDMF obtained at the ic-MRCI/ACV5Z level of theory with all electrons correlated that further includes a relativistic correction. root mean squared relative errors (RMSRE) for various rovibrational bands in HCN are given. They are calculated using the Comp I PEF and composite EDMF with different numbers of lines considered (columns 4-7 in Table 3.8). On the one hand results are quoted that take all the available experimental intensities into account (column 6-7) and on the other hand RMSRE values for the same lines considered by Makhnev *et al.* [242] are given in column 4-5. Additionally, calculated and experimental band intensities

$$A_v = \sum_{(i,f)} A_{if} \tag{3.7}$$

obtained by summing over a sufficient number of individual line intensities within a band are presented (column 8-9). Quoting both the RMSRE of individual lines and A_v helps to distinguish between systematic errors in the prediction of certain intensities and errors in experimental mea-

Table 3.8: Comparison of calculated[a] and experimental individual line intensities (root mean squared relative errors RMSRE in %) and band intensities[b] A_v (in $cm^{-2}atm^{-1}$) for transitions in HCN.

	Ref. [242]		$J''_{max} = 20$		all exp. lines		A_v	
Band	RMSRE	N_{lines}	RMSRE[a]	N_{lines}	RMSRE[a]	N_{lines}	calc.	exp.
ν_1	1.24	40	2.31	40	2.20	67	230.6	225.7(2)
ν_2	1.48	50	1.31	50	4.16	85	261.5	266.4(2)
ν_3	16.58	19	10.26	19	9.80	62	0.1108	0.1006
$\nu_1 + \nu_2 - \nu_2$	5.14	76	5.06	76	9.53	107	13.24	13.27
$2\nu_2^0$	0.98	40	1.15	40	6.13	59	31.00	30.82(5)
$2\nu_2^0 - \nu_2$	5.80	36	5.79	37	10.01	48	4.08	4.15
$2\nu_2^2 - \nu_2$	6.59	45	4.63	45	10.15	114	12.09	12.69
$3\nu_2^1 - \nu_2$	4.35	68	4.74	68	5.81	70	3.289	3.289
$2\nu_2^2$	6.74	37	8.07	37	10.99	67	0.2189	0.2356
$3\nu_2^3$	15.39	14	11.99	14	18.33	42	$2.370 \cdot 10^{-4}$	$2.210 \cdot 10^{-4}$
$\nu_1 + \nu_2^2$	23.95	19	23.02	19	25.97	38	$2.307 \cdot 10^{-4}$	$1.963 \cdot 10^{-4}$
$\nu_2^2 + \nu_3$	14.10	30	15.55	30	15.53	49	$2.282 \cdot 10^{-3}$	$2.699 \cdot 10^{-3}$

[a] Obtained from calculations using the Comp I PEF and composite EDMF.
[b] Calculated by summation of individual line intensities. For bands with quoted experimental uncertainties the calculated A_v values employ line intensities up to $J = 50$. All other experimental and theoretical band intensities obtained by summing up the available experimental intensities and the corresponding theoretical results, respectively.

surements. The latter will lead to differences in the RMSRE and the relative error of the calculated A_v with respect to experiment.

The strongest bands in the $H^{12}C^{14}N$ spectrum at about 296 K are the bending [24] and CH stretching fundamental [24]. Graphical comparisons of the composite results and the experimental line intensities for ν_1 and ν_2 are provided in Figure 3.8. The RMSRE of the present work amounts to about 2.2 % for ν_1 irrespective of the number of lines considered and the calculated band intensity of 230.6 $cm^{-2}atm^{-1}$ is in error by that same amount. Results for ν_1 of Makhnev *et al.* [242] are slightly better with a RMSRE of 1.24 % for the lowest 20 transitions in each the P- and the R-branch. For the bending fundamental ν_2 the largest errors are observed for high J'' lines. This leads to the difference in the calculated RMSRE values of 1.32 % and 4.16 % when considering the 50 lowest ($J''_{max} = 20$) and all 85 line intensities reported by Smith *et al.* [24]. Furthermore, the calculated band intensity of 261.5 $cm^{-2}atm^{-1}$ agrees to within 1.9 % with the experimental value [24].

The observed differences between calculated RMSRE from different sets of line intensities on the one hand and the error in the band intensities is especially pronounced for the weaker bending overton ν_2^0 ($\Delta\ell = 0$) and hot bands associated with ν_1, ν_2 and $2\nu_2$. The overtone $2\nu_2^0$ presents an extreme example. Considering 40 lines with $J''_{max} = 20$ yields an RMSRE of 1.15 % which increases to 6.13 % upon inclusion of the remaining 19 lines reported in Ref. [22]. Then again, the calculated and experimental band intensities agree to within 0.6 %. A closer look at the experimental results reveals that the measured P(30) and P(31) intensities are responsible for the almost sixfold

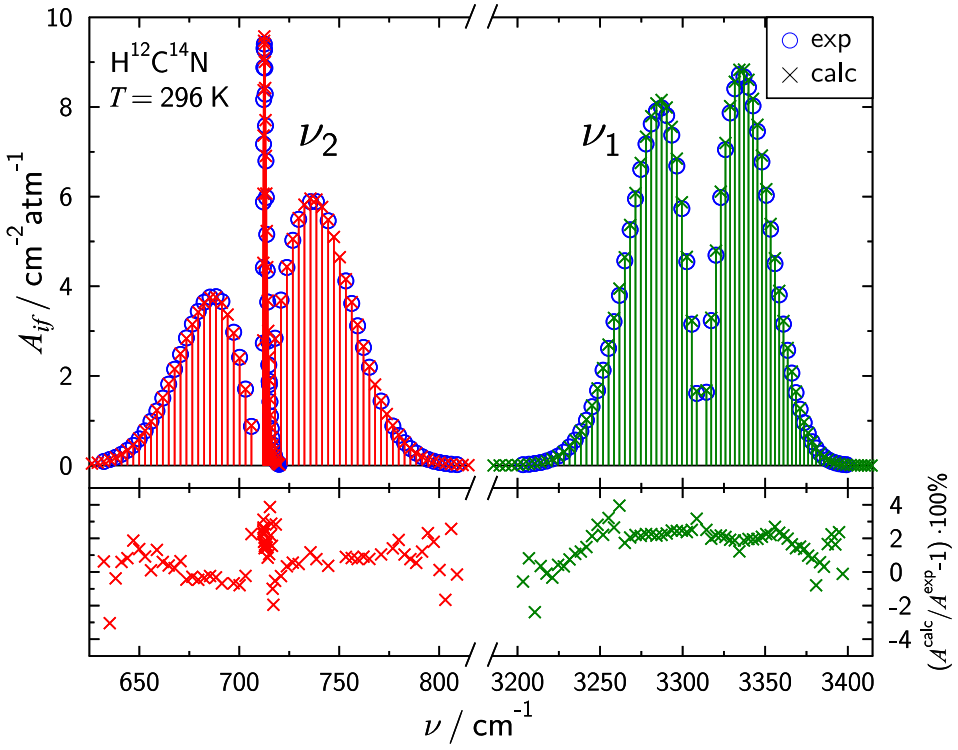

Figure 3.8: Comparison of experimental [21,24] and calculated absolute intensities for the bending (ν_2) and CH-stretching (ν_1) fundamental bands in $H^{12}C^{14}N$ at $T = 296$ K.

increase in the RMSRE. The former line deviates by as much as 43.5 % from the present *ab initio* value of $7.674 \cdot 10^{-3}$ cm^{-2}atm^{-1}. This clearly indicates an error in the experimental determination considering the overall accuracy of the composite results.

The CN stretch fundamental ν_3 of HCN deserves special attention. This band is exceptionally weak [18], which can be understood in the DHA by considering the contributions to the dipole moment derivative with respect to the normal coordinate Q_3 (in atomic units) according to

$$\begin{aligned} \left(\frac{\partial \boldsymbol{\mu}}{\partial Q_3}\right)_e &= \mathrm{L}_{13}\left(\frac{\partial \mu_\parallel}{\partial \Delta r}\right)_e + \mathrm{L}_{33}\left(\frac{\partial \mu_\parallel}{\partial \Delta R}\right)_e \\ &= 0.0038 \cdot (-0.2442) + 0.0086 \cdot 0.0763 \\ &= -0.0003, \end{aligned} \tag{3.8}$$

where L_{ij} are elements of the orthogonal matrix that transforms normal coordinates to internal coordinates. The presented numerical values are for $H^{12}C^{14}N$ and obtained from the Comp I PEF that defines the L_{ij} and the composite EDMF whose linear terms in Δr and ΔR give the required dipole derivatives. A near cancellation of the terms in Equation (3.8) is observed resulting a small value for the DHA transition dipole moment of $\mu_3^{\mathrm{DHA}} = -0.0068$ D. The further peculiar feature

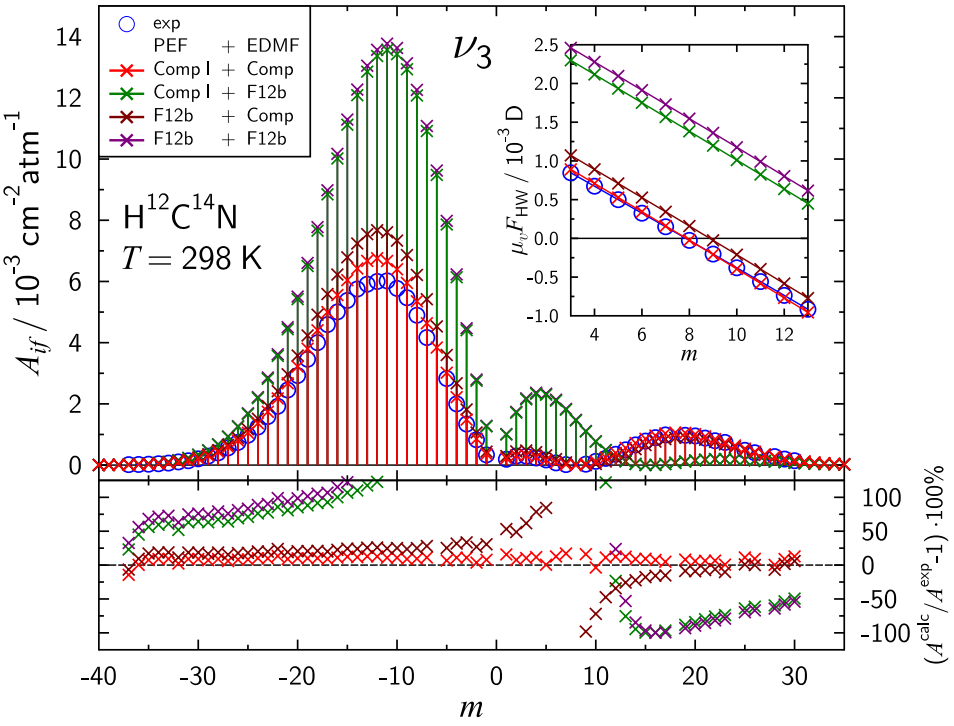

Figure 3.9: Comparison of experimental [18] and calculated absolute intensities for the CN-stretching (ν_3) fundamental band in $H^{12}C^{14}N$ at $T = 298$ K. Calculated results employ the rovibrational wavefunctions obtained with the Comp I and F12b PEFs in combination with the composite EDMF or the basic F12b contribution. In the lower panel the relative errors of calculated absolute intensities are given. For the combinations employing the F12b EDMF errors in the Range $m = -10$ to $m = 10$ are off scale. The inset depicts the m dependence of the Herman-Wallis factors obtained from the parameters of Table 3.9 in the R-branch region of the experimental intensity gap.

of the ν_3 band is a minimum in intensity of the R-branch which is due to the squared transition dipole moment μ_{if}^2 becoming zero for a certain value of m. This has been explained both experimentally [18] and theoretically [58] by the combination of a low vibrational transition moment and a relatively large first Herman-Wallis coefficient A_1 (cf. Equation (2.101)). A theoretical treatment therefore requires a highly accurate PEF and EDMF to reproduce this features.

A stick spectrum representation of the HCN ν_3 band is given in Figure 3.9. Theoretical absolute intensities obtained from different combinations of the PEF and EDMF employed in the variational calculations are compared to the experimental results of Maki and coworkers [18]. The best agreement is provided by the Comp I PEF + composite EDMF combination. The RMSRE calculated over the whole band system yields a value of 9.8 % which is significantly better than the recent theoretical study by Makhnev *et al.* [242] with a value of 16.58 % obtained from the P-branch transitions only. Changing only the PEF to F12b and thus the rovibrational wave func-

Table 3.9: Calculated[a] and experimental vibrational transition dipole moment μ_3 (in D), Herman-Wallis coefficients A_i and position of the R-branch intensity minimum for the ν_3 CN-stretching fundamental transition in HCN.

PEF	EDMF	μ_3	A_1	$10^3 A_2$	$10^3 \mu_3 A_1$	$R_{min}(J)$
F12b	F12b	0.00300	−0.0597	−0.11	−0.1791	R(15)
Comp I	F12b	0.00284	−0.0632	−0.12	−0.1795	R(14)
F12b	Comp	0.00161	−0.1108	−0.23	−0.1784	R(8)
Comp I	Comp	0.00143	−0.1250	−0.26	−0.1788	R(7)
	exp[b]	0.00136(1)	−0.1254(2)	−0.25(1)	−0.1708	R(7)

[a] Obtained from least-squares fits of squared transition dipoles according to Equation (2.100) and Equation (2.101) in the range $|m| \leq 30$.
[b] Experimental results from Ref. [18] with one standard deviation uncertainty in the last digit given in parentheses.

tions worsens the results especially for the P-branch transitions but the overall shape of the band is still reasonably reproduced. In contrast, changing the EDMF has a much more dramatic effect. P-branch transitions are obtained with intensities that are too large by a factor of about 2 and the minimum in the R-branch is shifted to higher m.

In order to provide a more detailed analysis, the calculated transition dipole moments in the range $|m| \leq 30$ were least-squares fit according to Equation (2.100) and 2.101. The results of these fits for the 4 PEF/EDMF combinations of Figure 3.9 are given in Table 3.9 together with the experimental results reported by Maki and coworkers [18]. Additionally the position of the R-branch minimum is quoted. Clearly, best performance is provided by the composite approach (PEF & EDMF). The transition dipole moment μ_3 is calculated to be 0.00143 D only 5 % larger than the experimental value of 0.00136(1) D. Comparing the former value to the DHA result of −0.0068 D shows that anharmonicity effects are important for a quantitative description of the ν_3 intensity. The experimental values for the first and second Herman-Wallis coefficients A_1 and A_2 are almost perfectly reproduced by the composite based calculations. Consequently, the theoretical and experimental [18] R-branch intensity minimum is observed for the same line, namely R(7). The calculations by Makhnev *et al.* [242] placed the minimum to low at R(6). Results obtained with the F12b EDMF are much worse with too large μ_3 values of and too small Herman-Wallis coefficients. Interestingly, the slope of the effective transition dipole moment curves $\sqrt{\frac{\mu_{if}^2}{F_{\mathrm{HL}}}}$ with respect to m, which is given by the product $\mu_3 A_1$, is nearly independent of the PEF/EDMF combination. The individual values vary by only 0.4 % between the different combinations and the mean value of $-0.1790 \cdot 10^{-3}$ D. This can also be observed from the inset of Figure 3.9 where the calculated and experimental effective transition dipole moments are depicted in the region of the R-branch minimum. The experimentally derived slope is $-0.1708 \cdot 10^{-3}$ D [18] about 5 % lower than the theoretical value due to the difference in the transition dipole moment μ_3. According to the work of Watson [238] on the Herman-Wallis factor, by employing a perturbational expansion of the dipole

operator [187] the product $\mu_3 A_1$ for the ν_3 band can be calculated by

$$\mu_3 A_1 = -2 \left(\frac{2B_\mathrm{e}}{\omega_3} \right)^{\frac{3}{2}} \zeta_{12} \mu_\mathrm{e} + 4B_\mathrm{e} \frac{\sqrt{\omega_3 \omega_2}}{\omega_3^2 - \omega_2^2} \zeta_{32} \mu_2 \,, \tag{3.9}$$

where μ_2 is the DHA transition dipole moment for the bending fundamental ν_2. The perturbational result calculated with the Comp I PEF and the composite EDMF is $-0.1803 \cdot 10^{-3}$ D in good agreement with the variational result. Since spectroscopic parameters related to the PEF (B_e and ω_i) as well as the EDMF (μ_e and μ_2) contribute to $\mu_3 A_1$ the observed independence can be attributed to a compensation effect when changing the PEF and/or EDMF.

3.2 Tricarbon - C_3

This Section is partly reproduced from References:

[294] B. Schröder, P. Sebald
High-level theoretical rovibrational spectroscopy beyond fc-CCSD(T): The C_3 molecule,
The Journal of Chemical Physics, **2016**, 7, 044307 (DOI: 10.1063/1.4940780),

[29] B. Schröder, K. D. Doney, P. Sebald, D. Zhao, H. Linnartz,
Stretching our understanding of C_3: Experimental and theoretical spectroscopy of highly excited $n\nu_1 + m\nu_3$ states ($n \leq 7$ and $m \leq 3$),
The Journal of Chemical Physics, **2018**, 149, 014302 (DOI: 10.1063/1.5034092),

with the permission of AIP Publishing. All theoretical computations were calculated on my own. The discussion of the equilibirum bond length in C_3 has been extended to include the recent results of Breier *et al.* [295]. Implementation of the integrated vibrational densities into C8VPRO was performed by P. Sebald. The spectra were recorded, assigned and fitted by Kirstin D. Doney of the Linnartz group.

3.2.1 Introduction

Tricarbon C_3 ($\tilde{X}^1\Sigma_g^+$) is an abundant species in astronomical environments, such as cool carbon stars and interstellar clouds, and has been identified in a number of sources [296–306]. The first astronomical observation of C_3 resulted from an investigation on the spectral lines of the Tebbutt comet around 4050 Å [296]. Unambigous assignment of these observations to the C_3 $\tilde{A}^1\Pi_u - \tilde{X}^1\Sigma_g^+$ electronic transition took more than 80 years. Spectral features of the 4050 Å band were first observed by Raffety [307] and Herzberg [308] in laboratory studies on discharges through methane, the latter initially attributing it CH_2. This was followed by the work of Douglas [168] who correctly assigned the 4050 Å band to C_3 based on a study of the spectrum obtained from discharges through ^{13}C labeled methane. Finally, flash photolysis of diazomethane carried out by Herzberg and coworkers [309, 310] revealed the origin of the bands as being due to the $\tilde{A}^1\Pi_u - \tilde{X}^1\Sigma_g^+$ electronic transition. Compared to other pure carbon chains with an odd number of carbon atoms (cf. Ref. [311] and references therein), C_3 is very "floppy", as seen by the extremely low lying bending vibrational frequency (ν_2) of 63 cm^{-1} [312]. As such, C_3 has attracted the interest of both experimentalists [295, 312–323] and theoreticians [25, 26, 84, 324]. Excellent accounts of earlier work on C_3 were compiled in the reviews by Weltner and Van Zee [325] as well as Van Orden and Saykally [326] and the reader is referred to these articles for an overview.
The first high-resolution spectroscopic study on C_3 was reported by Matsumura *et al.* in 1988 [313]. Using IR diode laser spectroscopy 28 lines within the antisymmetric stretching vibration ν_3 band

were observed and the band origin was determined to be 2040.0198(8) cm^{-1} with the error (1σ) in terms of the last significant digit being given in parentheses. Only one year later the same group extended their measurements of the ν_3 fundamental [314] and additionally detected the associated hot bands $\nu_2+\nu_3-\nu_2$, $2\nu_2+\nu_3-2\nu_2$ originating from excited bending vibrational states as well as the combination band $2\nu_2+\nu_3$. In 1990 Schmuttenmaer *et al.* were able to observe the exceptionally low-lying bending fundamental transition ν_2 at 63.416529(40) cm^{-1} by tunable Far-IR laser spectroscopy of jet-cooled C_3 molecules. Recently, Breier *et al.* [295] extended the ν_2 spectrum of the main C_3 species with spectra of all possible ^{13}C isotopologues using a terahertz-supersonic jet spectrometer in combination with a laser ablation source. Information on the IR inactive symmetric vibrational modes is available from studies on electronic transitions in the early 1990s employing laser induced flourescence and stimulated emission pumping spectroscopy [315–319]. In 2005 Zhang *et al.* [321] provided an accurate experimental characterisation of the first excited symmetric stretch vibrational state, yielding $\nu_1 = 1224.4933(29)$ cm^{-1} with three standard deviations in the last significant digit given in parentheses. Krieg *et al.* [322] reported a high-resolution study on the spectrum of C_3 in the 3 μm region. An optical parametric oscillator (OPO) was employed to probe C_3 molecules in a supersonic jet expansion enabling the detection of the $\nu_1+\nu_3$ combination band and the associated hot band $\nu_1+\nu_2+\nu_3-\nu_2$.

Besides the work of Breier *et al.* [295] on the ν_2 fundamental of C_3 isotopologues, experimental spectroscopic information on ^{13}C substituted C_3 is rather scarce. Moazzen-Ahmadi and McKellar [320] detected the the ν_3 fundamental of $^{13}C_3$ and $^{13}C^{12}C^{12}C$ and the $\nu_2+\nu_3-\nu_2$ hot band of $^{13}C_3$ around 5 μm by tunable diode laser spectroscopy in a hollow-cathode discharge. In their 2013 study on the $\nu_1+\nu_3$ transition of $^{12}C_3$ Krieg *et al.* [322] were also able to detect this transition for the $^{13}C^{12}C^{12}C$ and $^{12}C^{13}C^{12}C$ isotopologues, providing the first spectroscopic information for the latter species. Finally, following an extensive study of the 4051 Å electronic transition, Haddad *et al.* [323] quoted for the first time the ground state rotational constants for all six ^{12}C and ^{13}C isotopologues.

Earlier *ab initio* studies and experimental analysis suggested that the C_3 PES might show a small barrier to linearity [327]. Even more, Matsumura *et al.* [313] concluded from an analysis of the ν_3 fundamental spectrum that this barrier increases when the antisymmetric stretching vibration is excited. This was based on the observation that the rotational parameter B_v *increases* relative to the ground state parameter when the antisymmetric stretching vibration is excited. These observations motivated further theoretical investigations of C_3. In 1992 Jensen and coworkers [25] published a study of the C_3 ground state PES. This PES is based on CASSCF calculations with a basis set that comprises 102 cGTOs. The rovibrational term energies were subsequently calculated using the Morse oscillator rigid bender internal dynamics (MORBID) Hamiltonian [328]. For the three singly excited vibrational states term energies (in cm^{-1}) of 1191.9 (ν_1), 70.2 (ν_2) and 2007.3 (ν_3) were calculated. Compared to experiment they deviate by -34.7, 6.8 and -32.7 cm^{-1}, respectively. Two years later Botschwina and coworkers [26] published an extensive theoretical study of C_3 based on CCSD(T) coupled cluster calculations and a basis set of approximately quadruple-

zeta quality. The errors in the fundamental transition frequencies amount to -5.7 (ν_1), 0.9 (ν_2) and 0.6 (ν_3) obtained from DVR calculations [220]. However, the very good agreement in ν_2 and ν_3 is due to a fortuitous error compensation in the electronic structure calculations. Both these theoretical studies [25, 26] and the experimental work by Northrup [27] conclusively showed that C_3 has a linear equilibrium structure. The strong coupling between the stretching and the bending vibrational motions in C_3 which is responsible for the observed uncommon spectral features was clearly demonstrated by theory and experiment alike. Because of this unusual PES, perturbational methods even when employing an accurate PES were not able to reproduce experimental spectroscopic parameters with the same level of accuracy as seen for other molecules. Ahmed *et al.* [324] published a PES that employs MRCI+Q calculations with a VTZ basis set. The *ab initio* results are rather poor with differences in the fundamentals amounting to as much as -60.4, -27.3 and -44.2 cm^{-1} for ν_1, ν_2 and ν_3, respectively. These deficiencies were partly remedied by fitting the potential to experimental data reducing the above errors to -5.2, -2.9 and -2.0 cm^{-1}, respectively. A thorough theoretical study of C_3 was also performed by Rocha and Varandas [84]. They constructed a global C_3 PES within the double many-body expansion framework taking into account Jahn-Teller and pseudo-Jahn-Teller interactions occuring in the vicinity of equilateral triangular geometries. The PES is based on ic-MRCI calculations with a full valence CASSCF reference and employ the AVTZ basis set. Although this PES correctly describes the overall topology of the electronic ground state of C_3, the agreement of the calculated rovibrational term energies is rather poor. For the 53 calculated levels a RMS deviation of 50.4 cm^{-1} was obtained. While the agreement for the pure bending states is quite good, the description of the stretching vibrations is less accurate. The calculated term energies of the first excited symmetric and antisymmetric stretching vibrational states differ from the experimental values by as much as 63.2 and 53.9 cm^{-1}, respectively. One should note, however, that the latter quantities were not the main focus of that work.

Clearly the rovibrational spectrum of C_3 is dominated by anharmonic effects. Therefore, a theoretical spectroscopic treatment of C_3 will require both an accurate PES and an accurate treatment of the rovibrational problem. Section 3.2.2 summarizes the *ab initio* methods employed to construct such a PES for C_3 and Section 3.2.3 presents the results of extensive electronic structure and variational rovibrational calculations on C_3. Special attention on the interplay between experiment and theory will also be given, exemplified by a combined study of the C_3 spectrum in the region of the $\nu_1 + \nu_3$ combination band (Section 3.2.4).

3.2.2 Composite *ansatz*

For C_3 slightly different basis sets for some of the contributions employed for HCN were used enabled by the higher symmetry of the system ($\boldsymbol{D}_{\infty h}$(M)). The detailed components of the PEF are:

- Explicitly correlated fc-CCSD(T*)-F12b/AV5Z (abbreviated F12bs) calculations provide the

basic contribtution to the PEF. The AO basis set is combined with the sets AV5Z/OPTRI, AV5Z/JKFIT and AV5Z/MP2FIT [281–283] to provide the CABS and DF set. A geminal β of 1.5 $Å^{-1}$ is employed as recommended by Peterson and coworkers for AV5Z basis sets [124].

- The CV of the six inner shell electrons with themselves and the 12 valence electrons is obtained with a ACV5Z basis set (543 cGTOs) from conventional CCSD(T) as outlined in Section 2.2.5.

- SR effects are obtained from DKH2 CCSD(T) calculations using AVQZ-DK and AVQZ basis sets.

- Three HC contributions are included in the C_3 PEF:

  – The perturbative quadruples and full triples correction from the (Q)-(T) contribution is calculated as the CCSDT(Q) – CCSD(T) energy difference using a VQZ basis set

  – The tendency of CCSDT(Q) to overestimate the full CCSDTQ correlation energy [73] is corrected by the Q-(Q) contribution using a VTZ(*spd*) basis set (without f-functions on carbon).

  – Effects due to pentuple excitations are obtained from the P-Q contribution and a VDZ basis set.

The absence of light hydrogen atoms in the C_3 molecule justifies the neglect of the DBOC correction. Nevertheless, from all electron CCSD/CVQZ calculations on $^{12}C_3$ DBOC corrections to the equilibrium bond length R_e of +0.00004 Å and the harmonic vibrational frequencies of -0.03, -0.16, and -0.08 cm^{-1} for ω_1, ω_2 and ω_3, respectively, are calculated. This is reasonably well below the desired accuracy. Further non-adiabatic corrections (beyond DBOC) should have an even lower impact and, therefore, none of these corrections are included.
An EDMF is also calculated at the fc-CCSD(T*)-F12b/AV5Z level of theory with the finite field approach outlined in Section 2.2.4 using a field strength in atomic units of ±0.0003 and local transformation to the Eckart system. No high-level corrections to the EDMF (cf. Section 3.1.2) were included. The experimental determination of absolute rovibrational intensities requires a precise knowledge of the concentration of absorbing molecules over the optical path length (compare also Equation (2.94)). In fact, uncertainties in the partial pressure of the absorber are one of the main sources of error in gas phase intensity measurements. Given the highly reactive nature of C_3 as well as the rather harsh conditions for producing this transient molecule, it is virtually impossible to determine reliable estimate of p in Equation (2.94) and thus absolute line intensities. However, the relative intensities of rovibrational transitions can be rather reliably obtained for such systems. Therefore, in order to give a sound qualitative picture of the intensities from *ab initio* calculations, the chosen level of theory appears to be sufficient.

3.2.3 Construction of an accurate PES for C_3

Electronic structure calculations

The basis set dependence of the equilibrium bond length R_e and the two harmonic stretching vibrational wavenumbers ω_1 and ω_3 is investigated in Table 3.10 Either standard or explicitly correlated frozen core coupled cluster theory up to non-iterative triples has been employed in the calculations. As observed in previous studies [173, 287, 329] very similar results are obtained by fc-CCSD(T)/AV5Z and fc-CCSD(T)-F12b/AVTZ. Likewise, only very small differences are observed between fc-CCSD(T)/AV7Z and fc-CCSD(T*)-F12b/AV5Z. Comparing the different values in the table, the results for both R_e and the harmonic stretching vibrational frequencies ω_i appear to be well converged for the fc-CCSD(T) series, so that no further extrapolation beyond AV7Z is required. Without the use of triples scaling, a slight underestimation of the bond length can be observed, resulting in an overestimation of ω_s. Although the effect is rather small, better agreement between large-basis set calculations and explicitly correlated CCSD(T) is obtained with use of the (T*) correction [173, 287, 329, 330].

Figure 3.10 displays the dependence of the C_3 bending potential on the AVnZ basis set size. Basis sets of at least AV5Z quality are needed in order to converge the bending potential in the range $0° \leq \theta \leq 90°$. The inset of Figure 3.10 depicts the low θ region of the potential energy curves up to 25°. With increasing basis set size the potential becomes flatter leading to tiny values of the harmonic bending vibrational frequency (e.g. $\omega_2 = 13.1$ cm^{-1} for AV7Z).

The significance of smaller contributions to R_e and ω_i $(i = 1, 3)$ of C_3 is quoted in Table 3.11 which includes the F12bs results (corresponding to fc-CCSD(T*)-F12b/AV5Z) in the first line. As expected, CV effects have the largest influence of all the contributions. The calculated CV

Table 3.10: Frozen core CCSD(T) and CCSD(T)-F12b equilibrium bond length (in Å) and harmonic stretching vibratonal frequencies (in cm^{-1}) of C_3. Reproduced from Ref. [28] with the permission of AIP Publishing.

Method	Basis	R_e	ω_1	ω_3
CCSD(T)	AVTZ	1.30174	1191.5	2090.8
	AVQZ	1.29816	1200.6	2097.2
	AV5Z	1.29733	1202.0	2099.5
	AV6Z	1.29705	1202.6	2100.3
	AV7Z	1.29687	1203.0	2100.9
CCSD(T)-F12b[a]	AVTZ	1.29785	1201.5	2098.9
	AVQZ	1.29673	1203.6	2101.8
	AV5Z	1.29666	1203.5	2101.8
CCSD(T*)-F12b[a]	AV5Z	1.29681	1202.7	2100.4

[a] Geminal exponents (in Å^{-1}) chosen are 1.2, 1.4 and 1.5 for AVTZ, AVQZ and AV5Z, respectively.

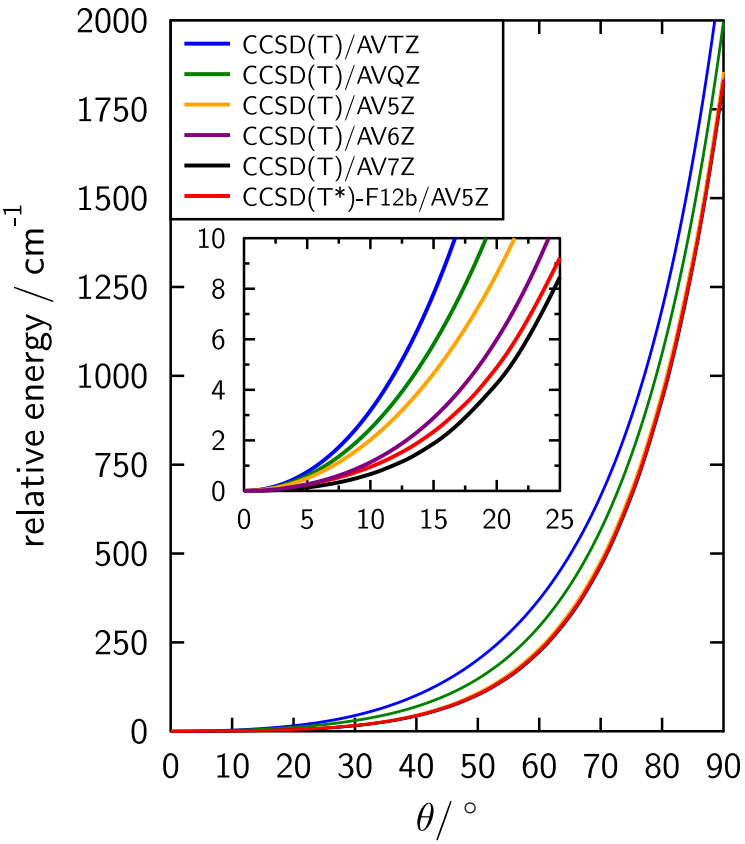

Figure 3.10: Basis set dependence of the C_3 bending potential. Reproduced from Ref. [28] with the permission of AIP Publishing.

Table 3.11: Influence of smaller contributions on the equilibrium bond length (in Å) and harmonic stretching vibrational fequencies (in cm^{-1}) of C_3. Reproduced from Ref. [28] with the permission of AIP Publishing.

Contribution	R_e	ω_1	ω_3
F12bs	1.29681	1202.7	2100.4
+ CV	−0.00349	+7.4	+10.8
+ SR	−0.00019	−0.3	−0.3
+ (Q)-(T)	+0.00103	−4.6	−15.1
+ Q-(Q)	−0.00029	+2.6	+4.4
+ P-Q	+0.00010	−0.7	+1.1
composite	1.29397	1206.7	2101.3

corrections $\Delta R_\mathrm{e} = -0.00349$ Å and $\Delta\omega_1 = +7.4$ cm^{-1}, respectively, are in reasonable agreement with the values reported by Mladenović *et al.* [26]. They obtained $\Delta R_\mathrm{e} = -0.00319$ Å and $\Delta\omega_1 = +6.0$ cm^{-1} from all electron CCSD(T) calculations compared to standard fc-CCSD(T) with a basis set of approximately ACVQZ quality. Scalar relativity leads only to slight, but still significant reductions in both R_e and ω_i. Among the contributions of higher-order electron correlation beyond CCSD(T), the difference (Q)-(T) plays the dominant role. The difference Q-(Q) corrects for the tendency of CCSDT(Q) to overestimate the effect of quadruples excitations. [73] The pentuples are still important when one is aiming at accuracies of $1 \cdot 10^{-4}$ Å in R_e and 1 cm^{-1} in the ω_i.

Figure 3.11 gives an impression of the dependence of the smaller contributions (CV, SR, (Q)-(T), Q-(Q) and P-Q) on the internal coordinates. In the upper part of Figure 3.11 the variation of the various contributions with ΔR (single CC stretch) is displayed. The above discussed effects of the contributions on R_e and the ω_i can be clearly observed.

The angular dependence of the smaller contributions is shown in the lower part of Figure 3.11. A blow up of the low θ region up to 50° is given as an inset. All contributions are rather small for low values of θ. However, considering the very flat bending potential they are still significant. The dominant contributions in this region are the CV and the Q-(Q) contribution. There is a drastic increase in the effects of quadruple excitations accounted for by the (Q)-(T) contribution. A maximum of 237 cm^{-1} in the relative (Q)-(T) contribution is observed for $\theta \approx 98°$. Such an increase in the effect of higher-order excitations indicates a higher multi-reference character. As has been shown by Rocha and Varandas, [84] there is a conical intersection in the region of $\theta = 120°$ on the C_3 ground state PES.

All contributions (denoted by the superscript α) are analytically represented as polynomials of the form

$$V^{(\alpha)} - V^{(\alpha)}_{ref} = \sum_{ijk} C^{(\alpha)}_{ijk} \Delta R_1^i \Delta R_2^j \theta^k \quad \text{(k: even)}\,. \tag{3.10}$$

In Equation (3.10), ΔR_i $(i = 1, 2)$ are the single CC bond stretching coordinates, θ measures the deviation from linearity and $C^{(\alpha)}_{ijk}$ are the coefficients determined through least-squares fits. All calculations employ the coordinate ranges -0.15 Å $\leq \Delta R_i \leq 0.20$ Å and $0° \leq \theta \leq 100°$. The recommended equilibrium bond length of Mladenović *et al.* [26] $R_\mathrm{e} = 1.2945$ Å is used as reference structure in the *ab initio* calculations.

Due to the strong stretch-bend coupling in C_3, the construction of the PES has to be carried out in a series of steps. The least-squares fits of the basic contribution include terms up to powers of 8 and 14 in ΔR_i and θ, respectively in the diagonal PES terms. Stretch-stretch coupling terms $C^{(\alpha)}_{ij0}$ were considered up to sextic order. For the stretch-bend coupling terms the following scheme was employed: for every even power in θ (up to eight) all single stretch-bend and stretch-stretch-bend coupling terms of type $C^{(\alpha)}_{ijk}$ with $i + j \leq 4$ were included. Fewer terms are needed to properly fit the smaller contributions. In order to obtain numerically stable results all contributions are put together from individual least-squares fits of the diagonal, stretch-stretch coupling and stretch-bend

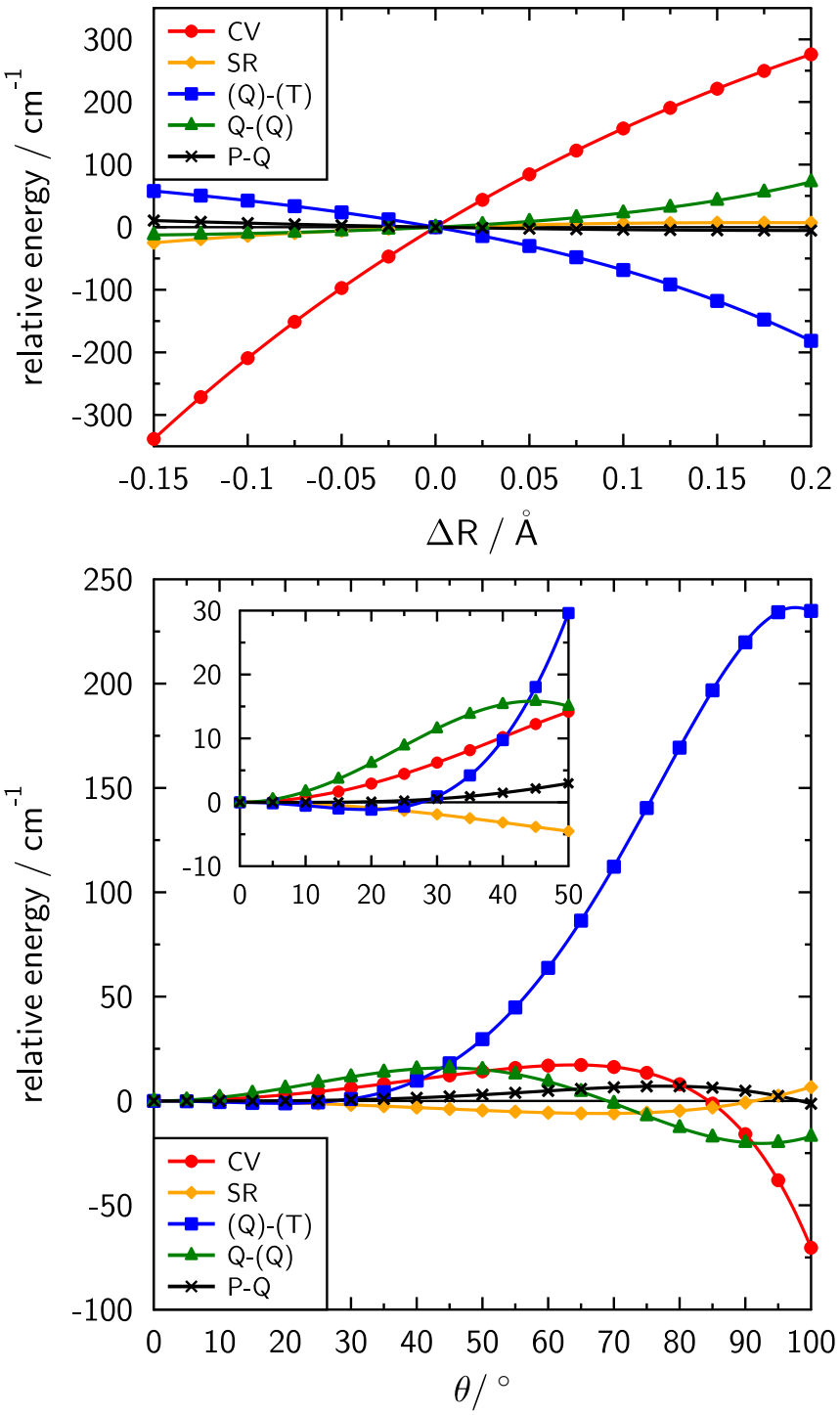

Figure 3.11: Dependence of the smaller contributions on the internal coordinates ΔR and θ. Reproduced from Ref. [28] with the permission of AIP Publishing.

coupling part. The standard deviation of the fit of the combined basic contribution is 0.05 cm^{-1}, which is better by a factor of about 40 compared the most accurate PES in the literature reported by Mladenović *et al.* [26]. The parameters of the various relative contributions $V^{(\alpha)} - V_{ref}^{(\alpha)}$ are supplied in Appendix B (Table B.1 and B.2). After summation of the individual contributions the resulting polynomial is transformed to its true minimum. The final composite PES thus obtained is given in Table B.3.

The EDMF of C_3 is constructed from calculations at 372 symmetry-unique nuclear configurations. Least-squares fits of the parallel ($\mu^{\parallel}$) and perpendicular ($\mu^{\perp}$) component of the electric dipole moment vector according to

$$\mu^{\parallel} = \sum_{ijk} D_{ijk}^{\parallel} \tilde{S}_1^i \tilde{S}_3^j \theta^k \quad j\text{: odd, } k\text{: even} \tag{3.11}$$

and

$$\mu^{\perp} = \sum_{ijk} D_{ijk}^{\perp} \tilde{S}_1^i \tilde{S}_3^j \theta^k \quad j\text{: even, } k\text{: odd} \tag{3.12}$$

have been carried out. In Equation (3.11) and (3.12) the coordinates $\tilde{S}_1$ and $\tilde{S}_3$ are defined as $\tilde{S}_1 = 2^{-1/2}(\Delta R_1 + \Delta R_2)$ and $\tilde{S}_3 = 2^{-1/2}(\Delta R_1 - \Delta R_2)$. Dipole moments are evaluated in the coordinate ranges $-0.1\text{Å} \leq \tilde{S}_1 \leq 0.2$ Å, $0.00\text{Å} \leq \tilde{S}_3 \leq 0.15$ Å and $0° \leq \theta \leq 60°$. The coefficients of the fits are provided in Table B.4.

Spectroscopic parameters

The PES and EDMF in Table B.3 and Table B.4 are employed in variational calculations of low-lying rovibrational states and electric transition dipole moments. Following the study on the "floppy" CNC^+ cation [167] a two step approach is employed. First, the Rvib3 program developed by Carter and Handy [203, 204] is used to calculate the term energies. By optimizing the basis set and the size of the final rovibrational Hamiltonian matrix a convergence of all rovibrational states of interest to within 10^{-4} cm^{-1} is achieved. Similar to the calculations on CNC^+ [167] the convergence of the rotational levels depends strongly on the size of the final rovibrational Hamiltonian matrix.

In a second step rovibrational wave functions are calculated using Sebald's C8vpro program [210]. Very large basis sets of harmonic oscillator/rigid rotor product functions (about 4000 per $K = \ell$) are required to obtain converged results for C_3. This due to the curvilinear nature of the bending vibration which is difficult to describe using rectilinear normal modes and a large number of basis functions that couple the bending and symmetric stretching vibration are needed. Additionally one-dimensional contractions of the bending basis functions are employed. Convergence of the wavefunction is monitored by comparing the calculated term energies for the states of interest with those of the Rvib3 program. Agreement to within some hundreths of a wavenumber or better

is observed. Squared transition dipole moments μ_{if}^2 between rovibrational states are evaluated following the procedure outlined in Section 2.3.4 up to a rotational quantum number of $J = 75$.
The spectroscopic parameters obtained from fitting the term energies calculated with both programs show only very small differences. In contrast, much larger differences are obtained when changing the range of J values considered in the fits (see below). This is a common phenomenon when even low lying vibrational states are influenced by avoided crossings or highly anharmonic vibrations are present. This issue has been studied in considerable detail for example in [293]. Therefore, only term energies calculated with RVIB3 in the range $J = 0$ to 30 are considered for the determination of spectroscopic parameters according to Equation (2.92) and Equation (2.93). Table 3.12 summarizes the calculated vibrational term energies and rotational constants as well as the quartic and sextic centrifugal distortion constants obtained for $^{12}C_3$. Where available experimental values are given for comparison. However, due to differences in the fitting procedures [314] care has to be taken when comparing some of the parameters.
For the vibrational ground state, the calculated rotational constants are $B_0 = 0.43063$ cm^{-1}, $D_0 = 1.537 \cdot 10^{-6}$ cm^{-1} and $H_0 = 1.77 \cdot 10^{-10}$ cm^{-1}. The relative deviations from the experimental values amount to no more than 0.01%, 4% and 33% for B_0, D_0 and H_0,respectively. Notice that the sextic centrifugal distortion parameter H_v is strongly dependent on the number of rovibrational states included in the fit. For example, a fit of the rovibrational ground state in the range $0 \leq J \leq 20$ yields $H_0 = 2.11 \cdot 10^{-10}$ cm^{-1}. However, the above mentioned level of agreement is an obvious improvement relative to previous theoretical works. Mladenović *et al.* [26] obtained $B_0 = 0.42767$ cm^{-1} (0.67 %) and Jensen *et al.* [25] calculated a B_0 of 0.4191 cm^{-1} (2.64 %) with the relative deviation given in parentheses.
For the first excited state of the bending vibration $(0, 1^1, 0)$ a vibrational term energy of 63.26 cm^{-1} is calculated only 0.16 cm^{-1} lower compared to experiment [322]. The B_v is overestimated by 0.007 %. Centrifugal distortion parameterss in the $(0, 1^1, 0)$ state differ from experiment [322] by 0.6 % and 2 % for D_v and H_v, respectively. The deviation from experiment [314] of the vibrational term energies G_v of the $\ell = 0$ and $\ell = 2$ components of the first overtone of the bending vibration $(0, 2^\ell, 0)$ are calculated to be 0.04 and -0.18 cm^{-1}, respectively. Agreement between the present and the experimental rotational parameters B_v, D_v and H_v is again excellent.
Calculate vibrational term energies for the two first excited stretching vibrational states are 1224.57 and 2039.60 cm^{-1} for ν_1 and ν_3, respectively. The corresponding absolute deviations from experiment are uniformly below 1 cm^{-1}. Calculated rotational constants for the two states show relative deviations of no more than 0.03 %. While the centrifugal distortion constants of the $(0, 1^1, 0)$ and $(1, 0^0, 0)$ states are in good agreement with experiment, the situation is slightly different for the first excited antisymmetric stretching vibrational state, again especially in case of H_v. Compared to experiment the calculations underestimate H_v by about 25 %. This is due to two reasons: the experimental fit includes terms up to M_v (tenth order in J) and covers the range P(40) to R(52) [314]. Refitting the line positions reported by Kawaguchi *et al.* [314] in the range P(30) to R(30) yields $B_v = 0.43571$ cm^{-1}, $D_v = 4.262 \cdot 10^{-6}$ cm^{-1} and $H_v = 7.57 \cdot 10^{-10}$ cm^{-1} now in

Table 3.12: Calculated and experimental[a] spectroscopic parameters (in cm^{-1}) of $^{12}C_3$. Reproduced from Ref. [28] with the permission of AIP Publishing.

State	G_v	B_v	$10^6 D_v$	$10^{10} H_v$
$(0, 0^0, 0)$	1705.06[b]	0.43063(0.43057)	1.537(1.471)	1.77(1.33)
$(0, 1^1, 0)$	63.26(63.42)	0.44243(0.44240)	2.349(2.336)	2.49(2.44)
$(0, 2^0, 0)$	132.84(132.80)	0.45155(0.45163)	2.349(2.57)	2.00
$(0, 2^2, 0)$	132.89(133.07)	0.45306(0.45304)	2.483(2.623)	2.79
$(0, 3^1, 0)$	207.66	0.46044	2.755	2.13
$(0, 3^3, 0)$	208.36	0.46284	3.256	2.72
$(1, 0^0, 0)$	1224.57(1224.49)	0.42501(0.42495)	0.719(0.52)	0.45
$(1, 1^1, 0)$	1315.19	0.43417	1.194	0.84
$(1, 2^0, 0)$	1404.87	0.44282	1.577	1.09
$(1, 2^2, 0)$	1408.79	0.44309	1.622	1.16
$(1, 3^1, 0)$	1498.29	0.45116	1.939	1.61
$(1, 3^3, 0)$	1505.51	0.45175	1.976	1.09
$(0, 0^0, 1)$	2039.60(2040.02)	0.43559(0.43570)	4.165(4.312)	7.42(9.84)
$(0, 1^1, 1)$	2078.27(2078.50)	0.44965(0.44992)	4.809(4.919)	6.67(7.38)
$(0, 2^2, 1)$	2127.56(2127.41)	0.46117(0.46157)	4.983(4.850)	5.29(1.40)
$(0, 2^0, 1)$	2134.40(2133.89)	0.45573(0.45607)	3.044(0.97)	1.50(-1.11)
$(0, 3^3, 1)$	2185.34	0.47136	4.935	2.92
$(0, 3^1, 1)$	2193.74	0.46521	3.786	4.74
$(1, 0^0, 1)$	3259.79(3260.13)	0.42424(0.42420)	1.210(1.076)	1.24
$(1, 1^1, 1)$	3330.17(3330.51)	0.43536(0.43542)	1.966(1.955)	1.98
$(1, 2^0, 1)$	3403.02	0.44487	2.331	2.28
$(1, 2^2, 1)$	3405.12	0.44574	2.550	2.51
$(1, 3^1, 1)$	3480.79	0.45392	2.654	2.58
$(1, 3^3, 1)$	3484.63	0.45550	3.024	2.81

[a] Experimental values from Ref. 322, 314 and 321 in parentheses.
[b] Zero-point energy (ZPE).

better agreement with the calculated values.

The vibrational term energy of the $(0, 1^1, 1)$ combination state is obtained as $G_v = 2078.27$ cm^{-1} only 0.23 cm^{-1} lower than the experimental value [322] of $G_v = 2078.50$ cm^{-1}. For the $(1, 0^0, 1)$ state the absolute difference in G_v compared to experiment [322] is 0.34 cm^{-1}. Furthermore, the rotational parameters B_v, D_v and H_v are in good agreement with the experimental values. Finally, for the stretch-bend combination state $(0, 2^\ell, 1)$ the calculated G_v values are 2133.89 and 2127.41 cm^{-1} for $\ell = 0$ and $\ell = 2$, respectively. As has been observed experimentally, [314] the energetic ordering of the $\ell = 0$ and $\ell = 2$ components is inverted compared to the $(0, 2^\ell, 0)$ manifold of states. Similar accuracy as discussed above is expected for the remaining states in Table 3.12.

Calculated l-type doubling parameters for $^{12}C_3$ are given in Table 3.13. Excellent agreement with the available experimental values for q_v and q_{vJ} is observed. The q_v parameters deviate by no more than 2×10^{-5} cm^{-1} from experiment. For the quartic q_{vJ} the mean relative deviation is about 10%. The sextic q_{vJJ} values agree less favourably with experiment with a rather large deviation

Table 3.13: Calculated and experimental[a] ℓ-type doubling parameters (in cm^{-1}) of $^{12}C_3$. Reproduced from Ref. [28] with the permission of AIP Publishing.

State	$10^3 q_v$	$10^6 q_{vJ}$	$10^{10} q_{vJJ}$
$(0,1,0)$	5.70(5.69)	−0.952(−0.89)	1.52(0.6)
$(0,2,0)$	5.41	−0.743	0.94
$(0,3,0)$	5.19	−0.600	0.53
$(1,1,0)$	4.16	−0.430	0.50
$(1,2,0)$	4.20	−0.420	0.47
$(1,3,0)$	4.22	−0.396	0.45
$(0,1,1)$	8.20(8.25)	−2.100(−2.00)	4.09(2.77)
$(0,2,1)$	6.69	−0.851	2.12
$(0,3,1)$	6.27	−0.786	0.17
$(1,1,1)$	5.19(5.18)	−0.790(−0.66)	1.10
$(1,2,1)$	5.09	−0.690	0.73
$(1,3,1)$	4.99	−0.617	0.48

[a] Experimental values from [322] in parentheses.

of ca. 150 % in case of the $(0,1^1,0)$ state. However, this parameter is also very sensitive to the number of states used in the fit. Furthermore, the experimental value of 0.60×10^{-10} cm^{-1} has a rather large error of 0.23×10^{-10} cm^{-1} or 38%.

It is well known that the PES of the electronic ground state of C_3 exhibits exceptionally strong stretch-bend couplings [25–27]. For *ab initio* methods it is a great challenge to precisely describe these couplings. A sensitive measure for these couplings is the ℓ-dependent splitting of vibrational states which according to VPT2 equals to $x_{\ell\ell}\ell^2$ (cf. Equation (2.49)). Although the usage of $x_{\ell\ell}$ is prohibitive for a floppy molecule like C_3, Equation (2.57) indicates that the ℓ-dependent splitting strongly depends on stretch-bend coupling terms in the PES. The present composite PEF yields a value of $x_{\ell\ell} = -2.12$ cm^{-1}. From experiment the splitting between some rovibrational levels $(v_1, v_2^{\ell=0,2}, 0)$ with $J = 2$ are known (cf. Ref. [25] and references therein). In Table 3.14 these splittings are compared with the present calculations and values obtained from the *ab initio* PES by Mladenović *et al.* [26].

The absolute value of the splittings decreases with increasing v_2. For states with $v_1 = v_3 = 0$ experimental differences become smaller from $v_2 = 2$ to $v_2 = 16$ by 1.01 cm^{-1}. While with the present composite PEF a reduction of 1.34 cm^{-1} is obtained, from the potential of Ref. [26] one yields a decrease of only 0.32 cm^{-1}. In case of states with $v_1 = 1$ one finds over the range of given v_2 values a decrease of 1.29 cm^{-1} in experiment. Calculations with the composite PEF yield a difference of 1.00 cm^{-1} and from the PES of Mladenović *et al.* [26] a slightly smaller value (0.83 cm^{-1}) is obtained. No experimental values are known for states with $v_3 = 1$. However, the two *ab initio* potentials again show large differences in the calculated splittings and the present results are expected to lie closer to forthcoming experimental results.

The calculated and experimental spectroscopic parameters of the vibrational ground state and the singly excited vibrational states in the five ^{13}C substituted C_3 isotopologues are given in Table 3.15.

Table 3.14: Splitting between rovibrational levels $T_{(v_1,v_2^0,v_3)}(J)$ and $T_{(v_1,v_2^2,v_3)}(J)$ (in cm^{-1}) for $J = 2$. Reproduced from Ref. [28] with the permission of AIP Publishing.

v_2	$T_{(v_1,v_2^0,v_3)}(J)$ - $T_{(v_1,v_2^2,v_3)}(J)$		
	Exp.[a]	this work	Ref. 26
$v_1 = 0 \quad v_3 = 0$			
2	1.56	1.75	0.85
4	1.25	1.26	0.67
6	1.05	0.97	0.67
8	0.86	0.77	0.65
10	0.73	0.63	0.61
12	0.68	0.49	0.58
14	0.61	0.46	0.55
16	0.55	0.41	0.53
$v_1 = 1 \quad v_3 = 0$			
2	−2.26	−2.14	−2.16
4	−1.74	−1.63	−2.06
6	−1.23	−1.33	−1.68
8	−0.97	−1.14	−1.33
$v_1 = 0 \quad v_3 = 1$			
2		8.65	5.96
4		4.89	3.70
6		3.28	2.72
8		2.38	2.17

[a] Ref. 316 and 318.

Available experimental values are given in parentheses. Notice that the experimental values given for the $(0, 1^1, 0)$ state of $^{13}C^{13}C^{12}C$ were originally assigned to $^{13}C^{12}C^{12}C$. Based on the present results, this assignment turned out to be wrong which has also been confirmed experimentally by the work of Breier *et al.* [295]. Again, excellent agreement with available experimental date is observed and the calculated parameters for yet unobserved states should provide reliable predictions. The ℓ-type doubling parameters for the first excited bending state in ^{13}C substituted C_3 isotopologues are quoted in Table 3.16. Experimental information for the bending fundamental of the ^{13}C isotopologues has been made available by the work of Breier *et al.* [295].

The equilibrium bond length of C_3

The near perfect agreement between calculated and experimental rotational constants for all the isotopologues considered suggests that the *ab initio* equilibrium bond length is correct to within $1{\cdot}10^{-4}$ Å. Hinkle *et al.* [301] determined an experimental equilibrium bond length of $R_e = 1.2968$ Å largely different from our best *ab initio* value. However, their analysis was based on the less reliable rotational constants available at that time. Using the accurate B_0 values reported by Breier *et al.* [295] given in Table 3.17 and the differences $\Delta B_0 = B_e - B_0$ from the variational calculations

Table 3.15: Calculated and experimental[a] spectroscopic parameters (in cm^{-1}) of ^{13}C substituted C_3 isotopologues. Reproduced from Ref. [28] with the permission of AIP Publishing.

Isotopologue	State	G_v	B_v	$10^6 D_v$	$10^{10} H_v$
$^{13}C^{12}C^{12}C$	$(0,0^0,0)$	1686.44[b]	0.41376(0.41373)	1.416(1.367)	1.59(1.14)
	$(0,1^1,0)$	62.98(63.14)	0.42509(0.42508)	2.170(2.055)	2.24
	$(1,0^0,0)$	1201.43	0.40837	0.655	0.40
	$(0,0^0,1)$	2026.79(2027.21)	0.41861(0.41874)	3.930(4.164)	7.34(10.44)
$^{13}C^{13}C^{12}C$	$(0,0^0,0)$	1656.70[b]	0.41350(0.41345)	1.408[1.459]	1.60
	$(0,1^1,0)$	60.56(60.75)	0.42452(0.42449)	2.146[2.305]	2.24(1.50)
	$(1,0^0,0)$	1198.78	0.40834	0.673	0.43
	$(0,0^0,1)$	1975.37	0.41786	3.728	6.81
$^{12}C^{13}C^{12}C$	$(0,0^0,0)$	1675.54[b]	0.43037(0.43031)	1.527(1.487)	1.79
	$(0,1^1,0)$	60.86(61.05)	0.44184(0.44181)	2.322(2.726)	2.49
	$(1,0^0,0)$	1221.99	0.42499	0.738	0.48
	$(0,0^0,1)$	1988.53	0.43482	3.965	7.05
$^{13}C^{12}C^{13}C$	$(0,0^0,0)$	1667.74[b]	0.39733(0.39730)	1.303[1.404]	1.42
	$(0,1^1,0)$	62.71(62.86)	0.40820(0.40819)	2.003(2.510)	2.00
	$(1,0^0,0)$	1178.74	0.39215	0.595	0.34
	$(0,0^0,1)$	2013.33	0.40204	3.620	6.46
$^{13}C^{13}C^{13}C$	$(0,0^0,0)$	1637.79[b]	0.39710(0.39706)	1.296(1.281)	1.43(1.05)
	$(0,1^1,0)$	60.26(60.45)	0.40767(0.40764)	1.981(2.011)	2.00(2.88)
	$(1,0^0,0)$	1176.10	0.39213	0.612	0.37
	$(0,0^0,1)$	1961.48(1961.95)	0.40135(0.40138)	3.450(3.470)	5.88(6.69)

[a] Experimental values from Ref. [320] and [295] are given in parentheses. Values in square brackets have been fixed in the experimental determination.
[b]Zero-point energy (ZPE).

Table 3.16: Calculated and experimental[a] ℓ-type doubling parameters (in cm^{-1}) for the first excited bending state of ^{13}C substituted C_3 isotopologues. Reproduced from Ref. [28] with the permission of AIP Publishing.

Isotopologue	$10^3 q_v$	$10^6 q_{vJ}$	$10^{10} q_{vJJ}$
$^{13}C^{12}C^{12}C$	5.29(5.29)	−0.852(−1.024)	1.31
$^{12}C^{13}C^{12}C$	5.91(5.89)	−0.987	1.56
$^{13}C^{13}C^{12}C$	5.48(5.78)	−0.888(−0.726)	1.37
$^{13}C^{12}C^{13}C$	4.91(4.90)	−0.764	1.15
$^{13}C^{13}C^{13}C$	5.09(5.08)	−0.797(−0.746)	1.20

[a] Experimental values from Breier *et al.* 295 in parentheses.

Table 3.17: Calculated and experimental rotational parameters (in cm^{-1}) of C_3 isotopologues.

Isotopologue	B_e [a]	B_0 [a]	ΔB_0 [a]	B_0 [b]	B_e [c]
12-12-12	0.419505	0.430633	−0.011128	0.430587	0.419459
13-12-12	0.403109	0.413763	−0.010654	0.413725	0.403071
12-13-12	0.419505	0.430366	−0.010861	0.430309	0.419448
13-13-12	0.403098	0.413503	−0.010405	0.413454	0.403049
13-12-13	0.387135	0.397335	−0.010200	0.397301	0.387101
13-13-13	0.387135	0.397099	−0.009964	0.397059	0.387095

[a] Calculated values from the composite PEF corresponding to a bond length of $R_e = 1.29397$ Å.
[b] Experimental results from [295].
[c] Mixed experimental/theoretical result yielding a fitted equilibrium bond length of $R_e = 1.29404(10)$ Å.

(also given in Table 3.17) a mixed theoretical/experimental R_e for these isotopologues can be obtained in a well established approach [331, 332]. From the results of Table 3.17 the equilibrium bond length of C_3 is determined to be 1.29404(10) Å with a conservative error estimate in units of the last significant digit given in parentheses. This is corresponds to a slight update compared to the original determination in [28] by using improved B_0 values of all 6 ^{12}C and ^{13}C isotopologues. From an experimental point of view ΔB_0 can only be determined in an indirect way by appropriately summing up the differences between rotational parameters in the three fundamental vibrational states and the vibrational ground state provided that an analysis within the framework of VPT2 is aimed at. Such an analysis for the main isotopologue of C_3 using the computed B_v values yields $\Delta B_0 = -0.011467$ cm^{-1} and a mixed experimental/theoretical equilibrium bond length of 1.29459 Å. Similarly, if one calculates ΔB_0 for $^{12}C_3$ from the available experimental rotational constants [321, 322] $\Delta B_0 = -0.011582$ cm^{-1} is obtained and a fully experimental R_e of 1.29476 Å. Both results for R_e are longer by 0.00052 Å and 0.00069 Å, respectively, compared to the value determined from Table 3.17 in a more direct way by subtracting the variationally calculated value for B_0 from B_e. The preceding discussion indicates that the bond length of $^{12}C_3$ determined with the aid of formulas according to 2nd order perturbation theory will be longer than the present Born-Oppenheimer bond length by about 0.0006 Å (see also [311] for a detailed discussion of this issue).

In their work on the ν_2 band Breier *et al.* [295] attempted to determine a bond length only from the experimental high-resolution THz data. Two assumptions were made: the rotational parameter B_v follows the VPT2 expansion according to Equation (2.65) and the contribution from the stretching vibrations α_1 and α_3 cancel each other. The approximate equilibrium rotational constant is then given by $B^{(0e0)} = B_0 + \alpha_2$. From the six experimental $B^{(0e0)}$ values an *approximate* equilibrium bond length $R^{(0e0)} = 1.29511(5)$ Å is obtained [295] which is larger by as much as 0.00107 Å compared to the present mixed experimental/theoretical value. It should be noted that the quoted uncertainty in $R^{(0e0)}$ is only the statistical error obtained from the spread of $R^{(0e0)}$ values for the

isotopologues and does not account for the error introduced through the approximations. The latter thus require some clarification.
From the rotational parameters for the $(1,0^0,0)$ and $(0,0^0,1)$ states the sum $\alpha_1+\alpha_3$ within VPT2 can be calculated according to $\alpha_1+\alpha_3 = 2B_0 - B_{(1,0^0,0)} - B_{(0,0^0,1)}$. Using the experimental B_v values given in Table 3.12 one yields $\alpha_1+\alpha_3 = 0.00049$ cm^{-1} from theoretical and experimental results, respectively. This translates to a contribution of -0.00035 Å to the equilibrium bond length. Neglect of the stretching vibrations thus yields bond lengths which are too large by 0.00035 Å. The error due to the VPT2 based approach can be deduced by comparing $\Delta B^{(0e0)} = B^{(0e0)} - B_0 = \alpha_2$ with the theoretical value for ΔB_0 obtained variationally in this work. For $^{12}C_3$ one obtains from $\alpha_2 = -0.011828$ cm^{-1} [295] and $\Delta B_0 = -0.011128$ cm^{-1} (cf. Table 3.17) a difference of $\Delta B_0 - \Delta B_{(0e0} = +0.0007$ cm^{-1} which corresponds to an error of +0.00107 Å exactly the difference between the mixed experimental/theoretical result and $B^{(0e0)}$. After subtracting the error due to the neglect of α_1 and α_3 the error of the VPT2 *ansatz* in $B^{(0e0)}$ is obtained with a value of +0.00072 Å. This matches the error deduced above which is introduced by assuming the validity of VPT2.

Rovibrational intensities

Using the analytical PES and EDMF given in Table B.3 and Table B.4 squared transition dipole moments between rovibrational states were calculated using C8VPRO. By employing Equation (2.100) and Equation (2.101), pure vibrational transition dipole moments $\mu_{vv'}$ are obtained from least-squares fits. Results for selected transitions in the main isotopologue of C_3 are quoted in Table 3.18 together with calculated band intensities A_v according to Equation (3.7). The two infrared active fundamental transitions as well as the two lowest combination bands together with associated hot bands originating from the first excited bending state are quoted in Table 3.18.
For the two fundamental transitions ν_2 and ν_3 values of 0.4320 and 0.3445 D, respectively, are calculated for $|\mu_{vv'}|$. The corresponding band intensities are calculated to be 0.90 and 60.99 cm^{-2}/atm for ν_2 and ν_3, respectively. Both IR active combination bands $\nu_1+\nu_2$ and $\nu_1+\nu_3$ show $|\mu_{vv'}|$ values that are lower by an order of magnitude compared to the fundamental transitions. However, due to the higher transition frequencies the band intensities are comparable to that of the ν_2 transition. Based on the present results the $\nu_1+\nu_2$ transition should also be observable albeit rather weak.
The intensity pattern of hot bands that involve a final state with $v_2 = 2$ show signs of a strong Coriolis interaction. For example, in the case of the $(0,2^\ell,0) \leftarrow (0,1^1,0)$ transitions, Figure 3.12 depicts the variation of $\sqrt{\frac{\mu_{if}^2}{F_{\mathrm{HL}}}}$ with m. While the f component of the $(0,2^2,0) \leftarrow (0,1^1,0)$ transition may be accurately represented by Equation (2.101), the corresponding e component and the $(0,2^0,0) \leftarrow (0,1^1,0)$ band clearly can not. As has been shown before, the expectation value of the vibrational angular momentum quantum number $\langle|\ell|\rangle$ provides a good indicator for the strength of Coriolis interactions. For the e components of the $(0,2^l,0)$ manifold $\langle|\ell|\rangle$ changes strongly with J as can be seen from the inset of Figure 3.12. At $J = 40$ a common value of 1.00 is calculated for $(0,2^0,0)$ and $(0,2^2,0)e$. This strong Coriolis resonance has already been observed experimentally

Table 3.18: Calculated vibrational term differences (in cm^{-1}), transition dipole moments (in D) and band intensities (in km/mol) for selected transitions of $^{12}C_3$. Reproduced from Ref. [28] with the permission of AIP Publishing.

Transition	ΔG	$\lvert\mu_{vv'}\rvert$	A_v
$(0,1^1,0) \leftarrow (0,0^0,0)$	63.2	0.4320	0.90
$(0,2^0,0) \leftarrow (0,1^1,0)$	69.6	0.3680	0.55
$(0,2^2,0) \leftarrow (0,1^1,0)e$	69.6	0.4118	1.27
$(0,2^2,0) \leftarrow (0,1^1,0)f$	69.6	0.4010	
$(1,1^1,0) \leftarrow (0,0^0,0)$	1315.2	0.0197	0.12
$(1,2^0,0) \leftarrow (0,1^1,0)$	1341.6	0.0234	0.12
$(1,2^2,0) \leftarrow (0,1^1,0)e$	1345.5	0.0205	0.19
$(1,2^2,0) \leftarrow (0,1^1,0)f$	1345.5	0.0201	
$(0,0^0,1) \leftarrow (0,0^0,0)$	2039.6	0.3445	60.99
$(0,1^1,1) \leftarrow (0,1^1,0)e$	2015.0	0.3306	79.97
$(0,1^1,1) \leftarrow (0,1^1,0)f$	2015.0	0.3315	
$(1,0^0,1) \leftarrow (0,0^0,0)$	3259.8	0.0431	1.52
$(1,1^1,1) \leftarrow (0,1^1,0)e$	3266.9	0.0419	2.07
$(1,1^1,1) \leftarrow (0,1^1,0)f$	3266.9	0.0419	

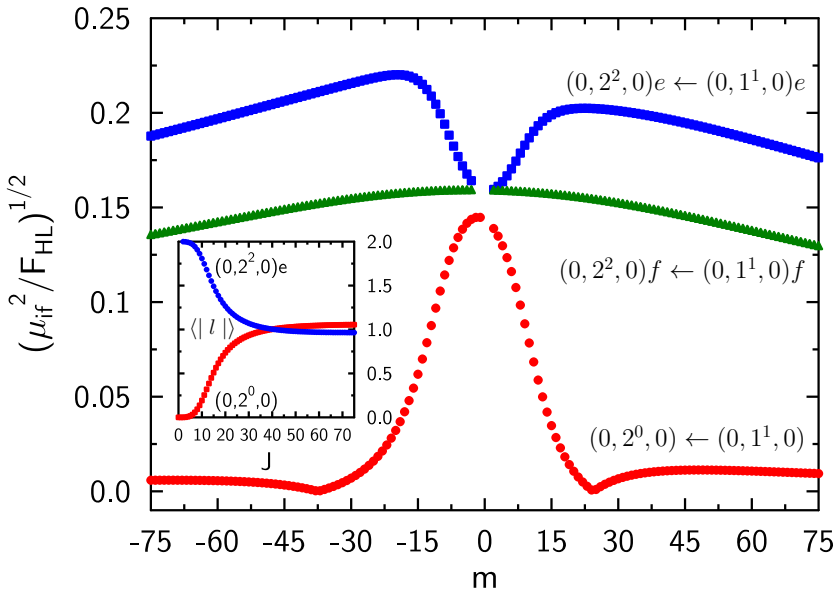

Figure 3.12: Variation of the expression $\sqrt{\frac{\mu_{if}^2}{F_{HL}}}$ with m for $^{12}C_3$. The inset shows the variation of $\langle|\ell|\rangle$ with J for the interacting bending states $(0,2^0,0)$ and $(0,2^2,0)$. Reproduced from Ref. [294] with the permission of AIP Publishing.

by Herzberg and coworkers 50 years ago [310].

3.2.4 Highly excited stretching states in C_3

A complete understanding of the C_3 PES requires that highly excited vibrational states, particularly those involving multiple vibrational modes, need to be studied. This requires high resolution IR measurements. In experimental measurements, C_3 molecules are commonly formed either through 1) photolysis of diacetylene, allene or furan, [313,314,318,321] 2) laser ablation of a carbon rod, [312,322] or 3) a discharge through acetylene [323,333]. To date, these methods have allowed measurements of vibrational states in the electronic ground state up to $v_2 = 34$, $v_1 = 3$, and $v_3 = 1$.

Experimental details

In the experimental study conducted by the Linnartz group, the vibrationally excited C_3 molecules are generated in a pulsed supersonically expanding planar plasma [334], using a precursor gas mixture of 0.5% propyne in 1:1 helium:argon mixture with a 5 bar backing pressure. The gas is expanded into the vacuum chamber through a slit discharge nozzle with an applied high voltage of ~ -550 V at the exit. In the past it was shown that such plasma sources are useful to study vibrationally highly excited species without losing much of the rotational cooling properties in the expansion typical for this type of adiabatic expansions [335,336]. The experimental setup has been described in detail in Ref. [337], and a similar setup working in the optical has been used to study the $\tilde{A}^1\Pi_u \leftarrow \tilde{X}^1\Sigma_g^+$ $(0, 0^0, 0)$ - $(0, 0^0, 0)$ band [306,323].
The high resolution infrared spectrum of the plasma products is recorded using continuous wave cavity ring-down spectroscopy (cw-CRDS), using a commercial cw-OPO that covers $\sim$ 3110 - 4200 cm^{-1}. The IR laser path intersects the expansion roughly 1 cm downstream from the nozzle body. The resulting spectrum is recorded in a series of $\sim$ 1.2 cm^{-1} parts that partially overlap to guarantee that spectra can be directly compared. In total some 170 cm^{-1} are covered. The Doppler width of the recorded transitions is about 0.004 cm^{-1}. At the same time the spectrum is recorded, the laser frequency is measured using a wavemeter, with a resulting maximum frequency uncertainty of $\pm$ 0.002 cm^{-1}. The frequency accuracy is independently checked by comparing the recorded absorption lines of trace water in the chamber against the corresponding HITRAN values [338], and typical frequency accuracies of the recorded transitions are better than 0.001 cm^{-1}.

Theoretical calculations

In order to provide the same level of convergence for higher lying excited rovibrational states, the basis set in the RVIB3 calculations is increased compared to the previous calculations presented above. The primitive basis set for the stretching vibrations comprised 200 symmetrized basis functions constructed from 20 functions for both the symmetric and antisymmetric stretching vibration. For the bending motion 42 basis functions per ℓ-block are employed. Combining 47 contractions for stretching vibrations per symmetry species with 33 contracted functions for the

bending vibration leads to Hamiltonian matrices of dimension 1551 for every value of ℓ. The size of the final Hamiltonian matrix for each symmetry species is adjusted appropriately in order to provide converged results.
Since all bands observed in the cw-CRDS spectrum are Σ - Σ bands, the vibrational angular momentum quantum number ℓ in the term energy formula Equation (2.91) equals to 0. Higher-order terms beyond D_v in the expansion Equation (2.91) are neglected due to the strong dependence of such terms on employed J values as has been shown above and this issue will also be addressed in more detail in the following. The transition frequencies between rovibrational states (v', J') and (v'', J'') can be calculated according to

$$\begin{aligned}\nu = T_{v'}(J') - T_{v''}(J'') = \nu_0 + (B_{v'} + B_{v''})\, m + [(B_{v'} - B_{v''}) - (D_{v'} - D_{v''})]\, m^2 \\ - 2(D_{v'} + D_{v''})m^3 - (D_{v'} - D_{v''})m^4\,,\end{aligned} \tag{3.13}$$

where $\nu_0 = G_{v'} - G_{v''}$ is the vibrational band origin (VBO).
While experimentally determined transition frequencies can only be fitted according to Equation (3.13) the variationally calculated term energies of an individual vibrational state can also be fitted according to Equation (2.91). The results of the latter procedure are termed Calc. I where ro-vibrational states up to $J_{\max} = 20$ were employed. Fits of the variationally calculated transition energies according to Equation (3.13) employing the same transitions as in the experimental fits are termed Calc. II.

Band assignment and spectroscopic parameters

The high resolution C_3 plasma spectrum is recorded between 3110 - 3341 cm^{-1}. Additional lines are observed which are due to other propyne plasma products, as well as C_3H_4 precursor material. Fifteen bands are observed between 3110 - 3280 cm^{-1}, with a rotational spacing of $\sim$ 1.6 cm^{-1}, which is consistent with a 1:0 intensity alternation of ro-vibrational transitions originating from stretching vibrations of C_3; no ro-vibrational bands are observed that can be assigned to transitions involving the bending states. An overview of the C_3 spectra is given in Fig. 3.13; the observed intensities cannot be directly compared, as these depend, for example, on small variations in the experimental plasma conditions, but general trends can be seen. For example, the C_3 band intensities decrease quickly with decreasing frequency. Assuming a Boltzmann population distribution, this suggests that the lower frequency bands involve transitions starting from higher quanta vibrational states relative to bands at higher frequencies.
The effective experimental band origin and rotational parameters for the lower and upper state of each band are determined using the spectral fitting software PGOPHER [339]. Preliminary spectral analysis of the fifteen bands is performed by fitting the observed transitions to simulated spectra assuming $B_v \sim 0.4$ cm^{-1} and using transition intensities near the band origins to determine the state symmetry (either Σ_g^+ or Σ_u^+). For most of the bands, transitions could be assigned up to $J" = 20$ (see supplementary material). From the rotational profiles, the rotational temperature

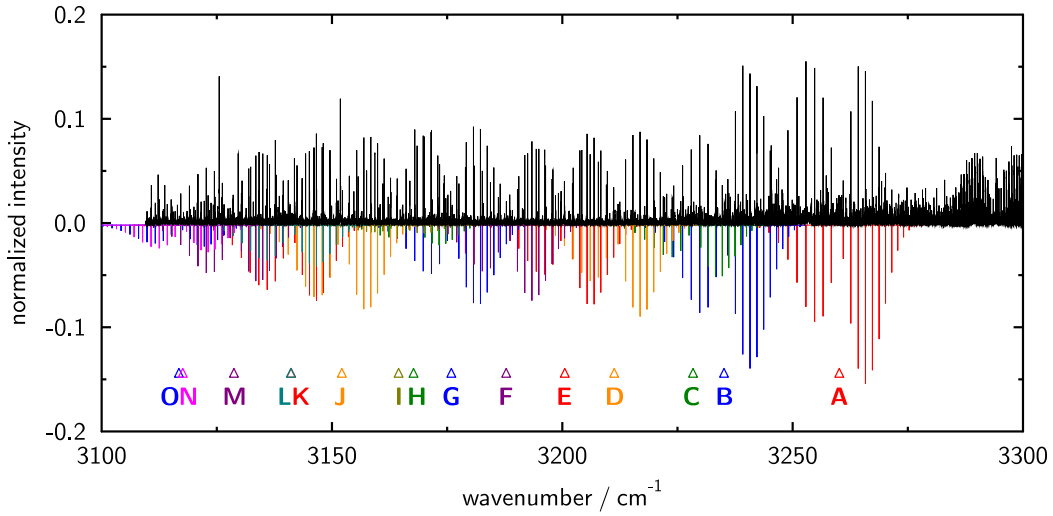

Figure 3.13: The experimental (in black) spectrum of the propyne plasma products showing a series of bands, which are assigned to vibrationally excited C_3 (simulated bands from PGOPHER, inverted). The strong bands at frequencies higher than 3275 cm^{-1} are assigned to propyne. The bands are assigned to the transitions: A) $(1,0^0,1)$ - $(0,0^0,0)$, B) $(2,0^0,1)$ - $(1,0^0,0)$, C) $(1,0^0,2)$ - $(0,0^0,1)$, D) $(3,0^0,1)$ - $(2,0^0,0)$, E) $(2,0^0,2)$ - $(1,0^0,1)$, F) $(4,0^0,1)$ - $(3,0^0,0)$, G) $(3,0^0,2)$ - $(2,0^0,1)$, H) $(2,0^0,3)$ - $(1,0^0,2)$, I) $(5,0^0,1)$ - $(4,0^0,0)$, J) $(4,0^0,2)$ - $(3,0^0,1)$, K) $(3,0^0,3)$ - $(2,0^0,2)$, L) $(6,0^0,1)$ - $(5,0^0,0)$, M) $(5,0^0,2)$ - $(4,0^0,1)$, N) $(7,0^0,1)$ - $(6,0^0,0)$, and O) $(4,0^0,3)$ - $(3,0^0,2)$. Reproduced from Ref. [29] with the permission of AIP Publishing.

of C_3 is determined to be about 55 K. This is slightly higher than typical for the plasma source in use [340, 341]. A least-squares fit analysis based on Equation (3.13) is then used to determine tentative vibrational band origins (VBOs) and lower and upper rotational parameters, $B_{v''}$ and $B_{v'}$, respectively. The bands are labeled A - O in descending value of their VBO.

Initial fits of the bands showed that some of them share vibrational states, i.e., the determined $B_{v'}$ for one band is the same as the $B_{v''}$ for another band. Based on the rotational parameters and state symmetry, twelve of the bands can be grouped into five vibrational series involving common states: A - E - K; B - G - O; C - H; D - J; and F - M. The other bands do not share common states. VBOs of each band in a series, regardless of the series, are separated by about 60 cm^{-1}, suggesting that in all five series the lower state of each band is increasing by the same number of quanta, which based on frequency region, is likely $\Delta v_1 = 1$ and $\Delta v_3 = 1$. This is also clearly visible from Fig. 3.13. In addition, seven of the bands: A, B, D, F, I, L, and N are evenly separated by about 23 cm^{-1}, suggesting that they are also part of a different progression that increases by $\Delta v_1 = 1$ in the lower state.

In order to confirm the initial assignment the experimental line positions are compared to the results of the variational calculations. Figure 3.14 depicts the difference between experimental and

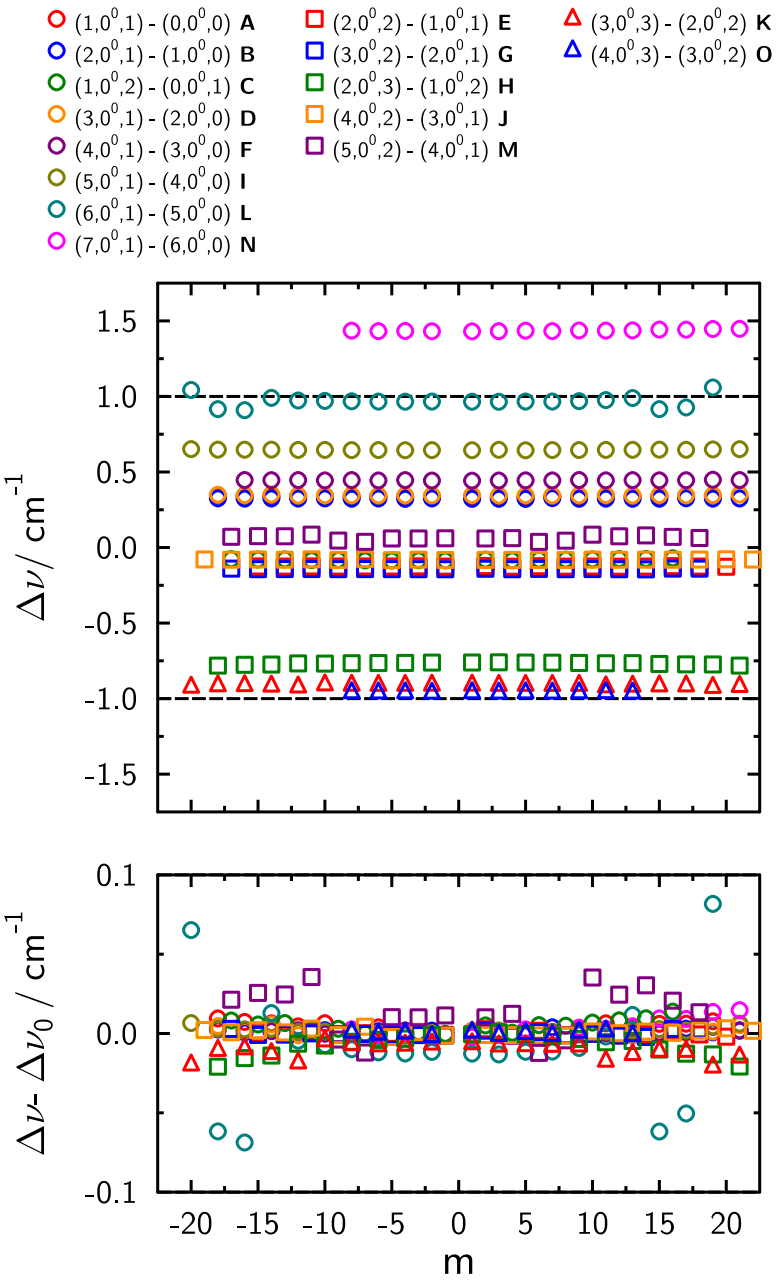

Figure 3.14: Comparison of experimental and variationally calculated line positions, $\Delta\nu$, for the fifteen observed combination bands of C_3 showing the accuracy in predicting the vibrational energy. The J dependent accuracy is highlighted in the plot of $\Delta\nu$ - $\Delta\nu_0$. Identical colors refer to bands in one series with the circle, square, and triangle markers referring to the first, second, and third band in the series, respectively. The larger deviations seen for bands L and M are due to a difference in the determined location of state crossings, as discussed in the text. Reproduced from Ref. [29] with the permission of AIP Publishing.

Table 3.19: Band origins (in cm^{-1}) and assignments (v_1, v_2^ℓ, v_3) of the observed C_3 combination bands. Reproduced from Ref. [29] with the permission of AIP Publishing.

		ν_0	
Label	Assignment	Expt.[a]	Calc. II
A	$(1,0^0,1)$ - $(0,0^0,0)$	3260.1265(4)	3259.79
B	$(2,0^0,1)$ - $(1,0^0,0)$	3235.0964(4)	3234.77
C	$(1,0^0,2)$ - $(0,0^0,1)$	3228.3796(4)	3228.46
D	$(3,0^0,1)$ - $(2,0^0,0)$	3211.2653(4)	3210.92
E	$(2,0^0,2)$ - $(1,0^0,1)$	3200.5361(4)	3200.66
F	$(4,0^0,1)$ - $(3,0^0,0)$	3187.8158(4)	3187.37
G	$(3,0^0,2)$ - $(2,0^0,1)$	3175.9066(4)	3176.05
H	$(2,0^0,3)$ - $(1,0^0,2)$	3167.7016(4)	3168.46
I	$(5,0^0,1)$ - $(4,0^0,0)$	3164.4665(4)	3163.82
J	$(4,0^0,2)$ - $(3,0^0,1)$	3152.1415(4)	3152.22
K	$(3,0^0,3)$ - $(2,0^0,2)$	3141.1229(4)	3142.03
L	$(6,0^0,1)$ - $(5,0^0,0)$	3141.0896(4)	3140.11
M	$(5,0^0,2)$ - $(4,0^0,1)$	3128.7178(4)	3128.66
N	$(7,0^0,1)$ - $(6,0^0,0)$	3117.6110(5)	3116.18
O	$(4,0^0,3)$ - $(3,0^0,2)$	3116.7759(5)	3117.74

[a] Experimental uncertainties are given in parentheses in units of the last significant digits.

variationally calculated line positions, $\Delta\nu$. For all bands the differences are smaller than 1 cm^{-1}, except for band N which has a difference of 1.5 cm^{-1}. This agreement confirms the vibrational assignment of the observed bands. Additionally, the lower panel of Figure 3.14 shows the differences when the error in the VBOs is subtracted, $\Delta\nu$ - $\Delta\nu_0$. The errors are decreased by more than an order of magnitude, unambiguously confirming the rotational assignment of the individual lines within the bands. For two of the observed bands, bands L and M, deviations from the expected independence of the errors from the rotational quantum number are observed. This indicates a local anharmonic resonance, which will be discussed in detail below.

Systematic rotational analysis of the observed bands is carried out by fitting the experimental transitions with linked states simultaneously according to Equation (3.13). The resulting experimental VBOs of the fifteen bands are given in Table 3.19 together with the corresponding variational results (Calc. II). The experimental and theoretical (Calc. I and Calc. II) rotational parameters are summarized in Table 3.20. Typically the results of the latter two fits are observed to deviate by less than 1% in the quartic centrifugal distortion parameter.

The strongest transitions in the experimental spectrum associated with C_3 (band A), belong to the known combination band $(1,0^0,1)$ - $(0,0^0,0)$ with a band origin at 3260.13 cm^{-1} [322]. The ground state rotational parameter is determined to be 0.430569(3) cm^{-1}, which is in agreement with the literature values [312,314,322,333] and the quartic centrifugal distortion parameter, D_v, is 1.399(12) $\times$ 10^{-6} cm^{-1}, smaller by about 5% compared to the value by Krieg *et al.* [322] of 1.471(13) $\times$

Table 3.20: Effective experimental and theoretical spectroscopic parameters of C_3 (in cm^{-1}). Reproduced from Ref. [29] with the permission of AIP Publishing.

	B_v			$10^6 D_v$		
State	Expt.[a]	Calc. I	Calc. II	Expt.[a]	Calc. I	Calc. II
$(0, 0^0, 0)$	0.430569(3)	0.43061	0.43062	1.399(12)	1.437	1.450
$(1, 0^0, 1)$	0.424211(8)	0.42423	0.42423	1.110(27)	1.143	1.144
$(2, 0^0, 2)$	0.418208(9)	0.41824	0.41823	0.894(21)	0.946	0.936
$(3, 0^0, 3)$	0.412448(8)	0.41252	0.41251	0.737(18)	0.812	0.806
$(1, 0^0, 0)$	0.424997(5)	0.42501	0.42501	0.704(16)	0.693	0.708
$(2, 0^0, 1)$	0.419489(5)	0.41950	0.41950	0.610(14)	0.613	0.614
$(3, 0^0, 2)$	0.414065(8)	0.41410	0.41412	0.530(28)	0.550	0.607
$(4, 0^0, 3)$	0.408807(14)	0.40880	0.40880	0.565(48)	0.499	0.520
$(0, 0^0, 1)$	0.435664(8)	0.43554	0.43556	3.890(10)	3.763	3.825
$(1, 0^0, 2)$	0.427040(6)	0.42690	0.42690	2.749(17)	2.691	2.696
$(2, 0^0, 3)$	0.419519(7)	0.41943	0.41643	2.035(17)	1.998	1.987
$(2, 0^0, 0)$	0.421603(6)	0.42164	0.42164	0.441(14)	0.462	0.461
$(3, 0^0, 1)$	0.416385(4)	0.41641	0.41642	0.416(9)	0.438	0.439
$(4, 0^0, 2)$	0.411212(6)	0.41123	0.41124	0.392(14)	0.406	0.410
$(3, 0^0, 0)$	0.419074(8)	0.41907	0.41908	0.467(21)	0.372	0.395
$(4, 0^0, 1)$	0.413969(6)	0.41395	0.41396	0.439(14)	0.355	0.372
$(5, 0^0, 2)$	0.408958(11)	0.40870	0.40876	0.529(33)	−0.195	0.023
$(4, 0^0, 0)$	0.416862(6)	0.41686	0.41687	0.345(14)	0.324	0.328
$(5, 0^0, 1)$	0.411807(6)	0.41180	0.41180	0.310(12)	0.314	0.314
$(5, 0^0, 0)$	0.414818(55)	0.41486	0.41487		0.292	0.316
$(6, 0^0, 1)$	0.409740(51)	0.41010	0.41027		1.056	1.797
$(6, 0^0, 0)$	0.412989(9)	0.41298	0.41299	0.743(24)	0.276	0.577
$(7, 0^0, 1)$	0.408009(8)	0.40795	0.40797	0.699(20)	0.276	0.540

[a] Experimental uncertainties are given in parentheses in units of the last significant digits.

10^{-6} cm^{-1}. Similarly, the VBO, which in this case is equal to G_v, and $(1,0^0,1)$ state rotational parameter are determined to be 3260.1265(4) and 0.424211(8) cm^{-1}, respectively, in agreement with the values determined by Krieg *et al.* [322] 3260.127048(91) and 0.4241990(25) cm^{-1}, respectively. D_v for the $(1,0^0,1)$ agrees to within 3% with the previous value [322]. Both the ground and $(1,0^0,1)$ state VBO and B_v agree to within 0.01% with the theoretical values (Tables 3.19 and 3.20). Notice that in the present spectrum and that of Krieg *et al.* [322] the best fit observed - calculated (o-c) values suggest a small perturbation around $J' = 9$. This slight anharmonic interaction in the $(1,0^0,1)$ state is successfully predicted by the present variational calculation, which is seen by no noticeable deviation in the $\Delta\nu$ - $\Delta\nu_0$ plot in Figure 3.14. An analysis of the term energies and state orderings showed that the most likely state responsible is the $(1,19^1,0)$ state, which crosses the $(1,0^0,1)$ state between $J = 8$ and 9. Simultaneous fitting of bands A, E, and K, gives VBOs for bands E and K of 3200.5361(4) and 3141.1229(4) cm^{-1}, which translate into upper state term energies of 6460.6640(3) and 9601.7887(5) cm^{-1}, respectively. The assignment is confirmed by comparing the experimental rotational parameters for the $(2,0^0,2)$ and the $(3,0^0,3)$ states to the corresponding values obtained variationally (cf. Table 3.19). The B_v values are in almost perfect agreement, with differences of less than 0.002%. Likewise, agreement of experimental and theoretical quartic centrifugal distortion, D_v, parameters is good except for the $(3,0^0,3)$ which might indicate a perturbation.

Based on the VBO and rotational parameter determined from the least-squares fitting, the lower state of the second strongest band (band B) is assigned to $(1,0^0,0)$. The rotational parameter, B_v, is determined to be 0.424997(5) cm^{-1} and agrees with the value of 0.424950(62) cm^{-1} determined for the ν_1 fundamental from the electronic spectra by Zhang *et al.* [321] as well as the current calculations (0.42501 cm^{-1}). A value of 0.704(16) $\times$ 10^{-6} cm^{-1} is obtained for the $(1,0^0,0)$ state D_v. This value is within the somewhat larger error bars of D_v determined from the electronic spectra [321] of 0.52(23) $\times$ 10^{-6} cm^{-1}. Assuming an increase of $\Delta v_1 = 1$ and $\Delta v_3 = 1$ in the quantum numbers, the bands in this series: B, G, and O are assigned to the $(2,0^0,1)$ - $(1,0^0,0)$, $(3,0^0,2)$ - $(2,0^0,1)$ and $(4,0^0,3)$ - $(3,0^0,2)$ combination bands, respectively. Simultaneous fitting of bands B, G, and O, gives VBOs consistent with those expected for all three bands according to the variational results in Table 3.19. Furthermore, the experimentally determined and variationally calculated rotational parameters B_v agree to within 0.002%. However, for the $(4,0^0,3)$ level, both theoretical fits (Calc. I and Calc. II) predict a D_v value smaller than that for $(3,0^0,2)$, which is not observed experimentally. This discrepancy is caused by the fact that band O is only observed up to P(8). While the spectroscopic parameters of the $(3,0^0,2)$ are constrained by transitions in band G, $(4,0^0,3)$ has no such additional information, and the limited observed transitions for band O severely skews the experimental fit, resulting in a large uncertainty in the determined D_v value. This effect can also be observed by comparing the D_v obtained from Calc. I and Calc. II. By employing the same lines as observed experimentally and fitting bands B, G and O simultaneously (Calc. II), D_v of $(4,0^0,3)$ increases by about 4% compared to the Calc. I result. A similar but less pronounced effect is also observed for the D_v of $(1,0^0,0)$, where the Calc. II is larger than

the Calc. I result almost coinciding with the experimental value, see Table 3.20. As such, the calculated values (Calc. I) are likely closer to the true value for the $(4, 0^0, 3)$ state.

Band D starts the next series of bands and is the third band in the large progression. From the least-squares fit analysis the VBO is determined to be 3211.2653(4) cm^{-1}, which agrees to within about 0.3 cm^{-1} with the variational result for the $(3, 0^0, 1)$ - $(2, 0^0, 0)$ band (Table 3.19). This assignment is further confirmed by the agreement of the experimental and theoretical rotational parameters (Table 3.20). Simultaneous fitting of transitions in band D and band J confirm that they share a common energy level, $(3, 0^0, 1)$. Consequently, band J is assigned to the $(4, 0^0, 2)$ - $(3, 0^0, 1)$ combination band. The experimental VBO is 3152.1415(4) cm^{-1} only 0.08 cm^{-1} lower than the value calculated variationally. For both bands D and J the experimental and calculated rotational B_v parameters differ by no more than 0.01% (Table 3.20).

As with the last series, the F-M series is assumed to start with the lower state of the first band being a vibrationally excited state of type $(v_1, 0^0, 0)$. Based on the comparison of experimental and theoretical VBO and rotational parameters (Table 3.19 and Table 3.20), band F is assigned to the $(4, 0^0, 1)$ - $(3, 0^0, 0)$ combination band. Simultaneous fitting of bands F and M confirms that they share an energy level, $(4, 0^0, 1)$, and band M is assigned to the $(5, 0^0, 2)$ - $(4, 0^0, 1)$ combination band. Band M shows signs of a small local anharmonic resonance likely within the $(5, 0^0, 2)$ state, which can be further deduced from the larger deviations in the D_v parameter for the $(5, 0^0, 2)$ state. Based on the (o-c) value of the experimental line positions, a perturbation occurs at around $J = 3$. According to the variational calculations, the $(5, 0^0, 2)$ state is expected to be crossed by the $(4, 10^2, 2)$ state between $J = 6$ and 7, and by the $(4, 10^0, 2)$ state between $J = 8$ and 9. The mismatch in the position of the crossing results in the observed down-up-down deviation seen in the $\Delta\nu$ - $\Delta\nu_0$ plot in Figure 3.14. The state density near 9900 cm^{-1} is extremely high, there are about 6 states for $J = 6$ and 8 states for $J = 8$ within $\pm$ 10 cm^{-1} of the $(5, 0^0, 2)$ state. Therefore, the influence of other nearby states might be non-negligible. However, inspection of expansion coefficients of the rovibrational wavefunction makes the two $(4, 10^\ell, 2)$ states the most likely ones that cause the local anharmonic resonances.

The bands I, L, and N do not share a state with any other observed band, but they are part of the larger $(v_1, 0^0, 0)$ progression. Based on their VBOs and relative intensities in the progression, the three bands are assigned to the $(5, 0^0, 1)$ - $(4, 0^0, 0)$, $(6, 0^0, 1)$ - $(5, 0^0, 0)$ and $(7, 0^0, 1)$ - $(6, 0^0, 0)$ bands, respectively. The experimental VBOs of 3164.4665(4), 3141.0896(4) and 3117.6110(5) for bands I, L and N, respectively, agree to within 0.65, 0.98 and 1.43 cm^{-1} with the variational VBOs (Table 3.19). The experimental B_v values for each band show differences of 0.0004% to 0.09% compared to the values obtained in the variational calculations, confirming the assignment. As seen with band O, the disagreement between the experimental and theoretical D_v values for band N is a result of the limited observation of P-branch transitions. Unlike any of the other observed bands, band L is heavily perturbed, with a strong perturbation in the form of an avoided crossing seen in the (o-c) values at $J' = 13$ and 15. In fact, for the $J' = 15$ transitions, the best fit o-c values are about -0.04 cm^{-1}, almost two orders of magnitude larger than the average residuals for

all other C_3 transitions. Because the perturbation occurs at a higher J", no D_v parameter can reliably be determined from our experimental fit. Indeed, an avoided crossing is predicted by the variational calculations for the $(6, 0^0, 1)$ state. The perturbing $(4, 3^1, 2)$ state lies at a frequency lower than the $(6, 0^0, 1)$ state for $J \leq 18$, and crosses to a higher frequency between $J = 18$ and 19. As discussed for the $(5, 0^0, 2)$ state, the down-up deviation seen in the $\Delta\nu$ - $\Delta\nu_0$ plot in Figure 3.14 for band L is due to a disagreement in the position of the crossing. Furthermore, the interaction between the $(6, 0^0, 1)$ and $(4, 3^1, 2)$ states is much stronger than that predicted for the $(5, 0^0, 2)$ state, which is seen in the larger magnitude of the deviations in the $\Delta\nu$ - $\Delta\nu_0$ plot in Figure 3.14. The last of the vibrational series, comprised of bands C and H, is unconnected to the other series. Based on the least-squares fit of band C, the lower state is assigned to $(0, 0^0, 1)$. The rotational parameter, B_v, is determined to be 0.435664(8) cm^{-1} to be compared with the value of 0.4356969(56) cm^{-1} obtained by Krieg and coworkers [322]. For the quartic centrifugal distortion parameter D_v a value of $3.890(10) \cdot 10^{-6}$ cm^{-1} is obtained, which is lower by 11 % compared to previous studies [322]. These discrepancies can be explained by the different truncations of the $J(J + 1)$ expansion of the rotational energy employed in this study (up to D_v) and previously (up to M_v) [322] as well as different J levels observed in both experiments. However, the strong increase in D_v by factor of about 3 compared to the vibrational ground state is consistent with an excited state of the antisymmetric stretching vibration. Therefore, band C is assigned the $(1, 0^0, 2)$ - $(0, 0^0, 1)$ transition. The assignment is also confirmed by comparing experimental and theoretical lower and upper state rotational parameters which agree to with 0.03 % and 3 % for B_v and D_v, respectively. Simultaneous fitting of bands C and H confirms a shared state, $(1, 0^0, 2)$. As such, band H is assigned to the $(2, 0^0, 3)$ - $(1, 0^0, 2)$ combination band. The corresponding VBO of 3167.7016(4) cm^{-1} agrees to within 0.76 cm^{-1} with the Calc. II value (Table 3.19). Both the upper and lower state rotational parameters, B_v, agree with the present variational results. In fact, the differences do not exceed 0.03% for the B_v and 2% for the centrifugal distortion parameter D_v.

Discussion

Fifteen combination bands of vibrationally excited gas-phase C_3 have been measured at high resolution; fourteen of which are reported for the first time. Fig 3.15 presents an energy level scheme of the detected vibrational states. Previously observed transitions are represented by dashed arrows. All term energies include the variationally calculated zero-point energy of 1705.06 cm^{-1}. VBOs of the fifteen observed bands as well as rotational and centrifugal distortion parameters for all twenty-three involved states have been determined. The present variational ro-vibrational calculations of the stretching modes give remarkable agreement between experimental values and theoretical estimates; the typical accuracy of the rotational parameters is a few 0.001 %. The experimental results offer a significant extension of the available data set for the C_3 molecule, since they extend the observed number of quanta in both v_1 and v_3.

Given the excellent agreement between the experimental and theoretical spectroscopic parameters a closer look at the trends observed for said parameters appears promising. Furthermore, the

results can also be discussed with respect to a VPT2 treatment. Therefore, using finite differences the PES (Table B.3) is transformed to a QFF in normal coordinates given in Table 3.21 and various spectroscopic parameters calculated from the QFF within VPT2 are given in Table 3.22. The normal coordinate force constants reflect the highly anharmonic nature of the C_3 molecule. For example, the diagonal quartic bending force constant k_{2222} is calculated to be 724.835 cm^{-1}, which is larger by a factor of about 17 compared to the harmonic bending frequency of $\omega_2 =$ 42.773 cm^{-1}. The strong coupling between the symmetric stretching and the bending vibration

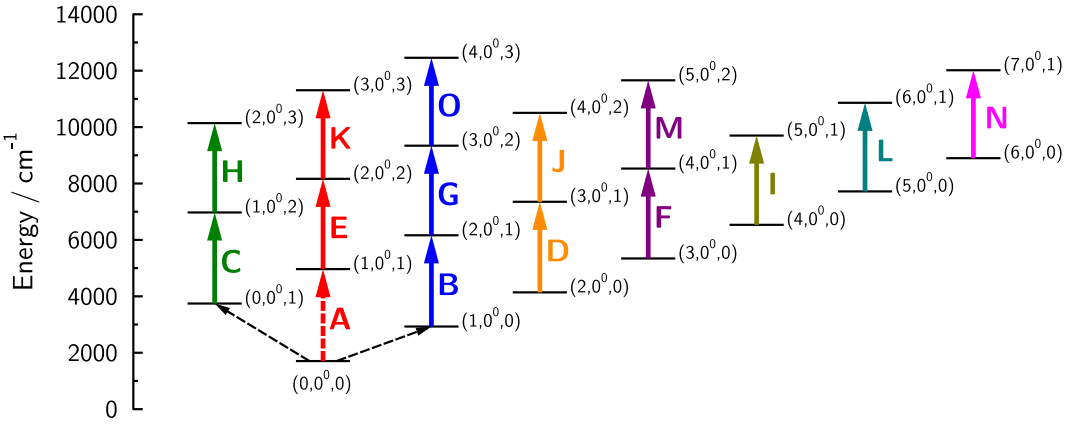

Figure 3.15: Energy level scheme of observed stretching states in C_3, including the variationally calculated zero-point energy. For the series of bands originating from the $(1, 0^0, 0)$ and $(0, 0^0, 1)$ states the lowest level is placed at the experimentally known term energy. [313,321] In case of bands D, F, I, L and N, the lower state term energy corresponds to the G_v of the present calculations: 2435.8, 3637.1, 4830.0, 6015.1, and 7192.9 cm^{-1}, respectively. The latter values are attributed a conservative error estimate of 3 cm^{-1}. Reproduced from Ref. [29] with the permission of AIP Publishing.

Table 3.21: Parameters (in cm^{-1}) of the quartic force field[a] in dimensionless normal coordinates for C_3. Reproduced from Ref. [29] with the permission of AIP Publishing.

Parameter[b]	Value	Parameter[b]	Value
ω_1	1206.698	k_{1111}	1.717
ω_2	42.773	k_{1122}	−177.462
ω_3	2101.276	k_{1133}	17.789
k_{111}	−41.975	k_{2222}	724.835
k_{122}	1315.426	k_{2233}	−294.533
k_{133}	−211.964	k_{3333}	5.131

[a] The equilibrium bond length is $R_e = 1.29397$ Å.
[b] The cubic k_{ijk} and quartic k_{ijkl} force field parameters are defined according to Nielsen [184].

Table 3.22: VPT2 spectroscopic parameters (in cm^{-1}) for C_3.

Parameter	Value	Parameter	Value
E_0	4.26	B_e	0.41950
x_{11}	−2.90	α_1	0.00143
x_{22}	9.98	α_2	−0.02000
x_{33}	−10.08	α_3	0.00338
x_{12}	61.98	ΔB_0	−0.01760
x_{13}	−15.98	$10^6 D_e$	0.203
x_{23}	−42.85	$10^{13} H_e$	0.35
$x_{\ell\ell}$	−2.12	$10^3 q_2^e$	8.242
ZPE	1713.32	$10^6 q_2^J$	−3.858

is apparent from the value of the cubic coupling constant $k_{122} = 1315.426$ cm^{-1}, which is even larger than the harmonic frequency of the symmetric stretching vibration ($\omega_1 = 1206.698$ cm^{-1}). These large third and fourth order force constants clearly show that a perturbational treatment of any order for the vibration-rotation problem in C_3 is problematic. This can also be observed when comparing the rotational parameters, e.g. D_e, H_e and q_2^e in Table 3.22 to the variational and experimental results for D_0 and H_0 (vibrational ground state) and q_v in the $(0, 1^1, 0)$ state presented above.

In Fig. 3.16, the differences $\Delta B_v = B_v - B_0$ for selected vibrational states of C_3 are depicted, where B_0 corresponds to the rotational parameter B_v of the vibrational ground state. Near perfect agreement of the experimental and theoretical results is observed, except for the perturbed states $(5, 0^0, 2)$ and $(6, 0^0, 1)$. In the case of a well behaved semi-rigid molecule this difference can be written within VPT2 as $\Delta B_v = -\sum_i \alpha_i \cdot v_i$. Hence, ΔB_v is a linear function of the quantum numbers v_i, and in general one observes only small deviations from linearity for higher values of v_i as a result of higher order perturbation effects. In C_3 strong deviations from linearity can be observed for *low* values of v_1 while for higher values of v_1 a near linear dependency is found (see left panel of Figure 3.16). In fact, a linear fit of the $(v_1, 0, 0)$ series from $v_1 = 3$ to 6 results in an effective α_1 of 0.0020 cm^{-1} for both the experimental and theoretical ΔB_v values. However, employing the standard procedure of determining an effective α_1 as the difference of B_v between the vibrational ground and $(1, 0^0, 0)$ state results in 0.0056 cm^{-1} from experimental and variational results. Finally, α_1 calculated within VPT2 using the present QFF is 0.0014 cm^{-1}. The latter value is close:nr to the results from the linear range than α_1 calculated from B_v in the $(0, 0^0, 0)$ and $(1, 0^0, 0)$ state. This behaviour will be explained below.

In the right panel of Figure 3.16 the variation of ΔB_v with v_3 is depicted. Again, a strong nonlinear dependency on v_3 can be seen. Here, even the sign of the slope changes when an excitation in v_1 is added. From the experimental and variationally calculated $(4, 0^0, v_3)$ ΔB_v series ($v_3 = 0$ to 3), an effective α_3 of 0.0027 cm^{-1} is obtained. Again, this value is intermediate between the VPT2 result of $\alpha_3 = 0.0034$ cm^{-1} and the α_3 values of -0.0051 and -0.0050 cm^{-1} (experimental and variational result, respectively) obtained by considering only the $(0, 0^0, 0)$ and $(0, 0^0, 1)$ states. Both findings

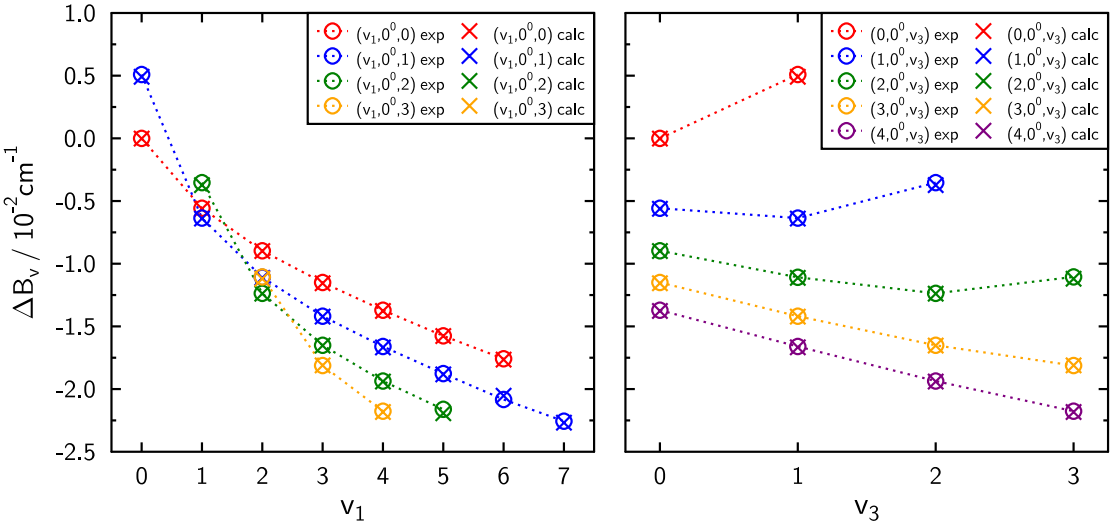

Figure 3.16: Left panel: variation of B_v with increasing stretching quantum numbers v_1 for different series of fixed quantum numbers v_3, and right panel: variation of B_v with increasing stretching quantum numbers v_3 for different series of fixed quantum numbers v_1. Reproduced from Ref. [29] with the permission of AIP Publishing.

can be explained by the fact that the bending part of the PES becomes more stiff upon excitation of the symmetric stretching vibration. From certain values of v_1 on a linear dependency of B_v with respect to the v_i can be observed which is characteristic for semi-rigid molecules.
The dependence of B_v on the stretching quantum numbers v_1 and v_3 can be understood by considering the vibrational wavefunctions. In order to quantify the relation between the vibrational wavefunctions and the rotational parameters, we have calculated the integrated density of the vibrational wavefunction as a function of the bond angle according to:

$$P_v(t) = \int_{q_2=0}^{t} q_2 \mathrm{d}q_2 \int_{q_1=-\infty}^{\infty} \mathrm{d}q_1 \int_{q_3=-\infty}^{\infty} \mathrm{d}q_3 \Psi_v^*(q_1, q_3, q_2)\Psi_v(q_1, q_3, q_2)\,. \tag{3.14}$$

In Equation (3.14) Ψ_v is the normalized vibrational wavefunction of the vibrational state under consideration obtained variationally with the C8VPRO program [210]. Integration over the complete configuration space of vibrational coordinates yields a value of 1. If one treats the upper limit t of the integration over q_2 as a parameter it is possible to calculate the dependency of the integrated density on the deviation of the bond angle from linearity, θ. The value of $q_2 = t$ can be connected to θ by

$$\theta = 2 \arctan\left(\frac{\gamma_2 q_2 (m_1^{-\frac{1}{2}} l_{1x,2} - m_2^{-\frac{1}{2}} l_{2x,2})}{R_\mathrm{e}}\right). \tag{3.15}$$

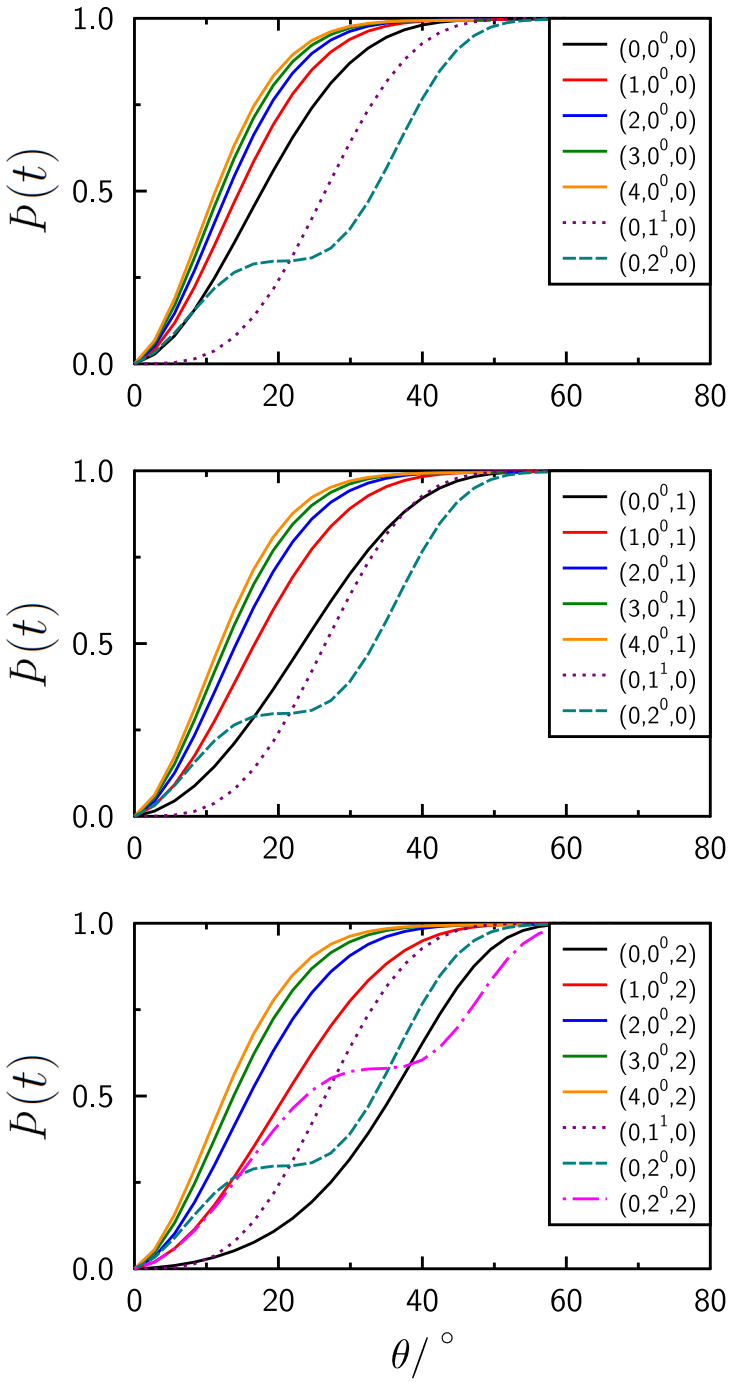

Figure 3.17: Integrated densities of vibrational wavefunctions as a function of the deviation from linearity θ for three series of C_3 states: top) $(v_1, 0^0, 0)$, middle) $(v_1, 0^0, 1)$, and bottom) $(v_1, 0^0, 2)$, using the $(0, 1^1, 0)$ and $(0, 2^0, 0)$ states as reference. Reproduced from Ref. [29] with the permission of AIP Publishing.

Here, γ_2 is the scaling parameter that defines the dimensionless normal coordinate (cf. Equation (4.3) and Equation (4.4)) and $l_{\mathrm{I}\alpha,j}$ are appropriate $\mathscr{L}$-matrix elements. Thus, $\dot{P}_v(t)$ gives a qualitative impression how the probability density accumulates as a function of the bond angle. The larger the angle where $\dot{P}_v(t)$ reaches the region of the asymptotic value of 1 the greater is the bent character of the state under consideration. In Fig. 3.17 $\dot{P}_v(t)$ is depicted for fifteen states investigated experimentally in this work and for a further four states, namely $(0, 1^1, 0)$, $(0, 2^0, 0)$, $(0, 2^0, 2)$ and $(0, 0^0, 2)$, for a better understanding. In a well behaved semi-rigid molecule, like CO_2, $\dot{P}_v(t)$ for a stretching vibrational state reaches a value close to the asymptote quite early ($\theta \approx 15°$), and nearly independent of the combination of stretching vibrational quantum numbers. A value of $\theta > 0$ is always to be expected because of the zero point motion of the molecule. In contrast, in C_3 one finds a strong dependence on the stretching vibrational quantum numbers.

In the upper panel of Figure 3.17 the vibrational ground state clearly exhibits the most bent character among the pure symmetric stretching states. In the middle panel one can observe that the fundamental antisymmetric stretching state $(0, 0^0, 1)$ reaches the asymptotic value as late as the fundamental bending state. Consequently B_v of the $(0, 0^0, 1)$ state is *larger* than the rotational parameter in the vibrational ground state. Figure 3.17 also suggests that the state $(1, 0^0, 2)$ collects its density at larger angles than $(1, 0^0, 1)$. Indeed, the state $(1, 0^0, 2)$ is a further example where the rotational parameter B_v becomes larger upon excitation of one quanta in the antisymmetric stretching vibration. In the lower panel of Figure 3.17 it can be seen that the first overtone of the antisymmetric stretching vibration $(0, 0^0, 2)$ accumulates most of its density at even *larger* θ values than the first overtone of the bending vibration $(0, 2^0, 0)$. The lower panel of Fig. 3.17 also suggests that the $(0, 2^0, 2)$ state accumulates most of its density at smaller angles than the $(0, 0^0, 2)$ state, resulting in a *smaller* rotational parameter for an excited bending state. This is really found from the variational calculations assuming the rotational pattern of a linear molecule in the range $J = 0$ to 10 with B_v of 0.4575 and 0.4565 cm^{-1} for $(0, 0^0, 2)$ and $(0, 2^0, 2)$, respectively.

These observations are in line with the well known fact that C_3 exhibits more and more the properties of a bent molecule with increasing excitation of the antisymmetric stretching vibration. [315] Therefore, the rotational pattern of stretching vibrational states which show more or less bent character cannot accurately be described by neither the formulas for a linear molecule (see Eq. 2.91) nor those of an asymmetric top molecule. Hence, more or less long progressions in $J(J + 1)$ are necessary to fit the rotational energies with the same accuracy as those states which are not affected by this issue. This has been done in previous experimental work [313, 314, 322] resulting in slightly different rotational parameters compared to those obtained in the present work. As C_3 has a linear equilibrium structure it is definitely no quasilinear molecule. The quasilinearity parameter γ_0 introduced by [342] equals to -0.91 which corresponds to an almost linear molecule. Given the growing bent character with increasing excitation of the antisymmetric stretching vibration it is more obvious to call it a "quasi-bent" molecule. By analogy $\gamma_0 = -0.64$ is obtained when considering the $(0, 1^1, 1)$ and $(0, 2^0, 1)$ states.

Using the VPT2 expansion of the vibrational term energy given by Equation (2.49) the VBOs

can be obtained by subtracting the $G_{v''}$ for a lower vibrational state from the $G_{v'}$ in the upper state. For example, the symmetric stretching fundamental frequency ν_1 can be calculated as the difference of the G_v in the $(0, 0^0, 0)$ and $(1, 0^0, 0)$ state according to:

$$G_{(0,0^0,0)} = E_0 + \frac{1}{2}\omega_1 + \omega_2 + \frac{1}{2}\omega_3 + \frac{1}{4}x_{11} + \frac{1}{2}x_{12} + \frac{1}{4}x_{13} + x_{22} + \frac{1}{2}x_{23} + \frac{1}{4}x_{33}\,, \tag{3.16}$$

$$G_{(1,0^0,0)} = E_0 + \frac{3}{2}\omega_1 + \omega_2 + \frac{1}{2}\omega_3 + \frac{9}{4}x_{11} + \frac{3}{2}x_{12} + \frac{3}{4}x_{13} + x_{22} + \frac{1}{2}x_{23} + \frac{1}{4}x_{33}\,, \tag{3.17}$$

$$\nu_1 = G_{(1,0^0,0)} - G_{(0,0^0,0)} = \omega_1 + 2x_{11} + x_{12} + \frac{1}{2}x_{13}\,. \tag{3.18}$$

and the anti-symmetric stretching fundamental frequency ν_3 according to

$$\nu_3 = \omega_3 + 2x_{33} + x_{23} + \frac{1}{2}x_{13}\,. \tag{3.19}$$

By subtracting appropriate VBOs one obtains formulas for the x_{ij}. Within the context of the present study two routes will be shown to obtain values for the anharmonicity parameters x_{11}, x_{33} and x_{13}.

The first route is termed Method $x_{ij} \rightarrow x_{ii}$ since first the offdiagonal parameter x_{13} is determined which then is used for obtaining the diagonal x_{11} and x_{22}. This involves the transitions $(1, 0^0, 1)$ - $(0, 0^0, 0)$ (band A), $(2, 0^0, 1)$ - $(1, 0^0, 0)$ (band B) and $(1, 0^0, 2)$ - $(0, 0^0, 1)$ (band C) with VBOs according to:

$$\nu_{\mathrm{A}} = \omega_1 + \omega_3 + 2x_{11} + x_{12} + 2x_{13} + x_{23} + 2x_{33}\,, \tag{3.20}$$

$$\nu_{\mathrm{B}} = \omega_1 + \omega_3 + 4x_{11} + x_{12} + 3x_{13} + x_{23} + 2x_{33} \tag{3.21}$$

and

$$\nu_{\mathrm{C}} = \omega_1 + \omega_3 + 2x_{11} + x_{12} + 3x_{13} + x_{23} + 4x_{33} \tag{3.22}$$

for band A, B and C, respectively. Then, the first step is calculating x_{13} via:

$$x_{13} = \nu_A - \nu_1 - \nu_3\,. \tag{3.23}$$

The difference $\nu_B - \nu_A$ is:

$$\nu_B - \nu_A = 2x_{11} + x_{13}\,, \tag{3.24}$$

which can be solved for x_{11} to yield

$$x_{11} = \frac{\nu_B - \nu_A - x_{13}}{2} \tag{3.25}$$

and in a similar manner x_{33} is obtained according to

$$x_{33} = \frac{\nu_C - \nu_A - x_{13}}{2}\,. \tag{3.26}$$

Table 3.23: Determination of anharmonicity parameters x_{11}, x_{13} and x_{33} from experimental and theoretical vibrational band origins by two different methods (see text for details). All values are given in units of cm^{-1}.

$x_{ij} \rightarrow x_{ii}$			$x_{ii} \rightarrow x_{ij}$	
Parameter	Exp.	Calc.[c]	Parameter	Calc.[c]
ν_1	1224.49[a]	1224.57	ν_1	1224.57
ν_3	2040.02[b]	2039.60	ν_3	2039.60
ν_A	3260.13[c]	3259.79	$2\nu_1$	2435.77
ν_B	3235.10[c]	3234.77	$2\nu_3$	4032.30
ν_C	3228.38[c]	3228.46	ν_A	3259.79
			ν_E	3200.66
x_{11}	−10.32	−10.32	x_{11}	−6.69
x_{13}	−4.38	−4.38	x_{13}	0.34
x_{33}	−13.68	−13.47	x_{33}	−23.45

[a] From Ref. [321]
[b] From Ref. [322]
[c] This work.

The second route termed Method $x_{ii} \rightarrow x_{ij}$ starts by determining x_{11} and x_{33} and then determines x_{13}. This involves the overtones $2\nu_i$ of the two stretching vibrations, which can be calculated according to

$$2\nu_1 = 2\omega_1 + 6x_{11} + 2x_{12} + x_{13} \tag{3.27}$$

and

$$2\nu_3 = 2\omega_3 + 6x_{33} + 2x_{23} + x_{13}. \tag{3.28}$$

The diagonal anharmonicity parameters x_{11} and x_{33} are then obtained as

$$x_{11} = \frac{2\nu_1 - 2 \cdot \nu_1}{2} \tag{3.29}$$

and

$$x_{33} = \frac{2\nu_3 - 2 \cdot \nu_3}{2}\,, \tag{3.30}$$

where $2 \cdot \nu_i$ corresponds to twice the VBO of the fundamental transition. The VBO of the $(2, 0^0, 2)$ - $(1, 0^0, 1)$ (band E) transition is:

$$\nu_E = \omega_1 + \omega_3 + 4x_{11} + x_{12} + 4x_{13} + x_{23} + 4x_{13}\,. \tag{3.31}$$

Hence, the difference $\nu_E - \nu_A$ can be used to determine x_{13} according to:

$$x_{13} = \frac{\nu_E - \nu_A - 2x_{11} - 2x_{33}}{2}\,. \tag{3.32}$$

The results of calculations following the Methods $x_{ij} \rightarrow x_{ii}$ and $x_{ii} \rightarrow x_{ij}$ as well as the employed VBOs are summarized in Table 3.23. Since no reliable experimental VBOs are available for $2\nu_1$ and $2\nu_3$, results are based on the present variational calculations only.
The anharmonicity parameters x_{11}, x_{33} and x_{13} determined from the experimental VBOs by Method $x_{ij} \rightarrow x_{ii}$ are $x_{11} = -10.32$ cm^{-1}, $x_{33} = -13.68$ cm^{-1} and $x_{13} = -4.38$ cm^{-1}. Employing the variational VBOs almost identical values are obtained. However, by combining the theoretical VBOs for ν_1, ν_3, $2\nu_1$, $2\nu_3$ as well as bands A and E in Method $x_{ii} \rightarrow x_{ij}$ one arrives at a different set of parameters: $x_{11} = -6.69$ cm^{-1}, $x_{33} = -23.45$ cm^{-1} and $x_{13} = 0.34$ cm^{-1}. Finally, the VPT2 result employing the QFF (Table 3.22) is $x_{11} = -2.90$ cm^{-1}, $x_{33} = -10.08$ cm^{-1} and $x_{13} = -15.98$ cm^{-1}. The strong variation of the anharmonicity parameters with the type of calculation used to obtain them shows that the underlying assumption of perturbation theory of any order, i.e. perturbations are small compared to the zeroth order (harmonic) solution, is not fulfilled for C_3, and hence, Equation (2.49) does not apply.

Chapter 4

C8v4: A variational program for tetraatomic linear molecules using Watsons isomorphic Hamiltonian

This chapter presents the development of a variational approach to obtain rovibrational term energies and wave functions for tetraatomic linear molecules. The basic form of the rovibrational Hamiltonian has been presented in Section 2.3.1. In Section 4.1 the theoretical considerations of a variational approach specific for tetraatomic linear molecules is presented. First, the employed basis functions and the subsequent transformation of the Hamiltonian are presented in Section 4.1.1 and 4.1.2, respectively. Details of the potential energy of a tetraatomic linear molecule are given in Section 4.1.3. Section 4.1.4 analyzes the structure of the Hamiltonian matrix and Section 4.1.5 gives the necessary discussion of symmetry related to the present approach. The implementation into the FORTRAN program C8v4 is described in Section 4.2. Special attention is given to the parallelization of the code (Section 4.2.6). Finally, Section 4.3 presents proof-of-principle calculations on two example molecules where results obtained with C8v4 are compared to literature.

4.1 Theoretical considerations

4.1.1 Variational *ansatz* and basis functions

The first step in the development of a variational approach is the choice of basis functions to represent the rovibrational wave functions. The *ansatz* adopted here is given by

$$\left|\psi_v^{(J)}\right\rangle = \sum_{k=-J}^{J} \sum_{i}^{N_k} c_{ki}^{(v,J)} \left|\mathbf{V}_i \boldsymbol{\ell} J k\right\rangle \,, \tag{4.1}$$

where N_k is the number of employed vibrational basis functions in each k-block (cf. Section 4.2.3), $c_{ki}^{(v,J)}$ the coefficients of the linear combination and $|\mathbf{V}_i \boldsymbol{\ell} J k\rangle$ is a product of harmonic oscillator and symmetric rotor functions:

$$|\mathbf{V}_i \boldsymbol{\ell} J k\rangle = |\mathbf{V}_i \boldsymbol{\ell}\rangle \, |J k\rangle \,. \tag{4.2}$$

In Equation (4.1) and (4.2) $\mathbf{V}_i$ is a collective variable for the vibrational quantum numbers $\mathbf{V}_i = (v_1, v_2, v_3, v_4, v_5)$ and $\boldsymbol{\ell} = (\ell_4, \ell_5)$. This choice of basis functions is advantageous since it allows almost all of the integrals needed for the KEO to be evaluated analytically, as will be discussed below.

Vibrational basis functions

The vibrational basis function $|\mathbf{V}_i \boldsymbol{\ell}\rangle$ is a product of harmonic oscillator functions. The individual functions are setup with respect to dimensionless normal coordinates q_i which are defined using a scaling factor

$$\gamma_i = \sqrt{\frac{\hbar}{2\pi c \omega_i}} \,, \tag{4.3}$$

where $\hbar$ is Planck's constant divided by 2π, c is the speed of light and ω_i is the harmonic vibrational frequency. Then, the q_i and their conjugate momenta $\hat{\mathrm{p}}_i$ are given by

$$Q_i = \gamma_i q_i \tag{4.4}$$

and

$$\hat{\mathrm{P}}_i = \frac{1}{\gamma_i} \hat{\mathrm{p}}_i \,. \tag{4.5}$$

For the stretching vibrations s the basis functions are the eigenfunctions of the one dimensional harmonic oscillator Hamiltonian

$$\hat{\mathrm{h}}_s^{\mathrm{1D}} = \frac{1}{2} \omega_s \left(\hat{\mathrm{p}}_s^2 + q_s^2\right) \,. \tag{4.6}$$

They are given by [343]

$$|v_s\rangle = \mathrm{H}_{v_s}(q_s) \mathrm{e}^{-\frac{1}{2} q_s^2} \,. \tag{4.7}$$

Table 4.1: Matrix elements of the one dimentional harmonic oscillator

$\langle v_s\|q_s\|v_s+1\rangle$	=	$\sqrt{\frac{v_s+1}{2}}$	=	$\mathrm{i}\,\langle v_s\|\hat{\mathrm{p}}_s\|v_s+1\rangle$
$\langle v_s\|q_s\|v_s-1\rangle$	=	$\sqrt{\frac{v_s}{2}}$	=	$-\mathrm{i}\,\langle v_s\|\hat{\mathrm{p}}_s\|v_s-1\rangle$
$\langle v_s\|q_s^2\|v_s+2\rangle$	=	$\frac{1}{2}\sqrt{(v_s+1)(v_s+2)}$	=	$-\langle v_s\|\hat{\mathrm{p}}_s^2\|v_s+2\rangle$
$\langle v_s\|q_s^2\|v_s\rangle$	=	$v_s+\frac{1}{2}$	=	$\langle v_s\|\hat{\mathrm{p}}_s^2\|v_s\rangle$
$\langle v_s\|q_s^2\|v_s-2\rangle$	=	$\frac{1}{2}\sqrt{v_s(v_s-1)}$	=	$-\langle v_s\|\hat{\mathrm{p}}_s^2\|v_s-2\rangle$
$\langle v_s\|q_s\hat{\mathrm{p}}_s\|v_s+2\rangle$	=	$-\frac{1}{2}\mathrm{i}\sqrt{(v_s+1)(v_s+2)}$	=	$\langle v_s\|\hat{\mathrm{p}}_s q_s\|v_s+2\rangle$
$\langle v_s\|q_s\hat{\mathrm{p}}_s\|v_s\rangle$	=	$\frac{1}{2}\mathrm{i}$	=	$-\langle v_s\|\hat{\mathrm{p}}_s q_s\|v_s\rangle$
$\langle v_s\|q_s\hat{\mathrm{p}}_s\|v_s-2\rangle$	=	$\frac{1}{2}\mathrm{i}\sqrt{v_s(v_s-1)}$	=	$\langle v_s\|\hat{\mathrm{p}}_s q_s\|v_s-2\rangle$

In Equation (4.7) $\mathrm{H}_n(x)$ is a (normalized) Hermite polynomial of degree $n = v_s$ [344]. The use of such a basis function enables the analytic evaluation of matrix elements when employing the Watson KEO and all the required one dimensional integrals are taken from [343] and summarized in Table 4.1.

The bending vibrations in a linear molecule are doubly degenerate with normal coordinates q_{t1} and q_{t2}. It is convenient to identify the directions 1 and 2 with the cartesian x and y directions such that $q_{t1} = q_{tx}$ and $q_{t2} = q_{ty}$. The vibrational Hamiltonian set up in these coordinates is

$$\hat{\mathrm{h}}_t^{\mathrm{2D},xy} = \frac{1}{2}\omega_t[(\hat{\mathrm{p}}_{tx}^2 + \hat{\mathrm{p}}_{ty}^2) + (q_{tx}^2 + q_{ty}^2)] \tag{4.8}$$

with eigenfunctions

$$|v_t\rangle = |v_{tx}\rangle\,|v_{ty}\rangle\ , \tag{4.9}$$

where the $|v_{t\alpha}\rangle$ are one dimensional harmonic oscillators given in Equation (4.7) and $v_t = v_{tx} + v_{ty}$. The energy eigenvalue associated with such a basis function is

$$\hat{\mathrm{h}}_t^{\mathrm{2D},xy}\,|v_t\rangle = \omega_t\left[\left(v_{tx}+\frac{1}{2}\right)+\left(v_{tx}+\frac{1}{2}\right)\right]|v_t\rangle = \omega_t(v_t+1)\,|v_t\rangle\ . \tag{4.10}$$

This choice of basis functions could in principal be used with the Hamiltonian in Equation (2.33). However, it would involve rather complicated transformations to select the correct functions according to Equation (2.43). Therefore, it is more convenient to set up the 2D Hamiltonian in polar coordinates that already incorporates the symmetry of the bending vibration

$$\rho_t = q_t^2 = q_{tx}^2 + q_{ty}^2 \tag{4.11}$$

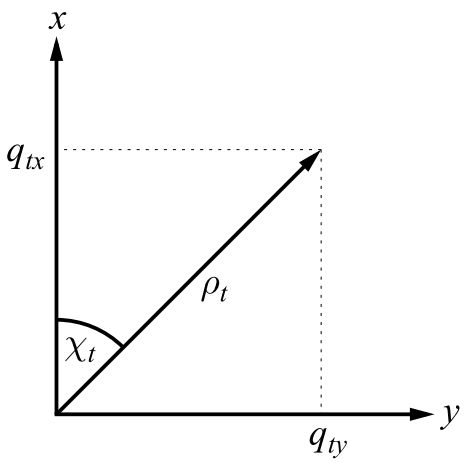

Figure 4.1: Representation of the relation between the set of degenerate coordinates (q_{tx}, q_{tx}) and the polar coordinates (ρ_t, χ_t) of a two-dimensional isotropic harmonic oscillator.

and

$$\tan(\chi_t) = \frac{q_{tx}}{q_{ty}}\,, \tag{4.12}$$

which implies

$$q_{tx} = q_t \cos\chi_t = \sqrt{\rho_t}\cos\chi_t \tag{4.13}$$

and

$$q_{ty} = q_t \sin\chi_t = \sqrt{\rho_t}\sin\chi_t\,. \tag{4.14}$$

The relation between the coordinates (q_{tx}, q_{ty}), the radial component ρ_t and the phase angle χ_t is graphically displayed in Figure 4.1. This change of coordinates results in the 2D isotropic harmonic oscillator Hamiltonian [233]

$$\hat{\mathrm{h}}_t^{\mathrm{2D,iso}} = -\frac{1}{2}\omega_t\left[\frac{1}{q_t}\frac{\partial}{\partial q_t}\left(q_t\frac{\partial}{\partial q_t}\right) + \frac{1}{q_t^2}\frac{\partial^2}{\partial\chi_t^2} - q_t^2\right] \tag{4.15}$$

and by making a product *ansatz* of the form $\psi = F(q_t)G(\chi_t)$ the desired basis functions are obtained as [345]

$$|v_t^{\ell_t}\rangle = |v_t\ell_t\rangle = \sqrt{\frac{1}{2\pi}}\mathrm{L}_{n_t}^{|\ell_t|}(\rho_t)\,\rho_t^{\frac{|\ell_t|}{2}}\mathrm{e}^{-\frac{1}{2}\rho_t}\mathrm{e}^{\mathrm{i}\ell_t\chi_t}\,, \tag{4.16}$$

where the substitution according to Equation (4.11) has been included. In Equation (4.16), the $\mathrm{L}_{n_t}^{|\ell_t|}(\rho_t)$ are (normalized) associated Laguerre polynomials [344] with $n_t = (v_t + |\ell_t|)/2$. The order

of the polynomial is given by $n_t - |\ell_t| = (v_t - |\ell_t|)/2$. The energy eigenvalue is given by

$$\hat{\mathrm{h}}_t^{\mathrm{2D,iso}} \, |v_t^{\ell_t}\rangle = \omega_t(v_t + 1) \, |v_t^{\ell_t}\rangle \; . \tag{4.17}$$

The factor of $(2\pi)^{-\frac{1}{2}}$ in Equation (4.16) originates from normalizing the χ_t phase factor of the basis function

$$|\ell_t\rangle = \sqrt{\frac{1}{2\pi}} \mathrm{e}^{\mathrm{i}\ell_t\chi_t} \, , \tag{4.18}$$

where ℓ_t is the vibrational angular momentum quantum number that can take the values $\ell_t = \pm v_t, \pm(v_t - 2), \pm(v_t - 4), \ldots, \pm 1$ or 0. Matrix elements of Equation (4.16) will be evaluated with respect to the ladder-like operators $q_t^{\pm}$ and $\hat{\mathrm{p}}_t^{\pm}$ which are defined as

$$q_t^{\pm} = q_{t_x} \pm \mathrm{i} q_{t_y} \tag{4.19}$$

and

$$\hat{\mathrm{p}}_t^{\pm} = \hat{\mathrm{p}}_{t_x} \pm \mathrm{i}\hat{\mathrm{p}}_{t_y} \, . \tag{4.20}$$

They have been worked out for example by Shaffer [345], Yamada [346] or in the monograph by Papoušek and Aliev [186]. Table 4.2 summarizes the necessary matrix elements for the integration of the KEO. The above transformation (Equation (4.19) and (4.20)) has to be applied accordingly also to the Hamiltonian in Equation (2.33) which will be presented in Section 4.1.2.

Rotational basis functions

Rigid rotor functions are used as basis functions for the rotation of the molecule. It can be shown that these functions are given by

$$\begin{aligned} |Jkm\rangle &= \sqrt{\frac{2J+1}{8\pi^2}} \mathrm{D}_{mk}^{J*}(\phi, \theta, \chi') \\ &= \sqrt{\frac{1}{2\pi}} S_{Jkm}(\theta, \phi) \mathrm{e}^{\mathrm{i}k\chi'} \, , \end{aligned} \tag{4.21}$$

where $\mathrm{D}_{mk}^{J*}(\phi, \theta, \chi')$ is a rotation matrix [234]. Matrix elements of the functions Equation (4.21) are obtained with respect to the angular momentum ladder operators

$$\hat{\Pi}'_{\pm} = \hat{\Pi}'_x \pm \mathrm{i}\hat{\Pi}'_y \tag{4.22}$$

and for the integration of the KEO the following analytic integrals are needed [347]

$$\langle Jk|\hat{\Pi}'_{\pm}\hat{\Pi}'_{\mp}|Jk\rangle = \left[J\,(J+1) - k^2\right] \, , \tag{4.23}$$

$$\langle Jk \mp 1|\hat{\Pi}'_{\pm}|Jk\rangle = \sqrt{J\,(J+1) - k\,(k \mp 1)} \, . \tag{4.24}$$

Table 4.2: Matrix elements of the two-dimentional isotropic harmonic oscillator.

$$
\begin{aligned}
\langle v_t,\ell_t|q_t^{\pm}|v_t+1,\ell_t\mp1\rangle &= \pm\sqrt{\tfrac{1}{2}(v_t\mp\ell_t)}\\
\langle v_t,\ell_t|\hat{\mathrm{p}}_t^{\pm}|v_t+1,\ell_t\mp1\rangle &= \mathrm{i}\,\langle v_t,\ell_t|q_t^{\pm}|v_t+1,\ell_t\mp1\rangle\\
\langle v_t,\ell_t|q_t^{\pm}|v_t-1,\ell_t\mp1\rangle &= \mp\sqrt{\tfrac{1}{2}(v_t\pm\ell_t+2)}\\
\langle v_t,\ell_t|\hat{\mathrm{p}}_t^{\pm}|v_t-1,\ell_t\mp1\rangle &= -\mathrm{i}\,\langle v_t,\ell_t|q_t^{\pm}|v_t+1,\ell_t\mp1\rangle\\
\langle v_t,\ell_t|q_t^{\pm}q_t^{\mp}|v_t+2,\ell_t\rangle &= -\tfrac{1}{2}\sqrt{(v_t+\ell_t+2)(v_t-\ell_t+2)}\\
\langle v_t,\ell_t|\hat{\mathrm{p}}_t^{\pm}\hat{\mathrm{p}}_t^{\mp}|v_t+2,\ell_t\rangle &= -\,\langle v_t,\ell_t|q_t^{\pm}q_t^{\mp}|v_t+2,\ell_t\rangle\\
\langle v_t,\ell_t|q_t^{\pm}q_t^{\mp}|v_t,\ell_t\rangle &= v_t+1\\
\langle v_t,\ell_t|\hat{\mathrm{p}}_t^{\pm}\hat{\mathrm{p}}_t^{\mp}|v_t,\ell_t\rangle &= \langle v_t,\ell_t|q_t^{\pm}q_t^{\mp}|v_t,\ell_t\rangle\\
\langle v_t,\ell_t|q_t^{\pm}q_t^{\mp}|v_t-2,\ell_t\rangle &= -\tfrac{1}{2}\sqrt{v_t^2-\ell_t^2}\\
\langle v_t,\ell_t|\hat{\mathrm{p}}_t^{\pm}\hat{\mathrm{p}}_t^{\mp}|v_t-2,\ell_t\rangle &= -\,\langle v_t,\ell_t|q_t^{\pm}q_t^{\mp}|v_t-2,\ell_t\rangle\\
\langle v_t,\ell_t|q_t^{\pm}\hat{\mathrm{p}}_t^{\mp}|v_t+2,\ell_t\rangle &= \tfrac{1}{2}\sqrt{(v_t+\ell_t+2)(v_t-\ell_t+2)}\\
\langle v_t,\ell_t|\hat{\mathrm{p}}_t^{\pm}q_t^{\mp}|v_t+2,\ell_t\rangle &= \langle v_t,\ell_t|q_t^{\pm}q_t^{\mp}|v_t+2,\ell_t\rangle\\
\langle v_t,\ell_t|q_t^{\pm}\hat{\mathrm{p}}_t^{\mp}|v_t,\ell_t\rangle &= \mp\mathrm{i}(\ell_t\mp1)\\
\langle v_t,\ell_t|\hat{\mathrm{p}}_t^{\pm}q_t^{\mp}|v_t,\ell_t\rangle &= -\,\langle v_t,\ell_t|q_t^{\pm}q_t^{\mp}|v_t,\ell_t\rangle\\
\langle v_t,\ell_t|q_t^{\pm}\hat{\mathrm{p}}_t^{\mp}|v_t-2,\ell_t\rangle &= -\tfrac{1}{2}\sqrt{v_t^2-\ell_t^2}\\
\langle v_t,\ell_t|\hat{\mathrm{p}}_t^{\pm}q_t^{\mp}|v_t-2,\ell_t\rangle &= \langle v_t,\ell_t|q_t^{\pm}q_t^{\mp}|v_t-2,\ell_t\rangle
\end{aligned}
$$

No term in the Hamiltonian involving the operators $\hat{\Pi}'_{\pm}$ has matrix element that are off-diagonal in J and since the basis functions Equation (4.21) are orthonormal J is a good quantum number, separating the Hamiltonian matrix in independent blocks for each J value.

4.1.2 Transformation of the Hamiltonian

In order to evaluate the necessary integrals efficiently, the coordinates and the individual operators of the KEO need to be transformed to those defined in Equation (4.19), (4.20) and (4.22). This is done in a term by term fashion.

For the linear vibrational momentum term $\hat{\mathrm{T}}_{\mathrm{P}}$ the operators for the degenerate bending vibrations are straightforward to rewrite by using Equation (4.19) and (4.20) to give

$$\hat{\mathrm{T}}_{\mathrm{P}} = \frac{1}{2}\sum_s \frac{1}{\gamma_s^2}\hat{\mathrm{p}}_s^2 + \frac{1}{2}\sum_t \frac{1}{\gamma_t^2}\hat{\mathrm{p}}_t^{\pm}\hat{\mathrm{p}}_t^{\mp}\,, \tag{4.25}$$

where the two summations run over stretching (s) and bending vibrations (t).
The first step in rewriting the term $\hat{\mathrm{T}}_\pi$ is the definition of the ladder-like operator

$$\hat{\pi}_\pm = \hat{\pi}_x \pm \mathrm{i}\hat{\pi}_y \,, \tag{4.26}$$

which after insertion yields

$$\hat{\mathrm{T}}_\pi = \frac{1}{2}\mu\left(\hat{\pi}_x^2 + \hat{\pi}_y^2\right) = \frac{1}{4}\mu\left(\hat{\pi}_+\hat{\pi}_- + \hat{\pi}_-\hat{\pi}_+\right) \,. \tag{4.27}$$

In Equation (4.26) the $\hat{\pi}_\alpha$ have been defined previously in Equation (2.40) and by insertion one obtains in terms of dimensionless normal coordinates

$$\hat{\pi}_\pm = \sum_{ij} \zeta_{ij}^x \frac{\gamma_j}{\gamma_i} q_i \hat{\mathrm{p}}_j \pm \mathrm{i} \sum_{kl} \zeta_{kl}^y \frac{\gamma_l}{\gamma_k} q_k \hat{\mathrm{p}}_l \,. \tag{4.28}$$

As discussed in Section 2.3.1 the only non-vanishing ζ_{ij}^α for linear molecules are those with $\{i,j\} = \{s,t_y\}$ and $\{i,j\} = \{s,t_x\}$ for $\alpha = x$ and $\alpha = y$, respectively. Thus, terms in Equation (4.28) can be grouped according to the summation indices into two cases:

1. $(ij,kl) = (st_y, st_x)$

2. $(ij,kl) = (t_y s, t_x s)$

Considering case 1. such a term can be rearranged by use of Equation (2.42) and Equation (4.20)

$$\zeta_{st_y}^x \frac{\gamma_t}{\gamma_s} q_s \hat{\mathrm{p}}_{t_y} \pm \mathrm{i}\zeta_{st_x}^y \frac{\gamma_t}{\gamma_s} q_s \hat{\mathrm{p}}_{t_x} = \mp \mathrm{i}\zeta_{st} \frac{\gamma_t}{\gamma_s} q_s \hat{\mathrm{p}}_t^\pm \,. \tag{4.29}$$

Analogously case 2. can be rearranged according to

$$\zeta_{t_y s}^x \frac{\gamma_s}{\gamma_t} q_{t_y} \hat{\mathrm{p}}_s \pm \mathrm{i}\zeta_{t_x s}^y \frac{\gamma_s}{\gamma_t} q_{t_x} \hat{\mathrm{p}}_s = \pm \mathrm{i}\zeta_{st} \frac{\gamma_s}{\gamma_t} q_t^\pm \hat{\mathrm{p}}_s \,, \tag{4.30}$$

where now Equation (4.19) has been used in the last step. Combining Equation (4.29) and Equation (4.30) one arrives at the final form of $\hat{\pi}_\pm$

$$\hat{\pi}_\pm = \mp \mathrm{i} \sum_{(st)} \zeta_{st} \left(\frac{\gamma_t}{\gamma_s} q_s \hat{\mathrm{p}}_t^\pm - \frac{\gamma_s}{\gamma_t} q_t^\pm \hat{\mathrm{p}}_s \right) \tag{4.31}$$

and the summation runs over all possible stretch-bend pairs (st). The same general result has been obtained by Suzuki [348] but with the sign exchanged since his formula uses $\zeta_{ts} = -\zeta_{st}$. Using

Equation (4.31) the sum $\hat{\pi}_+\hat{\pi}_- + \hat{\pi}_-\hat{\pi}_+$ is obtained as

$$
\begin{aligned}
&(\hat{\pi}_+\hat{\pi}_- + \hat{\pi}_-\hat{\pi}_+) = \\
&\sum_{(st)}\sum_{(st)'} \zeta_{st}\zeta_{s't'} \left[\frac{\gamma_t\gamma_{t'}}{\gamma_s\gamma_{s'}} q_s q_{s'} \left(\hat{\mathrm{p}}_t^+ \hat{\mathrm{p}}_{t'}^- + \hat{\mathrm{p}}_t^- \hat{\mathrm{p}}_{t'}^+ \right) - \frac{\gamma_t\gamma_{s'}}{\gamma_s\gamma_{t'}} q_s \hat{\mathrm{p}}_{s'} \left(\hat{\mathrm{p}}_t^+ q_{t'}^- + \hat{\mathrm{p}}_t^- q_{t'}^+ \right) \right. \\
&\qquad - \left. \frac{\gamma_s\gamma_{t'}}{\gamma_t\gamma_{s'}} \hat{\mathrm{p}}_s q_{s'} \left(q_t^+ \hat{\mathrm{p}}_{t'}^- + q_t^- \hat{\mathrm{p}}_{t'}^+ \right) + \frac{\gamma_s\gamma_{s'}}{\gamma_t\gamma_{t'}} \hat{\mathrm{p}}_s \hat{\mathrm{p}}_{s'} \left(q_t^+ q_{t'}^- + q_t^- q_{t'}^+ \right) \right] . \qquad (4.32)
\end{aligned}
$$

The rotational KEO is rewritten by use of Equation (4.22) which yields

$$\hat{\mathrm{T}}_{\mathrm{R}} = \frac{1}{2}\mu \left(\hat{\Pi}_x'^2 + \hat{\Pi}_y'^2 \right) = \frac{1}{2}\mu \hat{\Pi}_\pm' \hat{\Pi}_\mp' \,. \qquad (4.33)$$

Finally, the Coriolis term that couples rotation and vibration $\hat{\mathrm{T}}_{\mathrm{VR}}$ is obtained by employing Equation (4.31) together with Equation (4.22)

$$\hat{\mathrm{T}}_{\mathrm{VR}} = -\mu \left(\hat{\Pi}_x' \hat{\pi}_x + \hat{\Pi}_y' \hat{\pi}_y \right) = -\frac{1}{2}\mu \left(\hat{\Pi}_+' \hat{\pi}_- + \hat{\Pi}_-' \hat{\pi}_+ \right) = -\frac{1}{2}\mu \hat{\Pi}_\pm' \hat{\pi}_\mp \,, \qquad (4.34)$$

where the last equality results from the fact that either $\hat{\Pi}_+'$ or $\hat{\Pi}_-'$ will have a non-vanishing matrix element with the rotational basis functions depending on the value of k in the bra and ket.

4.1.3 The potential energy

The potential energy can be expressed as a Taylor expansion in terms of the dimensionless normal coordinates

$$V = \frac{1}{2}\sum_i \omega_i q_i^2 + \frac{1}{6}\sum_{ijk} \phi_{ijk} q_i q_j q_k + \frac{1}{24}\sum_{ijkl} \phi_{ijkl} q_i q_j q_k q_l + \ldots \qquad (4.35)$$

where ϕ_{ijk} and ϕ_{ijkl} are cubic and quartic force constants, respectively. The summations in Equation (4.35) are again over all $3N_{\mathrm{at}} - 5$ normal coordinates.
An important aspect of the potential energy in linear molecules with more than three atoms is the coupling between basis functions of different $(\ell_t, \ell_{t'})$. This can be realized by considering for example the following cubic terms in the potential energy of a tetraatomic linear molecule

$$\frac{1}{6}\phi_{s4x5x} q_s q_{4x} q_{5x} + \frac{1}{6}\phi_{s4y4y} q_s q_{4y} q_{5y} \,,$$

where due to symmetry $\phi_{s4x5x} = \phi_{s4y5y} = \phi_{s45}$. This sum can be rewritten by employing Equation (4.13) and (4.14) as well as introducing the difference of the phase angles $\xi = \chi_5 - \chi_4$

$$\frac{1}{6}\phi_{s45} q_s q_4 q_5 \cos\xi = \frac{1}{6}\phi_{s45} q_s q_4^\pm q_5^\mp \,,$$

where the right-hand side follows from Euler's formula and Equation (4.19). Forming a matrix element with a vibrational basis functions $|\mathbf{V}_i\boldsymbol{\ell}\rangle$ over the operators occurring in this term yields

$$\begin{aligned}\langle \mathbf{V}_i\boldsymbol{\ell}|q_s q_4^{\pm} q_5^{\mp}|\mathbf{V}_j\boldsymbol{\ell}'\rangle &= \langle v_s v_4 \ell_4 v_5 \ell_5|q_s q_4^{\pm} q_5^{\mp}|v_s v_4' \ell_4' v_5' \ell_5'\rangle \prod_{s'\neq s} \delta_{v_{s'} v_{s'}'} \\ &= \langle v_s|q_s|v_s'\rangle \langle v_4 \ell_4|q_4^{\pm}|v_4'\ell_4'\rangle \langle v_5\ell_5|q_5^{\mp}|v_5'\ell_5'\rangle \prod_{s'\neq s} \delta_{v_{s'} v_{s'}'}\,. \end{aligned} \tag{4.36}$$

Such a matrix element will only then be different from zero when the ℓ_t differ by ± 1. The potential energy thus can couple basis functions with different $(\ell_t, \ell_{t'})$ combinations. Similar terms can be obtained from quartic potential energy terms, which then have $\cos 2\xi$ dependence and therefore couple basis functions differing in the ℓ_t by ± 2. By using this finding the potential energy can be rewritten to yield

$$V = \sum_{n}^{n_{\max}} V^{(n)} \cos n\xi\,, \tag{4.37}$$

where $V^{(n)}$ can then be expressed again as a Taylor expansion (cf. Equation (4.35)) and the summations now run over the indices s and t. The number n indicates the $\Delta\ell_t$ that can be coupled and the maximum value $n_{\max}$ is determined by half the maximum degree of expansion employed in the coupling terms of the bending normal coordinates in the original potential Equation (4.35). Thus, for a so called quartic force field (QFF) which is a common degree of expansion $n_{\max} = 2$ and basis functions with at max $\Delta\ell_t = \pm 2$ are coupled through the potential energy. All higher $\Delta\ell_t$ couplings due to V vanish for a QFF.

The expansion of V in terms of the q_i is advantageous as this would allow the $\langle \mathbf{V}_i\boldsymbol{\ell}|V|\mathbf{V}_j\boldsymbol{\ell}'\rangle$ integrals to be reduced to sums of products of simple one dimensional integrals, which could be evaluated analytically. However, in most cases the potential energy is expanded in terms of geometrically defined curvilinear internal coordinates Я_i again as a Taylor expansion

$$V = \frac{1}{2}\sum_{ij} f_{ij}\text{Я}_i\text{Я}_j + \frac{1}{6}\sum_{ijk} f_{ijk}\text{Я}_i\text{Я}_j\text{Я}_k + \frac{1}{24} f_{ijkl}\text{Я}_i\text{Я}_j\text{Я}_k\text{Я}_l + \ldots \tag{4.38}$$

The transformation from normal coordinates to curvilinear internal coordinates is non-linear [233]

$$\text{Я}_n = \sum_i \gamma_i \mathrm{L}_i^n q_i + \frac{1}{2}\sum_{ij}\gamma_i\gamma_j \mathrm{L}_{ij}^n q_i q_j + \frac{1}{6}\sum_{ijk}\gamma_i\gamma_j\gamma_k \mathrm{L}_{ijk}^n q_i q_j q_k + \ldots\,, \tag{4.39}$$

where the L_i^n, L_{ij}^n and L_{ijk}^n are elements of the **L**-tensors [349] and the summations run over the $3N_{\text{at}} - 5$ normal coordinate indices. Cartesian displacement coordinates of nuclear positions $x_{\text{I}\alpha} = R_{\text{I}\alpha} - R_{\text{I}\alpha}^{\text{e}}$, where $R_{\text{I}\alpha}$ and $R_{\text{I}\alpha}^{\text{e}}$ are the instantaneous and equilibrium cartesian coordinates of nucleus I, respectively, are also related to the Я_n via a non-linear transformation [233]

$$\text{Я}_n = \sum_i \mathrm{B}_i^n x_i + \frac{1}{2}\sum_{ij}\mathrm{B}_{ij}^n x_i x_j + \frac{1}{6}\sum_{ijk}\mathrm{B}_{ijk}^n x_i x_j x_k + \ldots \tag{4.40}$$

In Equation (4.40), the summations run over all atoms I and cartesian components α. Inserting the definition of the $Я_n$ according to Equation (4.39) into Equation (4.38) shows that, when employing an curvilinear internal coordinate potential energy surface the expansion with respect to normal coordinates is infinite. This has important implications for the evaluation of potential energy matrix elements which will be discussed in Section 4.2.2 and the structure of the Hamiltonian matrix (cf. Section 4.1.4).
Hoy, Strey and Mills [349] have shown that it is possible to transform force constants from internal coordinates to normal coordinates and vice versa by use of only the L_i^n. The derivative of the potential energy with respect to the q_i ($\omega_i,\ \phi_{ijk},\ \ldots$) can be related to the derivates with respect to the $Я_i$ ($f_{ii},\ f_{ijk},\ \ldots$). For example the cubic force constants $\frac{\partial^3 V}{\partial q_i \partial q_j \partial q_j} = \phi_{ijk}$ can be obtained via [233]

$$\begin{aligned}\frac{\partial^3 V}{\partial q_i \partial q_j \partial q_k} = &\sum_{lmn}\left(\frac{\partial^3 V}{\partial Я_l \partial Я_m \partial Я_n}\right)\left(\frac{\partial Я_l}{\partial q_i}\frac{\partial Я_m}{\partial q_j}\frac{\partial Я_n}{\partial q_k}\right)\\ &+\sum_{lm}\left(\frac{\partial^2 V}{\partial Я_l \partial Я_m}\right)\left(\frac{\partial^2 Я_l}{\partial q_i \partial q_j}\frac{\partial Я_m}{\partial q_k}+\frac{\partial^2 Я_l}{\partial q_i \partial q_k}\frac{\partial Я_m}{\partial q_j}+\frac{\partial^2 Я_l}{\partial q_j \partial q_k}\frac{\partial Я_m}{\partial q_i}\right)\\ &+\sum_{l}\left(\frac{\partial V}{\partial Я_l}\right)\left(\frac{\partial^3 Я_l}{\partial q_i \partial q_j \partial q_k}\right). \end{aligned} \tag{4.41}$$

The order of expansion that can be transformed exactly thus is the same before and after, e.g. a QFF in internal coordinates determines the QFF in normal coordinates. Such an approach would allow a PEF to be first transformed to normal coordinates before usage in a variational calculation. All matrix elements could then be evaluted analytically. Expressions for force constants up to fourth order (ϕ_{ijkl}) have been developed by Hoy, Strey and Mills [349]. Expanding the approach up to arbitrary order, depending on the expansion of the provided internal coordinate PEF, would involve complicated transformations to be implemented.
Employing an internal coordinate PEF together with a KEO formulated in normal coordinates has the consequence that the potential energy matrix elements have to be evaluated numerically. Then, the potential energy needs to be evaluated at specific grid points of a numerical integration scheme. The transformation form normal coordinates to cartesian displacement coordinates $\mathbf{x}$ is linear

$$\mathbf{x} = \mathbf{M}^{-\frac{1}{2}}\mathbf{u} = \mathbf{M}^{-\frac{1}{2}}\mathscr{L}\mathbf{Q}\,, \tag{4.42}$$

where $\mathbf{M}$ is thr $3N_{\mathrm{at}} \times 3N_{\mathrm{at}}$ diagonal matrix of the atomic masses. Therefore, as long as the relation of the cartesian coordinates $\mathbf{R}_{\mathrm{I}}$ to the internal coordinates $\boldsymbol{Я}$ is known, any potential formulated in curvilinear coordinates can be employed in the calculation following the transformation scheme

$$\mathbf{Q} \xrightarrow{\mathbf{M}^{-\frac{1}{2}}\mathscr{L}} \mathbf{x}_{\mathrm{I}} \xrightarrow{\mathbf{R}_{\mathrm{I}}^{\mathrm{e}}} \mathbf{R}_{\mathrm{I}} \longrightarrow \boldsymbol{Я}\,. \tag{4.43}$$

Internal coordinates for tetraatomic linear molecules

A common set of curvilinear internal coordinates for tetraatomic linear A-B-C-D molecules is

$$\{\text{Я}_n\} = \{\Delta R_1, \Delta R_2, \Delta R_3, \theta_4, \theta_5, \tau\} \ , \tag{4.44}$$

where ΔR_s are the bond stretching coordinates, θ_t the deviations from linearity of the A-B-C and B-C-D units, respectively, and τ is the dihedral (torsional) angle between the A-B-C and B-C-D planes. Figure 4.2 shows the definition of the internal coordinates for a displaced tetraatomic linear molecule. Due to symmetry requirements the sum of exponents occurring in Equation (4.38) for the bending coordinates $\theta_4^l \theta_5^m$ have to be an even number. The internal coordinates are obtained from the instantaneous cartesian coordinates $\mathbf{R}_\mathrm{I}$ by introducing three bond vectors $\mathbf{R}_s$ according to

$$\mathbf{R}_1 = \mathbf{R}_\mathrm{B} - \mathbf{R}_\mathrm{A} \ , \tag{4.45}$$

$$\mathbf{R}_2 = \mathbf{R}_\mathrm{C} - \mathbf{R}_\mathrm{B} \tag{4.46}$$

and

$$\mathbf{R}_3 = \mathbf{R}_\mathrm{D} - \mathbf{R}_\mathrm{B} \, . \tag{4.47}$$

The bond stretching coordinates are then

$$\Delta R_s = \|\mathbf{R}_s\| - \|\mathbf{R}_s^\mathrm{e}\| = R_s - R_s^\mathrm{e} \, . \tag{4.48}$$

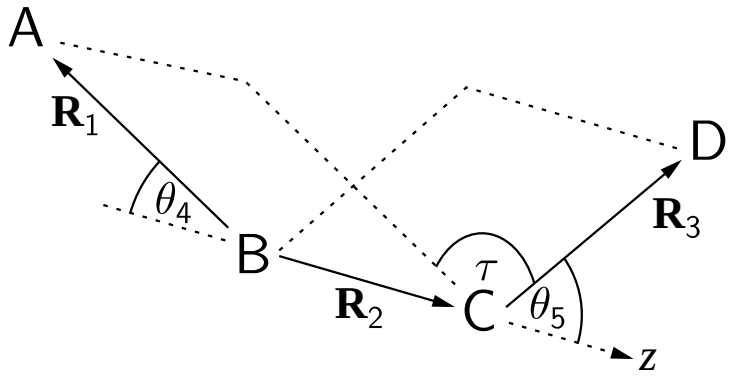

Figure 4.2: Definition of internal coordinates for a tetra atomic linear molecule based on three bond vectors $\mathbf{R}_s$.

where $\mathbf{R}_s^{\mathrm{e}}$ are the bond vectors for the equilibrium cartesian coordinates $\mathbf{R}_{\mathrm{I}}^{\mathrm{e}}$. The angles θ_t are obtained via vector products of the bond vectors according to

$$\sin(\theta_4) = \frac{\|\mathbf{R}_2 \times \mathbf{R}_1\|}{\|\mathbf{R}_1\|\|\mathbf{R}_2\|} \tag{4.49}$$

$$\sin(\theta_5) = \frac{\|\mathbf{R}_2 \times \mathbf{R}_3\|}{\|\mathbf{R}_2\|\|\mathbf{R}_3\|} \tag{4.50}$$

Finally, the torsional angle τ is obtained from the normal vectors $\mathbf{R}_4$ and $\mathbf{R}_5$ of the A-B-C and B-C-D planes, respectively. The latter are obtained from the vector products

$$\mathbf{R}_4 = \mathbf{R}_1 \times \mathbf{R}_2 \tag{4.51}$$

and

$$\mathbf{R}_5 = \mathbf{R}_3 \times \mathbf{R}_2 \tag{4.52}$$

and τ is given by

$$\cos(\tau) = \frac{\mathbf{R}_4 \cdot \mathbf{R}_5}{\|\mathbf{R}_4\|\|\mathbf{R}_5\|} \,. \tag{4.53}$$

These geometric definitions of the internal coordinates $\boldsymbol{\mathcal{R}}$ are valid for any nuclear configuration expressed in cartesian coordinates $\mathbf{R}_{\mathrm{I}}a$.
Hoy, Strey and Mills [349] have introduced a different set of bending coordinates

$$\left\{\mathcal{R}_t^{\mathrm{HSM}}\right\} = \{\theta_{4x}, \theta_{5x}, \theta_{4y}, \theta_{5y}\}$$

defined according to

$$\theta_{4x} = -\frac{\mathbf{e}_x \cdot (\mathbf{R}_2 \times \mathbf{R}_1)}{\|\mathbf{R}_1\|\|\mathbf{R}_2\|} \,, \tag{4.54}$$

$$\theta_{4y} = \frac{\mathbf{e}_y \cdot (\mathbf{R}_2 \times \mathbf{R}_1)}{\|\mathbf{R}_1\|\|\mathbf{R}_2\|} \,, \tag{4.55}$$

$$\theta_{5x} = -\frac{\mathbf{e}_x \cdot (\mathbf{R}_3 \times \mathbf{R}_2)}{\|\mathbf{R}_1\|\|\mathbf{R}_2\|} \tag{4.56}$$

and

$$\theta_{5y} = \frac{\mathbf{e}_y \cdot (\mathbf{R}_3 \times \mathbf{R}_2)}{\|\mathbf{R}_1\|\|\mathbf{R}_2\|} \,. \tag{4.57}$$

where $\mathbf{e}_x$ and $\mathbf{e}_y$ are the unit vectors of the molecule fixed reference system in x- and y-direction, respectively. These coordinates are defined for the linear equilibrium structure of the molecule such that the bond vectors are $\mathbf{R}_s = R_s\mathbf{e}_z$. Displacements in the HSM bending coordinates corresponds to displacement of atoms A or D out of the linear geometry. Then the HSM coordinates are the

projections of $\mathbf{R}_1$ and $\mathbf{R}_3$ on the xz- and yz-planes

$$\theta_{4x} = \sin(\theta_4)\cos(\chi_4)\,, \tag{4.58}$$

$$\theta_{4y} = \sin(\theta_4)\sin(\chi_4)\,, \tag{4.59}$$

$$\theta_{5x} = \sin(\theta_5)\cos(\chi_5) \tag{4.60}$$

and

$$\theta_{5y} = \sin(\theta_5)\sin(\chi_5)\,. \tag{4.61}$$

The angles χ_t are the polar angles of vectors $\mathbf{R}_1$ and $\mathbf{R}_3$ around the z-axis measured in a positive sense from the x-axis.
The HSM coordinates can be related to the curvilinear coordinates defined in (4.49), (4.50) and (4.53) by introducing the torsional angle as $\tau = \chi_5 - \chi_4$ yielding the relation

$$\sin(\theta_t') = \sqrt{\theta_{tx}^2 + \theta_{ty}^2}\,. \tag{4.62}$$

For the torsional angle τ one finds that it can be obtained from the HSM coordinates according to

$$\cos(\tau') = \frac{\theta_{4x}\theta_{5x} + \theta_{4y}\theta_{5y}}{\sqrt{\theta_{4x}^2 + \theta_{4y}^2}\sqrt{\theta_{5x}^2 + \theta_{5y}^2}}\,. \tag{4.63}$$

A detailed analysis of the HSM coordinates shows that they yield the same values for the angles $\theta_t' = \theta_t$ and the torsional angle $\tau' = \tau$ only in cases where the BC-bond is either parallel to the molecule fixed z-axis or lies in a plane that contains the z-axis. The latter conditions are not necessarily fulfilled when using normal coordinates. As an example, Figure 4.3 compares the dependence of the differences $\Delta\theta_t = \theta_t' - \theta_t$ and $\Delta\tau = \tau' - \tau$ on the bending normal coordinate q_4 of a linear A-B-C-D system (l-C_3H^+). The second bending normal coordinate is fixed to a value of $q_5 = 2.5$ with phase angle difference $\xi = \chi_5 - \chi_4 = \frac{\pi}{2}$. Details on the form of the normal coordinates can be found in Section 5.2. For small displacements in q_4 only small differences can be observed. This is due to the fact that the HSM coordinates are linearized internal coordinates. With increasing q_4 also the differences between the two sets of coordinates increase. The main reason for the differences arises from the inclusion of the normal vectors $\mathbf{e}_x$ and $\mathbf{e}_y$ in the definition of the HSM coordinates which are no longer orthogonal to an arbitrarily oriented $\mathbf{R}_2$. This problem is circumvented by using the geometrically defined coordinates in Equation (4.49), (4.50) and (4.53) which will also be used in the present variational approach to transform from normal coordinates to internal coordinates.
Comparison with the bending normal coordinates $\{q_{4x}, q_{4y}, q_{5x}, q_{5y}\}$ shows that HSM coordinates have Π-symmetry in the linear molecule point groups $\boldsymbol{C}_{\infty v}$ and $\boldsymbol{D}_{\infty h}$ [349]. The product $\theta_{4x}^l \theta_{5x}^m \theta_{4y}^n \theta_{5y}^o$ is then only allowed for specific combinations (l, m, n, o) such that it transforms according to the totally symmetric representation of the molecular point group. Combining Equa-

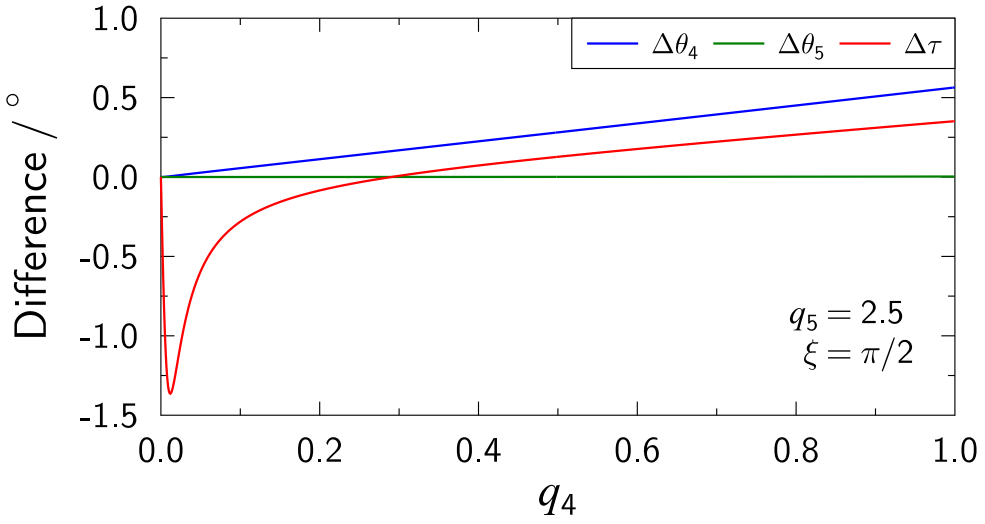

Figure 4.3: Differences in internal bending coordinates for tetraatomic linear molecules obtained from vector relations and from the definition of Hoy *et al.* [349].

tion (4.62) with the symmetry requirements on the products $\theta_{4x}^{l}\theta_{5x}^{m}\theta_{4y}^{n}\theta_{5y}^{o}$ leads to the following rules for the products $\theta_4^l\theta_5^m\cos(n\tau)$ that represent the bending-torsional dependence of the potential energy:

1. the sum $l+m$ is an even number
2. allowed values for the torsional part are $n = \begin{cases} [0, \min(l,m)] & \text{for } l \cdot m = \text{even} \\ [1, \min(l,m)] & \text{for } l \cdot m = \text{odd} \end{cases}$
3. n increments in units of 2 for a specific combination (l,m)

For example the allowed bending-torsion terms in a sextic force field are:

$l+m=2$	$l+m=4$	$l+m=6$
θ_4^2	θ_4^4	θ_4^6
$\theta_4^1\theta_5^1\cos(\tau)$	$\theta_4^3\theta_5^1\cos(\tau)$	$\theta_4^5\theta_5^1\cos(\tau)$
θ_4^2	$\theta_4^2\theta_5^2$	$\theta_4^4\theta_5^2$
	$\theta_4^2\theta_5^2\cos(2\tau)$	$\theta_4^4\theta_5^2\cos(2\tau)$
	$\theta_4^1\theta_5^3\cos(\tau)$	$\theta_4^3\theta_5^3\cos(\tau)$
	θ_5^4	$\theta_4^3\theta_5^3\cos(3\tau)$
		$\theta_4^2\theta_5^4$
		$\theta_4^2\theta_5^4\cos(2\tau)$
		$\theta_4^1\theta_5^5\cos(\tau)$
		θ_5^6

4.1.4 Structure of the Hamiltonian matrix

The structure of the Hamiltonian matrix set up using basis functions of type Equation (4.2) can be inferred from an analysis of the possible matrix elements. This allows to on the one hand identify blocks where all the possible matrix elements are zero which thus need not to be considered during the integration and on the other hand determine the specific terms which contribute to the matrix elements of the non-zero blocks.

As pointed out in Section 2.3.1 no operator in the Hamiltonian can couple basis functions differing in J which is an indication of a good quantum number that is strictly conserved. The matrix representation of the Hamiltonian will therefore have a block structure with unconnected blocks differing in J.

Analysis of the possible matrix elements of the Coriolis operator $\hat{\mathrm{T}}_{\mathrm{VR}}$ show that it couples basis functions within a J-block differing in k by ± 1. The J-block Hamiltonian will then have almost block-diagonal structure with the primary diagonal blocks formed by matrix elements diagonal in k and the secondary diagonal above and below coupling them through $\hat{\mathrm{T}}_{\mathrm{VR}}$.

The Sayvetz condition Equation (2.43) requires that the sum of vibrational angular momentum quantum numbers $\ell = \sum_t \ell_t$ has to be equal to k. Basis functions for a given k can therefore be grouped in blocks of equal vibrational angular momentum quantum number pairs (ℓ_4, ℓ_5). Equation (2.43) further implies that the presented basis set is not completable. For example when treating tetraatomic linear molecules and $k = 0$ an infinite number of possible combinations e.g. $(0,0)$ $(1,-1)$, $(-1,1)$ ... can be constructed. It is therefore necessary that, for a given k, one chooses a maximum absolute value ℓ^k_{max} for the ℓ_t occurring within the respective block. The operator $\hat{\pi}_{\pm}$ in $\hat{\mathrm{T}}_{\mathrm{VR}}$ couples basis functions differing in exactly one of the ℓ_t by ± 1. Thus, choosing $\ell^k_{\mathrm{max}} = \ell^0_{\mathrm{max}} + |k|$ ensures that for $J \geq |k| \geq 1$ all basis functions within such a block are coupled to the necessary functions in the $|k| - 1$ block and the remaining choice is the maximum value of $|\ell_t|$ for $k = 0$ (ℓ^0_{max}).

The grouping of basis functions within a k block according to (ℓ_4, ℓ_5) leads to a block structure with increasing differences in (ℓ_4, ℓ_5) but opposite signs in $\Delta\ell_4 = \ell_4 - \ell_4^{'}$ and $\Delta\ell_5 = \ell_5 - \ell_5^{'}$, where ℓ_t and $\ell_t^{'}$ are the vibrational angular momentum quantum numbers in the bra and ket, respectively. In a diagonal block $(\Delta\ell_4, \Delta\ell_5) = (0,0)$ all operators in the Hamiltonian except $\hat{\mathrm{T}}_{\mathrm{VR}}$ can contribute to a matrix element. The main contribution to off-diagonal k-subblocks are matrix elements of the potential energy (cf. Section 4.1.3). Additionally, for blocks with $(\Delta\ell_4, \Delta\ell_5) = (\pm 1, \mp 1)$ terms in $\hat{\mathrm{T}}_{\pi}$ with differing bending indices contribute to the matrix elements. As a summary, the individual contributions to the blocks of a Hamiltonian with $J_{\mathrm{max}} = 1$ and $\ell^0_{\mathrm{max}} = 1$ are schematically presented in Figure 4.4.

4.1.5 Symmetry considerations

The classification of the basis functions with respect to symmetry is an important step for the development of a variational procedure to treat the rovibrational problem in molecules. In case

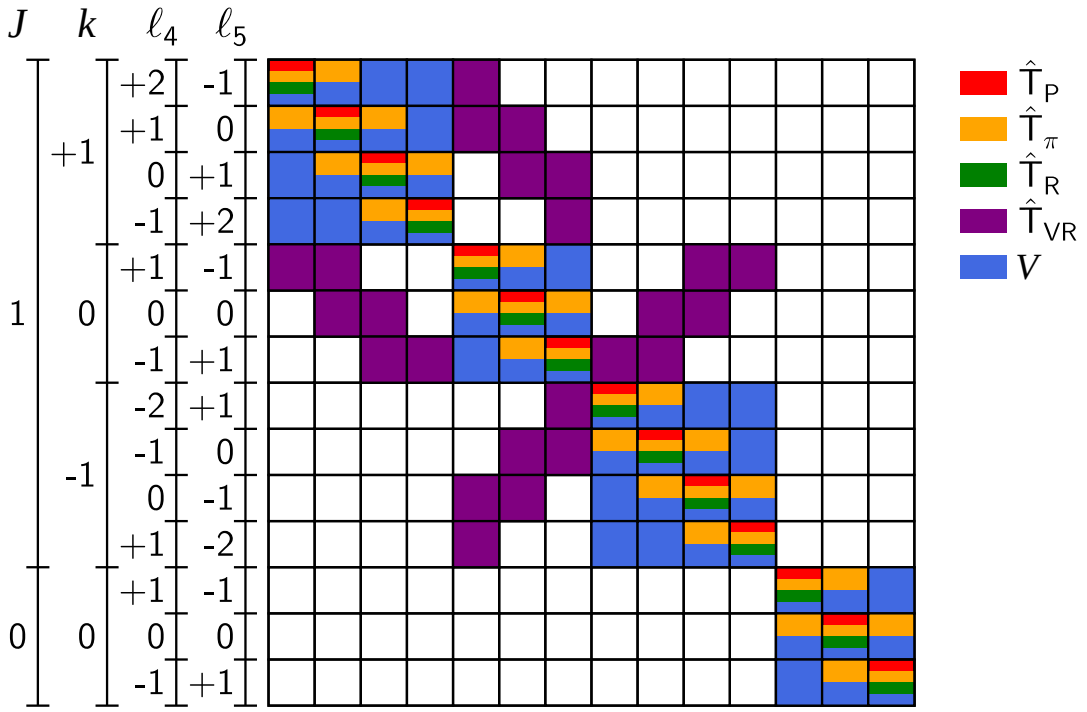

Figure 4.4: Block structure of a Hamiltonian matrix with $J_{\max} = 1$ and $\ell^0_{\max} = 1$. Colors indicate the different terms in the Hamiltonian that contribute to a specific block. Non colored blocks are zero.

of linear molecules two molecular symmetry (MS) groups are possible $\boldsymbol{C}_{\infty v}$(M) and $\boldsymbol{D}_{\infty h}$(M), depending on whether an inversion center is present or not.

The MS group $\boldsymbol{C}_{\infty v}$(M) has two symmetry operations E and E^*, which are the identity and the space inversion (parity), respectively. This gives rise to two irreducible representations Σ^+ and Σ^-, depending on the behaviour under the operation E^*. The behaviour of a rovibrational basis function under E^* determines the parity, which is a strictly conserved quantity. Therefore, basis functions that are eigenfunctions of E^* with eigenvalue $+1$ have positive parity $(+)$ and functions with eigenvalue -1 have negative parity $(-)$. Table 4.3 gives the character table of the MS group $\boldsymbol{C}_{\infty v}$(M).

Table 4.3: Character table of the MS group $\boldsymbol{C}_{\infty v}$(M).

$\boldsymbol{C}_{\infty v}$(M)	E	E^*
Σ^+	1	1
Σ^-	1	-1

To characterize the basis functions with respect to symmetry operations of the MS group $\boldsymbol{C}_{\infty v}(\mathrm{M})$ the behaviour of the coordinates (normal coordinates, phase angles, Euler angles) has to be determined. The operation E^* has the effect of inverting the molecule fixed z and y-axis as well as the radial components of the bending vibrations through the center of the space fixed coordinate system. This leaves all normal coordinate values unaffected and the set of normal coordinates transforms under E^* like

$$E^*(q_1,\ q_2,\ q_3,\ \rho_4,\ \rho_5) = (q_1,\ q_2,\ q_3,\ \rho_4,\ \rho_5) \tag{4.64}$$

and the Euler angles (θ, ϕ) transform under E^* according to

$$E^*(\theta,\ \phi) = (\pi - \theta,\ \phi + \pi)\,. \tag{4.65}$$

The part of a rovibrational basisfunction $|\mathbf{V}_i \boldsymbol{\ell} J k\rangle$ that depends on the phase angles χ_t and the Euler angles (θ, ϕ, χ') is given by

$$|\ell_4 \ell_5 J k\rangle = \sqrt{\frac{1}{8\pi^3}} S_{Jkm}(\phi, \theta) \mathrm{e}^{\mathrm{i}k\chi'} \mathrm{e}^{\mathrm{i}\ell_4\chi_4} \mathrm{e}^{\mathrm{i}\ell_5\chi_5}\,. \tag{4.66}$$

The Sayvetz condition (Equation (2.43)) shows the relation between the ℓ_t and k, so that for any given numerical combination of two of the quantum numbers ℓ_4, ℓ_5 or k the third one is fixed. One therefore can reformulate the bending-rotation basis function in a non-direct product form by, for example, requiring $\ell_4 = k - \ell_5$. Inserting this into Equation (4.66) yields

$$\begin{aligned}
|(k-\ell_5)\ell_5 J k\rangle &= \sqrt{\frac{1}{8\pi^3}} S_{Jkm}(\phi, \theta) \mathrm{e}^{\mathrm{i}k\chi'} \mathrm{e}^{\mathrm{i}(k-\ell_5)\chi_4} \mathrm{e}^{\mathrm{i}\ell_5\chi_5} \\
&= \sqrt{\frac{1}{8\pi^3}} S_{Jkm}(\phi, \theta) \mathrm{e}^{\mathrm{i}k(\chi'+\chi_4)} \mathrm{e}^{\mathrm{i}\ell_5(\chi_5-\chi_4)} \\
&= \sqrt{\frac{1}{8\pi^3}} S_{Jkm}(\phi, \theta) \mathrm{e}^{\mathrm{i}k(\chi_4')} \mathrm{e}^{\mathrm{i}\ell_5\xi}\,,
\end{aligned} \tag{4.67}$$

where the phase angle difference $\xi = \chi_5 - \chi_4$ defined earlier has been used and a new angle $\chi_4' = \chi' + \chi_4$ is introduced. Figure 4.5 graphically displays the relation between the different phase angles for a tetraatomic linear molecule.

Equation (4.67) shows that the wave function depends only on the difference of the phase angles ξ and the sum $\chi_4' = \chi' + \chi_4$. For fixed (non zero) values of all other coordinates the angle χ_4' has the same effect as the angle χ' on the cartesian coordinates of the molecule, resulting in a rotation about the z-axis with angular momentum $k\hbar$. Since χ' is arbitrary in the isomorphic Hamiltonian [191] so is the sum χ_4' and thus also χ_4. A rotation about an axis does not change the potential energy, the PES of linear molecules ($N_{\mathrm{at}} > 2$) do not depend on the phase angles χ_t independently but on $N_{\mathrm{at}} - 3$ differences $\chi_t - \chi_{t'}$. This has also been pointed out by Watson in his discussion of the cylindrical symmetry of linear molecules and the relation between $3N_{\mathrm{at}} - 5$

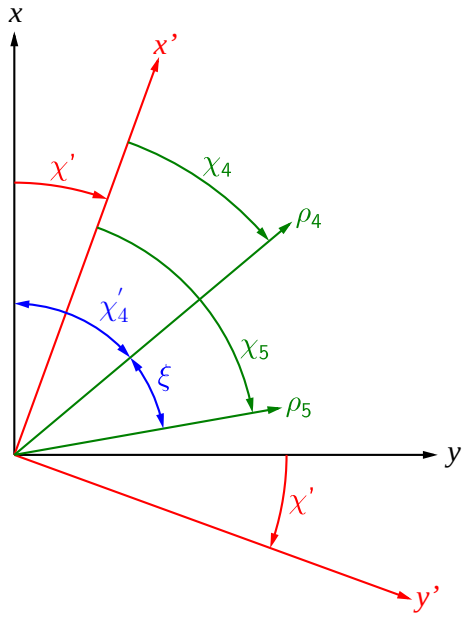

Figure 4.5: Graphical representation of the relation between the different phase angles of the rovibrational coordinates in a tetraatomic linear molecule.

and $3N_{\mathrm{at}} - 6$ approaches to the rovibrational problem in linear molecules [350].
The effect of E^* on the angles (χ_4', ξ) can be inferred from Figure 4.6 where the effect of E^* has been applied to the molecule fixed axes and bending normal coordinates (inverting y and the direction of the ρ_t). In summary the transformation properties of the phase angles are

$$E^* \chi_4^{'} = \pi - \chi_4^{'} \tag{4.68}$$

and

$$E^* \xi = -\xi \tag{4.69}$$

The transformation properties of the rovibrational basis functions under E^* can now be determined and one obtains

$$E^* \left| \mathbf{V} \boldsymbol{\ell} J k \right\rangle = (-1)^{J+k} \left| \mathbf{V} - \boldsymbol{\ell} J - k \right\rangle \ . \tag{4.70}$$

In Equation (4.70) the $\mathbf{V}$ is the vector containing all quantum numbers $\mathrm{V} = (v_1, v_2, v_3, v_4, v_5)$ and $\boldsymbol{\ell} = (\ell_4, \ell_5)$ collects all ℓ_t.
The MS group $\boldsymbol{D}_{\infty h}(\mathrm{M})$ cotains two additional symmetry operations (p) and $(p)^*$, which are the permutation of all pairs of like nuclei and the combination of (p) and E^* according to $(p)^* = (p)E^*$, respectively. The operation $(p)^*$ has the same effect on the rovibrational coordinates as the point

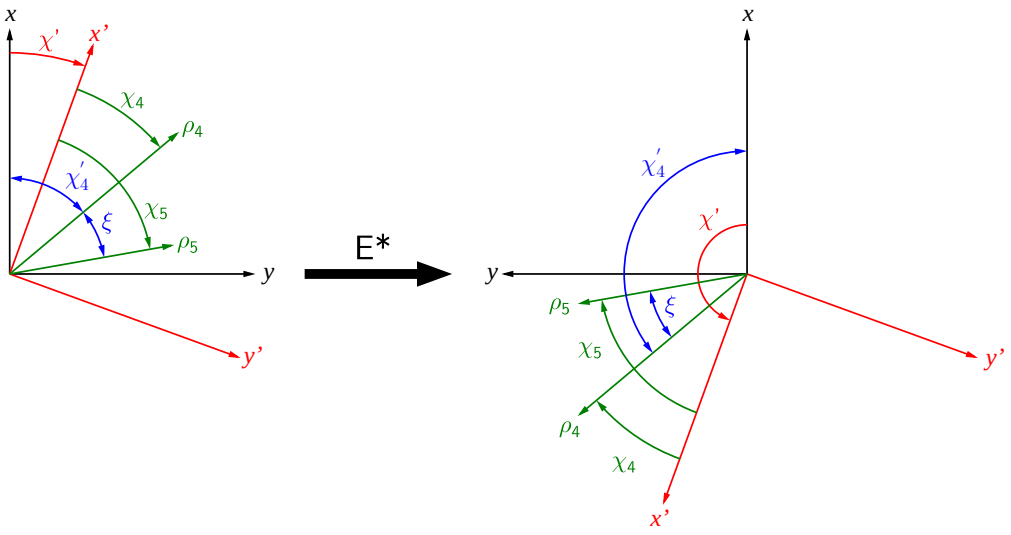

Figure 4.6: Effect of the parity operator E^* on the phase angles of rovibrational coordinates in a tetraatomic linear molecule.

group operation i (inversion operator) and thus determines whether the basis function is *gerade* (g) or *ungerade* (u). Table 4.4 gives the character table of the MS group.

A tetraatomic molecule A-B-B-A belongs to the MS group $\boldsymbol{D}_{\infty h}(\mathrm{M})$ and has three totally symmetric vibrations: two stretching vibrations (symmetric A-B stretch q_1 and B-B stretch q_2) and one bending vibration (trans-bending ρ_4). The remaining two vibrations are antisymmetric (antisymmetric A-B stretch q_3 and cis-bending ρ_5). The transformation of the normal coordinates under the operation $(p)^*$ are then given by

$$(p)^*(q_1,\ q_2,\ q_3,\ \rho_4,\ \rho_5) = (q_1,\ q_2,\ -q_3,\ \rho_4,\ \rho_5)\,. \tag{4.71}$$

Table 4.4: Character table of the MS group $\boldsymbol{D}_{\infty h}(\mathrm{M})$.

$\boldsymbol{D}_{\infty h}(\mathrm{M})$	E	(p)	E^*	$(p)^*$
Σ_g^+	1	1	1	1
Σ_u^-	1	−1	1	−1
Σ_g^-	1	−1	−1	1
Σ_u^+	1	1	−1	−1

The transformation properties of the phase angles are

$$(p)^*\chi_4' = \chi_4' \,, \tag{4.72}$$

$$(p)^*\xi = \xi + \pi \tag{4.73}$$

and finally the transformation of the Euler angles $(\theta,\ \phi)$

$$(p)^*(\theta,\ \phi) = (\theta,\ \phi)\,. \tag{4.74}$$

From these transformations the effect of $(p)^*$ on the rovibrational basis functions can be deduced. For the HO basis function of the antisymmetric stretching vibrational one obtains

$$\begin{aligned}(p)^*\,|v_3\rangle &= \mathrm{H}_{v_3}(-q_3)\mathrm{e}^{-\frac{1}{2}(-q_3)^2} \\ &= (-1)^{v_3}\mathrm{H}_{v_3}(q_3)\mathrm{e}^{-\frac{1}{2}q_3^2} \\ &= (-1)^{v_3}\,|v_3\rangle\ ,\end{aligned} \tag{4.75}$$

where the fact has been used that the Hermite polynomials $\mathrm{H}_n(x)$ are even functions in x when n is even or odd functions otherwise. The 2D HO basis function of the cis-bending vibration ρ_5 transforms under $(p)^*$ according to

$$\begin{aligned}(p)^*\,|v_5,\ell_5\rangle &= \sqrt{\frac{1}{2\pi}}\,(\rho_5)^{\frac{|\ell_5|}{2}}\,\mathrm{L}_{n_5}^{|\ell_5|}(\rho_5)\mathrm{e}^{-\frac{1}{2}\rho_5}\mathrm{e}^{\mathrm{i}\ell_5(\xi+\pi)} \\ &= (-1)^{|\ell_5|}\sqrt{\frac{1}{2\pi}}\,(\rho_5)^{\frac{|\ell_5|}{2}}\,\mathrm{L}_{n_5}^{|\ell_5|}(\rho_5)\mathrm{e}^{-\frac{1}{2}\rho_5}\mathrm{e}^{\mathrm{i}\ell_5\xi} \\ &= (-1)^{|\ell_5|}\,|v_5,\ell_5\rangle\ .\end{aligned} \tag{4.76}$$

The effect of $(p)^*$ on a rovibrational basis function $|\mathbf{V}\boldsymbol{\ell}Jk\rangle$ is then

$$(p)^*\,|\mathbf{V}\boldsymbol{\ell}Jk\rangle = (-1)^{v_3+|\ell_5|}\,|\mathbf{V}\boldsymbol{\ell}Jk\rangle\ , \tag{4.77}$$

showing that the basis functions are eigenfunctions of $(p)^*$. From Equation (4.70), Equation (4.77) and the definition $(p)^* = E^*(p)$ follows directly the effect of (p) on the basis functions

$$(p)\,|\mathbf{V}\boldsymbol{\ell}Jk\rangle = (-1)^{v_3+|\ell_5|+J+k}\,|\mathbf{V}-\boldsymbol{\ell}J-k\rangle\ . \tag{4.78}$$

The transformation of the rovibrational basis functions under the symmetry operations E^* (Equation (4.70)) and (p) (Equation (4.78)) reveal that they are not eigenfunctions of the symmetry operations. Since the Hamiltonian (Equation (2.33)) commutes with all symmetry operations of the MS group [347] they have a common set of eigenfunctions and an additional symmetrization of the basis functions is needed. This is achieved by forming Wang-type [351] linear combinations

Table 4.5: Parity and e/f assignment of symmetrized basis functions adopted in this work.

J	K	κ	partiy	e/f
even	even	0	$+$	e
even	even	1	$-$	f
even	odd	0	$-$	f
even	odd	1	$+$	e
odd	even	0	$-$	e
odd	even	1	$+$	f
odd	odd	0	$+$	f
odd	odd	1	$-$	e

of the basis functions

$$|\mathbf{V}\boldsymbol{\ell}JK\kappa) = \frac{1}{\sqrt{2}}\left[|\mathbf{V}\boldsymbol{\ell}JK\rangle + (-1)^{\kappa}\,|\mathbf{V}{-}\boldsymbol{\ell}J{-}K\rangle\right]\,, \tag{4.79}$$

where $\kappa = 0$ or 1 and $K = |k|$. In the special case that $\boldsymbol{\ell} = (0,0)$ no symmetrization is needed

$$|\mathbf{V0}J0\kappa) = |\mathbf{V0}J0\rangle\ . \tag{4.80}$$

and $\kappa = 0$ by definition. These functions are now eigenfunctions of the MS group operations

$$E|\mathbf{V}\boldsymbol{\ell}JK\kappa) = |\mathbf{V}\boldsymbol{\ell}JK\kappa)\,, \tag{4.81}$$

$$(p)|\mathbf{V}\boldsymbol{\ell}JK\kappa) = (-1)^{v_3+|\ell_5|+J+K+\kappa}|\mathbf{V}\boldsymbol{\ell}JK\kappa)\,, \tag{4.82}$$

$$E^*|\mathbf{V}\boldsymbol{\ell}JK\kappa) = (-1)^{J+K+\kappa}|\mathbf{V}\boldsymbol{\ell}JK\kappa) \tag{4.83}$$

and

$$(p)^*|\mathbf{V}\boldsymbol{\ell}JK\kappa) = (-1)^{v_3+|\ell_5|}|\mathbf{V}\boldsymbol{\ell}JK\kappa)\,, \tag{4.84}$$

which is readily verified by applying Equation (4.70), (4.77) and (4.78) to Equation (4.79). The effect of this symmetrization is the separation of basis functions into blocks of well determined parity $(+/-)$. The labeling of rovibrational states with respect to parity is done in the e/f scheme introduced by Brown *et al.* [200]. For molecules with an even number of electrons e-levels have parity $+(-1)^J$ and f-levels $-(-1)^J$. The assignment of the symmetrized basis functions (Equation (4.79)) is given in Table 4.5. Figure 4.7 shows the effect of this blockwise separation for the Hamiltonian presented in Figure 4.4. Equation (4.84) allows for a complete separation of the Hamiltonian matrix into blocks of *gerade* (g) and *ungerade* (u) symmetry by selecting only functions with an even or odd value for the sum $v_3 + |\ell_5|$, respectively.

With the basis functions now correctly symmetrized, the rovibrational wave functions can be

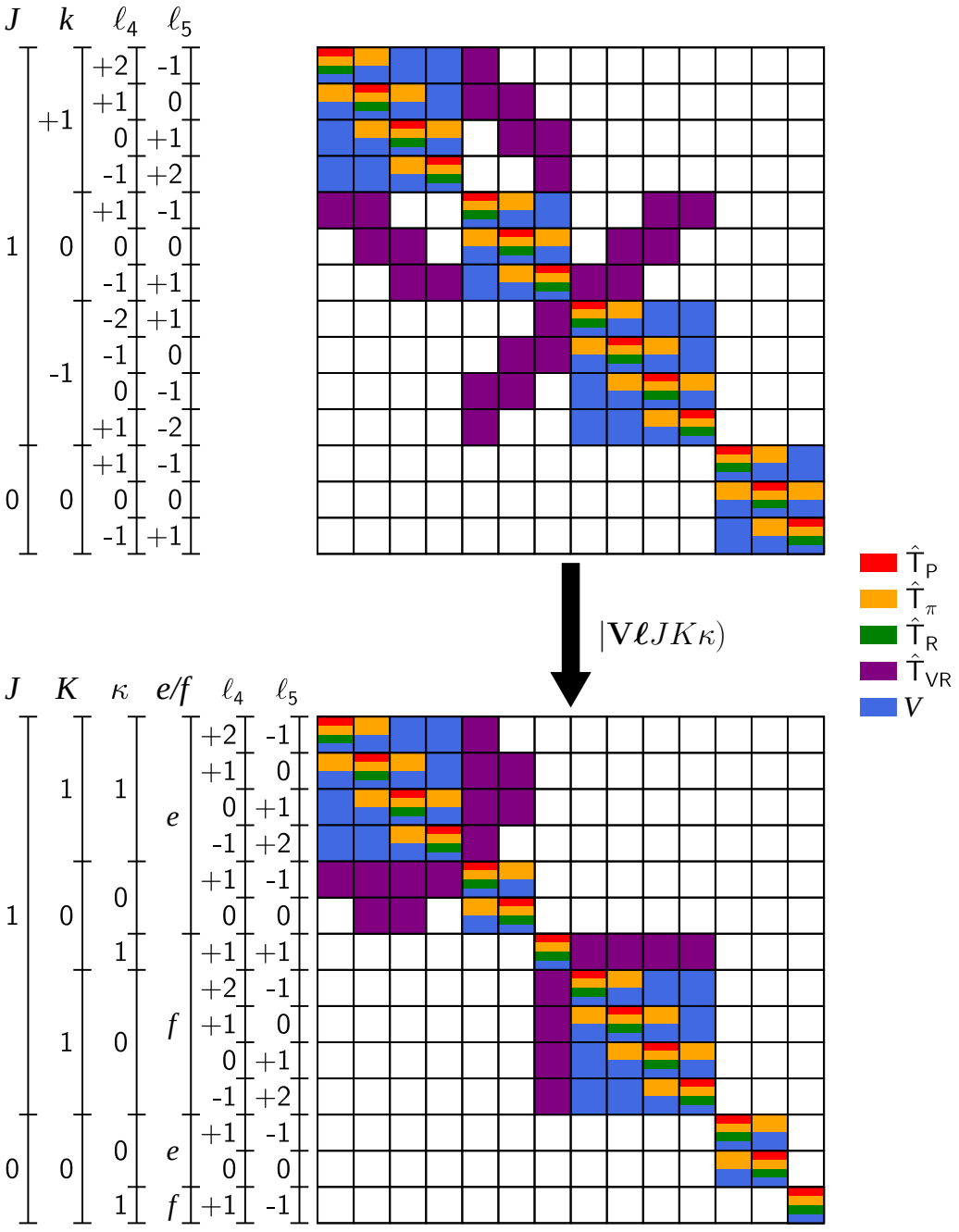

Figure 4.7: Structure of a Hamiltonian matrix with $J_{\max} = 1$ and $\ell^0_{\max} = 1$ before (upper part) and after (lower part) symmetrization. Colors indicate the different terms in the Hamiltonian that contribute to a specific block. Non colored blocks are zero.

written in the following form

$$\left|\psi_v^{(J,\mathrm{p})}\right\rangle = \sum_{K=0}^{J} \sum_{\ell_5=-\ell^0_{\max}}^{\sigma} \sum_{i}^{N_v} c^{(J,\mathrm{p})}_{K\ell_5 i} |\mathbf{V}_i \boldsymbol{\ell} J K \kappa) \,, \tag{4.85}$$

where

$$\sigma = \begin{cases} -\mathrm{p} & \text{for } K = 0 \\ \ell^K_{\max} & \text{for } K \neq 0 \end{cases} \,. \tag{4.86}$$

In Equation (4.85) and (4.86) p is either 0 or 1 for the e- and f-type wave functions, respectively, and N_v is the size of a (ℓ_4, ℓ_5)-block. The value of κ is determined by J, K and p combined with Table 4.5.

4.2 Implementation

The following section describes the implementation of the variational approach for rovibrational calculations on linear tetraatomic molecules into the Fortran program C8v4. A calculation can be divided into three steps. First a harmonic treatment of the vibrational problem is performed to determine the parameters that appear in the Hamiltonian and details are described in section Section 4.2.1. In the second step the matrix elements of the Hamiltonian in the chosen basis set are constructed as presented in Section 4.2.2. Finally, the Hamiltonian is diagonalised to obtain rovibrational term energies and wave functions (cf. Section 4.2.5). An important part of the implementation is the parallelisation of the program in order for the calculations to be feasible and the necessary considerations are presented in Section 4.2.6.

4.2.1 Solving the harmonic problem

The first step in the variational procedure is the determination of the various molecular parameters that appear in the Hamiltonian operator. From the equilibrium cartesian coordinates $\mathbf{r}^{\mathrm{e}}$ the equilibrium moment of inertia is calculated according to Equation (2.53). Harmonic vibrational frequencies ω_i and the $\mathscr{L}$-matrix are obtained by the GF-method [343]

$$\mathbf{GFL} = \mathbf{L}\lambda \,, \tag{4.87}$$

where $\mathbf{G}$ is the inverse kinetic energy matrix

$$\mathbf{G} = \mathbf{B}\mathbf{M}^{-1}\mathbf{B}^{\mathrm{T}} \tag{4.88}$$

and $\mathbf{F}$ the internal coordinate potential energy matrix

$$\mathbf{F} = \left(\mathbf{B}^{-1}\right)^{\mathrm{T}} \mathbf{f_x} \mathbf{B}^{-1} \,. \tag{4.89}$$

In Equation (4.89) $\mathbf{f_x}$ is the $3N_{\mathrm{at}} \times 3N_{\mathrm{at}}$ force constant matrix in cartesian coordinates (Hessian). The F-matrix can be obtained by collecting all quadratic force constants f_{ij} for simple Taylor expansions (cf. Equation (4.38)) or by numerical differentiation for more complex PEF forms. The $\mathbf{B}$ matrix defines the transformation from the $3N_{\mathrm{at}}$ cartesian displacement coordinates to the $3N_{\mathrm{at}} - 5$ linearized internal coordinates $\{s_n\}$ of the tetraatomic linear molecule. The relation is obtained by truncating Equation (4.40) after the linear term which yields

$$\mathrm{s}_n = \sum_{\mathrm{I}} \sum_{\alpha} \mathrm{B}^n_{\mathrm{I}\alpha} x_{\mathrm{I}\alpha} \tag{4.90}$$

or in matrix vector notation

$$\mathbf{s} = \mathbf{B}\mathbf{x}\,. \tag{4.91}$$

The solution to the eigenvalue problem in Equation (4.87) are the harmonic frequencies $\omega_i = \sqrt{\lambda_i}$ and the eigenvectors $\mathbf{L}$ that transform the normal coordinates to the linearized internal coordinates

$$\mathbf{s} = \mathbf{B}\mathbf{x} = \mathbf{B}\mathbf{M}^{-\frac{1}{2}}\mathbf{u} = \mathbf{B}\mathbf{M}^{-\frac{1}{2}}\boldsymbol{\mathscr{L}}\mathbf{Q} = \mathbf{L}\mathbf{Q} \tag{4.92}$$

From Equation (4.92) the definition of the $\boldsymbol{\mathscr{L}}$-matrix is obtained

$$\boldsymbol{\mathscr{L}}^{\mathrm{T}} = \mathbf{L}^{-1}\mathbf{B}\mathbf{M}^{-\frac{1}{2}} \tag{4.93}$$

With the $\boldsymbol{\mathscr{L}}$ matrix the $\boldsymbol{\zeta}^x$ matrix and a_k parameters can be calculated by the formulas given in Section 2.3.1.

4.2.2 Integration of the Hamiltonian

The next step in performing a FBR variational calculation is to build up the representation of the Hamiltonian in the chosen basis set

$$\mathrm{H}^{(J,\mathrm{p})}_{ij} = (\mathbf{V}_i \boldsymbol{\ell} J K \kappa | \hat{\mathrm{H}}_{\mathrm{W}} | \mathbf{V}_j \boldsymbol{\ell}' J K' \kappa')\,. \tag{4.94}$$

Such matrix elements can either be evaluated directly in the symmetrized basis set or in an unsymmetrized basis and the resulting blocks are combined afterwards when building the Hamiltonian that is to be diagonalised. The latter approach has been chosen here.
As outlined above most of the KEO matrix elements can be evaluated analytically with the employed basis functions. Matrix elements of the linear momentum term $\hat{\mathrm{T}}_{\mathrm{P}}$ are straight forward to evaluate by use of the analytic matrix elements presented in Section 4.1.1. Complications arise for the terms involving μ since there are no analytic matrix elements for the inverse effective moment of inertia. Consequentially a numerical integration has to be employed. The same is true for the generalized potential energy V (although analytic evaluation would be possible for a PES expanded with respect to normal coordinates).

First consider the pure rotational kinetic energy $\hat{\mathrm{T}}_{\mathrm{R}}$. A matrix element of this operator is given by

$$\begin{aligned}\left(\mathrm{T}_{\mathrm{R}}^{(J)}\right)_{ij} &= \langle \mathbf{V}_i \boldsymbol{\ell} Jk | \hat{\mathrm{T}}_{\mathrm{R}} | \mathbf{V}_j \boldsymbol{\ell}' Jk \rangle \\ &= \frac{1}{2} \langle \mathbf{V}_i \boldsymbol{\ell} | \mu | \mathbf{V}_j \boldsymbol{\ell}' \rangle \langle Jk | \hat{\Pi}'_{\pm} \hat{\Pi}'_{\mp} | Jk \rangle \\ &= \frac{1}{2} \mu_{ij} \left[J(J+1) - k^2 \right] . \end{aligned} \tag{4.95}$$

In Equation (4.95) the second braket has been evaluated analytically and the first braket corresponds to a matrix representation $\boldsymbol{\mu}$ in the chosen vibrational basis. The latter has to be evaluated numerically and in principle would require a six dimensional (3 stretch q_s, 2 bend ρ_t and the phase angle difference ξ) numerical integration. Equation (2.39) shows that μ depends only on the stretching normal coordinates q_s and a matrix element μ_{ij} can therefore be rewritten

$$\begin{aligned}\mu_{ij} &= \langle \mathbf{V}_i \boldsymbol{\ell} | \mu | \mathbf{V}_j \boldsymbol{\ell}' \rangle \\ &= \langle v_1 v_2 v_3 | \mu | v'_1 v'_2 v'_3 \rangle \langle v_4 v_5 \ell_4 \ell_5 | v'_4 v'_5 \ell'_4 \ell'_5 \rangle \\ &= \langle v_1 v_2 v_3 | \mu | v'_1 v'_2 v'_3 \rangle \, \delta_{v_4 v'_4} \delta_{v_5 v'_5} \delta_{\ell_4 \ell'_4} \delta_{\ell_5 \ell'_5} , \end{aligned} \tag{4.96}$$

indicating that the contribution of term $\hat{\mathrm{T}}_{\mathrm{R}}$ to a Hamiltonian matrix element is diagonal with respect to all v_t and ℓ_t. Therefore, the matrix representation $\boldsymbol{\mu}$ needs only to be evaluated once in the chosen primitive vibrational basis set and can then be added to the diagonal (ℓ_4, ℓ_5) blocks after appropriately scaling the matrix according the values of J and K. The evaluation of $\boldsymbol{\mu}$ is straight forward in a 3D Gauss-Hermite integration scheme that takes the orthogonality of the bending basis functions into account.

Evaluation of matrix elements due to $\hat{\mathrm{T}}_{\pi}$ is also complicated by the fact that it involves products of μ (depending only on the q_s) with the operators $\hat{\pi}_{\pm}$ that involve all normal coordinates q_i and momenta $\hat{\mathrm{p}}_i$. A matrix element would then be

$$\begin{aligned}\left(\mathrm{T}_{\pi}^{(J)}\right)_{ij} &= \langle \mathbf{V}_i \boldsymbol{\ell} Jk | \hat{\mathrm{T}}_{\pi} | \mathbf{V}_j \boldsymbol{\ell}' Jk \rangle \\ &= \frac{1}{4} \langle \mathbf{V}_i \boldsymbol{\ell} | \mu \left(\hat{\pi}_+ \hat{\pi}_- + \hat{\pi}_- \hat{\pi}_+ \right) | \mathbf{V}_j \boldsymbol{\ell}' \rangle \langle Jk | Jk \rangle \\ &= \frac{1}{4} \langle \mathbf{V}_i \boldsymbol{\ell} | \mu \left(\hat{\pi}_+ \hat{\pi}_- + \hat{\pi}_- \hat{\pi}_+ \right) | \mathbf{V}_j \boldsymbol{\ell}' \rangle , \end{aligned} \tag{4.97}$$

where the orthonormality of the rotational basis functions has been used. The integration would therefore need to proceed via an expensive six dimensional numerical integration. This can be avoided by introducing a truncated resolution-of-identity (RI)

$$1 = \sum_{k}^{N_v^{\mathrm{RI}}} | \mathbf{V}_k^{\mathrm{RI}} \boldsymbol{\ell}^{\mathrm{RI}} \rangle \langle \mathbf{V}_k^{\mathrm{RI}} \boldsymbol{\ell}^{\mathrm{RI}} | \tag{4.98}$$

where N_v^{RI} is the size of the RI basis and the $|\mathbf{V}_k^{\mathrm{RI}}\boldsymbol{\ell}^{\mathrm{RI}}\rangle$ are products of HO basis functions (cf. Section 4.1.1). Insertion of Equation (4.98) into Equation (4.97) yields

$$\left(\mathrm{T}_{\pi}^{(J)}\right)_{ij} = \frac{1}{4}\sum_{k}^{N_v^{\mathrm{RI}}} \underbrace{\langle \mathbf{V}_i\boldsymbol{\ell}|\mu|\mathbf{V}_k^{\mathrm{RI}}\boldsymbol{\ell}^{\mathrm{RI}}\rangle}_{\mu_{ik}^{\mathrm{RI}}} \underbrace{\langle \mathbf{V}_k^{\mathrm{RI}}\boldsymbol{\ell}^{\mathrm{RI}}|(\hat{\pi}_+\hat{\pi}_- + \hat{\pi}_-\hat{\pi}_+)|\mathbf{V}_j\boldsymbol{\ell}^{'}\rangle}_{\pi_{kj}^{\mathrm{RI}}} . \tag{4.99}$$

This shows that the matrix representation of $\hat{\mathrm{T}}_{\pi}$ can be reduced to a product of the matrices $\boldsymbol{\mu}^{\mathrm{RI}}$ and $\boldsymbol{\pi}^{\mathrm{RI}}$ which are the $N_v \times N_v^{\mathrm{RI}}$ and $N_v^{\mathrm{RI}} \times N_v$ matrices, respectively, evaluated in the mixed primitive vibrational and RI basis set. This *ansatz* for matrix elements of $\hat{\mathrm{T}}_{\pi}$ has also been employed by Császár and coworkers in their DVR based DEWE program [231].
The same approach as presented above for $\boldsymbol{\mu}$ can be applied to $\boldsymbol{\mu}^{\mathrm{RI}}$ reducing the integration to a three dimensional Gauss-Hermite integration that only needs to be done once. Since matrix elements of $\boldsymbol{\pi}^{\mathrm{RI}}$ depend on the combination of the ℓ_t in the bra and ket, they have to be evaluated for all required combinations $(\ell_4, \ell_5 // \ell_4^{'}, \ell_5^{'})$. Furthermore, the RI approximation can also be applied to evaluate the matrix elements due to $\hat{\mathrm{T}}_{\mathrm{VR}}$ according to

$$\begin{aligned}
\left(\mathrm{T}_{\mathrm{VR}}^{(J)}\right)_{ij} &= \langle \mathbf{V}_i\boldsymbol{\ell} Jk \mp 1|\hat{\mathrm{T}}_{\mathrm{VR}}|\mathbf{V}_j\boldsymbol{\ell}^{'} Jk\rangle \\
&= -\frac{1}{2}\langle \mathbf{V}_i\boldsymbol{\ell}|\mu\hat{\pi}_{\mp}|\mathbf{V}_j\boldsymbol{\ell}^{'}\rangle \langle Jk \mp 1|\hat{\Pi}_{\pm}^{'}|Jk\rangle \\
&= -\frac{1}{2}\sqrt{J(J+1) - k(k\mp 1)}\sum_{k}^{N_v^{\mathrm{RI}}} \underbrace{\langle \mathbf{V}_i\boldsymbol{\ell}|\mu|\mathbf{V}_k^{\mathrm{RI}}\boldsymbol{\ell}^{\mathrm{RI}}\rangle}_{\mu_{ik}^{\mathrm{RI}}} \underbrace{\langle \mathbf{V}_k^{\mathrm{RI}}\boldsymbol{\ell}^{\mathrm{RI}}|\hat{\pi}_{\mp}|\mathbf{V}_j\boldsymbol{\ell}^{'}\rangle}_{\left(\pi_{\mathrm{C}}^{\mathrm{RI}}\right)_{kj}} .
\end{aligned} \tag{4.100}$$

The remaining question is the size of the RI basis. The RI presented in Equation (4.98) is exact for a complete basis. However, since $\hat{\pi}_{\pm}\hat{\pi}_{\mp}$ in Equation (4.99) and $\hat{\pi}_{\mp}$ in Equation (4.100) can only couple vibrational basis functions that differ in the quantum numbers v_i by at max ± 2 (cf. Section 4.1.1), the RI basis can be truncated by requiring all quantum numbers v_i^{RI} occuring in the RI basis to fulfill $v_i^{\mathrm{RI}} \leq v_i + 2$. The ℓ_t^{RI} used in the evaluation of $\boldsymbol{\pi}^{\mathrm{RI}}$ is determined by the ℓ_t in the $\langle \mathbf{V}_i\boldsymbol{\ell}|$ of Equation (4.97).
Potential energy matrix elements are most expensive to calculate. They have to be evaluated using a six dimensional Gaussian integration. The use of HO basis functions for the vibrational degrees of freedom directly results in the use of Gauss-Hermite and Gauss-Laguerre integration for the stretching and bending modes, respectively. This accounts for the integration over the q_s and ρ_t. What remains to be chosen is the type of integration for the phase angles χ_4 and χ_5. Following Section 4.1.5 the χ_t dependent part of a basis function can be written in terms of χ_4 and $\xi = \chi_5 - \chi_4$ according to

$$|\ell_4\ell_5\rangle = |(k-\ell_5)\ell_5\rangle = \sqrt{\frac{1}{4\pi^2}}\mathrm{e}^{\mathrm{i}k\chi_4}\mathrm{e}^{\mathrm{i}\ell_5\xi} . \tag{4.101}$$

which is obtained from Equation (4.67) after multiplying with $\langle Jk|$ and integrating over the Euler angles (θ, ϕ, χ') since V does not depend on the Euler angles. On the other hand, Equation (4.37) shows that V depends on $\cos(n\xi)$ even when an internal coordinate potential is employed (cf. Equation (4.39)). An integral of $\cos(n\xi)$ over the functions $|\ell_4\ell_5\rangle$ is then

$$\langle(k-\ell_5)\ell_5|\cos(n\xi)|(k'-\ell_5')\ell_5'\rangle = \frac{1}{4\pi^2}\int_0^{2\pi}\int_0^{2\pi} \mathrm{e}^{-\mathrm{i}k\chi_4}\mathrm{e}^{-\mathrm{i}\ell_5\chi_5}\cos(n\xi)\mathrm{e}^{\mathrm{i}k'\chi_4}\mathrm{e}^{\mathrm{i}\ell_5'\xi}\mathrm{d}\chi_4\mathrm{d}\xi \tag{4.102}$$

and integration over $\mathrm{d}\chi_4$ yields

$$\langle(k-\ell_5)\ell_5|\cos(n\xi)|(k'-\ell_5')\ell_5'\rangle = \frac{1}{2\pi}\int_0^{2\pi} \mathrm{e}^{-\mathrm{i}\ell_5\chi_5}\cos(n\xi)\mathrm{e}^{\mathrm{i}\ell_5'\xi}\mathrm{d}\xi\delta_{kk'}\,. \tag{4.103}$$

Equation (4.103) implies that the integration over the phase angle χ_4 can always be done analytically. The remaining integration over $\mathrm{d}\xi$ can be rewritten by use of Euler's formula

$$\begin{aligned}\frac{1}{2\pi}\int_0^{2\pi} \mathrm{e}^{-\mathrm{i}\ell_5\chi_5}\cos(n\xi)\mathrm{e}^{\mathrm{i}\ell_5'\xi}\mathrm{d}\xi &= \frac{1}{2\pi}\int_0^{2\pi}\cos(n\xi)\mathrm{e}^{\mathrm{i}(\ell_5'-\ell_5)\xi}\mathrm{d}\xi \\ &= \frac{1}{2\pi}\int_0^{2\pi}\cos(n\xi)\mathrm{e}^{\mathrm{i}\Delta\ell_5\xi}\mathrm{d}\xi \\ &= \frac{1}{4\pi}\left[\int_0^{2\pi}\cos(n\xi)\cos(\Delta\ell_5\xi)\mathrm{d}\xi\right. \\ &\qquad \left.+\mathrm{i}\int_0^{2\pi}\cos(n\xi)\sin(\Delta\ell_5\xi)\mathrm{d}\xi\right]\end{aligned} \tag{4.104}$$

The second integral vanishes due to the orthogonality of the cos and sin functions. Introducing the Chebyshev polynomials $T_a(\cos(x)) = \cos(ax)$ where $a \in \mathbb{N}_0$ [344] gives

$$\begin{aligned}\frac{1}{2\pi}\int_0^{2\pi} \mathrm{e}^{-\mathrm{i}\ell_5\chi_5}\cos(n\xi)\mathrm{e}^{\mathrm{i}\ell_5'\xi}\mathrm{d}\xi &= \frac{1}{4\pi}\int_0^{2\pi}\cos(n\xi)\cos(\Delta\ell_5\xi)\mathrm{d}\xi \\ &= \frac{1}{4\pi}\int_0^{2\pi} T_n(\cos(\xi))T_{\Delta\ell_5}(\cos(\xi))\mathrm{d}\xi\,.\end{aligned} \tag{4.105}$$

The final step now is to change the integration coordinate to $\Xi = \cos(\xi)$ according to

$$\mathrm{d}\xi = -\frac{\mathrm{d}\cos(\xi)}{\sqrt{1-\cos^2(\xi)}} = -\frac{\mathrm{d}\Xi}{\sqrt{1-\Xi^2}}\,. \tag{4.106}$$

Inserting into Equation (4.105) and integrating over dx yields

$$\begin{aligned}\frac{1}{4\pi}\int_0^{2\pi} T_n(\cos(\xi))T_{\Delta\ell_5}(\cos(\xi))\mathrm{d}\xi &= -\frac{1}{2\pi}\int_1^{-1} T_n(\Xi)T_{\Delta\ell_5}(\Xi)\frac{\mathrm{d}\Xi}{\sqrt{1-\Xi^2}} \\ &= \frac{1}{2\pi}\int_{-1}^{1} T_n(\Xi)T_{\Delta\ell_5}(\Xi)\frac{\mathrm{d}\Xi}{\sqrt{1-\Xi^2}} \\ &= \begin{cases} \frac{1}{2} & \text{for } n = \Delta\ell_5 = 0 \\ \frac{1}{4} & \text{for } n = \Delta\ell_5 \neq 0 \\ 0 & \text{for } n \neq \Delta\ell_5 \end{cases}, \end{aligned} \tag{4.107}$$

where the orthogonality relations of the Chebyshev polinomials has been used [344]. This shows that for the integration over dξ a Gauss-Chebyshev integration is possible.
In summary the integration of the potential energy V over the basis functions is done via six dimensional Gaussian integration. The 1D HO stretching basis functions are integrated by Gauss-Hermite integration over the q_s, 2D HO bending basis functions employ Gauss-Laguerre for integration of the ρ_t and the integration over the phase angle difference ξ is performed using Gauss-Chebyshev integration. A general overview of the integration scheme employed by C8v4 is depicted in Figure 4.8. Further details of the approach related to the construction of the primitive vibrational basis set and the Gaussian integration grids as well as the parallelisation will be discussed in the following.

4.2.3 Basis set design

The primitive vibrational basis set that defines the size of a (ℓ_4, ℓ_5) block N_v is constructed from a direct product of sets of functions for each vibrational coordinate $\{|v_1\rangle\} \times \{|v_2\rangle\} \times \{|v_3\rangle\} \times \left\{|v_4^{\ell_4}\rangle\right\} \times \left\{|v_5^{\ell_5}\rangle\right\}$. The size of the individual sets is controlled by setting a maximum quantum number $v_i^{\max}$. For the stretching basis functions $|v_s\rangle$ this directly corresponds to the maximum degree of the employed Hermite polynomial and $(v_s^{\max}+1)$ basis functions are used. In case of the bending basis functions $(v_t^{\max}+1)$ corresponds to the number of Laguerre polynomials used. The size of the basis set is then given by $N_v = \prod_i (v_i^{\max}+1)$. A typical calculation employs 10 basis functions per coordinate ($v_i^{\max} = v^{\max} = 9$) resulting in a product basis set of $N_v = 10^5$ basis functions. Storing a single (ℓ_4, ℓ_5) block of this size using double precision would require about 75 GB of RAM making the calculation not feasible.
It is therefore necessary to reduce the size of the basis set. This can be done for example by so called pruning schemes (cf. e.g. Ref. [190, 352] and references therein). This places the following restriction on the quantum numbers of a product basis function

$$\sum_i g_i(v_i) \leq P\,. \tag{4.108}$$

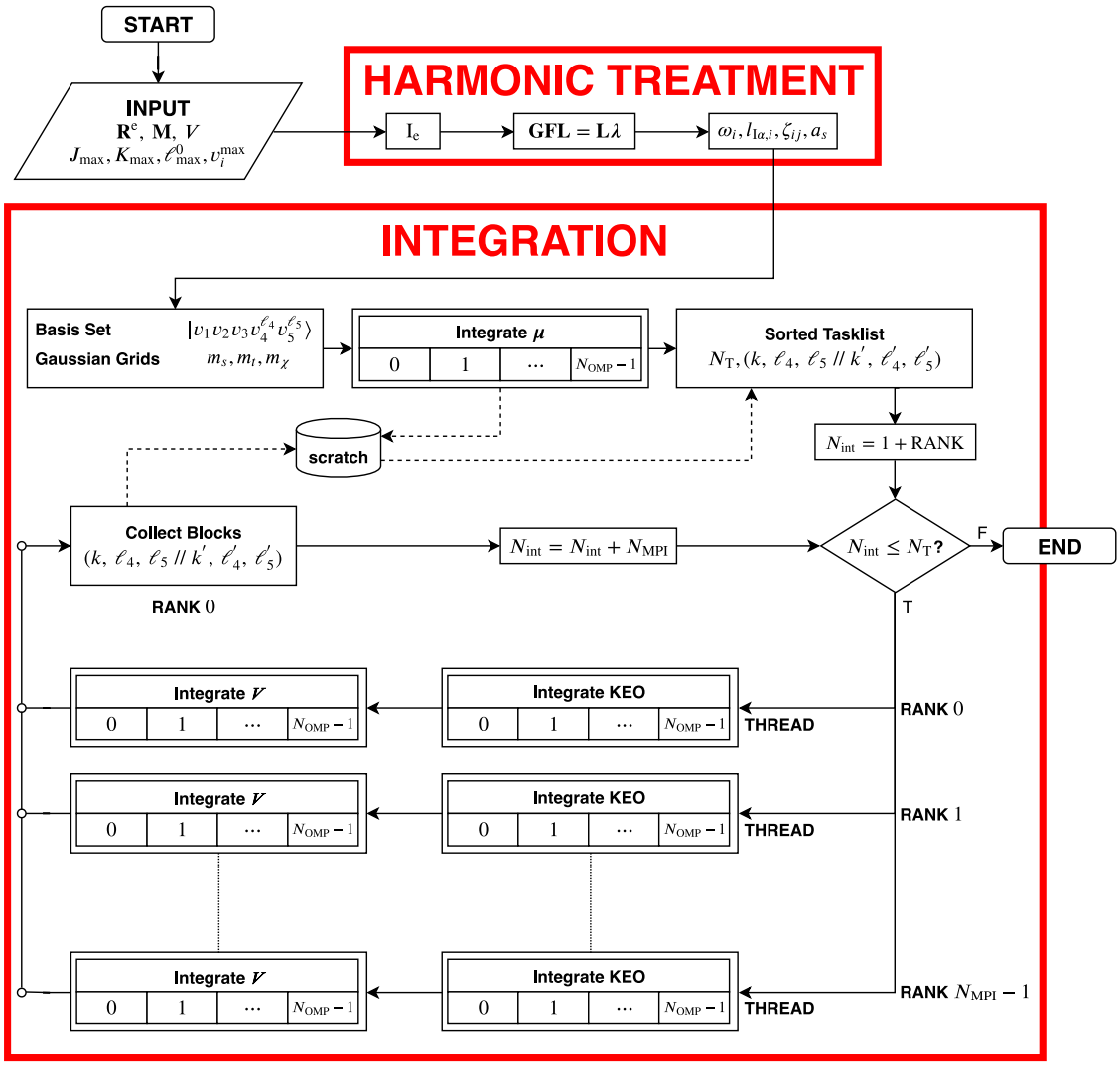

Figure 4.8: Flowchart representation of integration procedure implemented in C8V4 (see text for details). The scratch data (integral records) is read in the diagonalisation procedure.

In Equation (4.108) $g(v_i)$ is a suitable function that depends on the quantum number(s) v_i and P (sometimes called the polyad number) has to be chosen accordingly. In the present work P is set to 1 and the g-function is defined as

$$g(v_i) = \frac{v_i}{v_i^{\max}} \,. \tag{4.109}$$

This can be interpreted in the following way. Each basis function is assigned a vector $\boldsymbol{\eta}$ in the vector space $\mathbb{R}^5$ with components $\eta_i = \sqrt{v_i / v_i^{\max}}$. For a basis function to be accepted the scalar

product of such a vector with itself has to fulfill $\langle \boldsymbol{\eta}, \boldsymbol{\eta} \rangle \leq 1$. A graphical example in two dimensions $\mathbb{R}^2$ is shown in Figure 4.9 with $v_i^{\max} = v^{\max} = 3$.

Figure 4.10 displays the performance of the pruning scheme compared to a direct product basis set. In the left panel N_v of the basis sets obtained for different values of $v_i^{\max} = v^{\max}$ are compared on a logarithmic scale showing the reduced scaling of the basis set with $v^{\max}$. For the largest basis set $v^{\max} = 9$ the number of retained basis functions is lower by a factor almost two orders of magnitude. In the right panels the harmonic vibrational density of states (DOS) for basis sets with $v^{\max} = 9$ is given. Inspection of the upper right panel shows that, while the overall number of functions is reduced, the DOS for the pruned basis at the lower end of the spectrum is equal to the direct product basis set. This is desirable since it results in a comparable performance of the basis sets for low lying rovibrational states and the reduced N_v makes the calculation feasible.

Besides pruning the basis set based on the quantum numbers of the basis function an energy criterion could be used. Then, functions are selected based on whether their harmonic vibrational energy is below a cutoff energy $E_{\text{cut}}^{\text{bas}}$ and is straightforward to implement in a variational method. This pruning would then correspond to cutting off the DOS, as shown in Figure 4.10, above $E_{\text{cut}}^{\text{bas}}$. While the reduction in N_v would be significant, such a scheme can lead to an unbalanced basis set by favouring basis functions with high excitations in the low lying bending modes compared to the stretching vibrations.

The size of the rovibrational basis set depends on the rotational quantum number J, the e/f-parity block labeled by p = 0 or 1, respectively, the threshold on the vibrational angular momentum quantum number $\ell_0^{\max}$ and the size of the primitive vibrational basis set N_v. As discussed in Section 4.1.4, each Hamiltonian matrix $\mathbf{H}^{(J,p)}$ can be decomposed into $J+1$ blocks $\mathbf{H}_K^{(J,p)}$ with quantum numbers $K \leq J$ and Coriolis blocks $\mathbf{C}_K^{(J,p)}$ that couple K and $K-1$. For example the block matrix form of $\mathbf{H}^{(J,\mathrm{p})}$ for $J = 2$ in the e-block (p = 0) would be

$$\mathbf{H}^{(2,0)} = \begin{pmatrix} \mathbf{H}_2^{(2,0)} & \left(\mathbf{C}_1^{(2,0)}\right)^{\mathrm{T}} & \mathbf{0} \\ \mathbf{C}_2^{(2,0)} & \mathbf{H}_1^{(2,0)} & \left(\mathbf{C}_1^{(2,0)}\right)^{\mathrm{T}} \\ \mathbf{0} & \mathbf{C}_1^{(2,0)} & \mathbf{H}_0^{(2,0)} \end{pmatrix} . \tag{4.110}$$

The dimension of this matrix and thus the size of the rovibrational basis set can be obtained by summation over the K-block dimensions $N_K^{(\mathrm{p})}$ according to

$$N_{\text{VR}}^{(J,\mathrm{p})} = \sum_{K=0}^{J} N_K^{(\mathrm{p})} . \tag{4.111}$$

The size of the $\mathbf{H}_K^{(J,p)}$ blocks $N_K^{(\mathrm{p})}$ can be calculated as the product

$$N_K^{(\mathrm{p})} = N_\ell^{(\mathrm{p})} N_v \tag{4.112}$$

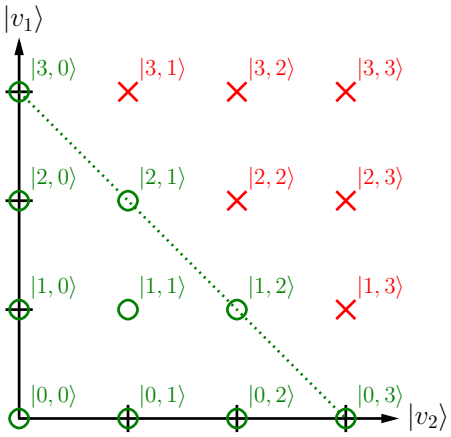

Figure 4.9: Schematic example of the pruning scheme applied to a 2D basis set with $v_i^{\max} = v^{\max} = 3$. Basis functions that are retained are represented by green circles and rejected basis functions by red crosses.

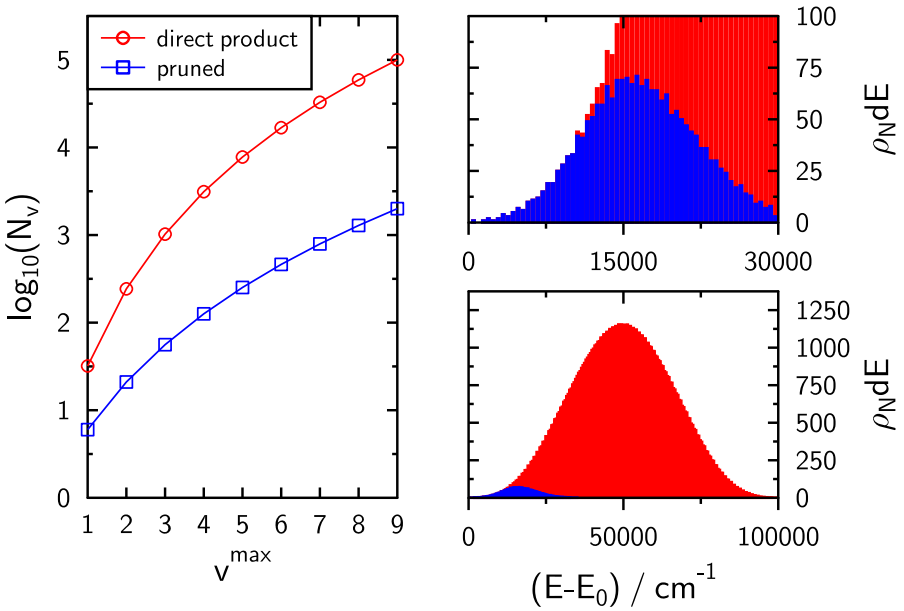

Figure 4.10: Comparison of direct product basis sets and pruned basis sets. Left: basis set sizes on a logarithmic scale with respect to $v_i^{\max} = v^{\max}$. Right: number densities of harmonic vibrational states for direct product (red) and pruned (blue) basis sets with $v^{\max} = 9$.

where $N_\ell^{(p)}$ and N_v are the number and size of the (ℓ_4, ℓ_5)-block, respectively. The former is given by

$$N_\ell^{(\mathrm{p})} = \begin{cases} 2\ell_{\max}^0 + 1 - \mathrm{p} & \text{for } K = 0 \\ 2\ell_{\max}^0 + K + 1 & \text{for } K \neq 0 \end{cases} \tag{4.113}$$

4.2.4 Gaussian integration grids

With the primitive basis set defined the next step is to set up the Gaussian integration grid. In Gaussian integration the integral of a function is replaced by a weighted sum

$$\int_a^b f(x)\mathrm{d}x \approx \sum_{i=1}^{m} f(x_i)w_i \,. \tag{4.114}$$

It can be shown [353] that this summation can be made exact when $f(x)$ is represented as a product $f(x) = p_n(x)W(x)$ where $p_n(x)$ is a polynomial of degree n and $W(x)$ is a weight function. Depending on the form of $W(x)$ there is an associated class of orthogonal polynomials $h_m(x)$. Choosing the x_i to be the m roots of polynomial $h_m(x)$ makes the Gaussian integration Equation (4.114) exact for all polynomials $p_n(x)$ with $n \leq 2m - 1$. In order to determine the number of integration points needed to integrate the Hamiltonian first consider the overlap integral of two orthonormal 1D HO basis functions

$$\langle v|v^{'}\rangle = \int_{-\infty}^{\infty} \underbrace{\mathrm{H}_v(q)\mathrm{H}_{v'}(q)}_{p_n(q)} \underbrace{\mathrm{e}^{-q^2}}_{W(q)} \mathrm{d}q \stackrel{!}{=} \delta_{vv'} \tag{4.115}$$

The product of the polynomials is again a polynomial now of degree $n = v + v'$. To make this integral exact $m \geq (v + v^{'} + 1)/2$ Gauss-Hermite integration points are needed and they are the roots of the Hermite polynomial $\mathrm{H}_m(q)$. The maximum order of Hermite polynomials employed for the stretching basis functions is $v_s^{\max}$ and the number of Gaussian integration points needed to make the overlap integrals exact is therefore $m_s \geq (2v_s^{\max} + 1)/2$.
The same argument can be applied to the Gauss-Laguerre integration

$$\langle v\ell|v'\ell^{'}\rangle = \frac{1}{4\pi} \int_0^{\infty} \underbrace{\mathrm{L}_n^{|\ell|}(\rho)\mathrm{L}_{n'}^{|\ell^{'}|}(\rho)}_{p_n(\rho)} \underbrace{\rho^{\frac{(|\ell|+|\ell^{'}|)}{2}}\mathrm{e}^{-\rho}}_{W(\rho)} \mathrm{d}\rho \int_0^{2\pi} \mathrm{e}^{\mathrm{i}(\ell^{'}-\ell)\chi}\mathrm{d}\chi \stackrel{!}{=} \delta_{nn'}\delta_{\ell\ell'} \,. \tag{4.116}$$

In this case the polynomial $p_n(\rho)$ is of order $n = (v - |\ell| + v' - |\ell^{'}|)/2$. Then, in order for the first integral to be exact $m \geq (v - |\ell| + v' - |\ell^{'}| + 2)/4$ Gauss-Laguerre integration points are needed. The latter are the roots of the associated Laguerre polynomial $\mathrm{L}_m^{(|\ell|+|\ell^{'}|)}(\rho)$.
Here it is important to consider the restrictions on the quantum numbers of the bending vibrations $v_t \geq |\ell_t| \leftrightarrow v_t - |\ell_t| \geq 0$ and since only $|\ell_t| = v_t, v_t - 2, v_t - 4, \ldots 1$ or 0 are the only allowed values for ℓ_t the degrees of the polynomials $\mathrm{L}_{n_t}^{|\ell_t|}(\rho)$ are $n_t - |\ell_t| = 2k \,\forall\, k \in \mathbb{N}_0$ independent of ℓ_t. For bending vibrations $v_t^{\max}$ corresponds to the number of basis functions which following the

above discussion then yields $n_t^{\max} - |\ell_t| = 2v_t^{\max}$. Therefore $m_t \geq (4v_t^{\max} + 2)/4$ Gauss-Laguerre integration points are needed for all overlap integrals.
So far only the overlap integrals of the basis set would be exact. The numerical integration of V, $\boldsymbol{\mu}$ and $\boldsymbol{\mu}^{\mathrm{RI}}$ have to be taken into consideration. For the two latter matrices one considers an Taylor expansion of μ in terms of the (stretching) normal coordinates up to an order $n_\mu^{\max}$. The integration of μ over the stretching coordinates then contains at max the one dimensional integrals

$$\langle v_s^{\max}|q_s^{n_\mu^{\max}}|v_s^{\max}\rangle = \int_{-\infty}^{\infty} q_s^{n_\mu^{\max}} \mathrm{H}_{v_s^{\max}}(q_s)\mathrm{H}_{v_s^{\max}}(q_s)\mathrm{e}^{-q_s^2}\mathrm{d}q_s \tag{4.117}$$

and to make the above integral exact a Gauss-Hermite integration of order $m_s \geq (2v_s^{\max} + n_\mu^{\max} + 1)/2$ is sufficient. Since the RI basis contains 1D HO basis functions up to order $v_s^{\max} + 2$ the integration of $\boldsymbol{\mu}^{\mathrm{RI}}$ requires $m_s + 2$ points in the Gauss-Hermite grids. The same approach can be applied to potential energy integrals. In case of normal coordinate PEFs the value of $n_V^{\max}$ is given by the maximum order of expansion in the q_i (e.g. $n_V^{\max} = 4$ for a QFF). For PEFs expanded in terms of curvilinear internal coordinates Я_i the situation is more complicated since even a finite order expansion of V in the internal coordinate space corresponds to an infinite order expansion in normal coordinate space due to Equation (4.39). One therefore has to determine a suitable value of $n_V^{\max}$ and subsequently m_i. This can be done by monitoring the convergence of matrix elements with respect to m_s and m_t in a trial and error fashion. Unfortunately such an approach is rather expensive, since it would require repeated six dimensional numerical integrations.
A more efficient way of estimating a suitable $n_{\mathrm{V}}^{\max}$ is by use of the chain rule as described in Section 4.1.3. A truncated internal coordinate expansion of order $n_{\mathrm{V}}^{\max}$ defines the corresponding normal coordinate potential only up to the same order exactly. To obtain accurate matrix elements the m_i are therefore calculated for each normal coordinate individually via

$$m_s \geq \frac{1}{2}(2v_s^{\max} + n_{\mathrm{V}s}^{\max} + 1) \Rightarrow m_s = v_s^{\max} + \frac{1}{2}n_{\mathrm{V}s}^{\max} + 1 \tag{4.118}$$

and

$$m_t \geq \frac{1}{4}(4v_t^{\max} + n_{\mathrm{V}t}^{\max} + 2) \Rightarrow m_t = v_t^{\max} + \frac{1}{4}n_{\mathrm{V}t}^{\max} + 1\,, \tag{4.119}$$

where the $n_{\mathrm{V}s}^{\max}$ and $n_{\mathrm{V}t}^{\max}$ are the maximum expansion orders in V for the stretching and angle bending internal coordinates. This directly ensures that integration of μ/μ^{RI} over basis functions $|v_s^{\max}\rangle$ is also exact up to order $n_{\mathrm{V}s}^{\max}$ in the q_s.
For the Gauss-Chebyshev integration over $\mathrm{d}\xi$ (cf. Equation (4.102) to (4.107)) the order of the Chebyshev polynomials n and $\Delta\ell_5$ are defined by the term in the potential expansion Equation (4.37) and the basis functions, respectively. The maximum values $n^{\max}$ and $\Delta\ell_5^{\max}$ that can occur in a given calculation can be derived from the maximum angular momentum quantum number $J^{\max} = K^{\max}$ and $\ell_{\max}^0$. By analyzing the possible (ℓ_4, ℓ_5) combinations in the $J^{\max}$ Hamiltonian (excluding vanishing blocks) one finds that $\Delta\ell_5^{\max} = n^{\max} = 2\ell_{\max}^0 + K^{\max}$. Therefore, the number

of Gauss-Chebyshev integration points needed is

$$m_\xi \geq 2\ell^0_{\max} + K^{\max} + \frac{1}{2} \Rightarrow m_\xi = 2\ell^0_{\max} + K^{\max} + 1\,. \tag{4.120}$$

The presented rules for m_s, m_t and m_ξ pertain to the evaluation of matrix elements of basis functions with the maximum value for the respective quantum numbers involved. Evaluating matrix elements between functions with a lower quantum number then is accurate to a higher degree than assumed to determine the m's. This is best understood by examining an example and for simplicity restricting the setup to a 1D case. Consider a basis of stretching functions $\{|v_s\rangle\}$ with $v_s^{\max} = 10$. When requiring the matrix element $\langle v_s^{\max} \,|\, V \,|\, v_s^{\max}\rangle$ over the generalized potential V to be accurate up to 4^{th} order in q_s ($n_{\text{V}s}^{\max} = 4$) the required number of Gauss-Hermite points is (Equation (4.118)) $m_s = 10 + \frac{1}{2}4 + 1 = 13$. Then, the matrix element $\langle 0 \,|\, V \,|\, 0\rangle$ for $v_s = 0$ will be accurate up to $n_{\text{V}s} = 2\,(m_s - v_s - 1)$ which yields the 24^{th} order in q_s for the present example.

4.2.5 Diagonalisation

With the matrix representation of the Hamiltonian $\mathbf{H}^{(J,\text{p})}$ set up in a suitable basis set, the rovibrational term energies and wave functions are obtained by diagonalisation. This corresponds to finding the orthogonal matrix $\mathbf{X}^{(J,\text{p})}$ such that

$$\left(\mathbf{X}^{(J,\text{p})}\right)^{\text{T}} \mathbf{H}^{(J,\text{p})} \left(\mathbf{X}^{(J,\text{p})}\right) = \mathbf{\Lambda}^{(J,\text{p})}\,, \tag{4.121}$$

where $\mathbf{\Lambda}^{(J,\text{p})}$ is the diagonal matrix of the rovibrational term energies $T_v(J)$. The size of the matrix $\mathbf{H}^{(J,\text{p})}$ typically is too large for direct eigensolvers, e.g. as implemented in LAPACK [354]. For example, a modest sized primitive basis set of $N_v = 2500$ and vibrational angular momentum threshold of $\ell^0_{\max} = 3$ leads to e-parity matrices of order 10000, 35000 and 62500 for $J = 0,\ 1$ and 2, respectively. The calculation of *all* eigenpairs of such large matrices is prohibitive. In order to reduce the matrix size a prediagonalisation scheme has been implemented. The approach is based on the fact that the matrix elements of Coriolis-blocks $\mathbf{C}_K^{(J,\text{p})}$ are small compared to $\mathbf{H}_K^{(J,\text{p})}$ and can thus be treated as perturbations to the K-diagonal eigenstates.
To this end, the $\mathbf{H}_K^{(J,\text{p})}$ blocks are diagonalised first

$$\left(\mathbf{X}_K^{(J,\text{p})}\right)^{\text{T}} \mathbf{H}_K^{(J,\text{p})} \mathbf{X}_K^{(J,\text{p})} = \mathbf{\Lambda}_K^{(J,\text{p})}\,, \tag{4.122}$$

where $\mathbf{X}_K^{(J,\text{p})}$ are the obtained eigenvectors and $\mathbf{\Lambda}_K^{(J,\text{p})}$ the corresponding eigenvalues. From this set of eigenpairs N_K^{red} are kept. This selection can be either based on a fixed number of eigenfunctions/eigenvalues or an energy criterion $E_{\text{cut}}^{\text{red}}$. In the latter case N_K^{red} is determined once based on the eigenvalues of $\mathbf{H}_K^{(K,\text{p})}$ eigenvalues.
After collecting the $N^{\text{red}} = \sum_K N_K^{\text{red}}$ eigenpairs $\mathbf{X}_K^{(J,\text{p})}$ and $\mathbf{\Lambda}_K^{(J,\text{p})}$, the full Hamiltonian matrix

$\mathbf{H}^{(J,\mathrm{p})}$ is transformed to the reduced basis $\tilde{\mathbf{H}}^{(J,\mathrm{p})}$

$$\tilde{\mathbf{H}}^{(J,\mathrm{p})} = \left(\mathbf{S}^{(J,\mathrm{p})}\right)^{\mathrm{T}} \mathbf{H}^{(J,\mathrm{p})} \mathbf{S}^{(J,\mathrm{p})}\,, \tag{4.123}$$

where a transformation matrix $\mathbf{S}^{(J,\mathrm{p})}$ is introduced according to

$$\mathbf{S}^{(J,\mathrm{p})} = \begin{pmatrix} \mathbf{X}_J^{(J,\mathrm{p})} & \mathbf{0} & \cdots & \mathbf{0} \\ \mathbf{0} & \mathbf{X}_{J-1}^{(J,\mathrm{p})} & & \vdots \\ \vdots & & \ddots & \mathbf{0} \\ \mathbf{0} & \cdots & \mathbf{0} & \mathbf{X}_0^{(J,\mathrm{p})} \end{pmatrix}. \tag{4.124}$$

Since the $\mathbf{X}_K^{(J,\mathrm{p})}$ are orthonormal

$$\left(\mathbf{X}_K^{(J,\mathrm{p})}\right)^{\mathrm{T}} \mathbf{X}_K^{(J,\mathrm{p})} = \mathbf{I}\,, \tag{4.125}$$

where $\mathbf{I}$ is the identity matrix ($\mathrm{I}_{ij} = \delta_{ij}$), the block diagonal matrix $\mathrm{S}^{(J,\mathrm{p})}$ is also orthonormal

$$\left(\mathbf{S}^{(J,\mathrm{p})}\right)^{\mathrm{T}} \mathbf{S}^{(J,\mathrm{p})} = \mathbf{I}\,. \tag{4.126}$$

Inserting Equation (4.123) into Equation (4.121) yields the secular equation for the reduced Hamiltonian matrix

$$\left(\mathbf{S}^{(J,\mathrm{p})}\right)^{\mathrm{T}} \mathbf{H}^{(J,\mathrm{p})} \mathbf{S}^{(J,\mathrm{p})} \left(\left(\mathbf{S}^{(J,\mathrm{p})}\right)^{-1} \mathbf{X}^{(J,\mathrm{p})}\right) = \left(\left(\mathbf{S}^{(J,\mathrm{p})}\right)^{-1} \mathbf{X}^{(J,\mathrm{p})}\right) \tilde{\mathbf{\Lambda}}^{(J,\mathrm{p})} \tag{4.127}$$

or

$$\tilde{\mathbf{H}}^{(J,\mathrm{p})} \tilde{\mathbf{X}}^{(J,\mathrm{p})} = \tilde{\mathbf{X}}^{(J,\mathrm{p})} \tilde{\mathbf{\Lambda}}^{(J,\mathrm{p})}\,. \tag{4.128}$$

The matrix $\tilde{\mathbf{H}}^{(J,\mathrm{p})}$ is now small enough that it can be diagonalised by a direct eigensolver to yield eigenvalues $\tilde{\mathbf{\Lambda}}^{(J,\mathrm{p})}$ and eigenvectors $\tilde{\mathbf{X}}^{(J,\mathrm{p})}$ with respect to the contracted functions $\mathbf{X}_K^{(J,\mathrm{p})}$. Using the latter, back transformation according to

$$\mathbf{X}^{(J,\mathrm{p})} = \mathbf{S}^{(J,\mathrm{p})} \tilde{\mathbf{X}}^{(J,\mathrm{p})} \tag{4.129}$$

yields the desired rovibrational wave functions in the original basis set. The eigenpairs obtained in this way are approximations to the exact results, but in the limit $N_K^{\mathrm{red}} \to N_K^{(\mathrm{p})}$ they are identical. For $J = 0$ calculations the presented scheme always yields exact eigenvalues/eigenvectors since $\mathbf{H}^{(0,\mathrm{p})} = \mathbf{H}_0^{(0,\mathrm{p})}$. Due to the underlying assumption on the numerical size relation between $\mathbf{C}_K^{(J,\mathrm{p})}$ and $\mathbf{H}_K^{(J,\mathrm{p})}$ matrix elements, this approach is best suited for low values of rotational excitation, since $\mathbf{C}_K^{(J,\mathrm{p})}$ scale with both J and K (cf. Equation (4.23)). The general procedure is summarized in Figure 4.11 which depicts a flowchart representation of the diagonalisation. Details of the shown

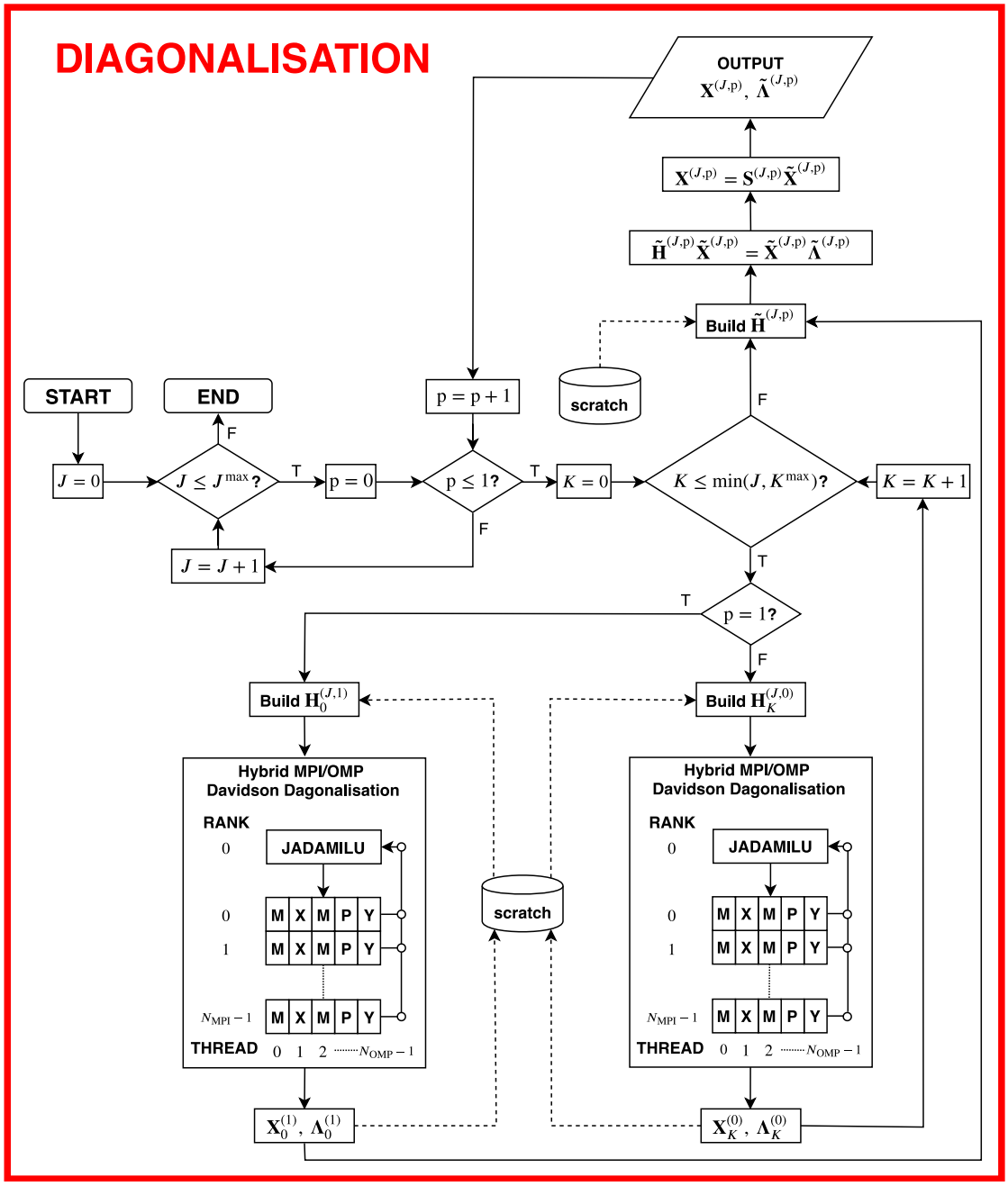

Figure 4.11: Flowchart representation of diagonalisation procedure implemented in C8V4 (see text for details). The scratch data contains the integral records determined during the integration.

parallelisation approach will be discussed in Section 4.2.6.
So far the computational effort of diagonalising the $\mathbf{H}^{(J,\mathrm{p})}$ Hamiltonian has been reduced from $\mathcal{O}((N_{\mathrm{VR}}^{(J,\mathrm{p})})^3)$ to $2J$ diagonalisations with $\mathcal{O}((N_K^{(\mathrm{p})})^3)$, where $N_{\mathrm{VR}}^{(J,\mathrm{p})} \gg N_K^{(\mathrm{p})}$. Furthermore, since the diagonal K-blocks $\mathbf{H}_K^{(J,\mathrm{p})}$ with $\mathrm{p} = 0$ and 1 are identical for $K > 0$ they have to be diagonalised only once for each J. The $\mathrm{p} = 1$ Hamiltonians then require only an additional prediagonalisation of the $\mathbf{H}_0^{(J,1)}$ block and in total $J + 1$ matrices of order $N_K^{(\mathrm{p})}$ have to be diagonalised for each J. A further reduction by applying the prediagonalisation scheme also to the $\mathbf{H}_K^{(J,\mathrm{p})}$ blocks is problematic since basis functions with different (ℓ_4, ℓ_5) combinations show strong coupling among each other due to the potential energy terms $V^{(n)}$ (cf. Equation (4.37)) especially for low values of $n = \Delta\ell_t$.
Since only a limited number of diagonal K-block eigenvalues are needed for the prediagonalisation, an iterative eigensolver based on the Davidson algorithm [355] is used to determine $\mathbf{\Lambda}_K^{(J,\mathrm{p})}$ and $\mathbf{X}_K^{(J,\mathrm{p})}$ in Equation (4.122). The Davidson method operates in the following manner. Given a matrix $\mathbf{H}$, a true eigenvector is denoted as $\mathbf{v}$, an approximate eigenvector as $\mathbf{x}$ and the error vector is $\boldsymbol{\delta} = \mathbf{v} - \mathbf{x}$. The eigenvalue equation is given by

$$\mathbf{H}(\mathbf{x} + \boldsymbol{\delta}) = \lambda(\mathbf{x} + \boldsymbol{\delta})\,. \tag{4.130}$$

In Equation (4.130) λ is the true eigenvalue which can be written as $\lambda = \rho + \epsilon$, with the Rayleigh quotient $\rho = \mathbf{x}^{\mathrm{T}}\mathbf{H}\mathbf{x}$ and error ϵ. Equation (4.130) can be rewritten as

$$\begin{aligned}(\mathbf{H} - \rho - \epsilon)\boldsymbol{\delta} = &= -(\mathbf{H} - \rho - \epsilon)\mathbf{x} \\ &= -\mathbf{r} + \epsilon\mathbf{x}\,,\end{aligned} \tag{4.131}$$

where the residue vector $\mathbf{r} = (\mathbf{H} - \rho\mathbf{I})\mathbf{x}$ has been introduced. Solving Equation (4.131) for $\boldsymbol{\delta}$ and updating the subspace in which $\mathbf{H}$ is diagonalised results in an iterative procedure for obtaining eigenvectors and eigenvalues of the Matrix $\mathbf{H}$. The present implementation is taken from the JADAMILU program [356]. It uses a diagonal preconditioner where $\mathbf{H}$ in Equation (4.131) is replaced by its diagonal $(\mathbf{D})_{ij} = \mathrm{H}_{ij}\delta_{ij}$ and assume the error ϵ is negligible. The correction vector $\boldsymbol{\delta}$ then becomes

$$\boldsymbol{\delta} = -(\mathbf{D} - \rho\mathbf{I})^{-1}\mathbf{r}\,. \tag{4.132}$$

Since $\mathbf{D}$ and $\boldsymbol{\rho}\mathbf{I}$ are diagonal matrices, the inversion in Equation (4.132) is trivial. The algorithm outlined so far can now be extended to the solution of the N_{eig} lowest eigenvalues.

Initialisation

Build a guess eigenspace of dimension $l \geq N_{\mathrm{eig}}$ with orthonormal vectors $\mathbf{b}_1, \mathbf{b}_2, \ldots, \mathbf{b}_l$.

Build Subspace

Form matrix vector products $\mathbf{H}\mathbf{b}_1, \mathbf{H}\mathbf{b}_2, \ldots, \mathbf{H}\mathbf{b}_l$, calculate $\tilde{H}_{ij} = \mathbf{b}_i^{\mathrm{T}}\mathbf{H}\mathbf{b}_j$ and solve for approximate eigenvalues $\{\rho_i\}$ and eigenvectors $\{\mathbf{x}_i\}$.

Residues

Calculate the k residue vectors $\mathbf{r}_i = (\mathbf{H} - \rho_i \mathbf{I})\mathbf{x}_i$ and check for convergence via $\|\mathbf{r}_i\| \leq$ tolerance. When no convergence for *all* N_{eig} eigenvectors is achieved, continue with next step.

Correction vectors

Calculate the correction vectors δ_i based on Equation (4.132). This is done only for those eigenvectors that are unconverged.

Subspace expansion

Orthogonalize the δ_i to the previous sub space, append the orthonormal correction vectors to the subspace and start from step 2 (only matrix elements involving the new vector need to be calculated).

For the present application N_{eig} is in general much smaller than the matrix dimensions $N_K^{(\text{p})}$. The diagonalization of the subspace therefore does not contribute significant to the computational cost. Forming the matrix vector products $\mathbf{Hx}$ of the trial vectors with the matrix is the main computational bottleneck. Then, the computational cost of the Davidson algorithm scales approximately like $N_{\text{eig}} N_{\text{it}} C_{\text{MX}}$, where N_{it} is the number of iterations needed to achieve convergence and the cost of a single matrix vector product is $C_{\text{MX}} \sim (N_K^{(\text{p})})^2$.

4.2.6 Parallelisation

The block structure of the Hamiltonian can be exploited for the parallelisation of the program. In order to maximize the usage of todays high performance computing facilities that consist of a network of compute nodes each representing a multi-CPU machine, a hybrid parallelisation scheme is implemented in the C8V4 variational program. Intuitively a distributed memory approach based on the Message Passing Interface (MPI) is applicable to the integration of the Hamiltonian matrix by distributing blocks among the network. Furthermore, the numerical Gaussian integration of $\boldsymbol{\mu}$, $\boldsymbol{\mu}^{\text{RI}}$ and potential energy matrix elements lends itself to a further layer of parallelisation. This is done with shared memory parallelisation based on OpenMP (OMP) routines.
The hybrid MPI/OMP integration of the Hamiltonian can be described by the following workflow (cf. also Figure 4.8):

Tasklist

First the list of N_{task} non-vanishing $(k, \ell_4, \ell_5 // k', \ell_4', \ell_5')$ blocks is constructed based on the values of $J^{\max}$, $K^{\max}$ and $\ell^0_{\max}$ employed in the calculations. The list is distributed by MPI to the N_{MPI} shared memory machines (ranks).

Integrate KEO

Each rank performs the necessary integration of KEO terms for a combination

$(k, \ell_4, \ell_5//k', \ell_4', \ell_5')$ assigned to it. This involves also a parallelised $\boldsymbol{\mu}$ ($\boldsymbol{\mu}^{\mathrm{RI}}$) integration and matrix multiplication for combinations coupled by $\hat{\mathrm{T}}_\pi$ ($\hat{\mathrm{T}}_{\mathrm{VR}}$).

Integrate V

The potential energy integration (if needed) is distributed among the N_{OMP} compute units (threads) of the shared memory machines. This can be done with different orderings of the loops over intergration points and matrix elements. Different choices of these loop orders are studied below.

Communication

After finishing integration of one $(k, \ell_4, \ell_5//k', \ell_4', \ell_5')$ block, each rank sends the matrix representation to the root rank (rank 0) which writes the data to temporary files (scratch). The ranks now proceed to integrate the next $(k, \ell_4, \ell_5//k', \ell_4', \ell_5')$ block.

This workflow only requires minor modification compared to a serial version of the program. The main addition is the communication that has to be done after each batch of blocks has been integrated by the ranks.

In order to reduce idling of the nodes when waiting for communication with rank 0 to transfer the finished blocks, work balancing is required. From the analysis of the block structure of the Hamiltonian one can deduce an ordering of different types of blocks with respect to the needed computational time. The most expensive blocks are the diagonal K-blocks for which $\Delta\ell = \pm 1$. These blocks involve integration over both $\hat{\mathrm{T}}_\pi$ and V. Furthermore, they are not symmetric and thus require the full $N_v \times N_v$ matrix to be calculated. Integration of blocks with $\Delta\ell = 0$ is the fastest

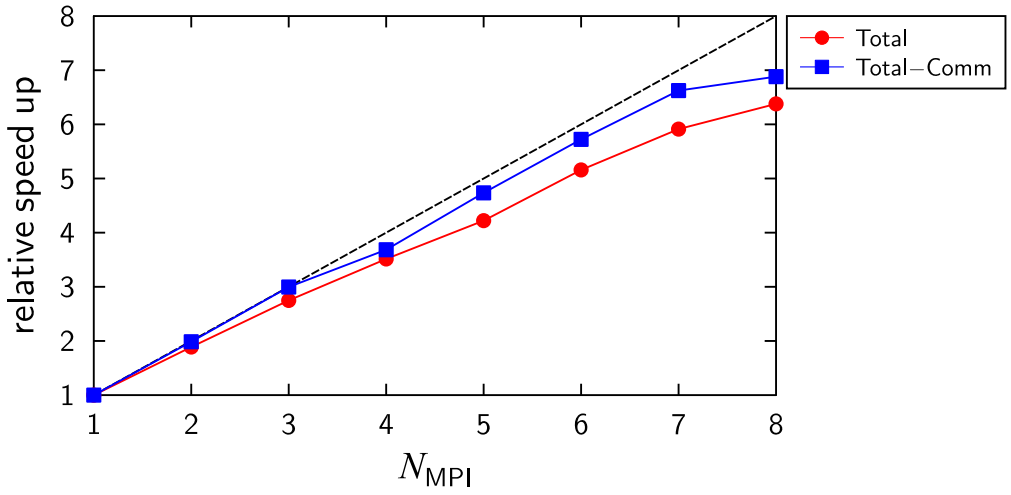

Figure 4.12: Relative speedup for the integration of a $K = 0$ block with $\ell^0_{\mathrm{max}} = 8$ (81 blocks) with respect to the number of MPI nodes N_{MPI}. The speed up is obtained either by comparing total run times (Total) or the actual computation time obtained after subtracting the MPI communication time (Total−Comm).

among the diagonal K-blocks although the full vibrational KEO and V have to be considered. The computational time is sped up by the symmetry of the blocks such that only half of the matrix needs to be calculated explicitly. Blocks with $|\Delta\ell| > 1$ fall in between these extreme cases. Only V needs to be integrated for such a block. Finally, Coriolis blocks with $\Delta k = k^{'} - k = \pm 1$ are also fast to construct once the matrix $\boldsymbol{\mu}^{\mathrm{RI}}$ is available and the required matrix multiplication $\boldsymbol{\mu}^{\mathrm{RI}}\boldsymbol{\pi}^{\mathrm{RI}}$ has been parallelised using OMP. Using these expected calculation times the task list can be sorted to balance the work load that is done for each batch of blocks across the nodes. The MPI based parallelisation of the Hamiltonian matrix integration is fully task parallel and should show almost linear speed up with increasing number of nodes N_{MPI}. Figure 4.12 clearly depicts this behaviour for the integration of a $K = 0$ block with $\ell_{\max} = 8$. Calculations were performed using up to 8 nodes (Intel E5-2670 v2) of the GWDG HPC cluster.
The OMP based parallelisation of the V integration can be done in different ways, depending on the order of loops (integration points and matrix elements) and which loop is distributed between the threads. Three different approaches have been tested:

Algorithm 1

Each thread performs part of the loop over the integration points and evaluates the full matrix $\mathbf{V}$. For each integration point the thread needs to first calculate the value of the potential energy at the integration point and then performes a rank-1 update (using BLAS routines DSYR or DGER) of the private $\mathbf{V}^{(N_{\mathrm{OMP}})}$ matrix. In the end the individual matrices are reduced to yield the final matrix $\mathbf{V}$.

Algorithm 2

In this case the loops are ordered such that the integration routine passes over the matrix V once. Each matrix element is then integrated by distributing the integration points among the threads. The weighted potential energy at the integration points is stored by each thread individually and thus needs only to be explicitly calculated once for the first matrix element.

Algorithm 3

This algorithm uses the same loop order as algorithm 2 but now the matrix elements that are calculated are distributed between threads. Again, the weighted potential energy is calculated only once but each thread performs the full summation over the integration points.

In order to judge the performance of the three algorithms, test calculations have been perfomed. Two primitive basis sets were used with $v_i^{\max} = v^{\max} = 7$ and 8 corresponding to about 800 and 1300 basis functions, respectively. Calculations were performed on a single node (Intel E5-2670 v2) of the GWDG HPC cluster. Figure 4.13 compares the relative speed ups t_1/t_n where t_1 and t_n are the wall times using 1 and n threads, respectively. While algorithm 1 achieves the highest peak η_s of about 10 for the smaller basis set and using 14 threads, the performance deteriorates with more threads and for larger basis sets. This is due to the high memory demand of the algorithm. For a fixed matrix size, the required memory scales linearly with the number of threads used and

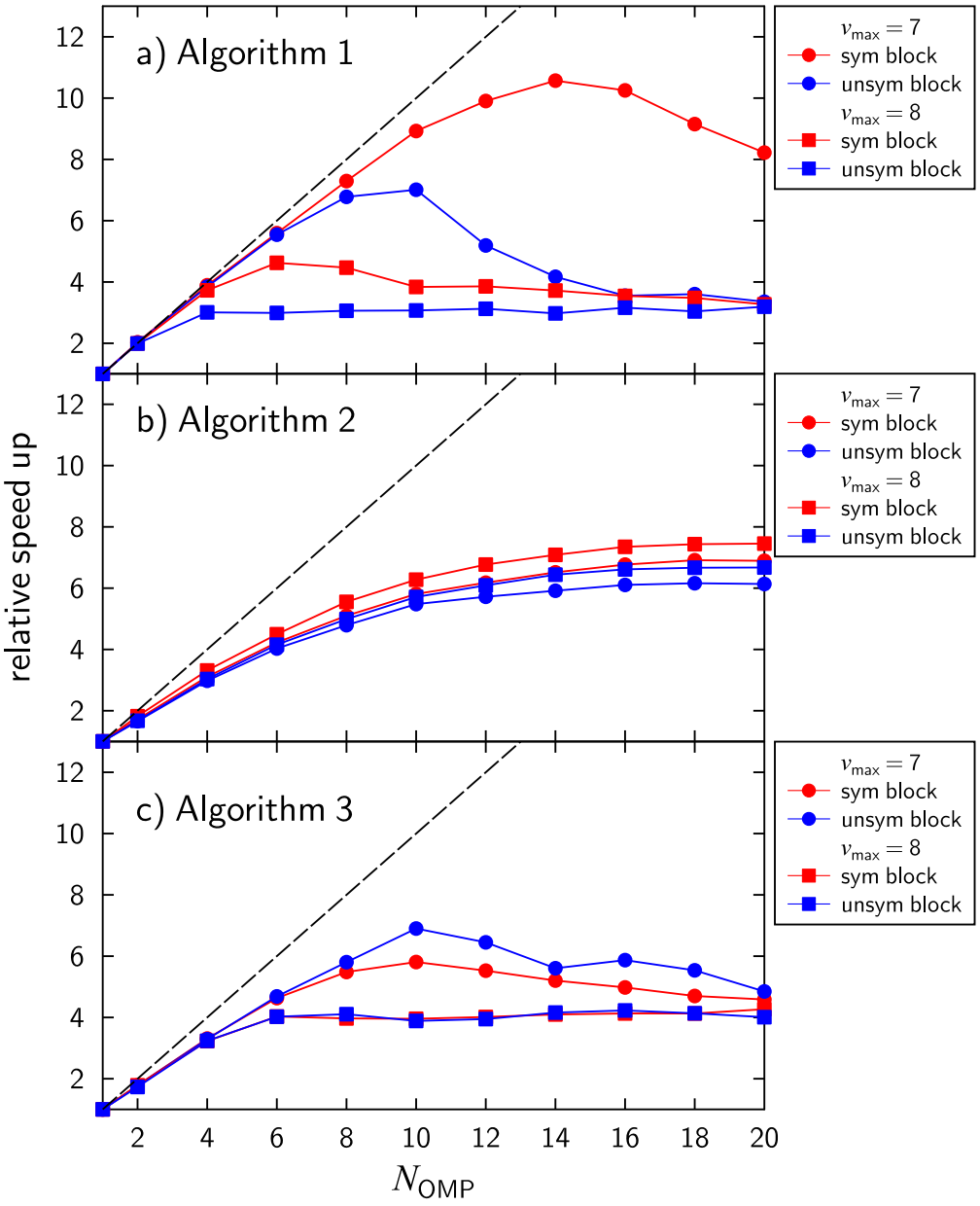

Figure 4.13: Comparison of relative speedups with respect to the number of OMP threads N_{OMP} for different potential energy integration algorithms. Calculations employ different numbers of basis functions determined by the $v_{\max}$ and are either performed for a symmetric (sym) block or a an unsymmetric (unsym) block. For details on the algorithms see text.

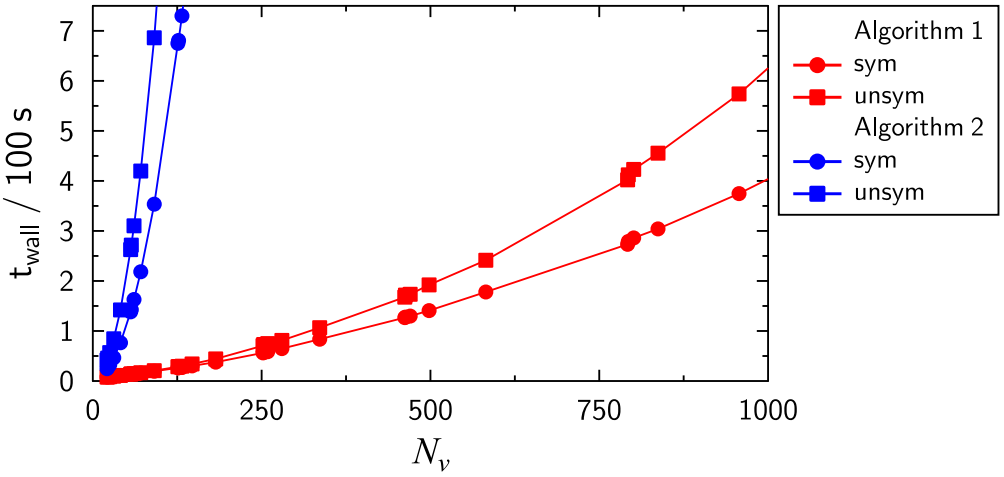

Figure 4.14: Comparison of wall times with respect to the size of the primitive vibrational basis set N_v for potential energy integration algorithms 1 and 2.Results are shown for symmetric (sym) and unsymmetric (unsym) blocks. For details on the algorithms see text.

for a fixed number of threads scales quadratically with the basis size. Algorithm 2 and 3 show somewhat similar speed up behaviour but algorithm 2 performs better. In that case, a peak speed up of about 7 is achieved when using all available CPUs of the node, a factor of 2 larger than algorithm 1. Furthermore, no strong dependence on the matrix size is observed. While these results suggest that algorithm 2 should be the preferred choice, analysis of the wall time scaling with respect to the size of the primitive vibrational basis N_v when $N_{\mathrm{OMP}} = 1$ contradicts this choice. Figure 4.14 compares this scaling behaviour for basis set sizes up to about 2000. Clearly, algorithm 2 shows a much worse scaling. Already for small basis sets of about 200 functions the wall time of algorithm 2 is orders of magnitude larger compared to 1 and thus overcompensating the possible increased speed up through parallelisation. Judging from these observations algorithm 1 should be preferred, since it gives the best over all performance in light of a typical basis set size exceeding 2000 functions.

The critical step in speeding up the Davidson diagonalisation of the $\mathrm{H}_K^{(J,\mathrm{p})}$ blocks is the matrix-vector multiplication (MXMPY). Again, a hybrid MPI/OMP partitioning of the calculation has been implemented in C8v4. Figure 4.15 shows a graphical representation of the scheme (also cf. Figure 4.11). The $\mathbf{H}_K^{(J,\mathrm{p})}$ blocks are constructed on each node individually and then the workload is distributed in a row-striped fashion to the individual ranks. The input vector is broadcasted by the root rank 0 which does all necessary calls to JADAMILU. Each rank thus calculates only a part of the product vector. Dot products (DDOT) of the matrix rows with the input vector are split up between the OMP threads of each MPI rank to further reduce the computational workload done by each CPU. The result vector is then gathered on rank 0 which enters the JADAMILU program again. This cycle repeats until convergence on all the desired eigenvalues/eigenvectors is achieved.

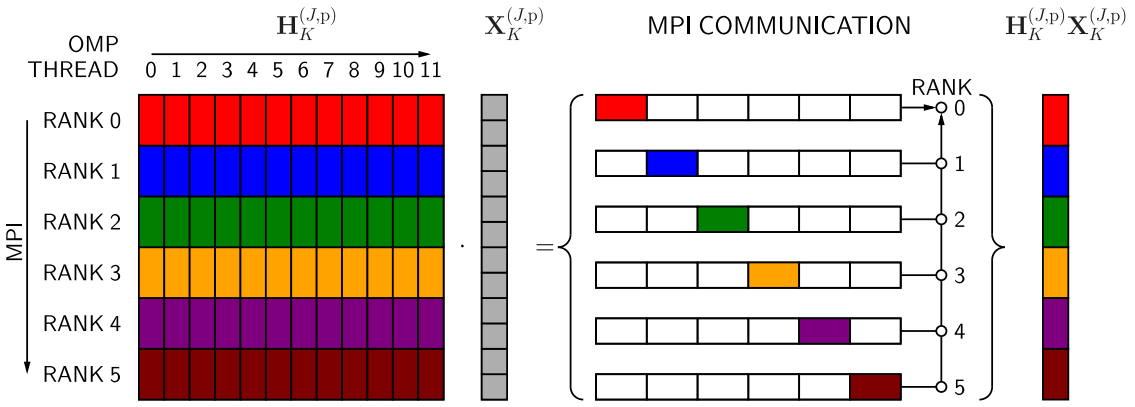

Figure 4.15: Schematic representation of the hybrid MPI/OMP parallelisation of the matrix-vector multplication (MXMPY) used within the Davidson diagonalisation.

The performance of the MXMPY parallelisation is shown in Figure 4.16. As a test case a $J = 0$ e-parity diagonalisation with $\ell_{\max} = 6$ and $N_v = 792$ was chosen, yielding a Hamiltonian of dimension $N_{\mathrm{VR}}^{(0,0)} = 5544$. In total 200 CPUs (10 nodes with 20 cores each) were employed in the test. The pure MPI based speed up (red data lower panel of Figure 4.16) shows a near linear speedup. Parallelisation of the DDOT based on OMP shows a speedup by a factor of about 4 for $N_{\mathrm{MPI}} = 1$ (red date upper panel of Figure 4.16). Increasing the number of threads per node leads to a super linear speed up of the MXMPY shown in the lower panel of Figure 4.16 which can be understood from the employed partitioning scheme. Increasing N_{MPI} reduces the number of rows of $\mathbf{H}_K^{(J,\mathrm{p})}$ each node has to multiply with the input vector and thus the size of the partial output vector. The latter reduces the overhead of the OMP parallelisation leading to the observed scaling. The OMP based parallelisation shows a drastic performance degradation when N_{OMP} is equal to the number of physical cores present on the nodes. This is likely due to background processes that take up CPU time during the excecution of C8v4.

4.3 Example calculations

The following sections present results of benchmark calculations in comparison to previously published variational calculations on tetraatomic linear molecules. In Section 4.3.1 the classic internal coordinate QFF for the acetylene electronic ground state (HCCH, $\mathrm{X}^1\Sigma_g^+$) by Strey and Mills [357] is employed and results are compared to those reported by Bramley and Handy [211] on the basis of an internal coordinate rovibrational Hamiltonian [358]. The second molecule is boranimine ($\mathrm{X}^1\Sigma^+$), where a PEF based on *ab initio* calculations is available [359]. Spectroscopic parameters calculated using C8v4 are checked by comparison to values published by Brites and Léonard [359] using the variational method developed by Bramley and Handy [212].

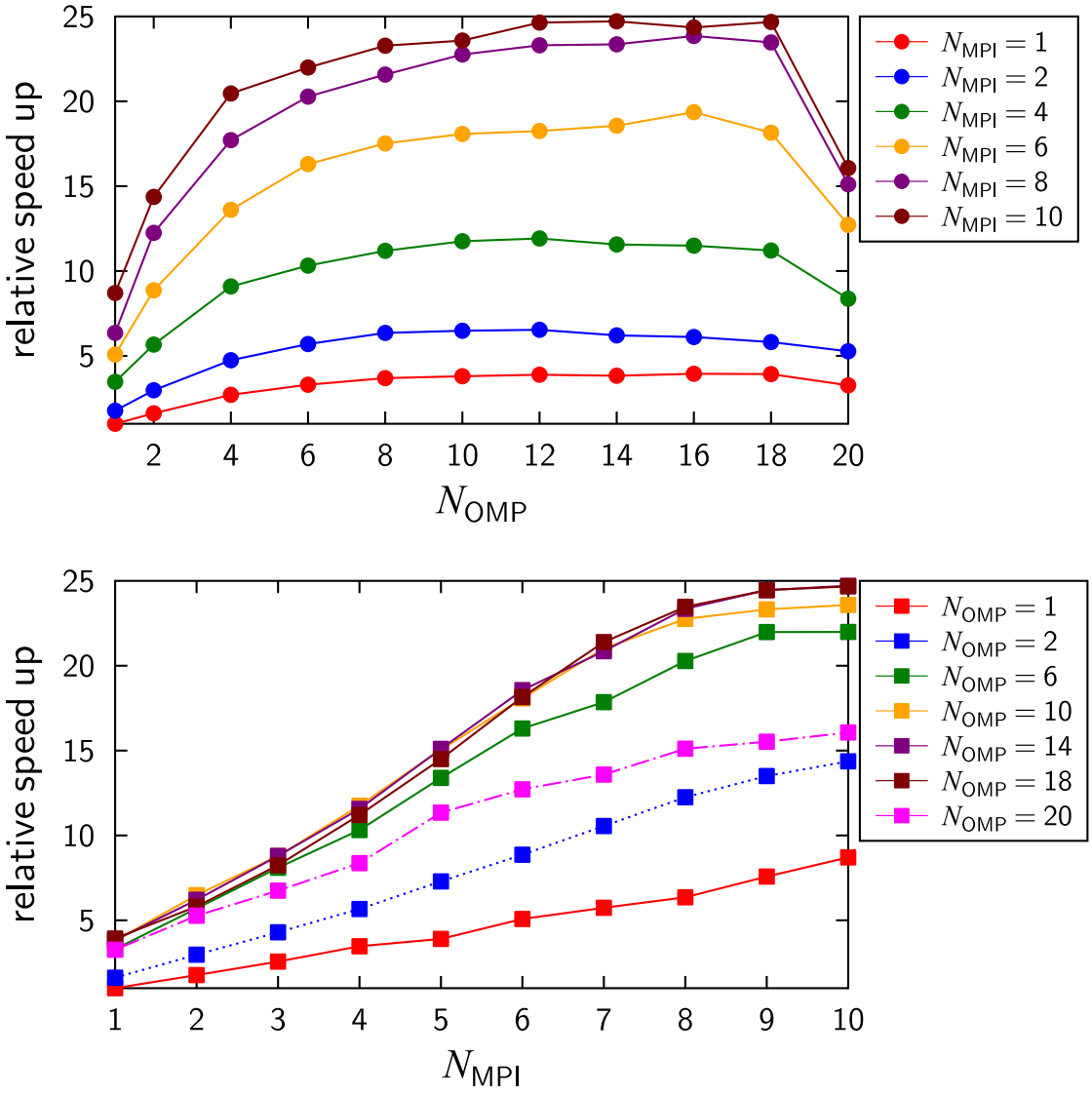

Figure 4.16: Relative speedups for the diagonalisation of a $J = 0$ e-parity Hamiltonian with $\ell_{\max} = 6$ and $N_v = 792$ ($N_{\mathrm{VR}}^{(0,0)} = 5544$) with respect to the number of MPI nodes N_{MPI} and OMP threads per node N_{OMP}.

4.3.1 Acetylene - HCCH

Acetylen is one of the simplest tetraatomic molecules. Because of its importance it has been subject to a tremendous amount of both experimental and theoretical spectroscopic investigations. A thorough review of the rovibrational spectrum of acetylene has been provided by Herman in the book by Quack and Merkt [360] and the reader is referred there for an overview.
Already in 1976 SM [357] developed a quartic force field for HCCH on the basis of available experimental spectroscopic data, using formulas of second order vibrational perturbation theory in normal coordinate space (VPT2). The QFF is expanded in the internal coordinates ΔR_1, ΔR_2 and ΔR_3 (stretching coordinates for the first CH, CC and the second CH bond, respectively). Angular coordinates are $\sin(\theta_t)$ which results from the symmetry requirements as discussed in Section 4.1.3 and the torsional angle enters as $\cos(n\tau)$. Bramley and Handy made two modifications to the SM QFF in their work

- The angular coordinates are transformed from $\sin(\theta_t)$ to θ_t. By use of the series expansion of the sin-functions one finds that this affects only quartic force constants of type f_{tttt} and $f_{tttt'}$. The relations between the $f_{tttt}/f_{tttt'}$ ($\sin(\theta_t)$ expansion) and the $F_{tttt}/F_{tttt'}$ (θ_t expansion) are found to be [194]

$$F_{tttt} = f_{tttt} - 4f_{tt} \tag{4.133}$$

  and

$$F_{tttt'} = f_{tttt'} - f_{tt'} \tag{4.134}$$

- The stretching coordinates are transformed to so called morse coordinates, first advocated by Dateo, Lee and Schwenke [361] for use in variational calculations

$$y_s = [1 - \exp(-\beta_s(\Delta R_s))] \ , \tag{4.135}$$

  where $\beta_s = -f_{sss}/(3f_{ss})$. Force constants with respect to the y_s (F_{ij}, F_{ijk} and F_{ijkl}) are then combinations of the simple internal coordinate force constants (f_{ij}, f_{ijk} and f_{ijkl}). The special choice of β_s causes the diagonal cubic force constants F_{sss} with respect to the y_s to vanish.

Both these changes yield the morse transformed QFF SM(M) [211] and have also been applied in the present work in order to facilitate comparison to the results by Bramley and Handy.
The $\{v_i^{\max}\}$ that define the primitive vibrational basis set were chosen after extensive convergence tests to be $\{14,\ 9,\ 11,\ 9,\ 9\}$ for the symmetric CH stretching vibration, CC stretching vibration, anti-symmetric CH stretching vibration, *trans*-bending vibration and *cis*-bending vibration, respectively. The direct product basis using this parameters would contain 180000 basis functions

and after pruning (cf. Section 4.2.3) a manageable size of 2785 is obtained. For the vibrational angular momentum threshold a value of $\ell^0_{\max} = 5$ has been chosen and is comparable to the 6 torsional basis functions (NBFT = 6) used by Bramley and Handy [211]. These parameters provide fundamental vibrational term energies converged to 0.01 cm^{-1}. Calculations were performed up to $J^{\max} = 2$ in both g- and u-symmetry. For the prediagonalisation (cf. Section 4.2.5) a fixed number of K-diagonal eigenvalues of $N_K^{\text{red}} = 200$ was employed.
From the rovibrational term energies $T_v(J)$ approximate rotational constants B_v were calculated from half the difference of $J = 0$ and 1 term energies for states of Σ symmetry, or from the $J = 1$ and 2 difference divided by 4 for Π states. The latter are evaluated for e- and f-parity

Table 4.6: Calculated spectroscopic parameters (in cm^{-1}) for HCCH obtained from C8v4 and by Bramley and Handy (Ref. [211]) using the morse transformed quartic force field SM(M) [357].

State	Symmetry	Method	G_v	B_v	q_v
$(0,0,0,0^0,0^0)$	Σ_g^+	C8v4	5766.436[a]	1.17662	
		Ref. [211]	5766.433[a]	1.1766	
$(0,0,0,1^1,0^0)e$	Π_g	C8v4	615.18	1.17526	0.00519
		Ref. [211]	615.18	1.1753	0.00519
$(0,0,0,1^1,0^0)f$		C8v4	615.18	1.18044	
		Ref. [211]	615.18	1.1804	
$(0,0,0,0^0,1^1)e$	Π_u	C8v4	732.61	1.17641	0.00471
		Ref. [211]	732.61	1.1764	0.00471
$(0,0,0,0^0,1^1)f$		C8v4	732.61	1.18112	
		Ref. [211]	732.61	1.1811	
$(0,0,0,2^0,0^0)$	Σ_g^+	C8v4	1237.67	1.17908	
		Ref. [211]	1237.67	1.1790	
$(0,0,0,1^1,1^{-1})$	Σ_u^+	C8v4	1331.51	1.18032	
		Ref. [211]	1331.50	1.1803	
$(0,0,0,1^1,1^{-1})$	Σ_u^-	C8v4	1347.79	1.17998	
		Ref. [211]	1347.79	1.1800	
$(0,0,0,0^0,2^0)$	Σ_g^+	C8v4	1453.41	1.18120	
		Ref. [211]	1453.41	1.1810	
$(0,1,0,0^0,0^0)$	Σ_g^+	C8v4	1972.92	1.17046	
		Ref. [211]	1972.92	1.1704	
$(0,1,0,1^1,1^{-1})$	Σ_u^+	C8v4	3271.34	1.17248	
		Ref. [211]	3271.33	1.1723	
$(0,0,1,0^0,0^0)$	Σ_u^+	C8v4	3303.09	1.17271	
		Ref. [211]	3303.08	1.1724	
$(1,0,0,0^0,0^0)$	Σ_g^+	C8v4	3373.27	1.16988	
		Ref. [211]	3373.30	1.1698	

[a] Zero-point energy.

individually and the difference in these effective rotational constants is used to approximate the ℓ-type doubling parameter q_v. Results are given in Table 4.6. Excellent agreement between the present calculations and the values reported by Bramley and Handy [211] is observed. Differences in the vibrational term energies G_v are almost negligible except for the $(1,0,0,0^0,0^0)$ state, where the term energy calculated from the C8v4 eigenvalues is smaller by 0.03 cm^{-1}. This can probably be atributed to a slightly better convergence. The present calculations use 15 basis functions for the symmetric stretching vibration compared to 10 functions which were included in the calculations by Bramley and Handy [211]. Rotational parameters B_v show the same level of agreement with all present values within the convergence range of 0.0003 cm^{-1} reported for the results of Bramley and Handy [211]. The largest differences are observed for the Σ_u^+ pair of states $(0,1,0,1^1,1^{-1})/(0,0,1,0^0,0^0)$ which are in strong resonance. Since the B_v of these states are mixed by this resonance, the small variations in the energetic position of these states lead to the observed differences compared to the previous results. Finally, the ℓ-type doubling parameters q_v for the fundamental bending vibrations exactly match those calculated by Bramley and Handy [211].

Table 4.7: Convergence of calculated vibrational term energies G_v (in cm^{-1}) for HCCH with respect to the vibrational angular momentum threshold $\ell^0_{\max}$.

			$\Delta G_v = G_v^{\mathrm{C8v4}} - G_v^{\mathrm{BH}}$				
state	G_v^{BH}	$\ell^0_{\max} =$	1	2	3	4	5
$(0,0,0,0^0,0^0)$	5766.43[a]		1.10	0.05	0.00	0.00	0.00
$(0,0,0,1^1,0^0)$	615.18		1.58	0.08	0.00	0.00	0.00
$(0,0,0,0^0,1^1)$	731.61		1.60	0.08	0.00	0.00	0.00
$(0,0,0,2^0,0^0)$	1237.67		7.29	0.53	0.04	0.01	0.00
$(0,0,0,1^1,1^{-1})e$	1331.50		68.96	3.38	0.22	0.02	0.01
$(0,0,0,1^1,1^{-1})f$	1347.79		83.22	4.53	0.31	0.03	0.01
$(0,0,0,0^0,2^0)$	1453.41		7.81	0.55	0.04	0.01	0.00
$(0,1,0,0^0,0^0)$	1972.92		1.22	0.06	0.01	0.00	0.00
$(0,1,0,1^1,1^{-1})e$	3271.33		15.88	1.47	0.11	0.02	0.01
$(0,0,1,0^0,0^0)$	3303.08		62.36	2.60	0.19	0.03	0.01
$(1,0,0,0^0,0^0)$	3373.30		1.10	0.03	−0.02	−0.02	−0.02

[a] Zero-point energy.

The rather modest size of the primitve vibrational basis set allows to efficiently study the behaviour of some of the thresholds that are used in a C8v4 calculation. Table 4.7 presents the results of these tests for the vibrational angular momentum threshold $\ell^0_{\max}$. Since this determines the size of the diagonal K-blocks it is primarily a vibrational effect through the potential energy term V. Its effect can be observed in the convergence of the C8v4 vibrational term energies towards the values reported by Bramley and Handy [211] which is calculated as $\Delta G_v = G_v^{\mathrm{C8v4}} - G_v^{\mathrm{BH}}$. Inspection of Table 4.7 shows that for the zero-point energy (ZPE) and the singly excited vibrational states convergence to within 0.1 cm^{-1} or better is achieved for $\ell^0_{\max} > 3$. The strong dependence in the ΔG_v for the first excited anti-symmetric stretching state $(0,0,1,0^0,0^0)$ is due to the resonance with the $(0,1,0,1^1,1^{-1})$ (Σ_u^+) state. As a general assumption a value of $\ell^0_{\max} > 2\max(\ell_t) + 3 - K$ appears appropriate, where $\max(\ell_t)$ is the largest value of ℓ_t in the states that one seeks to converge. This pattern of convergence will vary depending on the magnitude of the off-diagonal potential energy coupling blocks and thereby increasing or decreasing the value of $\ell^0_{\max}$ needed to converge a $\max(\ell_t)$ state. A possible indicator might be deduced from the size of the $r_{tt'}$ spectroscopic parameter, which determines the e/f-splitting for bend-bend combination states with $v_t = 1$ and $v_{t'} = 1$. According to VPT2 $r_{tt'}$ is directly proportional to the normal coordinate force constant $\phi^{(-)}_{ttt't'}$ (cf. Section 2.3.2) which occurs in the potential energy via a term $\phi^{(-)}_{ttt't'} q_t^2 q_{t'}^2 \cos(2(\chi_{t'} - \chi_t))$. This shows that $r_{tt'}$ can be used as a measure for the $\Delta\ell = 2$ off-diagonal potential energy coupling and a large value may indicate slow convergence with respect to $\ell^0_{\max}$. Using the results of Table 4.6 r_{45} is calculated to be $-8.4\ cm^{-1}$ from both variational approaches. A VPT2 treatment employing the SM force field yields a slightly lower value of -7.4 cm^{-1} and the corresponding experimental value is -6.24 cm^{-1} [360].

Figure 4.17 shows the convergence of the rotational parameters $\Delta B_v = B_v^{\mathrm{C8v4}} - B_v^{\mathrm{BH}}$ with respect to the prediagonalisation parameters N_K^{red} (right panel) and $E_{\mathrm{cut}}^{\mathrm{red}}$ (left panel) for the rovibrational ground state and the singly excited states. The prediagonalisation scheme affects only contributions due to the Coriolis operator and therefore the rotational parameters B_v. Both selection methods converge to the same value above $E_{\mathrm{cut}}^{\mathrm{red}} = 13750$ cm^{-1} or $N_K^{\mathrm{red}} = 125$. An analysis of the calculation timings reveals that for such low values $J^{\max} \leq 2$ both approaches take approximately the same amount of wall time e.g. the $J = 2$ diagonalisation took $t_{\mathrm{wall}} = 6766$ and 7690 s for $N_K^{\mathrm{red}} = 125$ and $E_{\mathrm{cut}}^{\mathrm{red}} = 13750$ cm^{-1}, respectively. The energy based selection is favoured for calculations that target low lying vibrational states (e.g. fundamentals) but high rotational excitations. In this case, the number of retained states N_K^{red} will decrease/vanish for the higher K-blocks, since the lowest lying K-diagonal eigenvalue increases in energy until it finally is above the threshold. Beyond this value the size of the reduced Hamiltonian N^{red} remains constant. This is not the case for the fixed number selection, where N^{red} increases linearly with J. However, the latter approach has the advantage that the number of eigenvalues that need to be determined is exactly know before entering the Davidson diagonalisation. For the energy based approach this value has to be estimated, for example, by inspection of the diagonal matrix elements that are below $E_{\mathrm{cut}}^{\mathrm{red}}$.

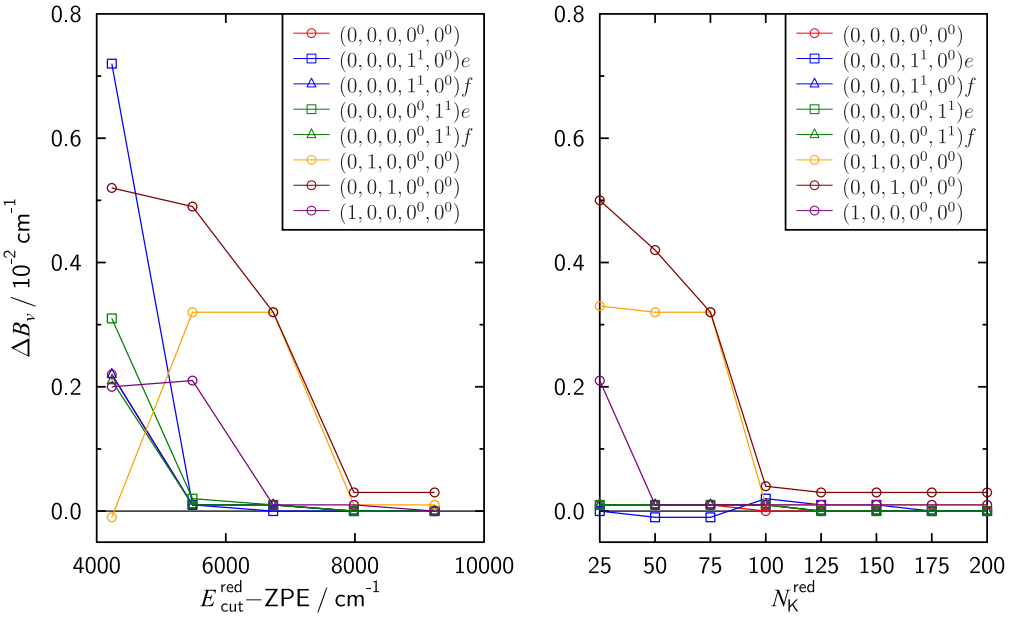

Figure 4.17: Convergence of the rotational parameters towards the BH [211] results with respect to the applied prediagonalisation scheme. Left panel: Energy threshold for selecting K-diagonal eigenvalues, right panel: fixed number of N_K^{red} eigenvalues per K-diagonal block.

4.3.2 Boranimine - HBNH

The boranimine molecule HBNH in its Σ^+ electronic ground state is the second example molecule used to test the C8v4 program. There is little experimental spectroscopic results on this tetraatomic system. Kawashima, Kawaguchi and Hirota [362] recorded the first gas phase infrared spectrum of the ν_3 fundamental band. The band origin and the ground state as well as excited state rotational constants of the H^{11}BNH isotopologue were determined to be $\nu_3 = 1786.19308(72)$, $B_0 = 1.099335(81)$, and $B_3 = 1.093481(72)$ cm^{-1}, respectively. In 2012 Brites and Léonard [359] engaged in the first full dimensional variational calculation of HBNH based on explicitly correlated coupled cluster calculations at the CCSD(T)-F12a level of theory in conjunction with an aug-cc-pVTZ basis set. The resulting PEF was expanded in so called Simons-Parr-Finlan (SPF) coordinates [363] $S_s = (R_s - R_s^{\mathrm{e}})/R_s$ for the bond stretches, deviations from linearity θ_t for the bending of the H-B-N and B-N-H angles and τ the torsional (dihedral) angle between the planes formed by the H-B-N and B-N-H subunits. Variational calculations were perfomed with the method developed by Bramley and Handy [211, 212] for $J = 0$ and $J = 1$.

The present calculations make use of a primitive vibrational basis set described by quantum numbers $\{v_i^{\max}\} = \{17,\ 10,\ 9,\ 10,\ 14\}$ for the N-H, H-B and B-N stretching vibrations and the B-N-H and H-B-N bending vibrations, respectively. Pruning reduces the direct product basis set from 326700 to 4728. This is roughly 2 times larger than the basis set used for HCCH and is in line with

Table 4.8: Comparison of rovibrational term energies (in cm^{-1}) for $H^{11}BNH$ obtained from C8v4 and by Brites and Léonard [359].

$J = 0$ (e) (Σ^+)			$J = 0$ (f) (Σ^-)		
state	C8v4	Ref. [359]	state	C8v4	Ref. [359]
$(0,0,0,0^0,0^0)$	5427.1[a]	5427.0[a]	$(0,0,0,1^1,1^1)$	1185.5	1185.4
$(0,0,0,0^0,2^0)$	921.8	921.0	$(0,0,1,1^1,1^1)$	2953.8	2953.4
$(0,0,0,1^1,1^1)$	1185.2	1185.0	$J = 1$ (e) (Σ^-)		
$(0,0,0,2^0,0^0)$	1428.4	1428.4	state	C8v4	Ref. [359]
$(0,0,1,0^0,0^0)$	1780.3	1780.2	$(0,0,0,0^0,1^1)$	465.9	465.9
$(0,0,0,2^0,2^0)$	2349.6	2347.3	$(0,0,0,1^1,0^0)$	723.1	723.2
$(0,1,0,0^0,0^0)$	2773.6	2773.5	$(0,0,1,0^0,1^1)$	2232.9	2232.7
$(0,0,1,1^1,1^1)$	2953.1	2952.5	$(0,0,1,1^1,0^0)$	2504.6	2504.6
$(0,0,2,0^0,0^0)$	3545.7	3545.2	$(0,1,0,0^0,1^1)$	3236.9	3236.7
$(1,0,0,0^0,0^0)$	3711.2	3711.0	$(0,1,0,1^1,0^0)$	3480.4	3480.4

[a] Zero-point energy.

the lower symmetry which requires more vibrational basis functions to describe the rovibrational wave functions. Using the experience obtained from the acetylene calculations, the vibrational angular momentum threshold was set to $\ell^0_{\max} = 4$. This choice is based on the observation that the vibrational ℓ-type doubling parameter r_{45} is calculated to be 0.4 cm^{-1} from the variational calculations by Brites and Léonard [359] and 0.1 cm^{-1} via VPT2. This is an order of magnitude smaller than the value of r_{45} for HCCH. Therefore, a less pronounced coupling between the (ℓ_4, ℓ_5) is expected for HBNH and $\ell^0_{\max}$ can be reduced compared to HCCH when calculating low lying rovibrational state. Calculations were performed up to $J^{\max} = 1$ and the fixed K-diagonal eigenvalue scheme ($N_K^{\text{red}} = 200$) was employed in the prediagonalisation.

Table 4.8 compares rovibrational term energies obtained with C8v4 and by Brites and L [359]. The observed differences are small. For the fundamental vibrations the largest deviation of 0.2 cm^{-1} is calculated for the $(1,0,0,0^0,0^0)$ state. The $(0,0,0,1^1,0^0)$ state is predicted by the C8v4 calculations to be slightly below the result by Brites and Léonard [359]. From the $J = 1$ and $J = 0$ term energies rotational constants B_v can be calculated analogous to the acetylene treatment. Brites and Léonard only quoted the ground state $J = 1 \leftarrow 0$ transition frequency of 65.555 GHz [359] which corresponds to an approximate rotational constant of $B_0 = 1.09334$ cm^{-1}. The C8v4 calculations exactly reproduce this value. For the $(0,0,1,0^0,0^0)$ state a rotational constant B_3 of 1.08762 cm^{-1} is calculated with C8v4, to be compared to the experimental value of 1.093481(72) cm^{-1}. The differences $B_3 - B_0$ obtained from the C8v4 and in experiment are -0.00572 and -0.00585 cm^{-1}, respectively, which are in good agreement. Therefore, the rather large differences observed for B_0 and B_3 can be attributed to the error in B_e and thus in the equilibrium geometry.

Chapter 5

Propynylidynium (l-C_3H^+) – the B11244 story retold

This chapter presents the results of a study on the rovibrational spectrum of l-C_3H^+. Using the composite approach presented in Chapter 3 the development of a six-dimensional PEF for this interesting molecular ion is detailed in Section 5.2. The results of variational rovibrational calculations using the C8v4 programm developed in Chapter 4 are presented in Section 5.3 which either focus on the vibrational ground state (Section 5.3.1) or excited vibrational states (Section 5.3.2).

5.1 Introduction

The linear propynylidynium l-C_3H^+ ($\tilde{X}^1\Sigma^+$) is part of the select group of interstellar cations. Its discovery was accompanied by a controversy in the astrophysical community [364–369]. In a line survey of the photo-dissociation region (PDR) of the Horsehead neubla Pety and coworkers [364] detected 9 harmonically related lines using the IRAM 30 m telescope. The spectral features were fit to the rotational term energy formula of a closed shell linear molecule according to Equation (2.50). Including terms up to the sextic centrifugal distortion parameter they obtained 11244.9512(15) MHz, 7.766(40) kHz and 0.56(19) Hz for B_0, D_0 and H_0. On the basis of somewhat older theoretical calculations [370–373] the carrier of the B11244 termed series of lines was tentatively assigned to l-C_3H^+.

The assignment was subsequently questioned by Huang *et al.* [365] who carried out *ab initio* calculations on l-C_3H^+. A composite QFF that combines CBS-extrapolated fc-CCSD(T) results with corrections for scalar relativistic effects and core-valence correlation was developed and spectroscopic parameters for various isotopologues of l-C_3H^+ were obtained from VPT2 calculations. Although the resulting ground state rotational constant of $B_0 = 11262.68$ MHz was only 0.16 % larger than the astronomical value, the quartic centrifugual distortion parameter $D_e = 4.248$ kHz was too small by as much as 45.3 %. Huang *et al.* [365] compared the deviation of D_e with respect to D_0 in presumed related molecules HCN (3.5 %, [374,375]), HCC^- (2.1 %, [376,377]) and HCCH (2.27 %, [56, 378]) from which they concluded that l-C_3H^+ might not be the carrier of B11244. Shortly afterwards Fortenberry *et al.* [379] suggested C_3H^- in its first excited $1^1A'$ electronic state as a possible candidate based on spectroscopic parameters calculated with an *ab initio* QFF obtained at the same level of theory as employed for l-C_3H^+.

This triggered further astronomical studies on the origin of B11244 by McGuire *et al.* [366] who detected B11244 toward Sgr B2(N), Sgr B2(OH) and TMC-1 as part of the PRebiotic Interstellar MOlecular Survey (PRIMOS) [380]. The $J = 6 \rightarrow 5$ and $7 \rightarrow 6$ transitions were observed at exactly the same frequency as obtained by Pety and coworkers [364]. Additionally, the $J = 1 \rightarrow 0$ and $J = 2 \rightarrow 1$ were detected leading to improved rotational parameters of $B_0 = 11244.9571(41)$ MHz, $D_0 = 7.745(80)$ kHz and $H_0 = 0.49(37)$ Hz from a combined fit of all observed emission lines. In a second study McGuire and coworkers [367] specifically searched for C_3H^- toward sources where B11244 has previously been observed. However, no evidence of the necessary $K_a = 1$ transitions of an asymmetric top where found which makes C_3H^- unlikely to be the source of B11244. The assignment of B11244 to l-C_3H^+ was ultimately confirmed by laboratory studies carried out by Brünken *et al.* [368]. Using a novel mass-selective action spectroscopy based on light induced reactions in the millimeter-wave band the rotational spectrum of l-C_3H^+ was obtained. Transition frequencies for $J = 1 \rightarrow 2$ to $J = 4 \rightarrow 5$ were recorded that agree with the astronomical data [364, 366] to within their respective error bars.

Theory and astronomical observation were reconciled by the group of Botschwina [369]. Combining explicitly correlated coupled-cluster calculations with corrections for core-valence correlation,

scalar relativity, higher-order correlation up to CCSDTQ and the DBOC in a composite scheme they developed a force field for l-C_3H^+ which includes coupling between the internal coordinates up to cubic terms. The corresponding VPT2 ground state rotational constant $B_0 = 11246.4$ MHz is in excellent agreement with the astronomical observation but the $D_e = 4.229$ kHz is again lower by 45.5 %. The explanation for this large deviation can be realized when considering the VPT2 formula for D_e (Equation (2.68)) which does not include contributions from bending vibrations. Much like the floppy C_3 molecule, l-C_3H^+ has a low-lying bending vibration ($\omega_5 = 129.6$ cm^{-1} [369]) associated with a shallow CCC bending potential. By correlating the ratio $f_D = D_0(\text{exp.})/D_e(\text{theor.})$ with the flatness of the CCC bending potential of C_3N^- ($f_D = 1.08$), C_3O ($f_D = 1.44$), l-C_3H^+ ($f_D = 1.80$) and C_3 ($f_D = 7.26$) Botschwina *et al.* [369] showed that the large f_D is a consequence of the floppiness of l-C_3H^+. The calculations were later extended [381] to a QFF that supports anharmonic VPT2 vibrational frequencies which were calculated to be (in cm^{-1}): $\nu_1 = 3168.9$, $\nu_2 = 2090.3$, $\nu_3 = 1186.7$, $\nu_4 = 783.0$ and $\nu_5 = 125.7$.

Besides the work of the Botschwina group [369, 381] there has been another theoretical treatment of the rovibrational problem in l-C_3H^+. Mladenović [30] reported results of DVR(+R)+FBR [222–224] calculations based on the Morse-transformed QFF constructed by Huang, Fortenberry and Lee [365] and a Hamiltonian set up in internal coordinates. The latter are of *diatom+diatom* type: three radial coordinates d_{HC} (H-C^a), d_{CC} (C^b-C^c) and R_{HC-CC} the latter between the centers of mass of the two diatom subunits, the angles θ_{HC} and θ_{CC} between the vectors $\mathbf{d}_i$ and $\mathbf{R}_{HC-CC}$ and the torsional coordinate χ_{HC-CC}. Calculations were performed with two different rovibrational basis sets. The first one termed Basis1 is characterized by the basis set $(n_{d_1}, n_{d_2}) = (3, 5)$ for 2D stretching basis functions and the truncation recoupling parameters $N_k^{\max} = 200$ and $N_z^{\max} = 750$ and the second larger set Basis2 employs $(n_{d_1}, n_{d_2}) = (4, 6)$, $N_k^{\max} = 300$ and $N_z^{\max} = 900$. Rovibrational parameter were then obtained from calculations up to $J_{\max} = 20$. The vibrational frequencies $\nu_1 = 3167.8$, $\nu_2 = 2096.1$, $\nu_3 = 1192.5$, $\nu_4 = 784.4$ and $\nu_5 = 117.6$ cm^{-1} agree well with the VPT2 results of Huang, Fortenberry and Lee [365]. However, the calculated rotational parameters $B_0 = 11271.84$ MHz, $D_0 = 8.992$ kHz and $H_0 = 9.894$ reveal a surprisingly large difference in H_0 with respect to the astronomical value of $H_0 = 0.49$ Hz.

Mladenović [30] also provided a comparison between theoretical and experimental line frequencies of rotational transitions up to $J = 11 \rightarrow 12$. A closer look at the $J = 0 \rightarrow 1$ theoretical transition frequencies 22544 MHz and 22548 MHz calculated with Basis1 and Basis2, respectively, reveals the rather strange behaviour that the transition frequency *increases* when employing the *larger* Basis2. The vibrational ground state $(0, 0, 0, 0^0, 0^0)$ corresponds to the lowest possible eigenvalue of the rovibrational Hamiltonian for every value of J. From the variational principle [201, 202] follows that an increase of the basis set will always lead to a lowering of the term energy. Since the size of Basis2 is larger than Basis1 in the DVR calculations, there is only one possible scenario that can lead to this increase in the transition frequency while fulfilling the variational principle. This would require both term energies to be lowered by the increased basis set but the shift in the $J = 0$ level to be larger than that in $J = 1$ leading to a net increase in the energy difference of the

two levels which appears unexpected. However, the preceding discussion clearly shows the need to revisit the theoretical spectroscopy of l-C_3H^+.
A new full dimensional PEF for l-C_3H^+ will be presented in Section 5.2 that is based upon the previous work of Stein *et al.* [381] but extends the employed coordinate ranges. Results of variational rovibrational calculations using the newly developed C8V4 program will be presented in Section 5.3. Section 5.3.1 focuses on the accurate calculation of rotational parameters in the rovibrational ground state of l-C_3H^+ bases on the QFF developed by Huang, Fortenberry and Lee [365] and the new composite PEF. In Section 5.3.2 results for excited vibrational states in l-C_3H^+ on the basis of the composite PEF are presented which should provide reliable predictions of spectroscopic parameters in such states.

5.2 An accurate composite PEF for l-C_3H^+

The work of Botschwina *et al.* [369] and Stein *et al.* [381] has shown that the main source of error in the l-C_3H^+ QFF constructed by Huang, Fortenberry and Lee [365] is the neglect of HC contributions to the PEF. The study of Stein *et al.* [381] yielded a QFF for l-C_3H^+ which is sufficient for VPT2 calculations but not well suited for variational calculations. In order to support the latter type of calculations an accurate description of the PEF over a large coordinate space is required. Therefore, in the following a new PEF for l-C_3H^+ will be developed which extends upon the earlier calculations of Stein and coworkers [381]. The detailed components of the PEF are:

- Explicitly correlated fc-CCSD(T)-F12b/VQZ-F12 (abbreviated F12b) is employed as basic contribtution. The CABS and DF sets use the MOLPRO defaults of VQZ-F12/OPTRI, VQZ/JKFIT and AVQZ/MP2FIT and a geminal β of 1.0 $Å^{-1}$ [124].
- The CV contribtuion is calculated with the CV6Z basis set (543 cGTOs) using conventional CCSD(T).
- DKH2 CCSD(T) calculations with VQZ-DK and VQZ basis sets provide the SR contribution to the PEF.
- The following HC contributions are included in the l-C_3H^+ PEF:
  - The (Q)-(T) contribution is calculated as the CCSDT(Q) – CCSD(T) energy difference using a VTZ basis set
  - The Q-(Q) contribution employs the smaller VDZ basis set and is obtained from the difference CCSDTQ – CCSDT(Q).
- The adiabatic DBOC for the main isotopologue of l-C_3H^+ is calculated at the ae-CCSD/CVQZ level of theory using the CFOUR [176] program.

Compared to the work of Stein *et al.* [381] the present PEF uses a different basic contribution that does not apply triples scaling in the explicitly correlated coupled-cluster calculations. Arguments

for this change can be drawn from close inspection of the basis set studies carried out by Botschwina and coworkers on the equilibrium bond lengths and the harmonic vibrational frequencies in l-C_3H^+ (Table 2 and 3 in Ref. [369]). The fc-CCSD(T*)-F12b/VQZ-F12 harmonic frequencies appear to show better agreement than the triples unscaled variant when compared with the results of standard fc-CCSD(T) obtained with a large V8Z basis set. However, the latter set does not include k- and l-type functions and the basis is therefore not exactly an octuple-zeta basis. Furthermore, the harmonic frequencies calculated with standard fc-CCSD(T) also do not show a smooth convergence. The effect of increasing the basis from V6Z to V7Z (no k-functions) is in all cases compensated when further increasing to the V8Z basis set. Considering this, fc-CCSD(T)-F12b/VQZ-F12 seems to provide somewhat better near-CBS results especially for ω_2 where triples scaling results in the largest difference of more than 1 cm^{-1}.
A polynomial representation of the contributions (α) is used, according to

$$V^{(\alpha)} - V^{(\alpha)}_{\mathrm{ref}} = \sum_{ijklmn} C^{(\alpha)}_{ijklmn} \Delta r^i \Delta R_1^j \Delta R_2^k \theta_4^l \theta_5^m \cos(n\tau) \quad \text{(l,m: even)}. \tag{5.1}$$

In Equation (5.1) the internal coordinates are defined, following Section 4.1.3, as the H-C^a, C^a-C^b and C^b-C^c bond stretching coordinates Δr, ΔR_1 and ΔR_2, respectively, and the angular coordinates θ_4 (HC^aC^b deviation from linearity), θ_5 (CCC deviation from linearity) and the dihedral angle τ between the planes spanned by the HC^aC^b and CCC subunits (per definition $\tau = 0°$ for *cis*-like displacements). The following coordinate ranges are employed:

$$\begin{gathered}
-0.225 \text{ Å} \leq \Delta r \leq 0.375 \text{ Å} \\
-0.150 \text{ Å} \leq \Delta R_1 \leq 0.225 \text{ Å} \\
-0.200 \text{ Å} \leq \Delta R_2 \leq 0.300 \text{ Å} \\
0° \leq \theta_4 \leq 70° \\
0° \leq \theta_5 \leq 90° \\
0° \leq \tau \leq 180° \,.
\end{gathered}$$

These ranges span energies of $\sim$ 10000 cm^{-1} above the minimum in the diagonal cuts along Δr, ΔR_1, ΔR_2 and θ_4. For the diagonal cut along the shallow θ_5 potential about 2700 cm^{-1} above the minimum are covered. The linear reference geometry is the same as used before [381]: $r^{\mathrm{ref}} = 1.079$ Å, $R_1^{\mathrm{ref}} = 1.236$ Å and $R_2^{\mathrm{ref}} = 1.340$ Å.
Table 5.1 presents the dependence of l-C_3H^+ equilibrium bond lengths and harmonic vibrational frequencies on the smaller contributions. For the equilibrium bond lengths and stretching vibrations this has been discussed by Stein *et al.* [381] and the numerical values given here are in virtual agreement with the latter results. For the bending vibrations ω_4 and ω_5 the observed frequency shifts due to the smaller effects match the trends observed for HCN and C_3. The final equilibrium distances $r^{\mathrm{e}} = 1.07896$, $R_1^{\mathrm{e}} = 1.23540$ and $R_2^{\mathrm{e}} = 1.34080$ Å agree to within 0.00002, 0.00022 and

Table 5.1: Influence of smaller contributions to the composite PEF on the equilibrium bond lengths (in Å) and harmonic vibrational frequencies (in cm^{-1}) for l-C_3H^+.

Contribution	r^e	R_1^e	R_2^e	ω_1	ω_2	ω_3	ω_4	ω_5
F12b	1.08042	1.23806	1.34318	3303.0	2134.2	1184.0	802.8	123.7
CV	−0.00131	−0.00301	−0.00357	+5.7	+9.3	+6.2	+4.2	+3.1
SR	−0.00014	−0.00024	−0.00015	+0.2	±0.0	−0.2	+0.2	−0.2
(Q)-(T)	−0.00019	+0.00096	+0.00181	+0.1	−11.4	−10.1	−4.4	+1.9
Q-(Q)	−0.00002	−0.00040	−0.00051	+0.9	+5.3	+4.0	+1.2	+1.1
DBOC[a]	+0.00021	+0.00003	+0.00004	−1.0	±0.0	±0.0	+0.2	−0.1
Total	1.07896	1.23540	1.34080	3308.9	2137.4	1183.9	804.2	129.5
Stein *et al.* [381]	1.07898	1.23562	1.34086	3308.4	2135.8	1183.0	803.2	129.6
Huang *et al.* [365]	1.07896	1.23536	1.33984	3309.7	2142.7	1189.3	805.8	124.0

[a] Diagonal Born-Oppenheimer correction for the $^{12}C_3H^+$ isotopologue.

0.00006 Å with the results of Stein *et al.* [381]. Of course, the main difference in R_1^e originates from the scaled perturbative triples fc-CCSD(T)-F12b contribution. These differences in the bond length translate into differences in the composite harmonic vibrational frequencies of 0.5 cm^{-1}, 1.6 cm^{-1} and 0.9 cm^{-1} for ω_1, ω_2 and ω_3, respectively. These latter values again reflect the effect of triples scaling (cf. also Tab. 3 in Ref. [369]). While the present CCC-bending harmonic frequency is almost unchanged compared to the work of Stein and coworkers [381], a somewhat larger difference of 1.0 cm^{-1} is observed for the HCC bend due to triples scaling. This is even larger then the effect of triples scaling observed for HCN. The differences obtained when comparing the present composite results with those of Huang *et al.* [365] are all significantly larger than those presented in the preceding discussion which is due to the neglect of higher-order correlation contributions in the latter work.

Figure 5.1 depicts the angular dependence of the smaller contributions for l-C_3H^+. The top left panel presents the θ_4 (HCC bend) dependence. The largest contributions are provided by the HC effects. (Q)-(T) shows a strong dependence on θ_4 reaching a relative energy of about −250 cm^{-1} at 70°. This is a surprisingly large effect. For comparison, in HCN (Q)-(T) reaches a relative contribution of only −60 cm^{-1} in the same coordinate range (cf. Figure 3.2). The increased importance of HC effects might be explained with a recent study on the collision of H^+ and C_3 by Chhabra and Dhilip Kumar [382]. On the basis of ic-MRCI/AVQZ calculations ground and excited state potential energy surfaces of H^+ and *rigid* C_3 (fixed at an approximate CC equilibrium distance of 1.279 Å [326]) were calculated with respect to Jacobi-type coordinates for the distance of H^+ to the CoM of C_3 R_{H-CCC} and the angular displacement of H^+ around C_3 γ_{H-CCC}. Inspection of Figure 4 in Ref. [382] shows that there are low-lying excited electronic states whose energy separation relative to the ground state decrease with increasing γ_{H-CCC}. While the angle γ_{H-CCC} is not equal to θ_4 this behaviour could still explain the observed trends in the HC contributions for HCC bent l-C_3H^+. The top right graph of Figure 5.1 shows the dependence on the CCC bending angle θ_5. An almost exact coincidence with the θ dependence in C_3 (Figure 3.11) is observed which

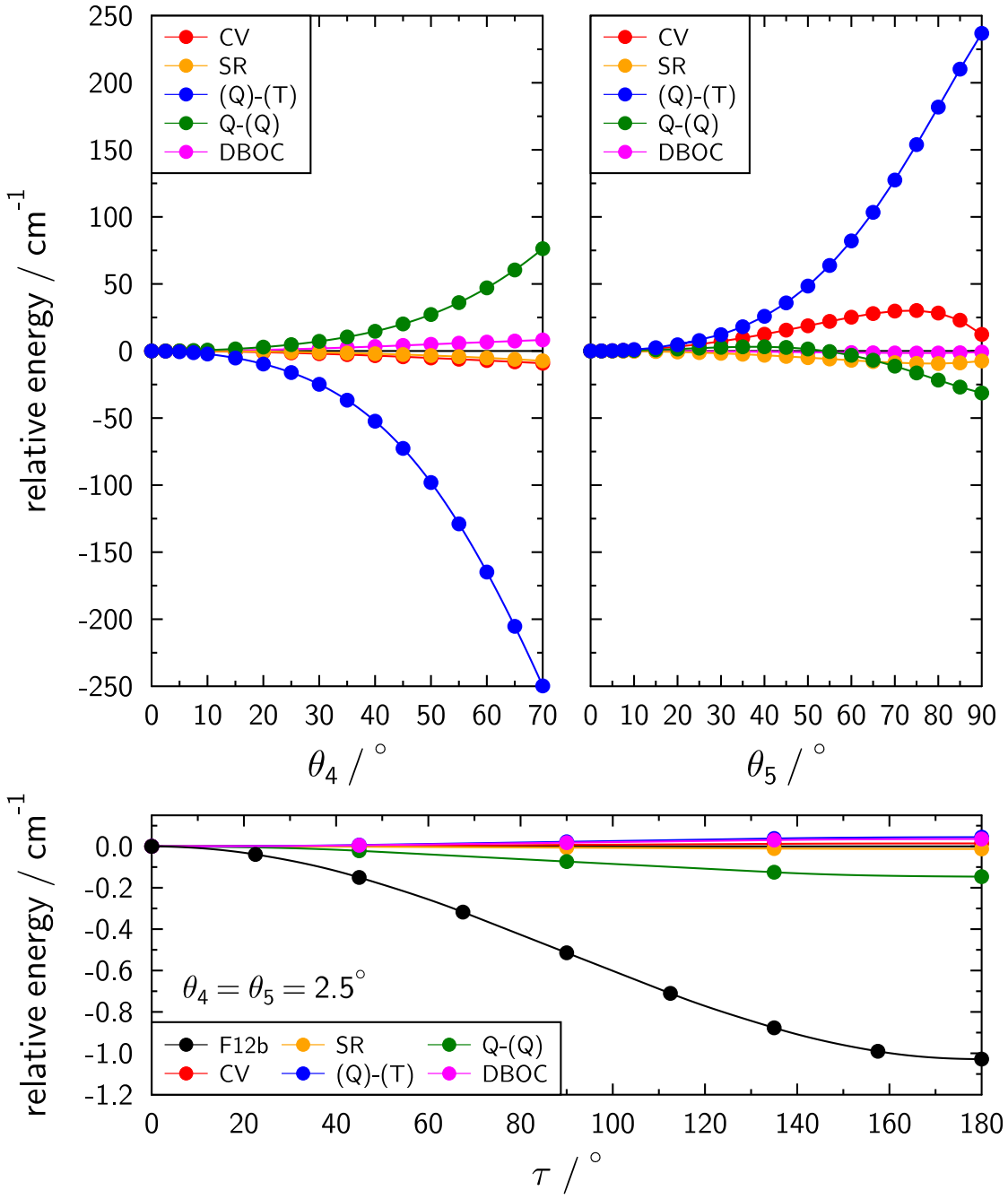

Figure 5.1: Dependence of contributions to the composite l-C_3H^+ PEF on the angular coordinates θ_4 (HCC), θ_5 (CCC) and τ (torsion).

further suggest a close relationship between l-C_3H^+ and C_3. Finally, the lower panel of Figure 5.1 depicts the dependence on the torsional angle τ for $\theta_4 = \theta_5 = 2.5°$. The overall dependency is weak with an F12b separation of only -1 cm^{-1} of the *trans*-like displacement with respect to the *cis* form. The effects of the smaller contributions are even weaker and compensate each other to a large degree, except for the Q-(Q) contribution which increases the *cis/trans* separation by about 10 %.

Coefficients $C^{(\alpha)}_{ijklmn}$ in Equation (5.1) are determined by least-squares fitting of the individual components. The F12b contribution is obtained from 3569 symmetry unique nuclear configurations. Adding the smaller contributions to this, in total about 7200 individual *ab initio* energies contribute to the composite PEF. The highest order diagonal polynomials employed in the fits are 10, 8, 8, 16 and 18 for Δr, ΔR_1, ΔR_2, θ_4 and θ_5, respectively. Coupling terms are considered up to sextic order in stretch-stretch, bend-bend and stretch-bend coupling. The rules outlined in Section 4.1.3 are to be applied to the bending indices $\{l, m, n\}$ from which follows that the highest n allowed is 3 corresponding to a term with coefficient $C^{(\alpha)}_{000333}$. The PEF defined in this way has 278 coefficients and yields a root-mean-square deviation of 0.002 cm^{-1} for fc-CCSD(T)-F12b/VQZ-F12. CV, SR, HC and DBOC contributions require less terms for an accurate fit to comparable accuracy. Individual coefficients contributing to the final composite PEF are given in Table C.1 and C.2 of Section C and the PEF obtained after summation and transformation to the minimum in Table C.3.

A direct comparison of harmonic spectroscopic properties in C_3 and l-C_3H^+ is provided in Fig-

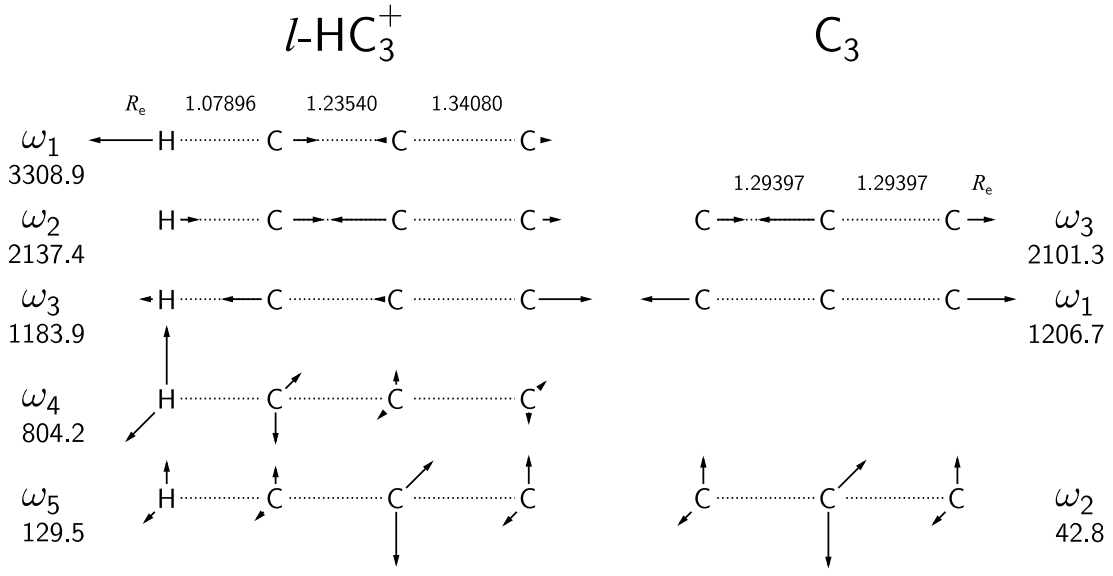

Figure 5.2: Comparison of equilibrium bond lengths R_e (in Å), harmonic vibrational frequencies ω_i and normal coordinates $l_{I\alpha i}$ for l-C_3H^+ and C_3.

ure 5.2. Addition of a proton contracts the C^a-C^b by 0.05857 Å and widens the C^b-C^c bond by 0.04683 Å compared to centro-symmetric C_3. The resulting CC bond lengths 1.23540 and 1.34080 Å are closer to what one would expect for a CC triple and a CC single bond for example in C_4H^- (1.2221 Å and 1.3680 Å [16]). From the normal coordinates the 2 CCC vibrations in l-C_3H^+ can be clearly identified as a pseudo-antisymmetric and a pseudo-symmetric stretching vibration for ω_2 and ω_3. The latter are shifted from the C_3 stretching vibrations ω_3 and ω_1 by $+31.3$ cm^{-1} and and -22.8 cm^{-1}, respectively. Because of the large mass differences between the proton and the C_3 unit as well as a small quadratic coupling force constant $f_{\theta_4\theta_5}$ the two bending vibrations are rather localized as a CH bending (ω_4) and CCC bending (ω_5). In fact, displacement of q_5 has almost no effect on the HCC angle θ_4. The largest relative effect due to the proton is calculated for the ω_5 bending vibration which has a harmonic vibrational frequency of 129.5 cm^{-1} about 3 times the value in C_3.

Going beyond the harmonic picture, Table 5.2 compares related anharmonic force constants with respect to dimensionless normal coordinates in l-C_3H^+ and C_3. The main differences occur for force constants that couple stretching and bending normal modes as well as the quartic CCC bending force constant. The exceptionally strong coupling between the symmetric stretching and

Table 5.2: Comparison of related anharmonic force constants (in cm^{-1}) in the quartic dimensionless normal coordinate force fields for l-C_3H^+ and C_3.

l-C_3H^+			C_3	
$k^{a,c}$	Value	Ratio	Value	$k^{b,c}$
k_{222}	41.252	–	0.000	k_{333}
k_{223}	−177.605	1.19	−211.964	k_{133}
k_{233}	−15.674	–	0.000	k_{113}
k_{333}	−43.888	0.96	−41.975	k_{111}
k_{255}	−133.333	–	0.000	k_{223}
k_{355}	383.084	3.43	1315.426	k_{122}
k_{2222}	4.709	1.09	5.131	k_{3333}
k_{2233}	14.266	1.25	17.789	k_{1133}
k_{3333}	2.080	0.83	1.717	k_{1111}
k_{2255}	−82.761	3.55	−293.533	k_{2233}
k_{3355}	−51.009	3.48	−177.462	k_{1122}
k_{5555}	71.624	10.12	724.835	k_{2222}

[a] Indices for l-C_3H^+ correspond to: $i = 2$ pseudo-antisymmetric stretch, $i = 3$ pseudo-symmetric stretch and $i = 5$ CCC bending.

[b] Indices for C_3 correspond to the usual ordering for centro-symmetric linear molecules: $i = 1$ symmetric stretch, $i = 2$ bending and $i = 3$ antisymmetric stretch.

[c] The cubic k_{ijk} and quartic k_{ijkl} force field parameters are defined according to Nielsen [184].

bending vibration in C_3 (k_{122} and k_{1122}) is reduced by more than a factor of 3 in l-C_3H^+ (k_{355} and k_{3355}). A similar ratio is observed for k_{2255} which couples the pseudo-antisymmetric stretching and CCC bending. The latter vibration is also much more harmonic in l-C_3H^+ compared to C_3. The ratio of harmonic frequency to diagonal quartic force constant in l-C_3H^+ is $\omega_5/k_{5555} = 1.8$ whereas in C_3 it is as low as $\omega_2/k_{2222} = 0.06$. Figure 5.3 further investigates the coupling between stretching and bending vibrations in l-C_3H^+ and C_3. The bending potential with respect to q_4 is almost unaffected by the CCC stretching normal coordinates q_2 and q_3 but shows a pronounced coupling with the CH stretching q_1 which is a consequence of the curvilinear nature of the HCC bending vibration. Comparing the q_5 potentials for l-C_3H^+ (middle row) and C_3 (bottom row)

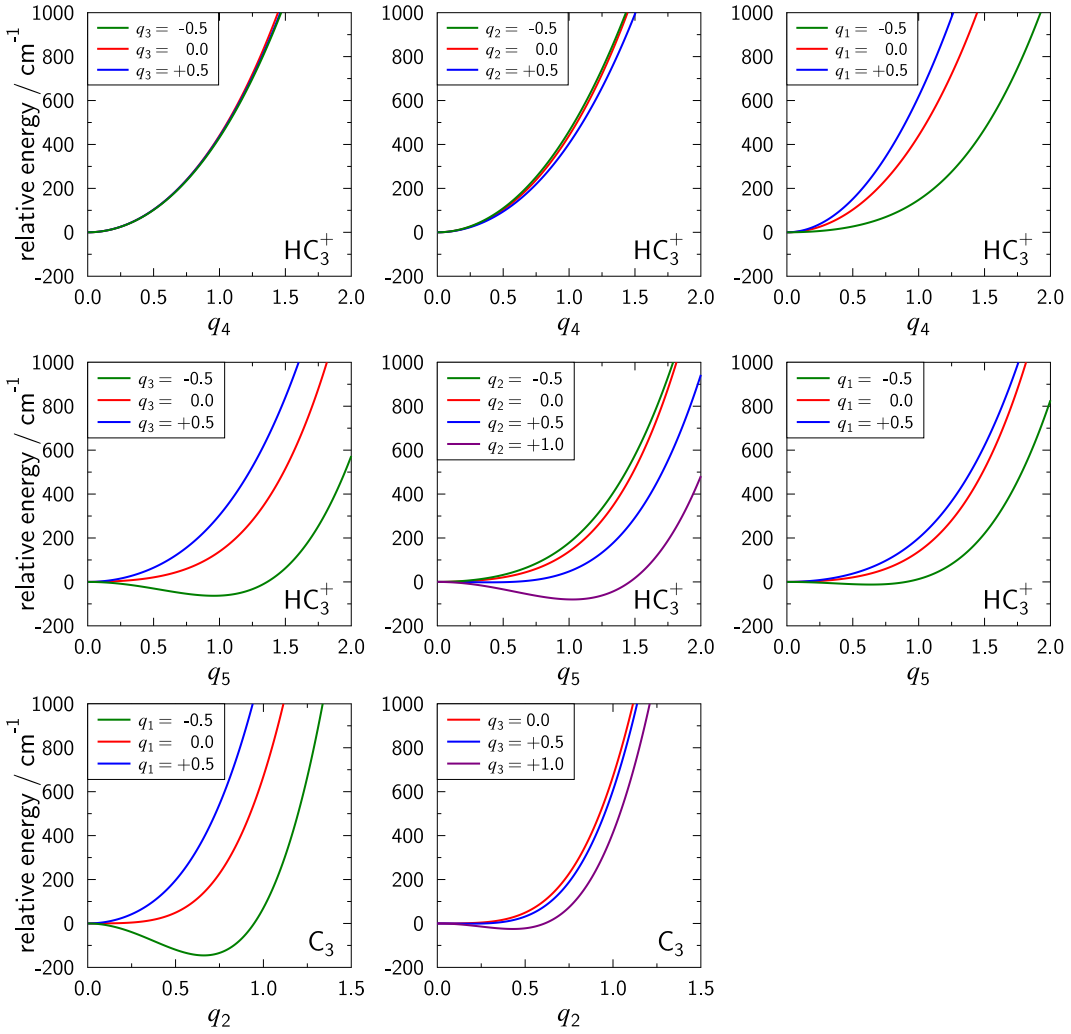

Figure 5.3: Variations of normal coordinate bending potentials in l-C_3H^+ (first and second row) and C_3 (third row) with different stretching normal coordinates.

they appear rather similar. The CCC stretching normal coordinates have the same effect on the q_5 potential as one observes for the corresponding potential curves in C_3. However, the effects are less pronounced in l-C_3H^+ which is a direct consequence of the reduced stretch-bend coupling force constants discussed above. From the preceeding discussion one can already make an important prediction about the rovibrational spectroscopy of l-C_3H^+: while effects due to rovibrational coupling as observed in C_3 (cf. e.g. Figure 3.16) are to be expected, they will be less pronounced.

5.3 Rovibrational calculations for l-C_3H^+

The aim of the present investigation of l-C_3H^+ is to put the results of Mladenović [30] under scrutiny. Therefore, the rovibrational calculations are required to be of the same quality as those presented earlier. The primitive vibrational basis set contains 5570 functions per $(\ell_4, \ell_5//\ell'_4, \ell'_5)$-block obtained from pruning the set $\{v_i^{\max}\} = \{13,\ 10,\ 16,\ 9,\ 14\}$. This set is chosen following extensive convergence tests on the Huang *et al.* QFF [365] that aim at converging the zero-point energy to within 0.005 cm^{-1} and the fundamental stretching vibrations and bending overtones to within 0.05 cm^{-1}. The latter corresponds to the convergence claimed by Mladenović [30]. For the vibrational angular momentum threshold a value of $\ell^0_{\max} = 4$ was chosen. Comparing $r^e_{45} = 2.17$ cm^{-1} calculated via VPT2 from the l-C_3H^+ QFF [365] with the value of -8.34 cm^{-1} obtained from the QFF for HCCH determined by Strey and Mills [357] justifies this choice. In the latter case convergence is observed for $\ell^0_{\max} \geq 3$ (cf. Section 4.2.3 and Section 4.3). These parameters yield a vibrational Hamiltonian for $J = 0$ of dimension 27850 in e-parity. While this is an order of magnitude smaller than the primary basis employed by Mladenović ($\sim$ 300000 to 700000) [30] it will be shown below that C8v4 results are in close agreement with the vibrational term energies reported by Mladenović for the QFF [30,365]. In the following vibrational states will be designate as $(v_1, v_2, v_3, v_4^{\ell_4}, v_5^{\ell_5})^{K\pm}$ where the sign is used to distinguish e (+) and f (−) parity states for $K = 0$. Results for the QFF [365] and the new composite PEF obtained with C8v4 will be denoted as QFF-C8v4 and Comp-C8v4, respectively. The DVR based results reported by Mladenović [30] are denoted as QFF-DVR accordingly.

Two series of $J > 0$ calculations are carried out. The first series focuses on the vibrational ground state $(0, 0, 0, 0^0, 0^0)^0$ and low-lying bending states $(0, 0, 0, v_4^{\ell_4}, v_5^{\ell_5})^K$ with $v_4 + v_5 \leq 2$. These calculations employ a maximum rotational quantum number of $J_{\max} = 12$. Because of the high computational cost of integrating and diagonalising the K-diagonal blocks with the above given vibrational basis set parameters the maximum value for the projection quantum number $K_{\max}$ is set to a value lower than $J_{\max}$. The offdiagonal Coriolis operator given in Equation (4.34) only couples basis functions with $\Delta K = \pm 1$. From a perturbational point of view, this means that the lowest order contribution of $\hat{T}_{VR}$ on a specific K-state is second order for coupling to $K' = K \pm 1$ states, third order for $K \pm 2$ and so on. Therefore, the influence of $K' = 2$ basis functions on the rovibrational term energies of the rovibrational ground state ($K = 0$) is expected to be small and for $K \geq 3$ should be negligible. On the other hand, for the bending states $K_{\max} = 3$

Table 5.3: Comparison of theoretical vibrational term energies for l-C_3H^+ calculated from the HFL QFF [365].

	G_v / cm^{-1}		
State	HFL-C8v4	HFL-DVR[a]	VPT2
$(0,0,0,0^0,0^0)^{0\,b}$	4204.62	4204.62	4201.85
$(0,0,0,0^0,1^1)^1$	117.6	117.6	114.2
$(0,0,0,1^1,0^0)^1$	784.4	784.4	782.3
$(0,0,1,0^0,0^0)^0$	1192.4	1192.5	1194.1
$(0,1,0,0^0,0^0)^0$	2095.6	2096.1	2096.3
$(1,0,0,0^0,0^0)^0$	3168.0	3167.8	3167.8

[a] Values reported by Mladenović [30].
[b] Zero-point energy (ZPE).

is the minimum value required to include Coriolis contributions to spectroscopic parameters for $K = 2$ states like the bend-bend combination state $(0,0,0,1^1,1^1)^2$. The prediagonalisation of the rovibrational Hamiltonian employs a fixed number of K-diagonal eigenvalues $N_K^{\mathrm{red}} = 200$. These parameters then provide converged rotational parameters up to H_v as well as rotational ℓ-type doubling paramters up to q_v^{JJ} in the target vibrational states.

The second series of calculations aims at the prediction of reliable parameters for excited stretching vibrational states in l-C_3H^+ based on the new composite PEF. Because of the low-lying CCC bending vibration the density of states in l-C_3H^+ for $J > 0$ is high which makes these calculations rather expensive and $J_{\max}$ is reduced to a value of 5 accordingly ($K_{\max} = 3$). The main reason for the increased cost is an increase in the prediagonalisation parameter which is needed to obtain converged rotational parameters for excited stretching states, especially the CH stretching state $(1,0,0,0^0,0^0)^0$ around 3170 cm^{-1}. Analysis of the offdiagonal matrix elements in the contracted Hamiltonian $\tilde{\mathbf{H}}^{(1,0)}$ shows that in order to describe the Coriolis contribution to the former state correctly it is necessary to include the K-diagonal state corresponding to $(2,0,0,1^1,0^0)^1$. This can be understood by considering the form of $\hat{\mathrm{T}}_{\mathrm{VR}}$ which contains vibrational operators $q_s\hat{\mathrm{p}}_t^{\pm}$ and $q_t^{\pm}\hat{\mathrm{p}}_s$ (cf. Equation (4.31)). The combinations have only offdiagonal matrix elements in the vibrational quantum numbers with $\Delta v_s = \pm 1$ and simultaneously $\Delta v_t = \pm 1$ (the signs are to be understood as independent). The strength of the coupling is then largely determined by the Coriolis coupling constant ζ_{st}. For the CH stretching fundamental $\zeta_{14} = 0.98614$ is the dominant contribution from which directly follows the importance of the $(2,0,0,1^1,0^0)^1$ and also $(0,0,0,1^1,0^0)^1$. A systematic analysis of all stretching vibrational states of interest yields a value of $N_K^{\mathrm{red}} = 1000$, in order to converge the rotational parameters. As will be shown, term energies up to $J_{\max} = 5$ only allows for the accurate determination of B_v and D_v.

5.3.1 Ground state rotational parameters in *l*-C_3H^+

Table 5.3 compares the ZPE and the vibrational term energies of the singly excited states in *l*-C_3H^+ determined from different rovibrational calculations and the Huang *et al.* QFF [365]. For the bending states $(0,0,0,1^1,0^0)^1$ and $(0,0,0,0^0,1^1)^1$ the QFF-C8v4 and QFF-DVR results correspond to the $J = 1$ term energy $T_v(J)$ and thus are larger by $B_v \sim 0.4$ cm^{-1} compared to G_v. The present C8v4 result for the ZPE (4204.62 cm^{-1}) perfectly reproduces the value determined by Mladenović [30], which gives confidence in the rotational parameters obtained with the former method. A rather large difference of 2.77 cm^{-1} is observed for the QFF-C8v4 ZPE with respect to the VPT2 result as a consequence of the anharmonicity of the system which makes a VPT2 treatment at least questionable [369]. The composite PEF yields a ZPE of 4208.97 cm^{-1} and 4205.47 cm^{-1} from variational C8v4 and VPT2 calculations, resulting in a slightly larger difference of 3.50 cm^{-1}. For comparison, in C_3 the difference in the ZPE between variational calculations and VPT2 amounts to as much as 7.31 cm^{-1}. Bending term energies agree to within the quoted accuracy between the QFF-C8v4 and -DVR results. Minor differences can be observed for the stretching term energies with the largest difference for the $(0,1,0,0^0,0^0)^0$ state obtained 0.5 cm^{-1} lower than the DVR calculations. The normal mode q_2 corresponding to the harmonic ω_2 can be characterized as a pseudo-antisymmetric CCC stretching vibration (cf. Figure 5.2). This motion expressed in terms of the diatom+diatom coordinates is highly coupled and all internal radial coordinates d_{HC}, d_{CC} and $R_{\mathrm{HC-CC}}$ change significantly with displacement according to q_2. Given the truncation/recoupling scheme employed Ref. [30] the difference in ν_2 might be attributed to a better description of this particular mode when employing normal coordinates and thus better convergence.

Rotational transition frequencies $J-1 \rightarrow J$ in the vibrational ground state of linear molecules can be obtained from Equation (2.90) upon inserting Equation (2.48) up to H_0 according to

$$\nu_{\mathrm{rot}} = 2B_0J - 4D_0J^3 + 2H_0J^3(3J^2+1) \tag{5.2}$$

Table 5.4 presents an overview of the experimental (astronomical & laboratory) rotational line frequencies [364, 366, 368] known for *l*-C_3H^+ as well as theoretical values obtained with the Huang *et al.* QFF [365] in this work using C8v4 (QFF-C8V4) and by Mladenović [30] (QFF-DVR) as well as the results of the new composite PEF (Comp-C8V4). Comparing the QFF-C8v4 and -DVR results shows that the C8v4 frequencies are uniformly lower than the DVR resulst with a difference of 0.12 MHz already for the $J = 0 \rightarrow 1$ transition up to as much as 15.45 MHz for $J = 11 \rightarrow 12$. Taking the difference 0.12 MHz as the approximate difference in the rotational parameters ΔB for the two theoretical methods accounts for only 2.64 MHz ($= 22\Delta B$) of the difference in the $J = 11 \rightarrow 12$ transition frequency according to Equation (5.2). This shows that the centrifugal distortion parameters D_0 and H_0 are also expected to differ between QFF-DVR and QFF-C8v4 results. In contrast, the Comp-C8v4 line frequencies show good agreement with the experimental results. The $J = 0 \rightarrow 1$ transition is predicted only 8.5 MHz higher than the astronomical value.

Table 5.4: Comparison of experimental and theoretical rotational transition frequencies (in MHz) for l-C_3H^+ in its vibrational ground state.

Transition	Experiment			Theoretical		
$J-1 \rightarrow J$	Pety[a]	McGuire[b]	Brünken[c]	QFF-C8v4[d]	QFF-DVR[e]	Comp-C8v4[d]
1		22489.86		22543.52	22543.64	22498.36
2		44979.54	44979.54	45086.84	45087.07	44996.54
3			67468.87	67629.72	67630.08	67494.34
4	89957.63		89957.64	90171.95	90172.48	89991.59
5	112445.64		112445.65	112713.34	112714.09	112488.09
6	134932.73	134932.73		135253.65	135254.78	134983.67
7	157418.72	157418.72		157792.68	157794.43	157478.14
8	179903.43			180330.23	180332.98	179971.31
9	202386.68			202866.07	202870.42	202463.01
10	224868.30			225400.02	225406.79	224953.05
11	247348.13			247931.84	247942.19	247441.25
12	269826.00			270461.35	270476.81	269927.43

[a] Astronomical data by Pety *et al.* [364].
[b] Astronomical data by McGuire *et al.* [366].
[c] Laboratory data by Brünken *et al.* [368].
[d] This work, see text for details.
[e] Derived from spectroscopic parameters reported by Mladenović [30].

Table 5.5: Comparison of rotational parameters and fit root-mean-squared (rms) deviations for l-C_3H^+ in its vibrational ground state[a] obtained by different methods.

Method	$K_{\max}$	B_0 / MHz	D_0 / kHz	H_0 / Hz	rms / kHz
QFF-DVR[b]	12	11271.67	6.439		678
		11271.84	8.992	9.89	35
QFF-C8v4[c]	0	11304.73	11.305		37.6
		11304.73	10.873	0.42	0.1
	1	11271.78	8.692		21.9
		11271.78	8.746	0.24	2.7
	2	11271.78	8.876		23.4
		11271.78	8.935	0.26	1.2
Comp-C8v4[d]	3	11249.19	7.681		72.4
		11249.20	7.741	0.15	0.4
exp.[e]		11244.96	7.745	0.49	31.9

[a] Theoretical results are obtained from calculations up to $J_{\max} = 12$.
[b] Results reported by Mladenović [30].
[c] Obtained using C8v4 ($N_K^{\text{red}} = 200$) and the Huang *et al.* QFF [365].
[d] Obtained using C8v4 ($N_K^{\text{red}} = 200$) and the composite PEF (Table C.3).
[e] Astronomical data by McGuire *et al.* [366].

Based on this an, error in B_0 of about 4.25 MHz is to be expected for the composite PEF.
Fitting the rotational line frequencies according to Equation (5.2) confirms the observations from comparing the rotational transition frequencies. The results of such fits are given in Table 5.5 and for QFF-C8v4 the convergence of the spectroscopic parameters with respect to $K_{\max}$ is shown additionally. Coriolis coupling reduces B_0 by about 33 MHz. The lowering of B_0 is straightforward to understand when remembering that the lowest $J > 0$ eigenvalues corresponding to the $(0, 0, 0, 0^0, 0^0)^0$ state will always be lowered upon inclusion of offdiagonal Coriolis matrix elements. The effect on D_0 and H_0 is somewhat more complicated. The differences in the spectroscopic parameters obtained from $K_{\max} = 1$ and 2 confirm the small indirect influence of $K \geq 2$ basis functions. Comparing QFF-C8v4 and QFF-DVR results shows that the latter grossly overestimated H_0. In fact, all rotational parameters obtained from the QFF-DVR calculations appear to be too large. Furthermore, the numerical accuracy of the least-squares fits according to the root-mean-squared (rms) deviation is at least one order of magnitude better for C8v4 results compared to DVR fits. Using the composite PEF the ground state rotational parameter B_0 is calculated to be 11249.20 MHz only 4.26 MHz (0.04 %) larger than the astronomical value [366]. The centrifugal distortion parameter $D_0 = 7.741$ kHz is in excellent agreement with the value determined by McGuire and coworkers [366] and the value of 0.15 Hz obtained for H_0 is within the error bounds of the experimental value $H_0 = 0.49 \pm 0.37$ Hz.
By combining the results of Table 5.4 and Table 5.5 another strong argument against the large H_0 obtained by Mladenović [30] can be made. To this end, the quantity $\Delta\nu_H$ is introduced according to

$$\Delta\nu_H = \frac{\nu_{\text{rot}} - 2B_0J}{-4J^3} = D_0 - \frac{1}{2}H_0 - \frac{3}{2}H_0J^2\,. \tag{5.3}$$

If the contribution of H_0 can be neglected a graph depicting the variation of $\Delta\nu_H$ with J will yield a straight line corresponding to D_0. In case the contribution of H_0 is non-negligible $\Delta\nu_H$ will have a parabolic shape according to Equation (5.3). Figure 5.4 depicts the variation of $\Delta\nu_H$ with J for the experimental and the theoretical results. The B_0 used in the calculation of $\Delta\nu_H$ corresponds to the respective value given in Table 5.5. For comparison the D_0 values are depicted by dashed lines. In the case of the QFF-C8v4, Comp-C8v4 and experimental result $\Delta\nu_H$ in the range $J = 4$ - 7 is close to the corresponding D_0, as expected. Only for larger values of J a *small* parabolic deviation of $\Delta\nu_H$ from D_0 can be observed indicating a small contribution from H_0. Notice that the experimental data originates from different sources. The employed experimental line frequencies for $J \geq 5$ are from Pety *et al.* [364], $J = 3$ and 4 from Brünken *et al.* [368] and $J = 2$ from McGuire *et al.* [366] ($J = 1$ given in the latter study yields a $\Delta\nu_H$ which is outside the depicted range and is not shown). Jumps in $\Delta\nu_H$ are observed when switching the underlying experimental data set which indicates some inconsistencies between the different sources. However, the data by Pety *et al.* is the most extensive and shows an internally consistent trend in $\Delta\nu_H$. As is obvious from the QFF-DVR results in Figure 5.4 H_0 determined by Mladenović [30] is way too large with $\Delta\nu_H$ showing a considerable parabolic shape already for low values of J.
Giving an explanation for the deviations in the DVR results is difficult since different factors may

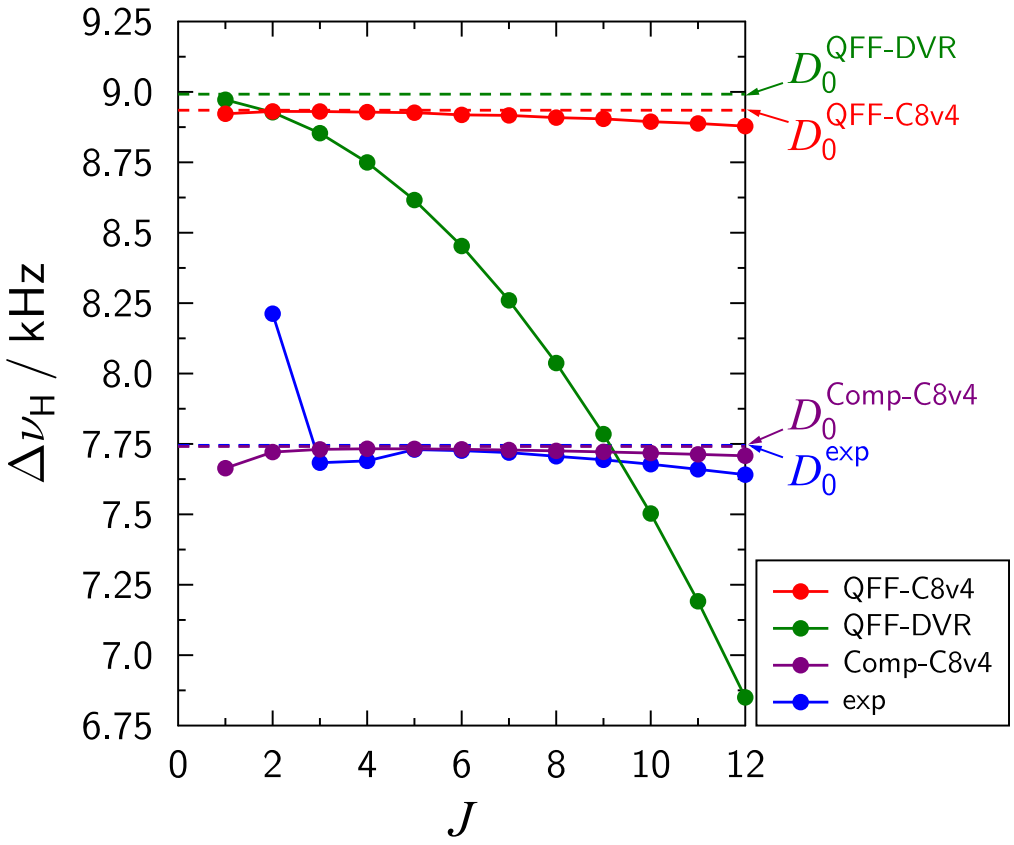

Figure 5.4: Variation of $\Delta\nu_H$ (see Equation (5.3) for definition) with J obtained from different sets of ground state rotational line frequencies (Table 5.4 and rotational parameters (Table 5.5). The dashed lines correspond to the respective value of the quartic centrifugal distortion parameter D_0.

add to them. One possibility could be the underlying DVR truncation/recoupling algorithm. At each step in such a scheme a Hamiltonian is obtained by neglecting certain degrees of freedom, subsequently diagonalised and eigenpairs are selected based on a given criterium. The following recoupling step then builds the Hamiltonian in an extended coordinate space using the eigenvalues and -vectors of the truncation step to couple the previous subspace with the added coordinate space. The accuracy of the off-diagonal coupling matrix elements in the extended Hamiltonian are largely defined by the accuracy of the eigenvectors. The former can be interpreted as linear combinations of the Hamiltonian matrix elements expressed in the primitive basis set with coefficients according to the elements of the eigenvectors. This scheme is repeated multiple times which emphasizes the need for accurate eigenvectors since numerical errors can be amplified by the subsequent steps. Another factor adding to the accuracy of the truncation/recoupling scheme is the intrinsic coupling of the

subspaces. The underlying assumption of the scheme is that each truncation of the Hamiltonian is a more or less good approximation to the motion described by the Hamiltonian. Specifically, for l-C_3H^+ Mladenović [30] used a diatom+diatom embedding of the rovibrational problem. This assumes that the molecule is accurately described by a CH and CC subsystem coupled by a intersystem coordinate $R_{\mathrm{HC-CC}}$. As has been pointed out before, this appears unfavourable for l-C_3H^+ which behaves more like a C_3 system with an added proton H^+. However, the numerical results presented above clearly show that the DVR results are less accurate than the C8V4 ones.

5.3.2 Vibrationally excited states in l-C_3H^+

The preceding discussion of the rotational parameters in the vibrational ground state has shown that due to the low value of H_0 high excitation in J is required to obtain a noticeable contribution to the term energy. Since reliable term energies up to only $J_{\max} = 5$ are available for the excited stretching states, the contribution of H_v can be neglected for these states. Following a similar argument, the quartic centrifugal distortion parameter D_v appear to be reasonably well determined from this number of rational states. Except for the erroneous QFF-DVR results the $\Delta\nu_H$ graphs in Figure 5.4 reach the maximum corresponding to D_0 for $J \approx 5$. Since no experimental results on vibrationally excited states in l-C_3H^+ are available for comparison the following results stand as predictions of forthcoming experimental results. Based on the previous results for the $(0,0,0,0^0,0^0)^0$ state (Table 5.5) the rotational parameters of the excited states are expected to be of similar accuracy.

The determination of spectroscopic parameters for bending states $(0,0,0,v_4^{\ell_4},v_5^{\ell_5})^{K\pm}$ in l-C_3H^+ has to take into account ℓ-type doubling and ℓ-type resonance effects. This is rather straightforward for states involving excitation in only one of the bending modes and can be done with the methods outlined in Section 2.3.4. The resulting least-squares fitting procedure then is the same as employed for linear triatomic molecules where effective Hamiltonians are set up and diagonalized for each J with matrix elements given by Equation (2.92) and Equation (2.93). For the bend-bend combination states $(0,0,0,1^{\ell_4},1^{\ell_5})^{|\ell_4+\ell_5|\pm}$ the vibrational ℓ-type doubling has to be also taken into account. This has been discussed by Amat and Nielsen [383] and the presented analysis follows their work. In an unsymmetrized basis the states belonging to $(0,0,0,1^{\ell_4},1^{\ell_5})^{|\ell_4+\ell_5|\pm}$ with $\{\ell_t\} = \pm 1$ can be described in an abbreviated form by $\left|v_4^{\ell_4},v_5^{\ell_5},J,k\right\rangle$ which gives the 4 required states: $\left|1^1,1^{-1},J,0\right\rangle$, $\left|1^{-1},1^1,J,0\right\rangle$, $\left|1^1,1^1,J,+2\right\rangle$ and $\left|1^{-1},1^{-1},J,-2\right\rangle$. The effective Hamiltonian using this basis functions has the following form [383]:

$$
\begin{array}{r}
 \\
\langle 1^1,1^1,J\,+2| \\
\langle 1^{-1},1^1,J\,0| \\
\langle 1^1,1^{-1},J\,0| \\
\langle 1^{-1},1^{-1},J\,-2|
\end{array}
\begin{array}{c}
\begin{array}{cccc}
\left|1^1,1^1,J,+2\right\rangle & \left|1^{-1},1^1,J,0\right\rangle & \left|1^1,1^{-1},J,0\right\rangle & \left|1^{-1},1^{-1},J,-2\right\rangle
\end{array} \\
\begin{pmatrix}
E^2_{45}(J) & K^{\mathrm{C}}_4 & K^{\mathrm{C}}_5 & 0 \\
K^{\mathrm{C}}_4 & E^0_{45}(J) & K^{\mathrm{V}}_{45} & K^{\mathrm{C}}_5 \\
K^{\mathrm{C}}_5 & K^{\mathrm{V}}_{45} & E^0_{45}(J) & K^{\mathrm{C}}_4 \\
0 & K^{\mathrm{C}}_5 & K^{\mathrm{C}}_4 & E^2_{45}(J)
\end{pmatrix}
\end{array}
= \mathbf{H}^{(J)}_{\mathrm{eff}}\,. \quad (5.4)
$$

where $E_{45}^{|k|}(J)$ are the diagonal matrix elements of the $k = \pm 2$ $(\pm, \pm)$ and $k = 0$ $(\pm, \mp)$ states. According to Equation (2.92) one has

$$\begin{aligned} E_{45}^{0}(J) &= G_{45} - x_{\ell_4\ell_5} + (B_{45} - \gamma_{\ell_4\ell_5})J(J+1) \\ &\quad - D\left[J(J+1)\right]^2 + H\left[J(J+1)\right]^3 \qquad (5.5) \\ E_{45}^{2}(J) &= G_{45} + x_{\ell_4\ell_5} + (B_{45} + \gamma_{\ell_4\ell_5})\left[J(J+1) - 4\right] \\ &\quad - D\left[J(J+1) - 4\right]^2 + H\left[J(J+1) - 4\right]^3 . \qquad (5.6) \end{aligned}$$

The off-diagonal ℓ-type resonance matrix elements K_t^{C} are given by

$$K_4^{\mathrm{C}} = \frac{1}{2}\left[q_4 + q_4^J J(J+1) + q_4^{JJ} J^2(J+1)^2\right]\sqrt{\left[J(J+1)\right]\left[J(J+1)-2\right]} \qquad (5.7)$$

$$K_5^{\mathrm{C}} = \frac{1}{2}\left[q_5 + q_5^J J(J+1) + q_5^{JJ} J^2(J+1)^2\right]\sqrt{\left[J(J+1)\right]\left[J(J+1)-2\right]}. \qquad (5.8)$$

Comparison with Equation (2.93) shows that the previous two equations describe the ℓ-type resonance of the individual bending modes contributing to the combination state. Notice that Amat and Nielsen [383] neglect the explicit K dependence in their offdiagonal matrix elements. The vibrational ℓ-type doubling matrix element K_{45}^{V} is given by [383]

$$\begin{aligned} K_{45}^{\mathrm{V}} &= \left\langle v_4^{\ell_4}, v_5^{\ell_5} \,\middle|\, \hat{\mathrm{H}}_{\mathrm{eff}} \,\middle|\, v_4^{\ell_4 \pm 2}, v_5^{\ell_5 \mp 2} \right\rangle \\ &= \frac{1}{4} r_{45} \sqrt{\left[v_4 \pm \ell_4 + 2\right]\left[v_4 \mp \ell_4\right]\left[v_5 \mp \ell_5 + 2\right]\left[v_5 \pm \ell_5\right]} \\ &= r_{45}\,, \qquad (5.9) \end{aligned}$$

where r_{45} contains additional rotational and centrifugal distortion contributions according to

$$r_{45} = r_{45}^0 + r_{45}^J J(J+1) + r_{45}^{JJ} J^2(J+1)^2 + r_{45}^{JJJ} J^3(J+1)^3 . \qquad (5.10)$$

In Equation (5.10), the spectroscopic paramter r_{45}^0 can be compared with the VPT2 parameter r_{45}^{e}. The parameters r_{45}^J, r_{45}^{JJ} and $r_{45}^{JJJ}$are responsible for differences in B_v, D_v and H_v, respectively, between the $+/-$ parity states for $K = 0$. This becomes obvious when factoring the Hamiltonian into said parity blocks by introducing the symmetrized wave functions $|1^1, 1^1, J, K, \pm)$ following Equation (4.79) which yields

$$\begin{array}{c} \\ (1^1,1^1,J,2,+| \\ (1^1,1^1,J,0,+| \\ (1^1,1^1,J,0,-| \\ (1^1,1^1,J,2,-| \end{array} \begin{array}{c} \begin{array}{cccc} |1^1,1^1,J,2,+) & |1^1,1^1,J,0,+) & |1^1,1^1,J,0,-) & |1^1,1^1,J,2,-) \end{array} \\ \begin{pmatrix} E_{45}^2(J) & K_4^{\mathrm{C}} + K_5^{\mathrm{C}} & 0 & 0 \\ K_4^{\mathrm{C}} + K_5^{\mathrm{C}} & E_{45}^0(J) + K_{45}^{\mathrm{V}} & 0 & 0 \\ 0 & 0 & E_{45}^0(J) - K_{45}^{\mathrm{V}} & K_4^{\mathrm{C}} - K_5^{\mathrm{C}} \\ 0 & 0 & K_4^{\mathrm{C}} - K_5^{\mathrm{C}} & E_{45}^2(J) \end{pmatrix} \end{array} = \mathbf{H}_{\mathrm{eff}}^{(J)} . \qquad (5.11)$$

Table 5.6: Calculated spectroscopic parameters for low lying bending states in l-C_3H^+.[a]

State	G_v / cm^{-1}	B_v / MHz	D_v / kHz	H_v / Hz
$(0,0,0,0^0,1^1)^1$	128.90	11403.35	11.451	0.32
$(0,0,0,0^0,2^0)^0$	252.65	11560.65	15.017	0.45
$(0,0,0,0^0,2^2)^2$	258.22	11560.05	14.758	0.42
$(0,0,0,1^1,0^0)^1$	788.86	11253.15	7.593	0.14
$(0,0,0,1^1,1^1)^{0+}$	915.57	11407.41	11.018	0.08
$(0,0,0,1^1,1^1)^{0-}$	918.00	11406.92	11.090	0.43
$(0,0,0,1^1,1^1)^2$	919.29	11407.91	11.054	0.26
$(0,0,0,2^0,0^0)^0$	1562.43	11260.59	7.673	0.14
$(0,0,0,2^2,0^0)^2$	1582.65	11254.98	7.222	0.11
State	q_t	q_v / MHz	q_v^J / kHz	q_v^{JJ} / Hz
$(0,0,0,0,1)$	q_5	68.57	−2.993	0.19
$(0,0,0,0,2)$	q_5	70.63	−3.144	0.17
$(0,0,0,1,0)$	q_4	14.19	−0.092	0.002
$(0,0,0,1,1)$	q_4	16.10	−4.750	13.74
$(0,0,0,1,1)$	q_5	65.93	−9.729	21.49
$(0,0,0,2,0)$	q_4	12.26	−0.181	0.65

[a] Obtained from C8v4 variational calculations ($N_K^{\mathrm{red}} = 200$) up to $J_{\max} = 12$ using the present l-C_3H^+composite PEF (Table C.3).

The results of least-squares fits to the variational rovibrational term energies for bending states $(0,0,0,v_4^{\ell_4},v_5^{\ell_5})^{K\pm}$ with $v_4 + v_5 \leq 2$ are given in Table 5.6. In the upper part the parameters that enter the diagonal matrix elements are given. Compared to the ground state parameters (Table 5.7) excitation of the CCC bend v_5 leads to larger changes in the rotational parameters then the HCC bend which is in line with the higher flexibility of the former mode. From the vibrational term energies for the overtone and bend-bend combination states effective anharmonicity constants (in cm^{-1}) can be calculated following Equation (2.49): $x_{\ell_4\ell_4} = 5.04$, $x_{\ell_5\ell_5} = 1.39$, $x_{\ell_4\ell_5} = 1.25$ cm^{-1} as well as the vibrational ℓ-type doubling parameter $r_{45}^0 = -1.22$ cm^{-1}. While the variational results for the $x_{\ell_t\ell_{t'}}$ parameters are in good agreement with the VPT2 result of 5.23, 1.55 and 1.29 cm^{-1}, the vibrational ℓ-type doubling parameter $r_{45}^{\mathrm{e}} = 5.23$ cm^{-1} predicts a too large splitting ($= 2r_{45}^{\mathrm{e}}$) by a factor of about 5 and even more severe reverses the energetic order of (+) and (−) parity states.

In the lower part of Table 5.6 the determined ℓ-type doubling parameters are quoted. These parameters take the phase choice made for the rovibrational wave functions into account. This issue has been discussed in detail by Yamada [346] and Sebald [384]. The q_v values only vary slightly with respect to the bending quantum numbers. From the normal coordinate transformed potential VPT2 values of $q_4^{\mathrm{e}} = 13.21$ MHz and $q_5^{\mathrm{e}} = 65.28$ MHz are obtained which are in quite good agreement with the q_v values given in Table 5.6. The centrifugal distortion contribution q_v^J shows larger variations with vibrational excitation. For the bending fundamentals ν_4 and ν_5 the ℓ-type doubling parameters q_t^J obtained with VPT2 (Equation (2.72)) are $q_4^J = -0.02$ kHz

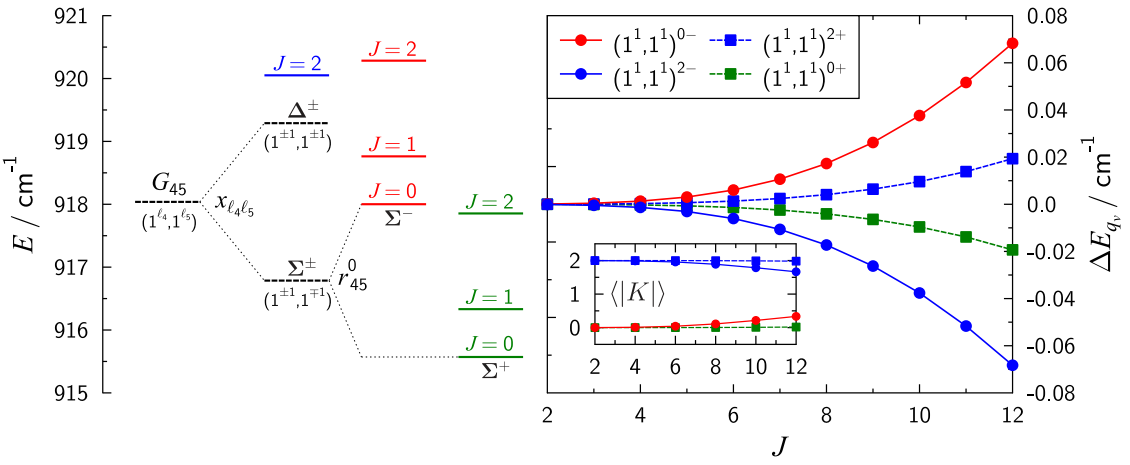

Figure 5.5: Effects of ℓ-type resonance in the bend-bend combination states $(0,0,0,1^{\ell_4},1^{\ell_5})^{K\pm}$ of l-C_3H^+. The left part gives an term energy diagram for rovibrational states up to $J = 2$. Dashed lines correspond to intermediate vibrational levels which are shown to display the different energy terms contributing to the rovibrational term energies. The right part gives the splitting ΔE_{q_v} between the diagonal matrix elements of the effective Hamiltonian Equation (5.11) and the variationally calculated term energies. The inset shows the expectation value of $\langle|K|\rangle$ evaluated with the eigenvectors of the effective Hamiltonian.

and $q_5^J = -2.5$ kHz which again agree rather well with the variational results of -0.092 kHz and -2.992 kHz, respectively. For C_3, on the other hand, still larger differences between VPT2 and variational results are observed as a consequence of the larger anharmonicity of the bending motion. For example, $q_2^e = 247.10$ MHz in C_3 is larger by a factor of about 1.45 compared to q_v in the ν_2 fundamental (Table 3.13).

Amat and Nielsen [383] have shown that the separation between the diagonal matrix elements in the individual parity blocks for the $(0,0,0,1^{\ell_4},1^{\ell_5})^K\pm$ states (Equation (5.11)) for low values of J is approximately $\Delta_\pm = 2x_{\ell_4\ell_4} \mp r_{45}^0 - 4B$ and thus independent of J. The rotational parameter of the bend-bend combination states expressed in units of cm^{-1} is $B \sim 0.38$ cm^{-1}. Using the parameters $x_{\ell_4\ell_4}$ and r_{45}^0 given above one obtains $|\Delta_+| = 2.2$ and $|\Delta_-| = 0.24$ cm^{-1} showing that the diagonal elements corresponding to $|1^1,1^1,J,K,-)$ functions are very close in energy. Up to $J = 2$ the energetic situation is graphically displayed in the left part of Figure 5.5. Notice that on the shown energy scale the splitting of the $\Delta^\pm$ states due to ℓ-type resonance is not resolvable. Nevertheless, since the offdiagonal matrix elements $K_4^C \pm K_5^C$ scale with $\sim J(J+1)$ [383] a quite pronounced ℓ-type resonance for the f-block states is observed. This is depicted on the right side of Figure 5.5 where the splitting ΔE_{q_v} between the diagonal matrix elements of the effective Hamiltonian Equation (5.5) and Equation (5.6) and the respective variational rovibrational term energy is given. The shift ΔE_{q_v} for the f $(-)$ levels is larger by a factor of about 3 compared to the e $(+)$ levels at $J = 12$. Due to the non-linear J scaling of the ℓ-type resonance matrix elements this difference will increase with J. The mixing of the $K = 0$ and $K = 2$ states is obvious from

the J-dependence of the expectation value $\langle|K|\rangle$ evaluated from the eigenvectors of the effective Hamiltonian shown in the inset in Figure 5.5. The situation is similar to the $2\nu_2^\ell$ bending overtone in C_3 which also shows a strong ℓ-type resonance due to the difference of the vibrational term energies ($\approx 4x_{\ell\ell}$) of the $(0, 2^0, 0)$ and $(0, 2^2, 0)$ state being almost zero (cf. Table 3.12 and the inset of Figure 3.12). In contrast, in l-C_3H^+ the $2\nu_5^K$ bending overtone does not show such a strong resonance, since a) $x_{\ell_5\ell_5} = 1.39$ leads to a significantly larger splitting of the l-C_3H^+ $2\nu_5^K$ sub-levels and b) $|q_5| \approx 70$ MHz in l-C_3H^+ is less than half the size of $|q_2| \approx 170$ cm^{-1} observed in C_3 [295, 322].

Table 5.7 summarizes spectroscopic parameters determined for low-lying stretching states in l-C_3H^+ obtained from calculations with $N_K^{\rm red} = 1000$ and up to $J_{\rm max} = 5$. For the vibrational term energies results obtained from a VPT2 treatment are also given in Table 5.7 for comparison. Differences between variational and and VPT2 results are small for the singly excited states except for the pseudo-symmetric CCC stretch fundamental $(0, 0, 1, 0^0, 0^0)^0$. In the latter case a difference of 1.96 cm^{-1} is observed and might be explained by a stronger coupling of q_3 and the CCC bending q_5 which is not well reproduced in a VPT2 treatment (cf. Figure 5.3). The VPT2+Fermi approach for the $\omega_1 \approx \omega_2 + \omega_3$ type-I Fermi resonance yields a quite good agreement in the vibrational term energies compared to the variational result indicating that the perturbational treament is applicable at least for the lowest dyade $(1, 0, 0, 0^0, 0^0)^0 // (0, 1, 1, 0^0, 0^0)^0$.

Interestingly, $\Delta B_v = B_v - B_0$ for both CCC stretching states is calculated to be negative which is different from C_3 where a sign change is observed between the ΔB_v of the two stretching vibrations. A more detailed discussion of the rotational parameters B_v and their differences with respect to the ground vibrational state will be given below. The centrifugal distortion parameters show a pronounced dependence on vibrational excitation. For the pseudo-symmetric stretching vibration a *decrease* in D_v by a factor of 0.38 is observed whereas for the pseudo-antisymmetric stretching vibration the results show an *increase* by a factor of 1.20. The direction of these changes are the same as observed for C_3.

Table 5.7: Calculated spectroscopic parameters for selected stretching states in l-C_3H^+.

	G_v / cm^{-1}			
State	VPT2[a]	C8v4[b]	B_v / MHz	D_v / kHz
$(0, 0, 1, 0^0, 0^0)^0$	1187.59	1185.63	11198.20	2.569
$(0, 1, 0, 0^0, 0^0)^0$	2091.81	2092.00	11188.93	9.344
$(0, 0, 2, 0^0, 0^0)^0$	2370.45	2364.22	11146.69	7.029
$(1, 0, 0, 0^0, 0^0)^0$	3169.86	3170.15	11215.85	7.982
$(0, 1, 1, 0^0, 0^0)^0$	3267.79	3267.51	11133.91	11.937
$(0, 2, 0, 0^0, 0^0)^0$	4166.20	4165.39	11137.26	10.466

[a] VPT2+Fermi vibrational term energies.
[b] Obtained from C8v4 variational calculations ($N_K^{\rm red} = 1000$) up to $J_{\rm max} = 5$ using the present l-C_3H^+composite PEF (Table C.3).

The rotational parameters of the CH stretching fundamental are influenced by the Fermi-resonance coupling to $(0,1,1,0^0,0^0)^{0+}$, therefore a more detailed analysis of this resonance is warranted. The resonance in the Fermi-dyad $(1,0,0,0^0,0^0)^0$ (State I) and $(0,1,1,0^0,0^0)^0$ (State II) can be modeled by setting up effective Hamiltonian matrices for each value of J according to

$$\mathbf{H}_{\text{eff}}^{(J)} = \begin{pmatrix} T_{\text{I}}(J) & K_{\text{F}} \\ K_{\text{F}} & T_{\text{II}}(J) \end{pmatrix}, \tag{5.12}$$

where $T_{\text{I}}(J)$ and $T_{\text{II}}(J)$ are the deperturbed rovibrational term energies which follow the expansion in Equation (2.92)

$$T_{\text{I}}(J) = G_{\text{I}} + B_{\text{I}}J(J+1) - D_{\text{I}}J^2(J+1)^2 \tag{5.13}$$

$$T_{\text{II}}(J) = G_{\text{II}} + B_{\text{II}}J(J+1) - D_{\text{II}}J^2(J+1)^2 \tag{5.14}$$

and the offdiagonal matrix element K_{F} is given by Equation (2.78) within VPT2. It is not possible to determine deperturbed G_{I}, G_{II} and K_{F} from the perturbed (variational) term energies alone. Given the good agreement of the VPT2 results in Table 5.7 for the two states in question, K_{F} is fixed to the VPT2 value of $\phi_{123}/\sqrt{8} = -20.64$ cm^{-1}. Matrix diagonalisation and least-squares fitting then yield the deperturbed spectroscopic parameters which are summarized in Table 5.8 together with the corresponding VPT2 vibrational term energies. Comparison of the deperturbed vibrational term energies shows excellent agreement between VPT2 and variational results with absolute differences of 0.32 and 0.69 cm^{-1} for G_{I} and G_{II}, respectively. The mixing ratio based on the eigenvectors obtained for $J = 0$ in the variational calculation is 96:4 which is in virtual

Table 5.8: Spectroscopic parameters for the lowest l-C_3H^+ Fermi resonance pair $(1,0,0,0^0,0^0)^{0+}$ (State I) and $(0,1,1,0^0,0^0)^{0+}$ (State II) obtained from VPT2 and variationally calculated term energies.

	Perturbed			Deperturbed	
	VPT2[a]	VPT2 + Fermi[b]	Variational[c]	VPT2+Fermi[d]	Variational[c]
G_{I} / cm^{-1}	3139.84	3170.15	3169.86	3174.42	3174.74
G_{II} / cm^{-1}	3297.81	3267.51	3267.79	3263.23	3262.92
ϕ_{123} / cm^{-1}				−58.39	[−58.39][e]
B_{I} / MHz			11215.85		11220.11
D_{I} / kHz			7.982		7.637
B_{II} / MHz			11133.91		11129.64
D_{II} / kHz			11.937		12.283

[a] Standard VPT2 treatment.
[b] VPT2 treatment accounting for the Fermi resonance.
[c] Results obtained from variational calculations.
[d] Matrix elements in the VPT2+Fermi treatment.

Table 5.9: Differences of rotational parameters in various vibrational states of l-C_3H^+ and C_3 obtained from VPT2 and variational calculations using the present composite PEFs.

ΔB_v	l-C_3H^+		C_3	
	$(0,0,0,0^0,0^0)^{0+}$		$(0,0^0,0)$	
VPT2	−81.78		−527.33	
Variational	−81.80		−333.62	
Difference	−0.02		+193.71	
	$(0,0,0,1^1,0^0)^1$	$(0,0,0,0^0,1^1)^1$	$(0,1^1,0)$	
VPT2	+3.19	+151.27	+599.53	
Variational	+3.95	+154.29	+353.70	
Difference	+0.76	+3.02	−245.83	
	$(0,0,1,0^0,0^0)^{0+}$	$(0,0,2,0^0,0^0)^{0+}$	$(1,0^0,0)$	$(2,0^0,0)$
VPT2	−37.82	−75.64	−101.43	−202.86
Variational	−51.00	−102.51	−168.60	−269.60
Difference	−13.18	−26.87	−67.17	−66.74
	$(0,1,0,0^0,0^0)^{0+}$	$(0,2,0,0^0,0^0)^{0+}$	$(0,0^0,1)$	$(0,0^0,2)$
VPT2	−74.67	−149.34	−42.98	−85.96
Variational	−60.27	−111.95	+147.14	+775.47
Difference	+14.40	+37.39	+190.12	+861.43
	$(1,0,0,0^0,0^0)^{0+}$	$(0,1,1,0^0,0^0)^{0+}$	$(1,0^0,1)$	
VPT2	−32.87	−112.49	−144.41	
Variational	−29.09	−119.55	−191.93	
Difference	+3.78	−7.06	−47.52	

agreement with the mixing predicted by a VPT2+Fermi treatment.

An important question to consider is how accurate the fundamental transition frequencies are with respect to the convergence of the PEF description. Compared to the triatomic molecules presented in Chapter 3 the l-C_3H^+ composite approach does not include the effect of pentuple excitations via the P-Q contribution. On the basis of the triatomic results an estimate of the importance of connected pentuples might be derived. Considering the P-Q corrections for ω_1 and ω_2 in HCN and for ω_1 and ω_3 in C_3 an error of ± 1 cm^{-1} for the corresponding fundamental transitions in l-C_3H^+ appears to be appropriate. Furthermore, the close agreement of angular dependence of smaller contributions with respect to θ_5 in l-C_3H^+ and θ in C_3 (compare Figure 5.1 and Figure 3.11, respectively) suggests that P-Q is only of minor importance for the CCC bending in l-C_3H^+. Nevertheless, a conservative error estimate of ± 1 cm^{-1} should be attributed to ν_5. In summary the fundamental transitions of l-C_3H^+ ν_i (in cm^{-1}) are predicted to occur at $\nu_1 = 3170 \pm 1$, $\nu_2 = 2092 \pm 1$, $\nu_3 = 1186 \pm 1$, $\nu_4 = 789 \pm 1$ and $\nu_5 = 129 \pm 1$.

With the rotational parameters determined for l-C_3H^+ a closer look at the vibrational dependence of B_v is possible. Table 5.9 compares $\Delta B_0 = B_e - B_0$ and $\Delta B_v = B_v - B_0$ obtained from varia-

tionally determined term energies and by VPT2 for both l-C_3H^+ and C_3. As has been pointed out before, within VPT2 the two differences can be calculated from the rotation-vibration interaction constants α_i according to $\Delta B_0 = -\sum_i d_i\alpha_i$ and $\Delta B_v = -\sum_i v_i\alpha_i$. ΔB_0 for l-C_3H^+ shows almost perfect agreement between VPT2 and variational calculations. In contrast, for C_3 a significant difference of +193.71 MHz can be observed. Similarly, in the singly excited l-C_3H^+ HCC bending state $(0,0,0,1^1,0^0)^1$ the difference between variational calculations and VPT2 does not exceed 1 MHz and for the low lying CCC bending fundamental a difference of +3.02 MHz is obtained. The latter value is much smaller and of opposite sign than the difference for ν_2 in C_3 where the variational ΔB_v is lower by as much as −245.53 MHz compared to VPT2. These observations are a direct consequence of the more harmonic CCC bending vibration in l-C_3H^+ which appears to be better described by VPT2 than ν_2 in C_3.

The differences between VPT2 and variational ΔB_v for stretching states are considerably smaller in l-C_3H^+ than in C_3. Nevertheless, the signs of the differences for the CCC stretching vibrations in l-C_3H^+ are the same as for the corresponding C_3 vibrations which follows from the similar albeit weaker stretch-bend couplings. A closer look at the changes when increasing the CCC stretch excitations from 1 to 2 shows an interesting effect. From $\Delta B_v = -\sum_i v_i\alpha_i$ one would expect the differences between variational and VPT2 results to also be a linear function of the v_s. This is approximately the case for l-C_3H^+ with excitation in a single CCC vibrational mode but not for C_3 which shows a significant non-linear behaviour for low values of v_s (cf. also Figure 3.16). In addition, the variational ΔB_v in l-C_3H^+ also does not show linear behaviour for the combination state $(0,1,1,0^0,0^0)^0$ which based on the differences for $(0,0,1,0^0,0^0)^0$ (−13.18 MHz) and $(0,1,0,0^0,0^0)$ (+14.40 MHz) should show nearly no difference between VPT2 and the variational result. Instead a difference of −7.06 MHz is obtained.

Adding up the variational ΔB_v for the singly excited vibrational states multiplied by the degeneracy factors d_i yields an approximate value ΔB_0 value of −88.06 MHz which is different form the value obtained directly from the variational B_0. This further indicates that the agreement of the variational and perturbational ΔB_0 is due to error compensation effects in the VPT2 treatment. Similar to C_3, these observations directly influence the quality of an equilibrium geometry determined from experimental results alone which relies on effective rotation-vibration interaction constants α_i determined from appropriate experimental ΔB_v values.

The preceding discussions confirms the presumption of Section 5.2 that rovibrational coupling in l-C_3H^+ will show similar albeit weaker effects compared to C_3. Furthermore, the vibrational term energies presented in Tables 5.6 and 5.7 also reveal difficulties in the description of the vibrational motion when a standard VPT2 treatment is applied together with an accurate PEF. Clearly, l-C_3H^+ is a rather flexible tetraatomic linear molecule evident from the f_D ratio of 1.80 which requires an exact treatment of the rovibrational problem beyond VPT2. A complete understanding of l-C_3H^+ thus will always require theoretical insight from variational calculations since the usual (perturbation theory-based) formulae for the interpretation of experimental rovibrational spectra are to be applied with caution.

Chapter 6

Summary and Outlook

Theoretical rovibrational spectroscopy of small polyatomic molecules yields some of the most impressive agreements between experiment and theory. By using modern *ab initio* methods the PES and EDMS can be sampled to very high accuracy yielding rovibrational transitions and intensities that allow direct comparison with experimental spectra. This enhances the capabilities of experimentalists to unambigously assign new lines in an otherwise dense spectrum which contains spectral signatures of a variety molecular species such as obtained from, e.g., plasma sources [29]. A theoretical treatment can also provide insight into aspects which are difficult address from an experimental point of view. This thesis has presented methods to generate such information *ab initio* with an accuracy of ~ 1 cm^{-1} in the fundamental transition frequencies and a few MHz in rotational constants B_v. For triatomic systems this has become a routine task in recent years [189]. Here, the focus is on linear species which require a special treatment of the rovibrational problem [191] compared to nonlinear systems [182]. Ultimately, the aim is to extend the range of accessible molecular systems to a larger size.

In Chapter 3 a high-level composite procedure for the generation of near-equilibrium PEFs and EDMFs has been applied to two molecules of great interest to astrochemistry, *i.e.*, hydrogen cyanide HCN and the tricarbon molecule C_3. In the case of HCN three different PEFs were calculated that are based on either single-reference coupled-cluster theory or the multi-reference methods MRCI and MR-ACPF. The comparison with experimental data for the fundamental transitions in HCN [17] has shown that the single-reference based PEF is clearly superior to the MR based ones due to the need for higher-order excitations in the treatment of dynamical correlation. Large-scale variational calculations with the single-reference PEF for states up to the first overtone of the CH streching vibrational $(2, 0^0, 0)$ and rotational excitation up to $J = 20$ yield almost perfect agreement with experiment. This encompasses term energies for more than 3000 rovibrational states. The results have also been compared to those presented by Makhnev and coworkers [241]. The

latter work claimed that it is important to include non-Born-Oppenheimer effects in order to reach an accuracy of better than 1 cm^{-1} in the vibrational term energies. However, the comparison with the present results has shown that the non-Born-Oppenheimer contribution used by Makhnev *et al.* is better understood as an empirical correction to the PEF which accounts for shortcomings of their *ab initio* treatment. The intensities of rovibrational transitions calculated with the present composite EDMF show excellent agreement with experiment even better than the second work by Makhnev *et al.* [242] on rovibrational intensities in HCN. Specifically, the strong CH stretching and bending fundamental intensities are within about 2 % of the experimental results [21, 23] thereby reaching the accuracy of experimental intensity measurments. The weak CN fundamental band with its R-branch intensity minimum is accurately reproduced by the present calculations. A comparison of different PEF/EDMF combinations has shown that the smaller contributions are of utmost importance to give quantitative agreement with experiment.
The rovibrational spectrum of C_3 is dominated by anharmonic effects and strong rovibrational coupling. As such it demonstrates the necessity of an appropriate treatment of the rovibrational problem. The PEF developed for C_3 when employed in variational calculations yields accurate spectroscopic parameters for low-lying vibrational states in comparison with experiment. In contrast, spectroscopic parameters obtained with VPT2 using the composite PEF results in large discrepancies with the variational calculations and the experimental data. The high quality of the PEF has allowed accurate predictions of spectroscopic parameters for virbational states previously unobserved. In a combined experimental/theoretical study 14 new $n\nu_1 + m\nu_3$ combination bands of C_3 ($n \leq 7$ and $m \leq 3$) have been detected in a supersonically expanding propyne plasma [29]. The excellent agreement between theory and experiment has justified taking the understanding of the rovibrational coupling present in C_3 a step further. This has been achieved by investigating the angular dependence of the integrated vibrational density (Equation (3.14)). The main conclusion is that, depending on the degree of stretching vibrational excitation (v_1 symmetric stretching, v_3 antisymmetric stretching) the vibrational wave function accumulates most of its density at larger ($v_3 > v_1$) or smaller ($v_1 > v_3$) deviations from linearity θ. Because of the growing bent character when the antisymmetric stretching vibration is excited C_3 might be referred to as a "quasi-bent" molecule.

With a reliable composite approach established the next step in this thesis has been the development of a variational program for tetraatomic linear molecules as presented in Chapter 4 where the implementation of C8V4 is discussed. The choice for a normal coordinate based approach is predicated on the requirement of simultaneously treating vibrational and rotational motion. While internal coordinates often lend themselves to a description of vibrational motion which converges faster in variational calculations [211], the kinetic coupling to the rotational motion is complicated. In case of normal coordinates, which are determined from the Eckart conditions [135], rovibrational coupling is minimized. In fact, the term $\hat{T}_{VR}$ in the Hamiltonian (Equation (4.34)) is the smallest contribution to the rovibrational term energy. The variational *ansatz* of the presented C8V4 program employs harmonic oscillator and rigid rotor product functions. The intricacies of the

vibrational angular momentum require a careful study of the symmetry properties of the rovibrational coordinates. This has lead to the formulation of a symmetry adapted basis which takes full account of the linear molecule MS groups $\boldsymbol{C}_{\infty v}(\mathrm{M})$ or $\boldsymbol{D}_{\infty h}(\mathrm{M})$.

An efficient integration of the Hamiltonian has been a key point in the development of C8V4. A typical calculation employs about 3000 to 5000 primitive vibrational basis functions and a maximum vibrational angular momentum $\ell^K_{\max} = 4 + K$ which results in a $J = 1$ Hamiltonian with ca. 60000 basis functions. This requires the accurate evaluation of more than $5 \cdot 10^8$ matrix elements. Kinetic energy matrix elements can be evaluated either by analytical integration or by a fast mixed numerical/analytical scheme based on a truncated resolution-of-the-identity approach. The main computational bottleneck is the calculation of potential energy matrix elements which is performed by six-dimensional Hermite-Laguerre-Chebyshev-Gaussian integration. To reduce the computational effort a hybrid parallelisation has been implemented. It is based on the block structure of the Hamiltonian Matrix and uses MPI to distribute the blocks between the nodes of a compute cluster as well as OMP to parallelize the the numerical integration. Analysis of the achievable speed ups has allowed to decide between three different implementations of the latter parallelisation.

The diagonalisation of the Hamiltonian presents another bottleneck in the variational procedure. The largest Hamiltonian encountered in this work contains about 180000 basis functions. Using double precision arithmetics this requires ca. 240 GB of memory to keep the full Hamiltonian in RAM which clearly is too large. Therefore, the block structure of the Hamiltonian is again exploited to reduce this number. As pointed out before, the Coriolis operator $\hat{\mathrm{T}}_{\mathrm{VR}}$ is the smallest contribution to the term energy and it only couples basis functions with $\Delta K = \pm 1$. A prediagonalisation scheme has been presented which reduces the diagonalisation of the full Hamiltonian for a given value of $J > 0$ into $J + 1$ diagonalisations of the much smaller K-diagonal blocks. Using a subset of the eigenvalues in each block the Coriolis matrix is transformed to the new basis. This effects a reduction of the rovibrational basis set by at least two orders of magnitude. The reduced Hamiltonian is then small enough to employ conventional dense matrix diagonalisers. The convergence of this approximation is controlled by the number of retained K-diagonal eigenvalue/eigenvector pairs. To further reduce the wall time of the diagonalisation, the K-block contraction is based on Davidson diagonalisation as implemented in the JADAMILU diagonaliser [355, 356] and has been hybrid parallelised with respect to the required matrix-vector products. Finally, example calculations for two linear tetraatomic molecules have been presented which confirm the correctness of the implementation.

Going forward, further developments of the C8V4 program are possible and would allow the extension of its capabilities. In its current implementation the rovibrational wave functions are only used to analyze the character of the rovibrational states and assign approximate quantum numbers on the basis of the dominant harmonic basis functions. The next step would be the calculation of squared transition dipole moments and the theoretical groundwork for this has been presented in Section 2.3.4. The main problem will be the calculation of the matrix elements of the dipole

operator (Equation (2.97) - (2.99)) over vibrational basis functions. By analysis of the expansion of dipole moment with respect to the normal coordinates the non-vanishing matrix elements can be worked out which could be evaluated by analytical integration. In the expansion of the EDMF in internal coordinates $\boldsymbol{\mathcal{R}}$ a similar treatment as presented in Section 4.1.3 is needed for the evaluation of the matrix elements. This raises an important challenge in the implementation of rovibrational intensities for tetraatomic linear molecules. With respect to the calculation of term energies the potential energy which requires numerical integration only contributes to the K-diagonal blocks. This is not the case for dipole moment matrix elements where $|\Delta K| = 1$ matrix elements are required. Furthermore, the non-linear transformation between $\boldsymbol{\mathcal{R}}$ and the normal coordinates does not allow to neglect certain blocks characterized by combinations $(\ell_4, \ell_5, K//\ell_4', \ell_5', K \pm 1)$ since these matrix elements will not be zero as was the case with the Coriolis operator $\hat{\mathrm{T}}_{\mathrm{VR}}$. The number of blocks to be evaluated with the numerical integration is then significantly larger than for the potential energy. A possible solution to this would be to transform the internal coordinate EDMF into a truncated normal coordinate expansion beforehand. This is similar to the approach commonly used in VPT applications where an arbitrary order internal coordinate PEF expansion is transformed to a finite order expansion normal coordinates. By truncating the EDMF in normal coordinates at a certain order n also the number of blocks to be evaluated is reduced since now matrix elements for certain combinations with $\Delta\ell_5 > n$ will vanish. Even more significant, the non-zero matrix elements can now be evaluated by fast analytical integration.

With the methods developed here, variational calculations beyond tetraatomic molecules becomes at least theoretically possible. Increasing the number of atoms from 4 to 5 results in $3N_{\mathrm{at}} - 5 = 10$ vibrational degrees of freedom where 3 are bending modes. The latter will thus result in 3 phase angles χ_t. Analogous to the tetraatomic case, only two differences of the χ_t are independent and one of the angles can be chosen to have the same effect on the rigid molecule as the Euler angle χ' (cf. Figure 4.5). The problem is again the Sayvetz condition Equation (2.43) which leads to a non-direct product basis structure (not all combinations of the ℓ_t are allowed for a given K). Restricting the vibrational angular moment quantum numbers for $K = 0$ to a value of, e.g., $\ell^0_{\mathrm{max}} = 2$ the number of possible (symmetry adapted) triples (ℓ_5, ℓ_6, ℓ_7) is 10: $(0, 0, 0)$ as well as three permutations each for the combinations $(1, -1, 0)$, $(2, -2, 0)$ and $(2, -1, -1)$. The number of K-diagonal blocks is therefore almost the same as for the $J = 1$ e-parity Hamiltonian in the tetraatomic case with $\ell^0_{\mathrm{max}} = 2$ which on top of it has been shown to be insufficient for converged results. Further taking the required size of the primitive vibrational basis set for converged calculations in the 5 atoms case into account, which could very well reach more 10000 even for pruned basis sets, renders an FBR approach and employing a Davidson diagonalisation unfeasible. A possible solution would be to change to an iterative eigensolver based on the Lanczos algorithm [385]. The eigenvalues of the Hamiltonian are then obtained by evaluating matrix-vector products with the M_L so called Lanczos-vectors to obtain a $M_L \times M_L$ tridiagonal matrix whose eigenvalue spectrum will contain the eigenvalues of the Hamiltonian. The matrix-vector products can then be formulated using for example Gaussian integration and does not require the explicit construction of the Hamiltonian

matrix. The Lanczos approach has been applied for example by Carrington *et al.* to calculate rovibrational energy levels of methane isotopologues [386] with $3N_{\mathrm{at}} - 6 = 9$ vibrational degrees of freedom.

Combining the results of Chapter 3 and 4 a study of the rovibrational spectrum of l-C_3H^+ has been presented in Chapter 5. The C8v4 calculations employing the QFF constructed by Huang *et al.* [365] conclusively show that the large H_0 value obtained by Mladenović [30] is incorrect. Building up on the previous work by Stein *et al.* [381] a full dimensional PEF designed for variational applications has been developed. Variational calculations yield ground state rotational parameters in excellent agreement with the astronomical data. For B_0 a deviation of less than 5 MHz is obtained. A close relation to "floppy" C_3 has been established by comparing the PEFs in both systems. This has lead to the assumption that l-C_3H^+ behaves in a sense like a “protonated” albeit much more rigid C_3. An analysis of the rotational parameters and their vibrational dependence has confirmed this expectation. The calculated spectroscopic parameters of excited vibrational states should facilitate forthcoming experimental spectroscopic studies on l-C_3H^+. In fact, the propyne plasma spectrum presented in Section 3.2.4 might contain transitions due to l-C_3H^+. The ν_1 CH fundamental around 3170 cm^{-1} and its Fermi-resonance partner $\nu_2 + \nu_3$ around 3268 cm^{-1} are well within the covered spectral range and the work of Stein and coworkers [381] suggested that ν_1 should have an intensity that allows detection. A search for l-C_3H^+ ν_1 and $\nu_2 + \nu_3$ rovibrational transitions in the propyne plasma spectrum informed by the results of Chapter 5 is currently underway in the Linnartz group. A positive detection of l-C_3H^+ will provide another example of the spectacular interplay of theory and experiment in rovibrational spectroscopy.

Bibliography

[1] M. Born and W. Heisenberg. Zur Quantentheorie der Molekeln. *Ann. Phys.*, 379:1–31, 1924.

[2] M. Born and J. R. Oppenheimer. Zur Quantentheorie der Molekeln. *Ann. Phys.*, 389:457–484, 1927.

[3] H. S. P. Müller, S. Thorwirth, D. A. Roth, and G. Winnewisser. The Cologne Database for Molecular Spectroscopy, CDMS. *Astron. Astrophys.*, 370:L49–L52, 2001.

[4] H. S. P. Müller, F. Schlöder, J. Stutzki, and G. Winnewisser. The Cologne Database for Molecular Spectroscopy, CDMS: a useful tool for astronomers and spectroscopists. *J. Mol. Struct.*, 742:215–227, 2005.

[5] C. P. Endres, S. Schlemmer, P. Schilke, J. Stutzki, and H. S. P. Müller. The Cologne Database for Molecular Spectroscopy, CDMS, in the Virtual Atomic and Molecular Data Centre, VAMDC. *J. Mol. Spectrosc.*, 327:95–104, 2016.

[6] R. C. Fortenberry. Quantum astrochemical spectroscopy. *Int. J. Quant. Chem.*, 117:81–91, 2017.

[7] D. Buhl and L. E. Snyder. Unidentified Interstellar Microwave Line. *Nature*, 228:267–269, 1970.

[8] W. Klemperer. Carrier of the Intersteller 89.190 GHz Line. *Nature*, 227:1230, 1970.

[9] R. C. Woods, T. A. Dixon, R. J. Saykally, and P. G. Szanto. Laboratory Microwave Spectrum of HCO^+. *Phys. Rev. Lett.*, 35:1269–1272, 1975.

[10] K. Kawaguchi, Y. Kasai, S.-I. Ishikawa, and N. Kaifu. A Spectral-Line Survey Observation of IRC +10216 between 28 and 50 GHz. *Publ. Astron. Soc. Jpn.*, 47:853–876, 1995.

[11] J. Cernicharo, M. Guélin, M. Agúndez, M. C. McCarthy, and P. Thaddeus. Detection of C_5N^- and Vibrationally Excited C_6H in IRC+10216. *Astrophys. J.*, 688:L83–L86, 2008.

[12] P. Botschwina. The two lowest electronic states of C_5N: results of coupled cluster calculations. *Chem. Phys. Lett.*, 259:627–634, 1996.

[13] Y. Kasai, Y. Sumiyoshi, Y. Endo, and K. Kawaguchi. Laboratory Detection of the C_5N Radical by Fourier Transform Microwave Spectroscopy. *Astrophys. J. Lett.*, 477:L65–L67, 1997.

[14] M. Guélin, N. Neininger, and J. Cernicharo. Astronomical detection of the cyanobutadiynyl radical C_5N. *Astron. Astrophys.*, 335:L1–L4, 1998.

[15] M. C. McCarthy, C. A. Gottlieb, H. Gupta, and P. Thaddeus. Laboratory and Astronomical Identification of the Negative Molecular Ion C_6H^-. *Astrophys. J. Lett.*, 652:L141–L144, 2006.

[16] P. Botschwina and R. Oswald. Carbon chains of type $C_{2n+1}N^-$ $(n = 2 - 6)$: A theoretical study of potential interstellar anions. *J. Chem. Phys.*, 129:044305, 2008.

[17] G. C. Mellau. Complete experimental rovibrational eigenenergies of HCN up to 6880 cm^{-1} above the ground state. *J. Chem. Phys.*, 134:234303, 2011.

[18] A. Maki, W. Quapp, S. Klee, G. C. Mellau, and S. Albert. The CN Mode of HCN: A Comparative Study of the Variation of the Transition Dipole and Herman-Wallis Constants for Seven Isotopomers and the Influence of Vibration-Rotation Interaction. *J. Mol. Spectrosc.*, 174:365–378, 1995.

[19] A. Maki, W. Quapp, and S. Klee. Intensities of Hot-Band Transitions: HCN Hot Bands. *J. Mol. Spectrosc.*, 171:420–434, 1995.

[20] A. Maki, W. Quapp, S. Klee, G. C. Mellau, and S. Albert. Intensity Measurements of $\Delta l > 1$ Transitions of Several Isotopomers of HCN. *J. Mol. Spectrosc.*, 185:356–369, 1997.

[21] V. M. Devi, D. C. Benner, M. A. H. Smith, C. P. Rinsland, , S. W. Sharpe, and R. L. Sams. A multispectrum analysis of the ν_1 band of $H^{12}C^{14}N$: Part I. Intensities, self-broadening and self-shift coefficients. *J. Quant. Spectrosc. Radiat. Transf.*, 82:319–341, 2003.

[22] V. M. Devi, D. C. Benner, M. A. H. Smith, C. P. Rinsland, , S. W. Sharpe, and R. L. Sams. A multispectrum analysis of the $2\nu_2$ spectral region of $H^{12}C^{14}N$: untensities, broadening and pressure-shift coefficients. *J. Quant. Spectrosc. Radiat. Transf.*, 87:339–366, 2004.

[23] V. M. Devi, D. C. Benner, M. A. H. Smith, C. P. Rinsland, A. Predoi-Cross, S. W. Sharpe, R. L. Sams, C. Boulet, and J. P. Bouanich. A multispectrum analysis of the ν_2 band of $H^{12}C^{14}N$: Part I. Intensities, broadening, and shift coefficients. *J. Mol. Spectrosc.*, 231:66–84, 2005.

[24] M. A. H. Smith, C. P. Rinsland, T. A. Blake, R. L. Sams, D. C. Benner, and V. M. Devi. Low-temperature measurments of HCN broadened by N_2 in the 14-μm spectral region. *J. Quant. Spectrosc. Radiat. Transf.*, 109:922–951, 2008.

[25] P. Jensen, C. M. Rohlfing, and J. Almlöf. Calculation of the complete-active-space self-consistent-field potential-energy surface, the dipole moment surfaces, the rotation-vibration

energies, and the vibrational transistion moments for C_3 ($\tilde{X}\,^1\Sigma_g^+$). *J. Chem. Phys.*, 89:3399–3411, 1992.

[26] M. Mladenović, S. Schmatz, and P. Botschwina. Large-scale *ab initio* calculations for C_3. *J. Chem. Phys.*, 101:5891, 1994.

[27] F. J. Northrup, T. J. Sears, and E. A. Rohlfing. A Semirigid Bender Analysis of an Extensive Set of Rotation-Vibration Levels in $\tilde{X}^1\Sigma_g^+$ C_3. *J. Mol. Spectrosc.*, 145:74–88, 1991.

[28] B. Schröder and P. Sebald. High-level theoretical rovibrational spectroscopy of HCS^+ isotopologues. *J. Mol. Spectrosc.*, 330:120–129, 2016.

[29] B. Schröder, K. D. Doney, P. Sebald, D. Zhao, and H. Linnart. Stretching our understanding of C_3: Experimental and theoretical spectroscopy of highly excited $n\nu_1 + m\mu_3$ states ($n \leq 7$ and $m \leq 3$). *J. Chem. Phys.*, 149:014302, 2018.

[30] M. Mladenović. The B11244 story: Rovibrational calculations for C_3H^+ and C_3H^- revisited. *J. Chem. Phys.*, 141:224304, 2014.

[31] I. Shavitt. The Method of Configuration Interaction. In H. F. Schaefer, editor, *Modern theoretical chemistry*, volume 3, page 189. Plenum Press, New York, 1977.

[32] D. R. Hartree. The Wave Mechanics of an Atom with a Non-Coulomb Central Field. Part I. Theory and Methods. *Math. Proc. Camb. Phil. Soc.*, 24:89—110, 1928.

[33] V. Fock. Näherungsmethode zur Lösung des quantenmechanischen Mehrkörperproblems. *Z. Physik*, 61:126–148, 1930.

[34] C. C. J. Roothaan. New Developments in Molecular Orbital Theory. *Rev. Mod. Phys.*, 23:69–89, 1951.

[35] C. C. J. Roothaan. Self-Consistent Field Theory for Open Shells of Electronic Systems. *Rev. Mod. Phys.*, 32:179–185, 1960.

[36] G. G. Hall. The molecular orbital theory of chemical valency VIII. A method of calculating ionization potentials. *Proc. Roy. Soc. A*, 205:541–552, 1951.

[37] L. Brillouin. La méthod du champ self-consistent. *Actualités sci. et ind.*, 71, 1933.

[38] L. Brillouin. Les champs 'self-consistent' de Hartree et de Fock. *Actualités sci. et ind.*, 159, 1934.

[39] J. A. Pople, R. Seeger, and R. Krishnan. Variational configuration interaction methods and comparison with perturbation theory. *Int. J. Quant. Chem.*, 12:149–163, 1977.

[40] S. R. Langhoff and E. R. Davidson. Configuration interaction calculations on the nitrogen molecule. *Int. J. Quant. Chemi.*, 8:61–72, 1974.

[41] F. Coester and Kümmel. Short-range correlations in nuclear wave functions. *Nucl. Phys.*, 17:477, 1960.

[42] J. Čížek. On the Correlation Problem in Atomic and Molecular Systems. Calculation of Wavefunction Components in Ursell-Type Expansion Using Quantum-Field Theoretical Methods. *J. Chem. Phys.*, 45:4256, 1966.

[43] T. Dunning. Gaussian Basis Sets for Use in Correlated Molecular Calculations. I. The Atoms Boron through Neon and Hydrogen. *J. Chem. Phys.*, 90:1007–1023, 1989.

[44] D. Feller. Application of systematic sequences of wave functions to the water dimer. *J. Chem. Phys.*, 96(8):6104–6114, 1992.

[45] A. J. C. Varandas. Basis-set extrapolation of the correlation energy. *J. Chem. Phys.*, 113:8880–8887, 2000.

[46] R. J. Gdanitz. Accurately solving the electronic Schrödinger equation of atoms and molecules by extrapolating to the basis set limit. I. The helium dimer (He_2). *J. Chem. Phys.*, 113:5145–5153, 2000.

[47] A. J. C. Varandas. Extrapolating to the one-electron basis-set limit in electronic structure calculations. *J. Chem. Phys.*, 126:244105, 2007.

[48] A. Karton, P. R. Taylor, and J. M. L. Martin. Basis set convergence of post-CCSD contributions to molecular atomization energies. *J. Chem. Phys.*, 127:064104, 2007.

[49] D. Feller and K. A. Peterson. High level coupled cluster determination of the structure, frequencies, and heat of formation of water. *J. Chem. Phys.*, 131:154306, 2009.

[50] D. Feller, K. A. Peterson, and B. Ruscic. Improved accuracy benchmarks of small molecules using correlation consistent basis sets. *Theor. Chem. Acc.*, 133:1407, 2014.

[51] W. Kutzelnigg and W. Klopper. Wave functions with terms linear in the interelectronic coordinates to take care of the correlation cusp. I. General theory. *J. Chem. Phys.*, 94:1985–2001, 1991.

[52] T. B. Adler, G. Knizia, and H.-J. Werner. A simple and efficient CCSD(T)-F12 approximation. *J. Chem. Phys.*, 127:221106, 2007.

[53] W. Kutzelnigg. *Ab initio* calculation of molecular properties. *J. Mol. Struct. (THEOCHEM)*, 202:11–61, 1989.

[54] T. B. Pedersen. Introduction to Response Theory. In J. Leszczynski, editor, *Handbook of Computational Chemistry*, pages 135–156. Springer, 2012.

[55] J. M. L. Martin, T. J. Lee, P. R. Taylor, and J.-P. François. The anharmonic force field of ethylene, C_2H_4, by means of accurate *ab initio* calculations. *J. Chem. Phys.*, 103:2589–2602, 1995.

[56] J. M. L. Martin, T. J. Lee, and P. R. Taylor. A purely *ab initio* spectroscopic quality quartic force field for acetylene. *J. Chem. Phys.*, 108:676–691, 1998.

[57] P. Botschwina, S. Seeger, M. Mladenović, B. Schulz, M. Horn, S. Schmatz, J. Flügge, and R. Oswald. Quantum-chemical investigations of small molecular anions. *Int. Rev. Phys. Chem.*, 169:14, 1995.

[58] P. Botschwina, M. Horn, M. Matuschewski, E. Schick, and P. Sebald. Hydrogen cyanide: theory and experiment. *J. Mol. Struct. (THEOCHEM)*, 400:119–137, 1997.

[59] A. Karton. A computational chemist's guide to accurate thermochemistry for organic molecules. *Wiley Interdiscip. Rev. Comput. Mol. Sci.*, 6:292–310, 2016.

[60] W. Kutzelnigg. The adiabatic approximation I. The physical background of the Born-Handy ansatz. *Mol. Phys.*, 90:909–916, 1997.

[61] G. Knizia, T. B. Adler, and H.-J. Werner. Simplified CCSD(T)-F12 methods: Theory and benchmarks. *J. Chem. Phys.*, 130:054104, 2009.

[62] R. Achilles and A. Bonfiglioli. The early proofs of the theorem of Campbell, Baker, Hausdorff, and Dynkin. *Arch. Hist. Exact Sci.*, 66:295–358, 2012.

[63] T. Helgaker, P. Jørgensen, and J. Olsen. *Molecular Electronic-Structure Theory.* John Wiley & Sons Ltd., 2000.

[64] G. D. Purvis and R. J. Bartlett. A full coupled-cluster singles and doubles model: The inclusion of disconnected triples. *J. Chem. Phys.*, 76:1910–1918, 1982.

[65] R. J. Bartlett and M. Musiał. Coupled-cluster theory in quantum chemistry. *Rev. Mod. Phys.*, 79:291–352, 2007.

[66] J. Noga and R. J. Bartlett. The full CCSDT model for molecular electronic structure. *J. Chem. Phys.*, 86:7041–7050, 1987.

[67] G. E. Scuseria and H. F. Schaefer. A new implementation of the full CCSDT model for molecular electronic structure. *Chem. Phys. Lett.*, 152:382–386, 1988.

[68] K. Raghavachari, G. W. Trucks, J. A. Pople, and M. Head-Gordon. A fifth-order perturbation comparison of electron correlation theories. *Chem. Phys. Lett.*, 157:479–483, 1989.

[69] M. E. Harding, J. Vázquez, B. Ruscic, A. K. Wilson, J. Gauss, and J. F. Stanton. High-accuracy extrapolated *ab initio* thermochemistry. III. Additional improvements and overview. *J. Chem. Phys.*, 128:114111, 2008.

[70] J. Řezáč and P. Hobza. Describing Noncovalent Interactions beyond the Common Approximations: How Accurate Is the "Gold Standard," CCSD(T) at the Complete Basis Set Limit? *J. Chem. Theory Comput.*, 9:2151–2155, 2013.

[71] J. M. L. Martin and M. K. Kesharwani. Assessment of CCSD(T)-F12 Approximations and Basis Sets for Harmonic Vibrational Frequencies. *J. Chem. Theory Comput.*, 10:2085–2090, 2014.

[72] M. Kállay and Surján. Higher excitations in Coupled-Cluster theory. *J. Chem. Phys.*, 115:2945–2954, 2001.

[73] Y. L. Bomble, J. F. Stanton, M. Kállay, and J. Gauss. Coupled-Cluster methods including noniterative corrections for quadriuple excitations. *J. Chem. Phys.*, 123:054101, 2005.

[74] M. Kállay, P. R. Nagy, Z. Rolik, D. Mester, G. Samu, J. Csontos, J. Csóka, B. P. Szabó, L. Gyevi-Nagy, I. Ladjánszki, L. Szegedy, B. Ladóczki, K. Petrov, M. Farkas, P. D. Mezei, and B. Hégely. MRCC, a quantum chemical program suite. See: `www.mrcc.hu`.

[75] Z. Rolik, L. Szegedy, I. Ladjánszki, B. Ladóczki, and M. Kállay. An efficient linear-scaling CCSD(T) method based on local natural orbitals. *J. Chem. Phys.*, 139:094105, 2013.

[76] M. Musiał and R. J. Bartlett. Critical comparison of various connected quadruple excitation approximations in the coupled-cluster treatment of bond breaking. *J. Chem. Phys.*, 122(22):224102, 2005.

[77] J. B. Robinson and P. J. Knowles. Benchmark Quasi-Variational Coupled Cluster Calculations of Multiple Bond Breaking. *J. Chem. Theory Comput.*, 8:2653–2660, 2012.

[78] K. R. Yang, A. Jalan, W. H. Green, and D. G. Truhlar. Which *Ab Initio* Wave Function Methods Are Adequate for Quantitative Calculations of the Energies of Biradicals? The Performance of Coupled-Cluster and Multi-Reference Methods Along a Single-Bond Dissociation Coordinate. *J. Chem. Theory Comput.*, 9:418–431, 2013.

[79] H. Lischka, D. Nachtigallová, A. J. A. Aquino, P. Szalay, F. Plasser, F. B. C. Machado, and M. Barbatti. Multireference Approaches for Excited States of Molecules. *Chem. Rev.*, 118:7293–7361, 2018.

[80] D. R. Yarkony. Diabolical conical intersections. *Rev. Mod. Phys.*, 68:985–1013, 1996.

[81] A. J. C. Varandas, A. I. Voronin, and P. Jimeno. Conical intersections between the two lowest $^1A'$ potential energy surfaces of HCN, and the role of three-body effects. *J. Chem. Phys.*, 107:10014–10028, 1997.

[82] A. J. C. Varandas and Z. R. Xu. Nuclear dynamics in the vicinity of the crossing seam: Theory and application to vibrational spectrum of H_3. *J. Chem. Phys.*, 112:2121–2127, 2000.

[83] T. Shiozaki and H.-J. Werner. Explicitly correlated multireference configuration interaction with multiple reference functions: Avoided crossings and conical intersections. *J. Chem. Phys.*, 134:184104, 2011.

[84] C. M. R. Rocha and A. J. C. Varandas. Accurate *ab initio*-based double many-body expansion potential energy surface for the adiabatic ground-state of the C_3 radical including combined Jahn-Teller plus pseudo-Jahn-Teller interactions. *J. Chem. Phys.*, 143:074302, 2015.

[85] C. M. R. Rocha and A. J. C. Varandas. The Jahn-Teller plus pseudo-Jahn-Teller vibronic problem in the C_3 radical and its topological implications. *J. Chem. Phys.*, 144:064309, 2016.

[86] P. Siegbahn, A. Heiber, B. Roos, and B. Levy. A Comparison of the Super-CI and the Newton-Raphson Scheme in the Complete Active Space SCF Method. *Phys. Scripta*, 21:323–327, 1979.

[87] B. O. Roos, P. R. Taylor, and P. E. M. Siegbahn. A complete active space SCF method (CASSCF) using a density matrix formulated super-CI approach. *Chem. Phys.*, 48:157–173, 1980.

[88] P. E. M. Siegbahn, J. Almlöf, A. Heiberg, and B. O. Roos. The complete active space SCF (CASSCF) method in a Newton–Raphson formulation with application to the HNO molecule. *J. Chem. Phys.*, 74:2384–2396, 1981.

[89] P. J. Knowles and H.-J. Werner. An efficient second-order MC SCF method for long configuration expansions. *Chem. Phys. Lett.*, 115:259–267, 1985.

[90] H.-J. Werner and P. J. Knowles. A second order multiconfiguration SCF procedure with optimum convergence. *J. Chem. Phys.*, 82:5053–5063, 1985.

[91] J. Olsen, B. O. Roos, P. Jørgensen, and H. J. A. Jensen. Determinant based configuration interaction algorithms for complete and restricted configuration interaction spaces. *J. Chem. Phys.*, 89:2185–2192, 1988.

[92] B. O. Roos, P. Per Linse, P. E. M. Siegbahn, and M. A. R. Blomberg. A simple method for the evaluation of the second-order-perturbation energy from external double-excitations with a CASSCF reference wavefunction. *Chem. Phys.*, 66:197–207, 1982.

[93] K. Andersson, P.-Å. Malmqvist, B. O. Roos, A. J. Sadlej, and K. Wolinski. Second-order perturbation theory with a CASSCF reference function. *J. Phys. Chem.*, 94:5483–5488, 1990.

[94] K. Hirao. Multirefernce Møller-Plesset method. *Chem. Phys. Lett.*, 190:374–380, 1992.

[95] K. Andersson, P.-Å. Malmqvist, and B. O. Roos. Second-order perturbation theory with a complete active space self-consistent field reference function. *J. Chem. Phys.*, 96:1218–1226, 1992.

[96] H.-J. Werner. Third-order multireference perturbation theory. The CASPT3 method. *Mol. Phys.*, 89:645–661, 1996.

[97] J. Finley, P.-Å. Malmqvist, B. O. Roos, and L. Serrano-Andrés. The multi-state CASPT2 method. *Chem. Phys. Lett.*, 288:299–306, 1998.

[98] P. Celani and H.-J. Werner. Multireference perturbation theory for large restricted and selected active space reference wave functions. *J. Chem. Phys.*, 112:5546–5557, 2000.

[99] C. Angeli, R. Cimiraglia, S. Evangelisti, T. Leininger, and J.-P. Malrieu. Introduction of n-electron valence states for multireference perturbation theory. *J. Chem. Phys.*, 114:10252–10264, 2001.

[100] F. Aquilante, P.-Å. Malmqvist, T. B. Pedersen, A. Ghosh, and B. O. Roos. Cholesky Decomposition-Based Multiconfiguration Second-Order Perturbation Theory (CD-CASPT2): Application to the Spin-State Energetics of Co^{III}(diiminato)(NPh). *J. Chem. Theory Comput.*, 4:694–702, 2008.

[101] Y. Kurashige and T. Yanai. Second-order perturbation theory with a density matrix renormalization group self-consistent field reference function: Theory and application to the study of chromium dimer. *J. Chem. Phys.*, 135:094104, 2011.

[102] R. J. Gdanitz and R. Ahlrichs. The averaged coupled-pair functional (ACPF): A size-extensive modification of MR CI(SD). *Chem. Phys. Lett.*, 143:413–420, 1988.

[103] U. S. Mahapatra, B. Datta, B. Bandyopadhyay, and D. Mukherjee. State-Specific Multi-Reference Coupled Cluster Formulations: Two Paradigms. In P.-O. Löwdin, editor, *Advances in Quantum Chemistry*, volume 30, pages 163–193. Academic Press, 1998.

[104] D. Mukherjee, R. K. Moitra, and A. Mukhopadhyay. Correlation problem in open-shell atoms and molecules. *Mol. Phys.*, 30:1861–1888, 1975.

[105] B. Jeziorski and H. J. Monkhorst. Coupled-cluster method for multideterminantal reference states. *Phys. Rev. A*, 24:1668–1681, 1981.

[106] U. S. Mahapatra, B. Datta, and D. Mukherjee. A size-consistent state-specific multireference coupled cluster theory: Formal developments and molecular applications. *J. Chem. Phys.*, 110:6171–6188, 1999.

[107] F. A. Evangelista and J. Gauss. An orbital-invariant internally contracted multireference coupled cluster approach. *J. Chem. Phys.*, 134:114102, 2011.

[108] M. Hanauer and A. Köhn. Pilot applications of internally contracted multireference coupled cluster theory, and how to choose the cluster operator properly. *J. Chem. Phys.*, 134:204111, 2011.

[109] D. Datta, L. Kong, and M. Nooijen. A state-specific partially internally contracted multireference coupled cluster approach. *J. Chem. Phys.*, 134:214116, 2011.

[110] F. A. Evangelista, W. D. Allen, and H. F. Schaefer. Coupling term derivation and general implementation of state-specific multireference coupled cluster theories. *J. Chem. Phys.*, 127(2):024102, 2007.

[111] F. A. Evangelista and J. Gauss. Insights into the orbital invariance problem in state-specific multireference coupled cluster theory. *J. Chem. Phys.*, 133(4):044101, 2010.

[112] R. J. Buenker and S. D. Peyerimhoff. CI method for the study of general molecular potentials. *Theor. Chim. Acta.*, 12:183–199, 1968.

[113] R. J. Buenker and S. D. Peyerimhoff. Individualized configuration selection in CI calculations with subsequent energy extrapolation. *Theor. Chim. Acta.*, 35:33–58, 1974.

[114] R. J. Buenker and S. D. Peyerimhoff. Energy extrapolation in CI calculations. *Theor. Chim. Acta.*, 39:217–228, 1975.

[115] W. Meyer. Configuration Expansion by Means of Pseudonatural Orbitals. In H. F. Schaefer, editor, *Modern theoretical chemistry*, volume 3, page 413. Plenum Press, New York, 1977.

[116] H.-J. Werner and E.-A. Reinsch. The self-consistent electron pairs method for multiconfiguration reference state functions. *J. Chem. Phys.*, 76:3144–3156, 1982.

[117] H.-J. Werner and P. J. Knowles. An efficient internally contracted multiconfiguration–reference configuration interaction method. *J. Chem. Phys.*, 89:5803–5814, 1988.

[118] E. R. Davidson and D. W. Silver. Size consistency in the dilute helium gas electronic structure. *Chem. Phys. Lett.*, 52:403–406, 1977.

[119] T. Kato. On the eigenfunctions of many-particle systems in quantum mechanics. *Commun. Pure Appl. Math.*, 10:151–177, 1957.

[120] E. A. Hylleraas. Neue Berechnung der Energie des Heliums im Grundzustande, sowie des tiefsten Terms von Ortho-Helium. *Z. Physik*, 54:347–366, 1929.

[121] V. Termath, W. Klopper, and W. Kutzelnigg. Wave functions with terms linear in the interelectronic coordinates to take care of the correlation cusp. II. Second-order Møller–Plesset (MP2-R12) calculations on closed-shell atoms. *J. Chem. Phys.*, 94:2002–2019, 1991.

[122] W. Klopper and W. Kutzelnigg. Wave functions with terms linear in the interelectronic coordinates to take care of the correlation cusp. III. Second-order Møller-Plesset (MP2-R12) calculations on molecules of first row atoms. *J. Chem. Phys.*, 94:2020–2030, 1991.

[123] S. Ten-no. Initiation of explicitly correlated Slater-type geminal theory. *Chem. Phys. Lett.*, 398:56–61, 2004.

[124] K. A. Peterson, T. B. Adler, and H.-J. Werner. Systematically convergent basis sets for explicitly correlated wavefunctions: The atoms H, He, B–Ne, and Al–Ar. *J. Chem. Phys.*, 128:084102, 2008.

[125] H.-J. Werner, P. J. Knowles, G. Knizia, F. R. Manby, M. Schütz, P. Celani, W. Györffy, D. Kats, T. Korona, R. Lindh, A. Mitrushenkov, G. Rauhut, K. R. Shamasundar, T. B. Adler, R. D. Amos, S. J. Bennie, A. Bernhardsson, A. Berning, D. L. Cooper, M. J. O. Deegan, A. J. Dobbyn, F. Eckert, E. Goll, C. Hampel, A. Hesselmann, G. Hetzer, T. Hrenar, G. Jansen, C. Köppl, S. J. R. Lee, Y. Liu, A. W. Lloyd, Q. Ma, R. A. Mata, A. J. May, S. J. McNicholas, W. Meyer, T. F. Miller III, M. E. Mura, A. Nicklass, D. P. O'Neill, P. Palmieri, D. Peng, K. Pflüger, R. Pitzer, M. Reiher, T. Shiozaki, H. Stoll, A. J. Stone, R. Tarroni, T. Thorsteinsson, M. Wang, and M. Welborn. MOLPRO, version 2019.1, a package of ab initio programs, 2012. see http://www.molpro.net.

[126] T. Shiozaki, G. Knizia, and H.-J. Werner. Explicitly correlated multireference configuration interaction: MRCI-F12. *J. Chem. Phys.*, 134:034113, 2011.

[127] T. Shiozaki and H.-J. Werner. Multireference explicitly correlated F12 theories. *Mol. Phys.*, 111:607–630, 2013.

[128] Knizia G. Adler T. B. Werner, H.-J. and O. Marchetti. Benchmark Studies for Explicitly Correlated Perturbation- and Coupled Cluster Theories. *Z. Phys. Chem.*, 224:493–511, 2010.

[129] C. Møller and M. S. Plesset. Note on an approximation treatment for many-electron systems. *Phys. Rev.*, 46:618–622, 1934.

[130] H.-J. Werner and F. R. Manby. Explicitly correlated second-order perturbation theory using density fitting and local approximations. *J. Chem. Phys.*, 124:054114, 2006.

[131] F. R. Manby, H.-J. Werner, T. B. Adler, and A. J. May. Explicitly correlated local second-order perturbation theory with a frozen geminal correlation factor. *J. Chem- Phys.*, 124:094103, 2006.

[132] H.-J. Werner, T. B. Adler, and F. R. Manby. General orbital invariant MP2-F12 theory. *J. Chem. Phys.*, 126:164102, 2007.

[133] D. Feller. Statistical Electronic Structure Calibration Study of the CCSD(T*)-F12b Method for Atomization Energies. *J. Phys. Chem. A*, 119(28):7375–7387, 2015.

[134] F. Jensen. *Introduction to Computational Chemistry.* John Wiley & Sons Ltd., 1999.

[135] C. Eckart. Some Studies Concerning Rotating Axes and Polyatomic Molecules. *Phys. Rev.*, 47:552–558, 1935.

[136] D. Feller, K. A. Peterson, and D. A. Dixon. Chemical accuracy in ab initio thermochemistry and spectroscopy: current strategies and future challenges. *Theor. Chem. Acc.*, 131:1079, 2012.

[137] J. A. Pople, M. Head-Gordon, D. J. Fox, K. Raghavachari, and L. A. Curtiss. Gaussian-1 theory: A general procedure for prediction of molecular energies. *J. Chem. Phys.*, 90:5622–5629, 1989.

[138] L. A. Curtiss, C. Jones, G. W. Trucks, K. Raghavachari, and J. A. Pople. Gaussian-1 theory of molecular energies for second-row compounds. *J. Chem. Phys.*, 93:2537–2545, 1990.

[139] L. A. Curtiss, K. Raghavachari, G. W. Trucks, and J. A. Pople. Gaussian-2 theory for molecular energies of first- and second-row compounds. *J. Chem. Phys.*, 94:7221–7230, 1991.

[140] L. A. Curtiss, K. Raghavachari, P. C. Redfern, and J. A. Pople. Assessment of Gaussian-2 and density functional theories for the computation of enthalpies of formation. *J. Chem. Phys.*, 106:1063–1079, 1997.

[141] L. A. Curtiss, K. Raghavachari, P. C. Redfern, V. Rassolov, and J. A. Pople. Gaussian-3 (G3) theory for molecules containing first and second-row atoms. *J. Chem. Phys.*, 109:7764–7776, 1998.

[142] L. A. Curtiss, K. Raghavachari, P. C. Redfern, and J. A. Pople. Gaussian-3 theory using scaled energies. *J. Chem. Phys.*, 112:1125–1132, 2000.

[143] L. A. Curtiss, P. C. Redfern, K. Raghavachari, and J. A. Pople. Gaussian-3X (G3X) theory: Use of improved geometries, zero-point energies, and Hartree–Fock basis sets. *J. Chem. Phys.*, 114:108–117, 2001.

[144] L. A. Curtiss, P. C. Redfern, and K. Raghavachari. Gaussian-4 theory. *J. Chem. Phys.*, 126:084108, 2007.

[145] A. Tajti, P. G. Szalay, A. G. Császár, M. Kállay, J. Gauss, E. F. Valeev, B. A. Flowers, J. Vázquez, and J. F. Stanton. HEAT: High accuracy extrapolated *ab initio* thermochemistry. *J. Chem. Phys.*, 121:11599, 2004.

[146] Y. J. Bomble, J. Vázquez, M. Kállay, C. Michauk, P.G. Szalay, A. G. Császár, J. Gauss, and J. F. Stanton. High-accuracy extrapolated *ab initio* thermochemistry. II. Minor improvements to the protocol and a vital simplification. *J. Chem. Phys.*, 125:064108, 2006.

[147] A. Karton, E. Rabinovich, J. M. L. Martin, and B. Ruscic. W4 theory for computational thermochemistry: In pursuit of confident sub-kJ/mol predictions. *J. Chem. Phys.*, 125:144108, 2006.

[148] N. Sylvetsky, K. A. Peterson, A. Karton, and J. M. L. Martin. Toward a W4-F12 approach: Can explicitly correlated and orbital-based ab initio CCSD(T) limits be reconciled? *J. Chem. Phys.*, 144:214101, 2016.

[149] W. D. Allen, A. L. L. East, and A. G. Császár. *Ab Initio* Anharmonic Vibrational Analyses of Non-Rigid Molecules. In J. Laane, M. Dakkouri, B. van der Veken, and H. Oberhammer, editors, *Structures and Conformations of Non-Rigid Molecules. NATO ASI Series*, volume 410. Springer, 1993.

[150] A. L. L. East and W. D. Allen. The heat of formation of NCO. *J. Chem. Phys.*, 99:4638–4650, 1993.

[151] S. J. Klippenstein, A. L. L. East, and W. D. Allen. A high level *ab initio* map and direct statistical treatment of the fragmentation of singlet ketene. *J. Chem. Phys.*, 105:118–140, 1996.

[152] A. G. Császár, W. D. Allen, and H. F. Schaefer. In pursuit of the *ab initio* limit for conformational energy prototypes. *J. Chem. Phys.*, 108:9751–9764, 1998.

[153] G. Tarczay, A. G. Császár, W. Klopper, V. Szalay, W. D. Allen, and H. F. Schaefer. The barrier to linearity of water. *J. Chem. Phys.*, 110:11971–11981, 1999.

[154] N. J. DeYonker, T. R. Cundari, and A. K. Wilson. The correlation consistent composite approach (ccCA): An alternative to the Gaussian-*n* methods. *J. Chem. Phys.*, 124:114104, 2006.

[155] G. A. Oyedepo and A. K. Wilson. Multireference Correlation Consistent Composite Approach [MR-ccCA]: Toward Accurate Prediction of the Energetics of Excited and Transition State Chemistry. *J. Phys. Chem. A*, 114:8806–8816, 2010.

[156] A. Mahler and A. K. Wilson. Explicitly Correlated Methods within the ccCA Methodology. *J. Chem. Theory Comput.*, 9:1402–1407, 2013.

[157] R. Weber and A. K. Wilson. Do composite methods achieve their target accuracy? *Comp. Theor. Chem.*, 1072:58–62, 2015.

[158] C. Peterson, D. A. Penchoff, and A. K. Wilson. Prediction of Thermochemical Properties Across the Periodic Table: A Review of the correlation consistent Composite Approach (ccCA) Strategies and Applications. In D. A. Dixon, editor, *Annual Reports in Computational Chemistry*, volume 12, pages 3–45. Elsevier, 2016.

[159] D. Feller, K. A. Peterson, and D. A. Dixon. A survey of factors contributing to accurate theoretical predictions of atomization energies and molecular structures. *J. Chem. Phys.*, 129:204105, 2008.

[160] D. Feller, K. A. Peterson, and D. A. Dixon. Refined Theoretical Estimates of the Atomization Energies and Molecular Structures of Selected Small Oxygen Fluorides. *J. Phys. Chem. A*, 114:613–623, 2010.

[161] D. Feller, K. A. Peterson, and D. A. Dixon. Further benchmarks of a composite, convergent, statistically calibrated coupled-cluster-based approach for thermochemical and spectroscopic studies. *Mol. Phys.*, 110:2381–2399, 2012.

[162] D. A. Dixon, D. Feller, and K. A. Peterson. A Practical Guide to Reliable First Principles Computational Thermochemistry Predictions Across the Periodic Table. In R. A. Wheeler, editor, *Annual Reports in Computational Chemistry*, volume 8, pages 1–28. Elsevier, 2012.

[163] R. A. Kendall, T. H. Dunning, and R. J. Harrison. Electron affinities of the first-row atoms revisited. Systematic basis sets and wave functions. *J. Chem. Phys.*, 96:6796–6806, 1992.

[164] D. E. Woon and T. H. Dunning. Gaussian basis sets for use in correlated molecular calculations. V. Core-valence basis sets for boron through neon. *J. Chem. Phys.*, 103:4572–4585, 1995.

[165] A. K. Wilson, T. van Mourik, and T. H. Dunning. Gaussian basis sets for use in correlated molecular calculations. VI. Sextuple-zeta correlation-consistent sets for boron through neon. *J. Mol. Struct. (THEOCHEM)*, 388:339–349, 1996.

[166] J. G. Hill, S. Mazumder, and K. A. Peterson. Correlation consistent basis sets for molecular core-valence effects with explicitly correlated wave functions: The atoms B-Ne and Al-Ar. *J. Chem. Phys.*, 132:054108, 2010.

[167] B. Schröder, O. Weser, P. Sebald, and P. Botschwina. Theoretical rovibrational spectroscopy beyond fc-CCSD(T): the cation CNC^+. *Mol. Phys.*, 113:1914–1923, 2015.

[168] M. Douglas and N. M. Kroll. Quantum electrodynamical corrections to the fine structure of helium. *Ann. Phys.*, 82:89–155, 1974.

[169] B. A. Hess. Relativistic electronic-structure calculations employing a two-component no-pair formalism with external-field projection operators. *Phys. Rev. A*, 33:3742–3748, 1986.

[170] W. A de Jong, R. J. Harrison, and D. A. Dixon. Parallel Douglas–Kroll energy and gradients in NWChem: Estimating scalar relativistic effects using Douglas–Kroll contracted basis sets. *J. Chem. Phys.*, 114:48–53, 2001.

[171] D. Feller and D. A. Dixon. Coupled Cluster Theory and Multireference Configuration Interaction Study of FO, F2O, FO2, and FOOF. *J. Phys. Chem. A*, 107:9641–9651, 2003.

[172] D. G. A. Smith, P. Jankowski, M. Slawik, H. A. Witek, and K. Patkowski. Basis Set Convergence of the Post-CCSD(T) Contribution to Noncovalent Interaction Energies. *J. Chem. Theory Comput.*, 10:3140–3150, 2014.

[173] B. Schröder, P. Sebald, C. Stein, O. Weser, and P. Botschwina. Challenging High-Level *ab initio* Rovibrational Spectroscopy: The Nitrous Oxide Molecule. *Z. Phys. Chem.*, 229:1663–1690, 2015.

[174] Amir Karton. Post-CCSD(T) contributions to total atomization energies in multireference systems. *J. Chem. Phys.*, 149:034102, 2018.

[175] N. C. Handy, Y. Yamaguchi, and H. F. Schaefer. The diagonal correction to the Born–Oppenheimer approximation: Its effect on the singlet–triplet splitting of CH_2 and other molecular effects. *J. Chem. Phys.*, 84:4481–4484, 1986.

[176] J. F. Stanton, J. Gauss, L. Cheng, M. E. Harding, D. A. Matthews, and P. G. Szalay. CFOUR, Coupled-Cluster techniques for Computational Chemistry, a quantum-chemical program package. With contributions from A.A. Auer, R.J. Bartlett, U. Benedikt, C. Berger, D.E. Bernholdt, Y.J. Bomble, O. Christiansen, F. Engel, R. Faber, M. Heckert, O. Heun, M. Hilgenberg, C. Huber, T.-C. Jagau, D. Jonsson, J. Jusélius, T. Kirsch, K. Klein, W.J. Lauderdale, F. Lipparini, T. Metzroth, L.A. Mück, D.P. O'Neill, D.R. Price, E. Prochnow, C. Puzzarini, K. Ruud, F. Schiffmann, W. Schwalbach, C. Simmons, S. Stopkowicz, A. Tajti, J. Vázquez, F. Wang, J.D. Watts and the integral packages MOLECULE (J. Almlöf and P.R. Taylor), PROPS (P.R. Taylor), ABACUS (T. Helgaker, H.J. Aa. Jensen, P. Jørgensen, and J. Olsen), and ECP routines by A. V. Mitin and C. van Wüllen. For the current version, see `http://www.cfour.de`.

[177] J. Gauss, A. Tajti, M. Kállay, J. F. Stanton, and P.G. Szalay. Analytic calculation of the diagonal Born-Oppenheimer correction within configuration-interaction and coupled-cluster theory. *J. Chem. Phys.*, 125:144111, 2006.

[178] D. W. Schwenke. Beyond the Potential Energy Surface: *Ab initio* Corrections to the Born-Oppenheimer Approximation for H_2O. *J. Phys. Chem. A*, 105:2352–2360, 2001.

[179] W. Kutzelnigg. Which masses are vibrating or rotating in a molecule? *Mol. Phys.*, 105:2627–2647, 2007.

[180] E. B. Wilson and J. B. Howard. The Vibration-Rotation Energy Levels of Polyatomic Molecules I. Mathematical Theory of Semirigid Asymmetrical Top Molecules. *J. Chem. Phys.*, 4:260–268, 1936.

[181] B. T. Darling and D. M. Dennison. The Water Vapor Molecule. *Phys. Rev.*, 57:128–139, 1940.

[182] J. K. G. Watson. Simplification of the molecular vibration-rotation hamiltonian. *Mol. Phys.*, 15:479–490, 1968.

[183] H. H. Nielsen. The Vibration-Rotation Energies of Molecules. *Rev. Mod. Phys.*, 23:90–136, 1951.

[184] H. H. Nielsen. The Vibration-rotation Energies of Molecules and their Spectra in the Infrared. In S. Flügge, editor, *Handbuch der Physik*, volume 37, Part I, pages 173–313. Springer, Berlin, 1959.

[185] Nielsen H. H. Amat, G. and G. Tarrago. *Rotation-Vibration of Polyatomic Molecules*. Dekker, New York, 1971.

[186] D. Papoušek and M. R. Aliev. *Molecular Vibrational-rotational Spectra: Theory and Applications of High Resolution Infrared, Microwave and Raman Spectroscopy of Polyatomic Molecules*. Elsevier Science Ltd, 1982.

[187] M. R. Aliev and J. K. G. Watson. Higher-order effects in the vibration-rotation spectra of semirigid molecules. In K. N. Rao, editor, *Molecular Spectroscopy: Modern Research*, pages 1–67. Academic Press, 1985.

[188] J. M. Bowman, T. Carrington, and H.-D. Meyer. Variational quantum approaches for computing vibrational energies of polyatomic molecules. *Mol. Phys.*, 106:2145–2182, 2008.

[189] Jonathan Tennyson. Perspective: Accurate ro-vibrational calculations on small molecules. *J. Chem. Phys.*, 145:120901, 2016.

[190] T. Carrington. Perspective: Computing (ro-)vibrational spectra of molecules with more than four atoms. *J. Chem. Phys.*, 146:120902, 2017.

[191] J. K. G. Watson. The vibration-rotation Hamiltonian of linear molecules. *Mol. Phys.*, 19:465–487, 1970.

[192] G. Amat and L. Henry. Sur les coefficients d'interaction entre la vibration et la rotation dans les molécules polyatomiques I. *Cah. Phys.*, 12:273, 1958.

[193] A. Sayvetz. The kinetic energy of polyatomic molecules. *J. Chem. Phys.*, 7:383–389, 1939.

[194] W. D. Allen, Y. Yamaguchi, A. G. Császár, D. A. Clabo, R. B. Remington, and H. F. Schaefer. A systematic study of molecular vibrational anharmonicity and vibration-rotation interaction by self-consistent-field higher-derivative methods. Linear polyatomic molecules. *Chem. Phys.*, 145:427–466, 1990.

[195] R. C. Herman and W. H. Shaffer. The Calculation of Perturbation Energies in Vibrating Rotating Polyatomic Molecules. *J. Chem. Phys.*, 16:453–465, 1948.

[196] J. Z. Gong, D. A. Matthews, P. B. Changala, and J. F. Stanton. Fourth-order vibrational perturbation theory with the Watson Hamiltonian: Report of working equations and preliminary results. *J. Chem. Phys.*, 149:114102, 2018.

[197] K. P. Huber and G. Herzberg. *Molecular Spectra and Molecular Structure II: Infrared and Raman Spectra of Polyatomic Molecules*. Van Nostrand Reinhold Co. Inc., 1979.

[198] G. Herzberg. l-Type Doubling in Linear Polyatomic Molecules. *Rev. Mod. Phys.*, 14:219–223, 1942.

[199] J. K. G. Watson. Higher-order l-doubling of linear molecules. *J. Mol. Spectrosc.*, 101:83–93, 1983.

[200] J.M. Brown, J. T. Hougen, K.-P. Huber, J. W. C. Johns, I. Kopp, H. Lefebvre-Brion, A. J. Merer, D. A. Ramsay, J. Rostas, and R. N. Zare. The labeling of parity doublet levels in linear molecules. *J. Mol. Spectrosc.*, 55:500–503, 1975.

[201] E. A. Hylleraas and B. Undheim. Numerische Berechnung der 2S-Terme von Ortho- und Par-Helium. *Z. Physik*, 65:759–772, 1930.

[202] J. K. L. MacDonald. Successive Approximations by the Rayleigh-Ritz Variation Method. *Phys. Rev.*, 43:830–833, 1933.

[203] S. Carter and N. C. Handy. An efficient procedure for the calculation of the vibrational energy levels of any triatomic molecule. *Molecular Physics*, 57(1):175–185, 1986.

[204] S. Carter, N. C. Handy, P. Rosmus, and G. Chambaud. A variational method for the calculation of spin-rovibronic levels of Renner-Teller triatomic molecules. *Mol. Phys.*, 71(3):605–622, 1990.

[205] B. T. Sutcliffe and J. Tennyson. A generalized approach to the calculation of ro-vibrational spectra of triatomic molecules. *Mol. Phys.*, 58(6):1053–1066, 1986.

[206] J. Tennyson. TRIATOM, SELECT and ROTLEV — For the calculation of the ro-vibrational levels of triatomic molecules. *Comput. Phys. Commun.*, 42:257–270, 1986.

[207] J. Tennyson and S. Miller. A program suite for the calculation of ro-vibrational spectra of triatomic molecules. *Comput. Phys. Commun.*, 55:149–175, 1989.

[208] J. Tennyson, S. Miller, and C. R. Le Sueur. TRIATOM: programs for the calculation of ro-vibrational spectra of triatomic molecules. *Comput. Phys. Commun.*, 75:339–364, 1993.

[209] R. J. Whitehead and N. C. Handy. Variational calculation of vibration-rotation energy levels for triatomic molecules. *J. Mol. Spectrosc.*, 55:356–373, 1975.

[210] P. Sebald. *Ab initio Berechnung spektroskopischer Eigenschaften kleiner linearer Moleküle. Dissertation*, University of Kaiserslautern, 1990.

[211] M. J. Bramley and N. C. Handy. Efficient calculation of rovibrational eigenstates of sequentially bonded four-atom molecules. *J. Chem. Phys.*, 98:1378–1397, 1993.

[212] M. J. Bramley, S. Carter, N. C. Handy, and I. M. Mills. A Refined Quartic Forcefield for Acetylene: Accurate Calculation of the Vibrational Spectrum. *J. Mol. Spectrosc.*, 157:301–336, 1993.

[213] K. L. Chubb, A. Yachmenev, J. Tennyson, and S. N. Yurchenko. Treating linear molecule HCCH in calculations of rotation-vibration spectra. *J. Chem. Phys.*, 149:014101, 2018.

[214] S. N. Yurchenko, W. Thiel, and P. Jensen. Theoretical ROVibrational Energies (TROVE): A robust numerical approach to the calculation of rovibrational energies for polyatomic molecules. *J. Mol. Spectrosc.*, 245:126–140, 2007.

[215] S. N. Yurchenko, A. Yachmenev, and R. I. Ovsyannikov. Symmetry-Adapted Ro-vibrational Basis Functions for Variational Nuclear Motion Calculations: TROVE Approach. *J. Chem. Theory Comput.*, 13:4368–4381, 2017.

[216] K. L. Chubb, P. Jensen, and S. N. Yurchenko. Symmetry Adaptation of the Rotation-Vibration Theory for Linear Molecules. *Symmetry*, 10:137, 2018.

[217] D. O. Harris, G. G. Engerholm, and W. D. Gwinn. Calculation of Matrix Elements for One-Dimensional Quantum-Mechanical Problems and the Application to Anharmonic Oscillators. *J. Chem. Phys.*, 43:1515–1517, 1965.

[218] A. S. Dickinson and P. R. Certain. Calculation of Matrix Elements for One-Dimensional Quantum-Mechanical Problems. *J. Chem. Phys.*, 49:4209–4211, 1968.

[219] J. V. Lill, G. A. Parker, and J. C. Light. Discrete variable representations and sudden models in quantum scattering theory. *Chem. Phys. Lett.*, 89:483–489, 1982.

[220] Z. Bačić and J. C. Light. Highly excited vibrational levels of "floppy" triatomic molecules: A discrete variable representation—Distributed Gaussian basis approach. *J. Chem. Phys.*, 85:4594–4604, 1986.

[221] J. C. Light and T. Carrington. Discrete-Variable Representations and their Utilization. In *Advances in Chemical Physics*, pages 263–310. John Wiley & Sons, Ltd, New York, 2007.

[222] M. Mladenović and M. Lewerenz. Converging multidimensional rovibrational variational calculations: the dissociation energy of $(HF)_2$. *Chem. Phys. Lett.*, 321:135–141, 2000.

[223] M. Mladenović. Discrete variable approaches to tetratomic molecules: Part I: DVR(6) and DVR(3)+DGB methods. *Spectrochim. Acta, Part A*, 58:795–807, 2002.

[224] M. Mladenović, P. Botschwina, and C. Puzzarini. Six-Dimensional Potential Energy Surface and Rovibrational Energies of the HCCN Radical in the Ground Electronic State. *J. Phys. Chem. A*, 110:5520–5529, 2006.

[225] M. Mladenović. Rovibrational Hamiltonians for general polyatomic molecules in spherical polar parametrization. I. Orthogonal representations. *J. Chem. Phys.*, 112:1070–1081, 2000.

[226] M. Mladenović. Rovibrational Hamiltonians for general polyatomic molecules in spherical polar parametrization. II. Nonorthogonal descriptions of internal molecular geometry. *J. Chem. Phys.*, 112:1082–1095, 2000.

[227] M. Mladenović. Rovibrational Hamiltonians for general polyatomic molecules in spherical polar parametrization. III. Global vs local axis system and angular coordinates. *J. Chem. Phys.*, 113:10524–10534, 2000.

[228] I. N. Kozin, M. M. Law, J. Tennyson, and J. M. Hutson. New vibration–rotation code for tetraatomic molecules exhibiting wide-amplitude motion: WAVR4. *Comput. Phys. Commun.*, 163:117–131, 2004.

[229] I. N. Kozin, M. M. Law, J. Tennyson, and J. M. Hutson. Calculating energy levels of isomerizing tetra-atomic molecules. II. The vibrational states of acetylene and vinylidene. *J. Chem. Phys.*, 122:064309, 2005.

[230] A. Urru, G. Kozin, I. N. Mulas, B. J. Braams, and Tennyson J. Ro-vibrational spectra of C_2H_2 based on variational nuclear motion calculations. *Mol. Phys.*, 108:1973–1990, 2010.

[231] E. Mátyus, G. Czakó, B. T. Sutcliffe, and A. G. Császár. Vibrational energy levels with arbitrary potentials using the Eckart-Watson Hamiltonians and the discrete variable representation. *J. Chem. Phys.*, 127:084102, 2007.

[232] E. R. Cohen, T. Cvitaš, J. G. Frey, B. Holmström, K. Kuchitsu, R. Marquardt, I. Mills, F. Pavese, M. Quack, J. Stohner, H. L. Strauss, M. Takami, and A. J. Thor. *Quantities, Units and Symbols in Physical Chemistry.* RSC Publishing, 3. edition, 2007.

[233] S. Califano. *Vibrational States.* John Wiley & Sons, Inc., London, 1976.

[234] R. N. Zare. *Angular momentum : understanding spatial aspects in chemistry and physics.* John Wiley & Sons, Inc., New York, 1988.

[235] H. Hönl and F. London. Über die Intensitäten der Bandenlinien. *Z. Physik*, 33:803–809, 1925.

[236] A. Hansson and J. K. G. Watson. A comment on Hönl-London factors. *J. Mol. Spectrosc.*, 233:159–173, 2005.

[237] R. Herman and R. F. Wallis. Influence of Vibration-Rotation Interaction on Line Intensities in Vibration-Rotation Bands of Diatomic Molecules. *J. Chem. Phys.*, 23:637–646, 1955.

[238] J. K. G. Watson. Quadratic Herman-Wallis Factors in the Fundamental Bands of Linear Molecules. *J. Mol. Spectrosc.*, 125:428–441, 1987.

[239] J. K. G. Watson. Intensities of Linear-Molecule Vibration-Rotation Transitions with $|\Delta k| = 2$, with Applications to HCN, DCN, and HCCH. *J. Mol. Spectrosc.*, 188:78–84, 1998.

[240] R. A. Toth. Line strengths (900-3600 cm^{-1}), self-broadened linewidths, and frequency shifts (1800-2360 cm^{-1}) of N_2O. *Appl. Opt.*, 32:7326–7365, 1993.

[241] V. Y. Makhnev, A. A. Kyuberis, N. F. Zobov, L. Lodi, J. Tennyson, and O. L. Polyansky. High Accuracy *ab initio* Calculations of Rotational–Vibrational Levels of the HCN/HNC System. *J. Phys. Chem. A*, 122:1326–1343, 2018.

[242] V. Y. Makhnev, A. A. Kyuberis, O. L. Polyansky, I. I. Mizus, J. Tennyson, and N. F. Zobov. A new spectroscopically-determined potential energy surface and *ab initio* dipole moment surface for high accuracy HCN intensity calculations. *J. Mol. Spectrosc.*, 353:40–53, 2018.

[243] I. E. Gordon, L. S. Rothman, C. Hill, R. V. Kochanov, Y. Tan, P. F. Bernath, M. Birk, V. Boudon, A. Campargue, K. V. Chance, B. J. Drouin, J.-M. Flaud, R. R. Gamache, J.T. Hodges, D. Jacquemart, V. I. Perevalov, A. Perrin, K. P. Shine, M.-A. H. Smith, J. Tennyson, G. C. Toon, H. Tran, V. G. Tyuterev, A. Barbe, A. G. Császár, V. M. Devi, T. Furtenbacher, J. J. Harrison, J.-M. Hartmann, A. Jolly, T. J. Johnson, T. Karman, I. Kleiner, A. A. Kyuberis, J. Loos, O. M. Lyulin, S. T. Massie, S. N. Mikhailenko, N. Moazzen-Ahmadi, H. S. P. Müller, O. V. Naumenko, A. V. Nikitin, O. L. Polyansky, M. Rey, M. Rotger, S.W. Sharpe, K. Sung, E. Starikova, S. A. Tashkun, J. Vander Auwera, G. Wagner, J. Wilzewski, P. Wcisło, S. Yu, and E. J. Zak. The HITRAN2016 molecular spectroscopic database. *J. Quant. Spectrosc. Radiat. Transf.*, 203:3–69, 2017.

[244] Y. Gao and P. M. Solomon. HCN survey of normal spiral, infrared-luminous, and ultraluminous galaxies. *Astrophys. J. Suppl. Ser.*, 152:63–80, 2004.

[245] L. E. Snyder and D. Buhl. Observations of radio emission from interstellar hydrogen cyanide. *Astrophys. J.*, 163:L47–L52, 1971.

[246] B. Zuckerman, M. Morris, P. Palmer, and B. E. Turner. Observations of CS, HCN, U89.2, and U90.7 in NGC 2264. *Astrophys. J. Lett.*, 173:L125, 1972.

[247] J. Hatchell, T. J. Millar, and S. D. Rodgers. The DCN/HCN abundance ratio in hot molecular cores. *Astron. Astrophys.*, 332:695–702, 1998.

[248] T. Hirota, S. Yamamoto, Mikami, and Masatoshi Ohishi. Abundances of HCN and HNC in dark cloud cores. *Astrophys. J.*, 503:717–728, 1998.

[249] W.F. Huebner, L.E. Snyder, and D. Buhl. HCN radio emission from Comet Kohoutek (1973f). *Icarus*, 23:580–584, 1974.

[250] W. M. Irvine, D. Bockelee-Morvan, D. C. Lis, H. E. Matthews, N. Biver, J. Crovisier, J. K. Davies, W. R. F. Dent, D. Gautier, P. D. Godfrey, J. Keene, A. J. Lovell, T. C. Owen, T. G. Phillips, H. Rauer, F. P. Schloerb, M. Senay, and K. Young. Spectroscopic evidence for interstellar ices in comet Hyakutake. *Nature*, 383:418–420, 1996.

[251] J. H. Bieging, S. Shaked, and P. D. Gensheimer. Submillimeter- and Millimeter-Wavelength Observations of SiO and HCN in Circumstellar Envelopes of AGB Stars. *Astrophys. J.*, 543:897–921, nov 2000.

[252] W. Aoki, T. Tsuji, and K. Ohnaka. Infrared spectra of carbon stars observed by the ISO SWS. I. Molecular absorption in N-type and SC-type stars. *Astron. Astrophys.*, 340:222–231, 1998.

[253] A. Dutrey, S. Guilloteau, and M. Guélin. Chemistry of Protosolar-like nebulae: The molecular content of the DM Tau and GG Tau disks. *Astron. Astrophys.*, 317:L55–L58, 1997.

[254] C. Qi, D. J. Wilner, Y. Aikawa, G. A. Blake, and M. R. Hogerheijde. Resolving the Chemistry in the Disk of TW Hydrae. I. Deuterated Species. *Astrophys. J.*, 681(2):1396–1407, 2008.

[255] A. Tsiaras, M. Rocchetto, I. P. Waldmann, O. Venot, R. Varley, G. Morello, M. Damiano, G. Tinetti, E. J. Barton, S. N. Yurchenko, and J. Tennyson. Detection of an atmosphere around the super-earth 55 Cancri E. *Astrophys. J.*, 820(2):99, 2016.

[256] W. L. Ebenstein and J. S. Muenter. Dipole moment and hyperfine properties of the ground state and the C-H excited vibrational state of HCN. *J. Chem. Phys.*, 80:3989–3991, 1984.

[257] Y. Gao. Dense Molecular Gas in Galaxies and the Evolution of Luminous Infrared Galaxies. *Publ. Astron. Soc. Pac.*, 109:1189, 1997.

[258] K. Eriksson, B. Gustafsson, U. G. Jørgensen, and A. Nordlund. Effects of HCN molecules in carbon star atmospheres. *Astron. Astrophys.*, 132:37–44, 1984.

[259] U. G. Jørgensen, J Almlöf, B. Gustafsson, M. Larsson, and P. Siegbahn. CASSCF and CCI calculations of the vibrational band strengths of HCN. *J. Chem. Phys.*, 83:3034–3041, 1985.

[260] W. Burmeister. Untersuchungen über die ultraroten Absorptionsspektra einiger Gase. *Verh. Dtsch. Phys. Ges.*, 15:589, 1913.

[261] A. Karton, S. Daon, and J. M. L. Martin. W4-11: A high-confidence benchmark dataset for computational thermochemistry derived from first-principles W4 data. *Chem. Phys. Lett.*, 510:165–178, 2011.

[262] L. A. Curtiss, P. C. Redfern, and K. Raghavachari. Assessment of Gaussian-3 and density-functional theories on the G3/05 test set of experimental energies. *J. Chem. Phys.*, 123:124107, 2005.

[263] J. H. Baraban, P. B. Changala, G. C. Mellau, J. F. Stanton, A. G. Merer, and R. W. Field. Spectroscopic characterization of isomerization transition states. *Science*, 350:1338–1342, 2015.

[264] G. C. Mellau, A. A. Kyuberis, O. L. Polyansky, N. Zobov, and R. W. Field. Saddle point localization of molecular wavefunctions. *Sci. Rep.*, 6:33068, 2016.

[265] G. E. Hyde and D. F. Hornig. The Measurement of Bond Moments and Derivatives in HCN and DCN from Infrared Intensities. *J. Chem. Phys.*, 20:647–652, 1952.

[266] K. Kim and W. T. King. Integrated intensities in hydrogen cyanide. *J. Chem. Phys.*, 71:1967–1972, 1979.

[267] I. W. M. Smith. Integrated intensities for some infrared absorption bands of HCN. *J. Chem. Soc., Faraday Trans. 2*, 77:2357–2363, 1981.

[268] M. A. H. Smith, G. A. Harvey, G. L. Pellett, A. Goldman, and D. J. Richardson. Measurements of the HCN ν_3 Band Broadened by N_2. *J. Mol. Spectrosc.*, 105:105–112, 1984.

[269] P. L. Varghese and R. K. Hanson. Tunable diode laser measurements of spectral parameters of HCN at room temperature. *J. Quant. Spectrosc. Radiat. Transf.*, 31:545–559, 1984.

[270] A. J. C. Varandas and S. P. J. Rodrigues. Double many-body expansion potential energy surface for ground-state HCN based on realistic long range forces and accurate AB INITIO calculations. *J. Chem. Phys.*, 106:9647–9658, 1997.

[271] J. M. Bowman, B. Gazdy, J. A. Bentley, T. J. Lee, and C. E. Dateo. *Ab initio* calculation of a global potential, vibrational energies, and wave functions for HCN/HNC, and a simulation of the $\tilde{A} - \tilde{X}$ emission spectrum. *J. Chem. Phys.*, 99:308–323, 1993.

[272] T. van Mourik, G. J. Harris, O. L. Polyansky, J. Tennyson, A. G. Császár, and P. J. Knowles. *Ab initio* global potential, dipole, adiabatic, and relativistic correction surfaces for the HCN–HNC system. *J. Chem. Phys.*, 115:3706–3718, 2001.

[273] R. Dawes, A. F. Wagner, and D. L. Thompson. *Ab Initio* Wavenumber Accurate Spectroscopy: $^1CH_2$ and HCN Vibrational Levels on Automatically Generated IMLS Potential Energy Surfaces. *J. Phys. Chem. A*, 113:4709–4721, 2009.

[274] J. N. Murrel, S. Carter, and L. O. Halonen. Frequency optimized potential energy surface for the ground-state of HCN and HCP. *J. Mol. Spectrosc.*, 93:307–316, 1982.

[275] S. R. Carter, N. C. Handy, and I. M. Mills. Variational calculations of rovibrational states: a precise high-energy potential surface for HCN. *Philos. Trans. R. Soc. London Ser. A*, 332:309–327, 1990.

[276] A. J. C. Varandas and S. P. J. Rodrigues. New Double Many-Body Expansion Potential Energy Surface for Ground-State HCN from a Multiproperty Fit to Accurate *ab initio* Energies and Rovibrational Calculations. *J. Phys. Chem. A*, 110:485–493, 2006.

[277] P. Botschwina, B. Schulz, M. Horn, and M. Matuschewski. *Ab initio* calculations of stretching vibrational transitions for the linear molecules HCN, HNC, HCCF and HC3N up to high overtones. *Chem. Phys.*, 190:345–362, 1995.

[278] S. R. Carter, I. M. Mills, and N. C. Handy. Vibration-rotation variational calculations: Precuse results on HCN up to 25000 cm^{-1}. *J. Chem. Phys.*, 99:4379–4390, 1993.

[279] G. J. Harris, O. L. Polyansky, and J. Tennyson. *Ab initio* rotation–vibration spectra of HCN and HNC. *Spectrochim. Acta A*, 58:673–690, 2002.

[280] K. E. Yousaf and K. A. Peterson. Optimized auxiliary basis sets for explicitly correlated methods. *J. Chem. Phys.*, 129:184108, 2008.

[281] F. Weigend. A fully direct RI-HF algorithm: Implementation, optimised auxiliary basis sets, demonstration of accuracy and efficiency. *Phys. Chem. Chem. Phys.*, 4:4285–4291, 2002.

[282] C. Hättig. Optimization of auxiliary basis sets for RI-MP2 and RI-CC2 calculations: Core–valence and quintuple-ζ basis sets for H to Ar and QZVPP basis sets for Li to Kr. *Phys. Chem. Chem. Phys.*, 7:59–66, 2005.

[283] K. E. Yousaf and K. A. Peterson. Optimized complementary auxiliary basis sets for explicitly correlated methods: auc-cc-pV*n*Z orbital basis sets. *Chem. Phys. Lett.*, 476:303–307, 2009.

[284] S. R. Carter, I. M. Mills, and N. C. Handy. The equilibrium structure of HCN. *J. Chem. Phys.*, 97:1606–1607, 1992.

[285] W. Quapp, M. Hirsch, G. C. Mellau, S. Klee, M. Winnewisser, and A. Maki. Climbing the Bending Vibrational Ladder in $D^{13}C^{15}N$ by Hot Gas Emission Spectroscopy. *J. Mol. Spectrosc.*, 195:284–298, 1999.

[286] A. Maki, G. C. Mellau, S. Klee, M. Winnewisser, and W. Quapp. High-Temperatur Infrared Measurements in the Region of the Bending Fundamental of $H^{12}C^{14}N$, $H^{12}C^{15}N$, and $H^{13}C^{14}N$. *J. Mol. Spectrosc.*, 202:67–82, 2000.

[287] P. Botschwina, A. Bargholz, P. Sebald, B. Schröder, and R. Oswald. Theoretical rovibrational spectroscopy of NO_2^+. *J. Mol. Spectrosc.*, 311:12–18, 2015.

[288] A. Halkier, W. Klopper, T. Helgaker, and P. Jørgensen. Basis-set convergence of the molecular electric dipole moment. *J. Chem. Phys.*, 111:4424–4430, 1999.

[289] R. L. DeLeon and J. S. Muenter. The vibrational dipole moment function of HCN. *J. Chem. Phys.*, 80:3992–3999, 1984.

[290] X. Yang, C. A. Rogaski, and A. M. Wodtke. Vibrational structure of hydrogen cyanide up to 18900 cm^{-1}. *J. Opt. Soc. Am. B*, 7:1835–1850, 1990.

[291] A. M. Smith, S. L. Coy, W. Klemperer, and K. L. Lehmann. Fourier transform spectra of overtone bands of HCN from 5400 to 15100 cm^{-1}. *J. Mol. Spectrosc.*, 134:134–153, 1989.

[292] P. Sebald, H. Vennekate, R. Oswald, P. Botschwina, and H. Stoll. A theoretical study of ZnH_2: a case of very strong Darling–Dennison resonance. *Mol. Phys.*, 108:487–499, 2010.

[293] P. Sebald, A. Bargholz, R. Oswald, C. Stein, and P. Botschwina. FHF^- Isotopologues: Highly Anharmonic Hydrogen-Bonded Systems with Strong Coriolis Interaction. *J. Phys. Chem. A*, 117:9695–9703, 2013.

[294] B. Schröder and P. Sebald. High-level theoretical rovibrational spectroscopy beyond fc-CCSD(T): The C_3 molecule. *J. Chem. Phys.*, 144:044307, 2016.

[295] A. A. Breier, T. Büchling, R. Schnierer, V. Lutter, G. W. Fuchs, K. M. T. Yamada, B. Mookerjea, J. Stutzki, and T. F. Giesen. Lowest bending mode of ^{13}C-substituted C_3 and an experimentally derived structure. *J. Chem. Phys.*, 145:234302, 2016.

[296] W. Huggins. Preliminary Note on the Photographic Spectrum of Comet b 1881. *Proc. Royal Soc. Lond.*, 33:1–3, 1881.

[297] A. McKellar. The Far Violet Region in the Spectra of the Cool Carbon Stars. *Astrophys. J.*, 108:453, 1948.

[298] R. G. W. Norrish, G. Porter, and B. A. Thrush. Studies of the Explosive Combustion of Hydrocarbons by Kinetic Spectroscopy. I. Free Radical Absorption Spectra in Acetylene Combustion. *Proc. Roy. Soc. Lond. A*, 216:165–183, 1953.

[299] P. Swings, A. McKellar, and K. Narahari Rao. Spectra of the Late N-type Stars in the Ultra-violet, Violet and Blue-green Regions. *Mon. Notices Royal Astron. Soc.*, 113:571–581, 1953.

[300] D. Crampton, A. P. Cowley, and R. M. Humphreys. Spectroscopic observations of CRL 2688. *Astrophys. J. Lett.*, 198:L135–L137, 1975.

[301] K. W. Hinkle, J. J. Keady, and P. F. Bernath. Detection of C_3 in the Circumstellar Shell of IRC+10216. *Science*, 241:1319–1322, 1988.

[302] J. Cernicharo, J. R. Goicoechea, and E. Caux. Far-infrared Detection of C_3 in Sagittarius B2 and IRC +10216. *Astrophy. J. Lett.*, 534:L199–L202, 2000.

[303] J. P. Maier, N. M. Lakin, G. A. H. Walker, and D.A. Bohlender. Detection of C_3 in Diffuse Interstellar Clouds. *Astrophys. J.*, 553:267–273, 2001.

[304] T. Oka, J. A. Thorburn, B. J. McCall, S. D. Friedman, L. M. Hobbs, P. Sonnentrucker, D. E. Welty, and D. G. York. Observations of C_3 in Translucent Sight Lines. *The Astrophysical Journal*, 582:823, 2003.

[305] Mookerjea, B., Giesen, T., Stutzki, J., Cernicharo, J., Goicoechea, J. R., De Luca, M., Bell, T. A., Gupta, H., Gerin, M., Persson, C. M., Sonnentrucker, P., Makai, Z., Black, J., Boulanger, F., Coutens, A., Dartois, E., Encrenaz, P., Falgarone, E., Geballe, T., Godard, B., Goldsmith, P. F., Gry, C., Hennebelle, P., Herbst, E., Hily-Blant, P., Joblin, C., Kaźmierczak, M., Kołos, R., Krełowski, J., Lis, D. C., Martin-Pintado, J., Menten, K. M., Monje, R., Pearson, J. C.,

Perault, M., Phillips, T. G., Plume, R., Salez, M., Schlemmer, S., Schmidt, M., Teyssier, D., Vastel, C., Yu, S., Dieleman, P., Güsten, R., Honingh, C. E., Morris, P., Roelfsema, P., Schieder, R., Tielens, A. G. G. M., and Zmuidzinas, J. Excitation and abundance of C_3 in star forming cores - Herschel/HIFI observations of the sight-lines to W31C and W49N. *Astron. & Astrophys.*, 521:L13, 2010.

[306] M. R. Schmidt, J. Krełowski, G. A. Galazutdinov, D. Zhao, M. A. Haddad, W. Ubachs, and H. Linnartz. Detection of vibronic bands of C_3 in a translucent cloud towards HD 169454. *Mon. Notices Royal Astron.*, 441:1134–1146, 2014.

[307] C. W. Raffety. On some Investigations of the Spectra of Carbon and Hydrocarbon. *Phil. Mag. Ser. 6*, 32:546–559, 1916.

[308] G. Herzberg. Laboratory Production of the λ 4050 Group occuring in cometary Spectra; Further Evidence for the Presence of CH_2 Molecules in Comets. *Astrophys. J.*, 96:314–315, 1942.

[309] L. Gausset, G. Herzberg, A. Lagerqvist, and B. Rosen. Spectrum of the C_3 molecule. *Discuss. Faraday Soc.*, 35:113–117, 1963.

[310] L. Gausset, G. Herzberg, A. Lagerqvist, and B. Rosen. Analysis of the 4050-Å group of the C_3 molecule. *Astrophys. J.*, 142:45, 1965.

[311] P. Botschwina. Coupled Cluster Study of the Linear Carbon Chains C_{2n+1} $(n = 5 - 9)$. *J. Phys. Chem. A*, 111:7431–7436, 2007.

[312] C. A. Schmuttenmaer, R. C. Cohen, N. Pugliano, J. R. Heath, A. L. Cooksy, K. L. Busarow, and R. J. Saykally. Tunable Far-IR Laser Spectroscopy of Jet-Cooled Carbon Clusters: The ν_2 Bending Vibration of C_3. *Science*, 249:897–900, 1990.

[313] K. Matsumura, H. Kanamori, K. Kawaguchi, and E. Hirota. Infrared diode laser kinetic spectroscopy of the ν_3 band of C_3. *J. Chem. Phys.*, 89:3491–3494, 1988.

[314] K. Kawaguchi, K. Matsumura, H. Kanamori, and E. Hirota. Diode laser spectroscopy of C_3: The $\nu_2 + \nu_3 - \nu 2$, $2\nu_2 + \nu_3 - 2\nu_2$, and $2\nu_2 + \nu_3$ bands. *J. Chem. Phys.*, 91:1953–1957, 1989.

[315] E. A. Rohlfing. Laser-induced-flourescence spectroscopy of jet-cooled C_3. *J. Chem. Phys.*, 91:4531–4542, 1989.

[316] F. J. Northrup and T. J. Sears. Observation of stimulated emission pumping spectra of jet-cooled NCS and C_3. *Chem. Phys. Lett.*, 159:421–425, 1989.

[317] E. A. Rohlfing and J. E. M. Goldsmith. Stimulated-emission pumping spectroscopy study of jet-cooled C_3: antisymmetric stretch-bend levels. *J. Opt. Soc. Am. B*, 7:1915–1923, 1990.

[318] F. J. Northrup and T. J. Sears. Stimulated-emission pumping spectroscopy study of jet-cooled C_3: pure bending levels and bend-symmetric-stretch combination levels of $\tilde{X}^1\Sigma_g^+$. *J. Opt. Soc. Am. B*, 7:1924–1934, 1990.

[319] J. Baker, S. K. Bramble, and P. A. Hamilton. A Hot Band LIF Study of the $A^1\Pi_u$-$X^1\Sigma_g^+$ Transition in C_3. *Chem. Phys. Lett.*, 213:297–302, 1993.

[320] N. Moazzen-Ahmadi and A. R. W. McKellar. Infrared diode laser spectroscopy of the ν_3 fundamental an $\nu_3 + \nu_2 - \nu_2$ sequence bands of $^{13}C_3$ and of the ν_3 $^{12}C^{12}C^{13}C$. *J. Chem. Phys.*, 98:7757–7762, 1993.

[321] G. Zhang, K.-S. Chen, A. J. Merer, Y.-C. Hsu, W.-J. Chen, C. Shaji, and Y.-A. Liao. The 4051-Å band of C_3 ($\tilde{A}^1\Pi_u - \tilde{X}^1\Sigma_g^+, 000 - 000$): Perturbed low-$J$ lines and lifetime measurments. *J. Chem. Phys.*, 122:244308, 2005.

[322] J. Krieg, V. Lutter, C. P. Endres, I. H. Keppeler, P. Jensen, M. E. Harding, J. Vázquez, S. Schlemmer, T. F. Giesen, and S. Thorwirth. High-resolution spectroscopy of C_3 around 3μm. *J. Phys. Chem. A.*, 117:3332–3339, 2013.

[323] M. A. Haddad, D. Zhao, H. Linnartz, and W. Ubachs. Rotational resolved spectra of the 4051 Å comet band of C_3 for all six ^{12}C and ^{13}C isotopologues. *J. Mol. Spectrosc.*, 297:41–50, 2014.

[324] K. Ahmed, G. G. Balint-Kurti, and C. M. Western. *Ab initio* calculations and vibrational energy level fits for the lower singlet potential-energy surfaces of C_3. *J. Chem. Phys.*, 121:10041–10051, 2004.

[325] W. Jr. Weltner and W. J. Van Zee. Carbon molecules, ions, and clusters. *Chem. Rev.*, 97:1713–1747, 1989.

[326] A. Van Orden and R. J. Saykally. Small Carbon Clusters: Spectroscopy, Structure, and Energetics. *Chem. Rev.*, 98:2313–2357, 1998.

[327] W. P. Kraemer, P. R. Bunker, and M. Yoshimine. A theoretical study of the rotation-vibration energy levels and dipole moment functions of CCN^+, CNC^+, and C_3. *J. Mol. Spectrosc.*, 107:191–207, 1984.

[328] P. Jensen. A New Morse Oscillator-Rigid Bender Interal Dynamics (MORBID) Hamiltonian for Triatomic Molecules. *J. Mol. Spectrosc.*, 128:478–501, 1988.

[329] P. Sebald, C. Stein, R. Oswald, and P. Botschwina. Rovibrational States of N_3^- and CO_2 Up to High J: A Theoretical Study Beyond fc-CCSD(T). *J. Phys. Chem. A*, 117:13806–13814, 2013.

[330] P. Botschwina, P. Sebald, B. Schröder, A. Bargholz, K. Kawaguchi, and T. Amano. Rovibrational states of HBF^+ isotopologues: Theory and experiment. *J. Mol. Spectrosc.*, 302:3–8, 2014.

[331] J. Demaison. Experimental, semi-experimental and *ab initio* equilibrium structures. *Mol. Phys.*, 105:3109–3138, 2007.

[332] C. Puzzarini, J. F. Stanton, and J. Gauss. Quantum-chemical calculation of spectroscopic parameters for rotational spectroscopy. *Int. Rev. Phys. Chem.*, 29:273–367, 2010.

[333] R. Gendriesch, K. Pehl, T. Giesen, G. Winnewisser, and F. Lewen. Terahertz spectroscopy of linear triatomic CCC: High precision laboratory measurement and analysis of the rovibrational bending transitions. *Z. Naturforsch. A*, 58:129–138, 2003.

[334] T. Motylewski and H. Linnartz. Cavity ring down spectroscopy on radicals in a supersonic slit nozzle discharge. *Rev. Sci. Instrum.*, 70:1305–1312, 1999.

[335] G. Bazalgette Courrèges-Lacoste, J. P. Sprengers, J. Bulthuis, S. Stolte, T. Motylewski, and H. Linnartz. Vibrationally excited state spectroscopy of radicals in a supersonic plasma. *Chem. Phys. Lett.*, 335:209–214, 2001.

[336] G. Bazalgette Courrèges-Lacoste, J.P. Sprengers, W. Ubachs, S. Stolte, and H. Linnartz. The $A^2\Sigma^+ \leftarrow X^2\Pi$ Transition of CF Starting from Highly Excited Vibrational States. *J. Mol. Spectrosc.*, 205:341–343, 2001.

[337] D. Zhao, J. Guss, A. J. Walsh, and H. Linnartz. Mid-infrared continuous wave cavity ring-down spectroscopy of a pulsed hydrocarbon plasma. *Chem. Phys. Lett.*, 565:132–137, 2013.

[338] L.S. Rothman, I.E. Gordon, Y. Babikov, A. Barbe, D. C. Benner, P. F. Bernath, M. Birk, L. Bizzocchi, V. Boudon, L. R. Brown, A. Campargue, K. Chance, E. A. Cohen, L. H. Coudert, V. M. Devi, B. J. Drouin, A. Fayt, J.-M. Flaud, R.R. Gamache, J. J. Harrison, J.-M. Hartmann, C. Hill, J. T. Hodges, D. Jacquemart, A. Jolly, J. Lamouroux, R. J. Le Roy, G. Li, D. A. Long, O. M. Lyulin, C. J. Mackie, S.T. Massie, S. Mikhailenko, H. S. P. Müller, O. V. Naumenko, A. V. Nikitin, J. Orphal, V. Perevalov, A. Perrin, E. R. Polovtseva, C. Richard, M. A. H. Smith, E. Starikova, K. Sung, S. Tashkun, J. Tennyson, G. C. Toon, V. G. Tyuterev, and G. Wagner. The HITRAN2012 molecular spectroscopic database. *J. Quant. Spectrosc. Radiat. Transf.*, 130:4–50, 2013.

[339] C. M. Western. PGOPHER version 8.0, 2014. University of Bristol Research Data Repository See: `www.dx.doi.org/10.5523/bris.huflggvpcuc1zvliqed497r2`.

[340] D. Zhao, M.A. Haddad, H. Linnartz, and W. Ubachs. C_6H and C_6D: Electronic spectra and Renner-Teller analysis. *J. Chem. Phys.*, 135:044307, 2011.

[341] K. D. Doney, D. Zhao, and H. Linnartz. High-resolution infrared spectrum of triacetylene: The ν_5 state revisited and new vibrational states. *J. Mol. Spectrosc.*, 316:54–63, 2015.

[342] K. Yamada and M. Winnewisser. A Parameter to Quantify Molecular Quasilinearity. *Z. Naturforsch. A*, 31:139–144, 1976.

[343] E. B. Wilson, J. C. Decius, and P. C. Cross. *Molecular Vibrations: The Theory of Infrared and Raman Vibrational Spectra*. Dover Publications, 1980.

[344] M. Abramowitz and I. A. Stegun. *Handbook of Mathematical Functions: With Formulas, Graphs, and Mathematical Tables*. Dover Publications, 1965.

[345] W. H. Shaffer. Degenerate modes of vibration and perturbations in polyatomic molecules. *Rev. Mod. Phys.*, 16:245–259, 1944.

[346] K. Yamada. Effect of Phase Choices in Rovibrational Wavefunctions on the Labeling of K- and l-type Doubling in Molecular Energy Levels. *Z. Naturforsch.*, 38a:821–834, 1983.

[347] P. R. Bunker and P. Jensen. *Molecular Symmetry and Spectroscopy*. NRC Research Press, 2nd edition, 2006.

[348] I. Suzuki. Anharmonic Potential Functions of Simple Molecules. III. Computation of Vibration-Rotation Energies of XYZ and X_2Y_2 Type Linear Molecules through Direct Numerical Diagonalization: Application to the N_2O Molecule. *B. Chem. Soc. Jpn.*, 52:1606–1613, 1979.

[349] A. R. Hoy, I. M. Mills, and G. Strey. Anharmonic force constant calculations. *Mol. Phys.*, 24:1265–1290, 1972.

[350] J. K. G. Watsonm. Vibration-rotation Hamiltonians of linear molecules. *Mol. Phys.*, 79(5):943–951, 1993.

[351] S. C. Wang. On the asymmetrical top in quantum mechanics. *Phys. Rev.*, 34:243–252, 1929.

[352] G. Avila, J. Cooper, and T. Carrington. Using pruned basis sets to compute vibrational spectra. *AIP Conf. Proc.*, 1504:925–927, 2012.

[353] A. Ralston. *A first course in numerical analysis*. McGraw-Hill, New York, 1965.

[354] E. Anderson, Z. Bai, C. Bischof, S. Blackford, J. Demmel, J. Dongarra, J. Du Croz, A. Greenbaum, S. Hammarling, A. McKenney, and D. Sorensen. LAPACK *Users' Guide*. Society for Industrial and Applied Mathematics, Philadelphia, PA, 3. edition, 1999.

[355] E. R. Davidson. The iterative calculation of a few of the lowest eigenvalues and corresponding eigenvectors of large real-symmetric matrices. *J. Comp. Phys.*, 17:87–94, 1975.

[356] M. Bollhöfer and Y. Notay. JADAMILU: a software code for computing selected eigenvalues of large sparse symmetric matrices. *Comp. Phys. Comm.*, 177:951–964, 2007.

[357] G. Strey and I. M. Mills. Anharmonic force field of acetylene. *J. Mol. Spectrosc.*, 59:103–115, 1976.

[358] M. J. Bramley, W. H. Green Jr., and N. C. Handy. Vibration-rotation coordinates and kinetic energy operators for polyatomic molecules. *Mol. Phys.*, 73:1183–1208, 1991.

[359] V. Brites and C. Léonard. CCSD(T)-F12 Investigations on HBNH and its Isotopologues. *Int. J. Quant. Chem.*, 112:2051–2061, 2012.

[360] M. Herman. High-resolution Infrared Spectroscopy of Acetylene: Theoretical Background and Research Trends. In M. Quack and F. Merkt, editors, *Handbook of High-Resolution Spectroscopy*. John Wiley & Sons, Ltd., 2011.

[361] C. E. Dateo, T. J. Lee, and D. W. Schwenke. An accurate quartic force field and vibrational frequencies for HNO and DNO. *J. Chem. Phys.*, 101:5853–5859, 1994.

[362] Y. Kawashima, K. Kawaguchi, and E. Hirota. Detection of HBNH by infrared diode laser spectroscopy. *J. Chem. Phys.*, 87:6331, 1987.

[363] G. Simons, R. G. Parr, and J. M. Finlan. New alternative to the Dunham potential for diatomic molecules. *J. Chem. Phys.*, 59:3229–3234, 1973.

[364] J. Pety, P. Gratier, Guzmán, E. Roueff, M. Gerin, J. R. Goicoechea, S. Bardeau, A. Sievers, F. Le Petit, J. Le Bourlot, A. Belloche, and D. Talbi. The IRAM-30 m line survey of the Horsehead PDR II. First detection of the l-C_3H^+ hydrocarbon cation. *Astron. Astrophys.*, 548:A68, 2012.

[365] X. Huang, R. C. Fortenberry, and T. J. Lee. Spectroscopic constants and vibrational frequencies of l-C_3H^+ and isotopologues from highly accurate quartic force fields: The detection of l-C_3H^+ in the Horsehead nebula PDF questioned. *Astrophys. J. Lett.*, 768:L25, 2013.

[366] B. A. McGuire, P. B. Carrol, R. A. Loomis, G. A. Blake, J. M. Hollis, F. J. Lovas, P. R. Jewell, and A. J. Remijan. A search for l-C_3H^+ in Sgr B2(N), Sgr B2(OH), and the dark cloud TMC-1. *Astrophys. J.*, 774:56, 2013.

[367] B. A. McGuire, P. B. Carroll, P. Gratier, V. Guzmán, J. Pety, E. Roueff, M. Gerin, G. A. Blake, and A. J. Remijan. An observational investigation of the identity of B11244 (l-C_3H^+/C_3H^-). *Astrophys. J.*, 783:36, 2014.

[368] S. Brünken, L. Kluge, A. Stoffels, O. Asvany, and S. Schlemmer. Laboratory rotational spectrum of l-C_3H^+ and confirmation of its astronomical detection. *Astrophys. J. Lett.*, 783:L4, 2014.

[369] P. Botschwina, C. Stein, P. Sebald, B. Schröder, and R. Oswald. Strong theoretical support for the assignment of B11244 to l-C_3H^+. *Astrophys. J.*, 787:72, 2014.

[370] S. Wilson and S. Green. Theoretical microwave spectral constants for C_3H^+ and C_4H^+. *Astrophys. J.*, 240:968–970, 1980.

[371] S. Wilson and S. Green. Erratum: Theoretical Microwave Spectral Constants for C_3H^+ and C_4H^+. *Astrophys. J.*, 253:989, 1982.

[372] D. L. Cooper and S. C. Murphy. *Ab initio* Geometries for $C_{2n+1}H$, $C_{2n+1}H^+$, and $C_{2n+1}H_2$ Species for $n = 1,\ 2,\ 3$. *Astrophys. J.*, 333:482, 1988.

[373] S. Ikuta. An *ab initio* MO study on structures and energetics of C_3H^-, C_3H, and C_3H^+. *J. Chem. Phys.*, 106(11):4536–4542, 1997.

[374] G. Winnewisser, A. G. Maki, and D. R. Johnson. Rotational constants for HCN and DCN. *J. Mol. Spectrosc.*, 39:149–158, 1971.

[375] T. J. Lee, C. E. Dateo, B. Gazdy, and J. M. Bowman. Accurate quartic force fields and vibrational frequencies for hydrogen cyanide and hydrogen isocyanide. *J. Phys. Chem.*, 97:8937–8943, 1993.

[376] X. Huang and T. J. Lee. Accurate ab initio quartic force fields for NH_2^- and CCH^- and rovibrational spectroscopic constants for their isotopologs. *J. Chem. Phys.*, 131(10):104301, 2009.

[377] S. Brünken, C. A. Gottlieb, H. Gupta, M. C. McCarthy, and P. Thaddeus. Laboratory detection of the negative molecular ion CCH^-. *Astron. Astrophys.*, 464:L33–L36, 2007.

[378] Y. Kabbadj, M. Herman, G. Di Lonardo, L. Fusina, and J. W. C. Johns. The bending energy levels of C_2H_2. *J. Mol. Spectrosc.*, 150:535–565, 1991.

[379] R. C. Fortenberry, X. Huang, T. D. Crawford, and T. J. Lee. High-accuracy quartic force filed calculations for the spectroscopic constants and vibrational frequencies of $1^1A'$ *l*-C_3H^-: A possible link to lines observed in the Horsehead nebula photodissociation region. *Astrophys. J.*, 772:39, 2013.

[380] J. L. Neill, M. T. Muckle, D. P. Zaleski, A. L. Steber, B. H. Pate, V. Lattanzi, S. Spezzano, M. C. McCarthy, and A. J. Remijan. Laboratory and Tentative Interstellar Detection of Trans-Methyl Formate Using the Publicly Available Green Bank Telescope Primos Survey. *Astrophys. J.*, 755:153, 2012.

[381] C. Stein, O. Weser, B. Schröder, and P. Botschwina. High-level theoretical spectroscopic parameters for three ions of astrochemical interest. *Mol. Phys.*, 113:2169–2178, 2015.

[382] S. Chhabra and T. Dhilip Kumar. *Ab Initio* potential energy surfaces of c_3 collision with proton and quantum dynamics of rotational transition. *J. Phys. Chem. A*, 122(24):5437–5444, 2018.

[383] G. Amat and H. H. Nielsen. Vibrational ℓ-Type Doubling and ℓ-type Resonance in Linear Polyatomic Molecules. *J Mol. Spectrosc.*, 2:152–162, 1958.

[384] P. Sebald. A note on ℓ-type doubling constants in linear triatomic molecules $ClHCl^-$: A molecular anion with an unusual q. *Chem. Phys.*, 346:77–80, 2008.

[385] C. Lanczos. An iteration method for the solution of the eigenvalue problem of linear differential and integral operators. *J. Res. Nat. Nur. Std.*, 45:255–282, 1950.

[386] Z. Zhao, J. Chen, Z. Zhang, D. H. Zhang, X.-G. Wang, T. Carrington, and F. Gatti. Computing energy levels of CH_4, CHD_3, CH_3D, and CH_3F with a direct product basis and coordinates based on the methyl subsystem. *J. Chem. Phys.*, 148:074113, 2018.

Appendix A

Supplemental material for hydrogen cyanide HCN

Table A.1: Basic (F12b), core-valence correlation (CV), scalar relativisitic (SR) and diagonal Born-Oppenheimer correction (DBOC) contributions to the composite potential energy function (PEF) of HCN.[a]

			$C_{ijk}^{(\alpha)}$			
i	j	k	F12b[b]	CV[c]	SR[d]	DBOC[e]
1	0	0	−0.00116912	0.00100145	0.00010266	−0.00011639
2	0	0	0.20197271	−0.00077485	−0.00014996	0.00009530
3	0	0	−0.20226561	0.00048225	0.00009294	−0.00004102
4	0	0	0.13690782	−0.00020827	−0.00004920	0.00002056
5	0	0	−0.07977321	0.00003107	0.00002147	−0.00001110
6	0	0	0.04237125	−0.00006207	−0.00000625	0.00000458
7	0	0	−0.02139640	0.00016910	0.00000156	0.00000066
8	0	0	0.01108800	−0.00009889	−0.00000072	−0.00000132
9	0	0	−0.00540408			
10	0	0	0.00150074			
0	1	0	−0.00425664	0.00587638	0.00043363	−0.00001886
0	2	0	0.60802976	−0.00492761	−0.00098987	0.00009279
0	3	0	−0.70969765	0.00277814	0.00077348	−0.00005046
0	4	0	0.50776193	−0.00124084	−0.00038498	0.00002713
0	5	0	−0.29401587	0.00060466	0.00018278	−0.00002112
0	6	0	0.15249370	−0.00023131	−0.00005919	0.00000871

To be continued on next page

Table A.1: *Continued from previous page*

i	j	k	F12b[b]	CV[c]	SR[d]	DBOC[e]
0	7	0	−0.07242603			
0	8	0	0.02426924			
0	0	2	0.03009963	−0.00004358	−0.00003170	0.00001473
0	0	4	0.00021860	0.00001484	0.00000115	−0.00000613
0	0	6	−0.00017278	0.00002471	−0.00000332	0.00000005
0	0	8	0.00006146	−0.00003429	0.00000130	0.00000111
0	0	10	−0.00021166	0.00002342	−0.00000039	−0.00000018
0	0	12	0.00014270	−0.00000807	0.00000006	
0	0	14	−0.00005041	0.00000112		
0	0	16	0.00000691			
1	1	0	−0.01371002	0.00019761	−0.00004437	−0.00001665
2	1	0	0.00377003	−0.00007075	−0.00001313	0.00002854
1	2	0	0.00019181	−0.00008152	−0.00000324	0.00000522
3	1	0	−0.00464398	0.00002832	0.00001233	−0.00002290
2	2	0	−0.00649325	0.00005696	0.00001493	0.00000089
1	3	0	−0.00042478	0.00005849	0.00001033	−0.00000903
4	1	0	0.00329840	−0.00002191	−0.00000359	0.00001222
3	2	0	0.00529365	−0.00003040	−0.00000345	0.00000120
2	3	0	0.00385709	−0.00004097	−0.00000679	0.00000178
1	4	0	0.00142678	−0.00004995	0.00000383	0.00000114
5	1	0	−0.00186863			
4	2	0	−0.00281481			
3	3	0	−0.00286502			
2	4	0	−0.00210504			
1	5	0	0.00023421			
1	0	2	−0.00889861	0.00002914	−0.00000251	0.00000416
0	1	2	−0.04013552	0.00008586	0.00001439	0.00002023
2	0	2	−0.00067626	−0.00001290	0.00001198	−0.00000184
1	1	2	0.01030078	0.00001699	0.00000372	−0.00002349
0	2	2	0.00481683	0.00000457	0.00001780	0.00000307
3	0	2	0.00107576	0.00002210	−0.00000250	0.00000089
2	1	2	0.00182247	−0.00003150	−0.00000148	0.00001007
1	2	2	−0.00446861	0.00007289	−0.00000801	−0.00000346
0	3	2	−0.00114852	0.00018544	0.00002221	−0.00001252
1	0	4	−0.00188796	0.00005543	−0.00000256	0.00000425

To be continued on next page

Table A.1: *Continued from previous page*

i	j	k	F12b[b]	CV[c]	SR[d]	DBOC[e]
0	1	4	0.00554524	0.00003633	0.00000519	−0.00000869
4	0	2	−0.00030827			
3	1	2	−0.00047450			
2	2	2	−0.00109319			
1	3	2	0.00154862			
0	4	2	0.00437934			
2	0	4	0.00084497			
1	1	4	−0.00222173			
0	2	4	0.00092086			

[a] PEF coefficients are quoted in atomic units; see Equation (3.1) for their definition. Expanded around $r_{\text{ref}} = 1.0650$ and $R_{\text{ref}} = 1.1532$ Å.

[b] F12b: fc-CCSD(T)-F12b/VQZ-F12.

[c] CV: [ae-CCSD(T) − fc-CCSD(T)]/CV6Z.

[d] SR: DKH2-fc-CCSD(T)/VQZ-DK − fc-CCSD(T)/VQZ.

[e] DBOC ($H^{12}C^{14}N$): ae-CCSD/CVQZ.

Table A.2: Higher-order correlation (HC) contributions to the composite potential energy function (PEF) of HCN.[a]

			$C_{ijk}^{(\alpha)}$			
i	j	k	(Q)-(T)[b]	Q-(Q)[c]	P-Q[d]	S-P[e]
1	0	0	0.00001656	0.00003551	−0.00000513	0.00000023
2	0	0	−0.00012037	0.00002797	−0.00001052	−0.00000077
3	0	0	−0.00005433	0.00001108	0.00000093	−0.00000012
4	0	0	−0.00001877	0.00000349	−0.00000091	−0.00000018
5	0	0	0.00002552	0.00000062	0.00000011	0.00000005
6	0	0	−0.00001548	0.00000311	−0.00000028	−0.00000005
7	0	0	−0.00001766	0.00000225	−0.00000028	
8	0	0	0.00001711	−0.00000202	0.00000024	
0	1	0	−0.00231045	0.00068707	−0.00047291	−0.00005284
0	2	0	−0.00233715	0.00111642	−0.00064471	−0.00010642
0	3	0	−0.00157199	0.00123247	−0.00048098	−0.00013748
0	4	0	−0.00068487	0.00094603	−0.00007575	−0.00011589
0	5	0	0.00014061	0.00031730	0.00025199	−0.00003663
0	6	0	0.00068692	−0.00037527	0.00027632	0.00005990
0	0	2	−0.00027652	0.00002211	−0.00003391	−0.00000344
0	0	4	0.00003220	−0.00000673	0.00000641	0.00000052
0	0	6	0.00000146	0.00000390	0.00000436	0.00000027
0	0	8	0.00002932	−0.00000250	−0.00000205	0.00000004
0	0	10	−0.00001766	0.00000038	0.00000102	
0	0	12	0.00000322	−0.00000004	−0.00000019	
1	1	0	0.00008995	0.00008351	−0.00000570	−0.00000038
2	1	0	−0.00017042	0.00008109	−0.00002818	−0.00000399
1	2	0	0.00008031	0.00006565	−0.00000553	−0.00000437
3	1	0	−0.00006965	0.00001529	0.00000597	−0.00001338
2	2	0	−0.00003580	0.00009297	−0.00004259	−0.00001343
1	3	0	0.00008277	−0.00002113	−0.00000205	−0.00000836
4	1	0	−0.00003348	0.00001277	−0.00000396	
3	2	0	0.00003861	−0.00001864	0.00000725	
2	3	0	0.00008994	0.00003045	−0.00002588	
1	4	0	0.00001126	−0.00010597	0.00001074	
1	0	2	−0.00004013	−0.00001047	−0.00000581	−0.00000204
0	1	2	−0.00037033	0.00003508	−0.00007082	−0.00000965

To be continued on next page

Table A.2: *Continued from previous page*

i	j	k	(Q)-(T)[b]	Q-(Q)[c]	P-Q[d]	S-P[e]
2	0	2	−0.00000039	−0.00000812	−0.00001072	0.00000375
1	1	2	−0.00002702	−0.00003541	−0.00001239	0.00000530
0	2	2	0.00007870	−0.00002443	0.00002807	−0.00001297
3	0	2	0.00004240	−0.00000556	0.00000506	
2	1	2	0.00001359	−0.00004104	−0.00002000	
1	2	2	−0.00005089	−0.00008531	0.00001248	
0	3	2	0.00055855	−0.00015168	0.00024902	
1	0	4	−0.00003655	−0.00000129	−0.00000446	
0	1	4	0.00019657	−0.00000426	0.00006011	

[a] PEF coefficients are quoted in atomic units; see Equation (3.1) for their definition. Expanded around $r_{\mathrm{ref}} = 1.0650$ and $R_{\mathrm{ref}} = 1.1532$ Å.

[b] (Q)-(T): [CCSDT(Q) − CCSD(T)]/VTZ.

[c] Q-(Q): [CCSDTQ − CCSDT(Q)]/VDZ.

[d] P-Q: [CCSDTQP − CCSDTQ]/VDZ.

[e] S-P: [CCSDTQPS − CCSDTQP]/VDZ.

Table A.3: Basic contributions to the multi-reference based composite potential energy functions (PEF) of HCN.[a]

			$C_{ijk}^{(\alpha)}$					$C_{ijk}^{(\alpha)}$	
i	j	k	MR-F12[b]	AC-F12[c]	i	j	k	MR-F12[b]	AC-F12[c]
1	0	0	0.00056545	0.00078610	2	2	0	−0.00498928	−0.00492849
2	0	0	0.20198573	0.20202689	1	3	0	−0.00143568	−0.00137559
3	0	0	−0.20239983	−0.20250331	4	1	0	0.00271637	0.00267088
4	0	0	0.13642868	0.13662391	3	2	0	0.00498593	0.00526697
5	0	0	−0.08023057	−0.07992443	2	3	0	0.00303279	0.00306132
6	0	0	0.04409142	0.04220139	1	4	0	−0.00015833	−0.00027818
7	0	0	−0.02167561	−0.02151887	5	1	0	−0.00247533	−0.00253062
8	0	0	0.00589788	0.01108851	4	2	0	−0.00168987	−0.00342995
9	0	0		−0.00524868	3	3	0	−0.00303016	−0.00322601
10	0	0		0.00115256	2	4	0	−0.00269636	−0.00292343
0	1	0	−0.01026532	−0.01003347	1	5	0	0.00312699	0.00295688
0	2	0	0.60860430	0.60866085	1	0	2	−0.01035744	−0.01034393
0	3	0	−0.70963826	−0.70971306	0	1	2	−0.03738453	−0.03755904
0	4	0	0.50454728	0.50458590	2	0	2	−0.00134155	−0.00126944
0	5	0	−0.28997715	−0.28989707	1	1	2	0.01422533	0.01413685
0	6	0	0.14994384	0.14990963	0	2	2	0.00273121	0.00275336
0	7	0	−0.06857133	−0.07029248	3	0	2	0.00090315	0.00112877
0	8	0	0.02096874	0.02351016	2	1	2	0.00362616	0.00358693
0	0	2	0.02855601	0.02862887	1	2	2	−0.00724080	−0.00712036
0	0	4	0.00032039	0.00033183	0	3	2	−0.00221073	−0.00216466
0	0	6	0.00005305	−0.00001734	1	0	4	−0.00156230	−0.00151914
0	0	8	−0.00009742	0.00005242	0	1	4	0.00597078	0.00606814
0	0	10	−0.00006607	−0.00023504	4	0	2	0.00105439	−0.00024560
0	0	12	0.00004725	0.00015086	3	1	2	−0.00029645	−0.00023622
0	0	14	−0.00001914	−0.00005194	2	2	2	−0.00013900	−0.00124620
0	0	16	0.00000293	0.00000713	1	3	2	0.00069770	0.00045718
1	1	0	−0.01693529	−0.01684458	0	4	2	0.01004115	0.00994179
2	1	0	0.00206170	0.00204767	2	0	4	0.00159004	0.00111664
1	2	0	0.00350451	0.00341900	1	1	4	−0.00255435	−0.00272873
3	1	0	−0.00528095	−0.00531778	0	2	4	0.00083351	0.00094154

[a] PEF coefficients are quoted in atomic units; see Equation (3.1) for their definition.
Expanded around $r_{\text{ref}} = 1.0650$ and $R_{\text{ref}} = 1.1532$ Å.

[b] MR-F12: fc-MRCI-F12+Q/VQZ-F12 (full-valence CASSCF reference).

[c] AC-F12: fc-MRACPF-F12/VQZ-F12 (full-valence CASSCF reference).

Table A.4: Adiabatic composite potential energy functions for $H^{12}C^{14}N$.[a]

			C_{ijk}		
i	j	k	Comp I[b]	Comp II[c]	Comp III[d]
2	0	0	0.20083522	0.20341705	0.20379582
3	0	0	−0.20159018	−0.20391158	−0.20432057
4	0	0	0.13654049	0.13769472	0.13810569
5	0	0	−0.07964376	−0.08118152	−0.08097406
6	0	0	0.04209174	0.04458740	0.04277888
7	0	0	−0.02092684	−0.02167672	−0.02172555
8	0	0	0.01126159	0.00579748	0.01118998
9	0	0	−0.00629466		−0.00529770
10	0	0	0.00200900		0.00115256
0	2	0	0.60002232	0.59588523	0.59636403
0	3	0	−0.70695780	−0.69959688	−0.70007376
0	4	0	0.50612613	0.49825356	0.49858352
0	5	0	−0.29243803	−0.28630712	−0.28640873
0	6	0	0.15240104	0.14810170	0.14812758
0	7	0	−0.07254773	−0.06802385	−0.06971668
0	8	0	0.02548365	0.02096874	0.02351016
0	0	2	0.02974019	0.02841196	0.02849742
0	0	4	0.00026095	0.00035530	0.00036647
0	0	6	−0.00013791	0.00007496	0.00000457
0	0	8	0.00004028	−0.00012980	0.00002004
0	0	10	−0.00018243	−0.00004298	−0.00021195
0	0	12	0.00011994	0.00003920	0.00014282
0	0	14	−0.00004250	−0.00001802	−0.00005082
0	0	16	0.00000590	0.00000293	0.00000713
1	1	0	−0.01340313	−0.01679122	−0.01670455
2	1	0	0.00358819	0.00203271	0.00203020
1	2	0	0.00024451	0.00344789	0.00336871
3	1	0	−0.00470311	−0.00527118	−0.00531339
2	2	0	−0.00643242	−0.00494233	−0.00489502
1	3	0	−0.00031599	−0.00140020	−0.00134501
4	1	0	0.00324981	0.00273789	0.00269041
3	2	0	0.00528407	0.00494873	0.00526314
2	3	0	0.00388754	0.00298526	0.00302069

To be continued on next page

Table A.4: *Continued from previous page*

i	j	k	Comp I[b]	Comp II[c]	Comp III[d]
1	4	0	0.00128691	−0.00013235	−0.00025306
5	1	0	−0.00168461	−0.00247533	−0.00253062
4	2	0	−0.00266485	−0.00168987	−0.00342995
3	3	0	−0.00267942	−0.00303016	−0.00322601
2	4	0	−0.00194360	−0.00269636	−0.00292343
1	5	0	0.00020335	0.00312699	0.00295688
1	0	2	−0.00892587	−0.01027039	−0.01025913
0	1	2	−0.04043397	−0.03729857	−0.03748147
2	0	2	−0.00070119	−0.00134308	−0.00127635
1	1	2	0.01026294	0.01414902	0.01406059
0	2	2	0.00481749	0.00276376	0.00279089
3	0	2	0.00116731	0.00090713	0.00115280
2	1	2	0.00184090	0.00360565	0.00355942
1	2	2	−0.00462987	−0.00717150	−0.00704412
0	3	2	−0.00015910	−0.00188705	−0.00184968
1	0	4	−0.00187218	−0.00152528	−0.00147986
0	1	4	0.00593142	0.00601852	0.00611836
4	0	2	−0.00009980	0.00105439	−0.00024560
3	1	2	−0.00059637	−0.00029645	−0.00023622
2	2	2	−0.00074087	−0.00013900	−0.00124620
1	3	2	0.00108839	0.00069770	0.00045718
0	4	2	0.00566913	0.01004115	0.00994179
2	0	4	0.00075011	0.00159004	0.00111664
1	1	4	−0.00309489	−0.00255435	−0.00272873
0	2	4	0.00202416	0.00083351	0.00094154

[a] PEF coefficients are quoted in atomic units; see Equation (3.1) for their definition.

[b] Equilibrium geometry: $r_e = 1.06518$ and $R_e = 1.15325$ Å.

[c] Equilibrium geometry: $r_e = 1.06304$ and $R_e = 1.15493$ Å.

[d] Equilibrium geometry: $r_e = 1.06275$ and $R_e = 1.15482$ Å.

Table A.5: Basic (F12b), core-valence correlation (CV) and scalar relativisitic (SR) contributions to the parallel component of the composite electric dipole moment function (EDMF) of HCN.[a]

			$D^{(\alpha)}_{ijk}$		
i	j	k	F12b[b]	CV[c]	SR[d]
0	0	0	−1.18949174	−0.00053667	0.00117691
1	0	0	−0.24399323	−0.00209792	0.00027657
2	0	0	0.00548214	−0.00064584	0.00022127
3	0	0	0.02012629	0.00008863	0.00014486
4	0	0	0.02178174	0.00008292	−0.00002121
5	0	0	−0.00464751		
6	0	0	0.00488381		
7	0	0	−0.00578131		
8	0	0	0.00262302		
0	1	0	0.06797994	−0.00178167	0.00123295
0	2	0	0.13203384	0.00036472	−0.00037834
0	3	0	−0.00678975	−0.00034491	−0.00016132
0	4	0	−0.00221881	−0.00031823	0.00002894
0	5	0	0.01541951	−0.00193781	−0.00007748
0	6	0	−0.00143455		
0	0	2	0.32648394	0.00012526	−0.00007472
0	0	4	−0.01540756	0.00002052	0.00000286
0	0	6	0.00508354	−0.00002174	−0.00000408
0	0	8	−0.00073688		
0	0	10	0.00041841		
0	0	12	−0.00010365		
1	1	0	−0.00020553	−0.00077624	0.00040331
2	1	0	0.03564703	−0.00008437	0.00019467
1	2	0	0.05167953	0.00058743	−0.00030395
3	1	0	0.02799005		
2	2	0	0.01516749		
1	3	0	−0.02424434		
4	1	0	0.00345838		
3	2	0	−0.00711140		
2	3	0	−0.01710382		
1	4	0	0.03665014		
5	1	0	−0.01662741		

To be continued on next page

Table A.5: *Continued from previous page*

i	j	k	F12b[b]	CV[c]	SR[d]
4	2	0	−0.00635046		
3	3	0	−0.01596217		
2	4	0	0.01707007		
1	5	0	−0.02721503		
1	0	2	0.06673151	0.00049727	−0.00008968
0	1	2	0.06989130	−0.00024501	−0.00038266
2	0	2	−0.03276690		
1	1	2	0.11496275		
0	2	2	−0.08195165		
3	0	2	−0.01570139		
2	1	2	0.00547634		
1	2	2	−0.01902668		
0	3	2	−0.02605798		
1	0	4	−0.01539005		
0	1	4	−0.06889530		
4	0	2	0.00982692		
3	1	2	−0.06503746		
2	2	2	0.06479547		
1	3	2	−0.03435372		
0	4	2	0.03465946		
2	0	4	0.01430168		
1	1	4	−0.01848149		
0	2	4	0.01868350		

[a] EDMF coefficients are quoted in atomic units; see Equation (3.3) for their definition. Expanded around $r_e = 1.06518$ and $R_e = 1.15325$ Å.

[b] Basic contribution calculated using fc-CCSD(T)-F12b/AV5Z.

[c] CV contribution: [ae-CCSD(T) − fc-CCSD(T)]/ACV6Z.

[d] SR contribution: DKH2-fc-CCSD(T)/AVQZ-DK − fc-CCSD(T)/AVQZ.

Table A.6: Higher-order correlation (HC) contributions to the perpendicular component of the composite electric dipole moment function (EDMF) of HCN.[a]

			$D^{(\alpha)}_{ijk}$			
i	j	k	(Q)-(T)[b]	Q-(Q)[c]	P-Q[d]	S-P[e]
0	0	0	0.00313225	−0.00019976	0.00055618	0.00006233
1	0	0	0.00208280	−0.00072321	0.00018757	0.00004146
2	0	0	0.00217750	−0.00062574	0.00006011	0.00001408
3	0	0	0.00160178	−0.00039519	0.00003740	0.00008897
4	0	0	0.00106781	−0.00018771	−0.00000210	−0.00001045
0	1	0	0.00760111	−0.00156488	0.00215881	0.00063964
0	2	0	0.01092062	−0.00471590	0.00319996	0.00306174
0	3	0	0.01500450	−0.00810803	0.00161952	0.00917050
0	4	0	0.01743273	−0.01028927	−0.00247467	0.01436590
0	5	0	0.01075631	−0.01133754	−0.00519122	
0	0	2	−0.00005938	0.00035851	−0.00000404	
0	0	4	−0.00003669	−0.00017241	−0.00021753	
0	0	6	−0.00238279	0.00023377	0.00003200	
0	0	8	0.00212001	−0.00025721	0.00000372	
0	0	10	−0.00069787	0.00012781		
0	0	12	0.00008135	−0.00002235		
1	1	0	0.00470461	−0.00306622	0.00093836	0.00040143
2	1	0	0.00440244	−0.00215042	0.00040394	−0.00099218
1	2	0	0.00366507	−0.00507449	0.00149556	0.00896146
1	0	2	−0.00086870	0.00036867	0.00011028	
0	1	2	−0.00301246	0.00207564	−0.00062107	

[a] EDMF coefficients are quoted in atomic units; see Equation (3.3) for their definition. Expanded around $r_e = 1.06518$ and $R_e = 1.15325$ Å.

[b] (Q)-(T) contribution: [CCSDT(Q) − CCSD(T)]/AVTZ.

[c] Q-(Q) contribution: [CCSDTQ − CCSDT(Q)]/VTZ(H: *sp*; C,N: *spd*).

[d] P-Q contribution: [CCSDTQP − CCSDTQ]/VDZ.

[e] S-P contribution: [CCSDTQPS − CCSDTQP]/VDZ.

Table A.7: Basic (F12b), core-valence correlation (CV) and scalar relativisitic (SR) contributions to the perpendicular component of the composite electric dipole moment function (EDMF) of HCN.[a]

			$D_{ijk}^{(\alpha)}$		
i	j	k	F12b[b]	CV[c]	SR[d]
0	0	1	0.32531217	0.00013822	0.00084932
0	0	3	−0.04390968	0.00009202	−0.00030593
0	0	5	−0.00429512	0.00014892	0.00004877
0	0	7	0.00464616	−0.00004553	−0.00000875
0	0	9	−0.00168032		
0	0	11	0.00061728		
0	0	13	−0.00010725		
1	0	1	0.17272654	0.00109839	−0.00000420
0	1	1	0.22228125	−0.00050285	−0.00027956
2	0	1	0.01693034	0.00017564	−0.00013308
1	1	1	0.04180358	0.00023877	−0.00025929
0	2	1	−0.09404360	0.00049243	−0.00039765
3	0	1	−0.03918161		
2	1	1	0.00653699		
1	2	1	−0.09168395		
0	3	1	−0.00665124		
1	0	3	−0.02058270		
0	1	3	−0.14997535		
4	0	1	−0.00546913		
3	1	1	−0.00872279		
2	2	1	−0.01583606		
1	3	1	0.00395622		
0	4	1	−0.00050651		
2	0	3	0.00445088		
1	1	3	−0.06965528		
0	2	3	0.02124966		
5	0	1	−0.00200378		
4	1	1	−0.01841213		
3	2	1	0.01136647		
2	3	1	−0.00362564		
1	4	1	0.01826154		
0	5	1	0.01955804		

To be continued on next page

Table A.7: *Continued from previous page*

i	j	k	F12b[b]	CV[c]	SR[d]
3	0	3	0.01338442		
2	1	3	0.01939271		
1	2	3	−0.02821246		
0	3	3	0.07927730		
1	0	5	0.01376848		
0	1	5	0.02434506		

[a] EDMF coefficients are quoted in atomic units; see Equation (3.4) for their definition. Expanded around $r_e = 1.06518$ and $R_e = 1.15325$ Å.

[b] Basic contribution calculated using fc-CCSD(T)-F12b/AV5Z.

[c] CV contribution: [ae-CCSD(T) − fc-CCSD(T)]/ACV6Z.

[d] SR contribution: DKH2-fc-CCSD(T)/AVQZ-DK − fc-CCSD(T)/AVQZ.

Table A.8: Higher-order correlation (HC) contributions to the perpendicular component of the composite electric dipole moment function (EDMF) of HCN.[a]

			$D^{(\alpha)}_{ijk}$		
i	j	k	(Q)-(T)[b]	Q-(Q)[c]	P-Q[d]
0	0	1	0.00100713	0.00017191	0.00004963
0	0	3	−0.00170811	0.00033749	−0.00029893
0	0	5	−0.00085467	−0.00017075	0.00002176
0	0	7	0.00102802	0.00006473	0.00003008
0	0	9	−0.00022808	−0.00001232	−0.00000501
1	0	1	0.00005826	0.00012222	0.00000983
0	1	1	0.00094391	0.00091739	−0.00009326
2	0	1	−0.00092417	0.00016839	−0.00002604
1	1	1	0.00055891	0.00053482	0.00018711
0	2	1	−0.00121810	0.00212096	−0.00074306

[a] EDMF coefficients are quoted in atomic units; see Equation (3.4) for their definition. Expanded around $r_e = 1.06518$ and $R_e = 1.15325$ Å.

[b] (Q)-(T) contribution: [CCSDT(Q) − CCSD(T)]/AVTZ.

[c] Q-(Q) contribution: [CCSDTQ − CCSDT(Q)]/VTZ(H: *sp*; C,N: *spd*).

[d] P-Q contribution: [CCSDTQP − CCSDTQ]/VDZ.

Table A.9: Composite electric dipole moment function for HCN.[a]

$\mu_{\parallel}$				$\mu_{\perp}$			
i	j	k	D_{ijk}	i	j	k	D_{ijk}
0	0	0	-1.18530049	0	0	1	0.32752838
1	0	0	-0.24422597	0	0	3	-0.04579315
2	0	0	0.00668353	0	0	5	-0.00510109
3	0	0	0.02169275	0	0	7	0.00571470
4	0	0	0.02271099	0	0	9	-0.00192573
5	0	0	-0.00464751	0	0	11	0.00061728
6	0	0	0.00488381	0	0	13	-0.00010725
7	0	0	-0.00578131	1	0	1	0.17401103
8	0	0	0.00262302	0	1	1	0.22326688
0	1	0	0.07626591	2	0	1	0.01619108
0	2	0	0.14448664	1	1	1	0.04306390
0	3	0	0.01039050	0	2	1	-0.09378903
0	4	0	0.01652658	3	0	1	-0.03918161
0	5	0	0.00763177	2	1	1	0.00653699
0	6	0	-0.00143455	1	2	1	-0.09168395
0	0	2	0.32682956	0	3	1	-0.00665124
0	0	4	-0.01581080	1	0	3	-0.02058270
0	0	6	0.00294069	0	1	3	-0.14997535
0	0	8	0.00112965	4	0	1	-0.00546913
0	0	10	-0.00015165	3	1	1	-0.00872279
0	0	12	-0.00004465	2	2	1	-0.01583606
1	1	0	0.00239972	1	3	1	0.00395622
2	1	0	0.03742111	0	4	1	-0.00050651
1	2	0	0.06101060	2	0	3	0.00445088
3	1	0	0.02799005	1	1	3	-0.06965528
2	2	0	0.01516749	0	2	3	0.02124966
1	3	0	-0.02424434	5	0	1	-0.00200378
4	1	0	0.00345838	4	1	1	-0.01841213
3	2	0	-0.00711140	3	2	1	0.01136647
2	3	0	-0.01710382	2	3	1	-0.00362564
1	4	0	0.03665014	1	4	1	0.01826154
5	1	0	-0.01662741	0	5	1	0.01955804
4	2	0	-0.00635046	3	0	3	0.01338442

To be continued on next page

Table A.9: *Continued from previous page*

i	j	k	D_{ijk}	i	j	k	D_{ijk}
3	3	0	-0.01596217	2	1	3	0.01939271
2	4	0	0.01707007	1	2	3	-0.02821246
1	5	0	-0.02721503	0	3	3	0.07927730
1	0	2	0.06674935	1	0	5	0.01376848
0	1	2	0.06770574	0	1	5	0.02434506
2	0	2	-0.03276690				
1	1	2	0.11496275				
0	2	2	-0.08195165				
3	0	2	-0.01570139				
2	1	2	0.00547634				
1	2	2	-0.01902668				
0	3	2	-0.02605798				
1	0	4	-0.01539005				
0	1	4	-0.06889530				
4	0	2	0.00982692				
3	1	2	-0.06503746				
2	2	2	0.06479547				
1	3	2	-0.03435372				
0	4	2	0.03465946				
2	0	4	0.01430168				
1	1	4	-0.01848149				
0	2	4	0.01868350				

[a] EDMF coefficients are quoted in atomic units; see Equation (3.3) and (3.4) for their definitions. Expanded around $r_e = 1.06518$ and $R_e = 1.15325$ Å.

Table A.10: Calculated[a] and experimental[b] spectroscopic parameters (in cm^{-1}) for $H^{12}C^{14}N$ up to the first overtone of the CH stretching vibrationa $(2, 0^0, 0)$.

State	Method	G_v	B_v	$10^6 D_v$
$(0, 0^0, 0)e$	calc.	0.00	1.47825	-2.907
	exp.	0.00	1.47822	-2.909
$(0, 1^1, 0)e$	calc.	711.89	1.47807	-2.930
	exp.	711.98	1.47804	-2.932
$(0, 1^1, 0)f$	calc.	711.89	1.48556	-3.018
	exp.	711.98	1.48552	-3.019
$(0, 2^0, 0)e$	calc.	1411.21	1.48584	-6.673
	exp.	1411.41	1.48580	-6.679
$(0, 2^2, 0)e$	calc.	1426.34	1.48510	0.573
	exp.	1426.53	1.48506	0.576
$(0, 2^2, 0)f$	calc.	1426.34	1.48507	-3.028
	exp.	1426.53	1.48502	-3.030
$(0, 0^0, 1)e$	calc.	2097.13	1.46817	-2.912
	exp.	2096.85	1.46814	-2.916
$(0, 3^1, 0)e$	calc.	2113.14	1.48191	-4.301
	exp.	2113.45	1.48186	-4.304
$(0, 3^1, 0)f$	calc.	2113.14	1.49740	-4.946
	exp.	2113.45	1.49734	-4.948
$(0, 3^3, 0)e$	calc.	2143.48	1.48800	-1.814
	exp.	2143.76	1.48795	-1.815
$(0, 3^3, 0)f$	calc.	2143.48	1.48792	-1.349
	exp.	2143.76	1.48787	-1.348
$(0, 4^0, 0)e$	calc.	2802.57	1.49368	-13.616
	exp.	2802.97	1.49357	-13.535
$(0, 1^1, 1)e$	calc.	2805.78	1.46782	-2.782
	exp.	2805.58	1.46782	-2.881
$(0, 1^1, 1)f$	calc.	2805.78	1.47536	-3.022
	exp.	2805.58	1.47532	-3.024
$(0, 4^2, 0)e$	calc.	2817.78	1.49347	5.599
	exp.	2818.16	1.49340	5.602
$(0, 4^2, 0)f$	calc.	2817.79	1.49311	-4.522
	exp.	2818.18	1.49304	-4.523
$(0, 4^4, 0)e$	calc.	2863.42	1.49049	-1.743

To be continued on next page

Table A.10: *Continued from previous page*

State	Method	G_v	B_v	$10^6 D_v$
	exp.	2863.78	1.49043	-1.744
$(0, 4^4, 0)f$	calc.	2863.42	1.49050	-1.770
	exp.	2863.78	1.49044	-1.771
$(1, 0^0, 0)e$	calc.	3311.85	1.46783	-2.882
	exp.	3311.48	1.46780	-2.884
$(0, 5^1, 0)e$	calc.	3494.69	1.48592	-6.432
	exp.	3495.12	1.48586	-6.484
$(0, 5^1, 0)f$	calc.	3494.68	1.51004	-8.639
	exp.	3495.11	1.50996	-8.637
$(0, 2^0, 1)e$	calc.	3502.18	1.47551	-6.717
	exp.	3502.12	1.47545	-6.711
$(0, 2^2, 1)e$	calc.	3516.96	1.47479	0.626
	exp.	3516.87	1.47474	0.633
$(0, 2^2, 1)f$	calc.	3516.97	1.47475	-3.028
	exp.	3516.87	1.47470	-3.022
$(0, 5^3, 0)e$	calc.	3525.24	1.49632	-1.282
	exp.	3525.67	1.49624	-1.283
$(0, 5^3, 0)f$	calc.	3525.25	1.49600	0.676
	exp.	3525.68	1.49592	0.675
$(0, 5^5, 0)e$	calc.	3586.28	1.49263	-1.837
	exp.	3586.70	1.49256	-1.841
$(0, 5^5, 0)f$	calc.	3586.28	1.49263	-1.836
	exp.	3586.70	1.49256	-1.840
$(1, 1^1, 0)e$	calc.	4004.49	1.46780	-2.907
	exp.	4004.16	1.46776	-2.908
$(1, 1^1, 0)f$	calc.	4004.49	1.47541	-3.001
	exp.	4004.16	1.47537	-3.003
$(0, 0^0, 2)e$	calc.	4173.65	1.45804	-2.919
	exp.	4173.07	1.45800	-2.921
$(0, 6^0, 0)e$	calc.	4174.23	1.50134	-22.110
	exp.	4174.64	1.50124	-22.101
$(0, 6^2, 0)e$	calc.	4189.52	1.50298	11.403
	exp.	4189.93	1.50288	11.404

To be continued on next page

Table A.10: *Continued from previous page*

State	Method	G_v	B_v	$10^6 D_v$
$(0, 6^2, 0)f$	calc.	4189.56	1.50166	-6.849
	exp.	4189.97	1.50156	-6.846
$(0, 3^1, 1)e$	calc.	4201.14	1.47148	-4.315
	exp.	4201.21	1.47143	-4.330
$(0, 3^1, 1)f$	calc.	4201.14	1.48690	-4.969
	exp.	4201.20	1.48684	-4.979
$(0, 3^3, 1)e$	calc.	4230.81	1.47756	-1.801
	exp.	4230.84	1.47750	-1.801
$(0, 3^3, 1)f$	calc.	4230.82	1.47748	-1.321
	exp.	4230.84	1.47742	-1.320
$(0, 6^4, 0)e$	calc.	4235.61	1.49885	-0.890
	exp.	4236.02	1.49876	-0.889
$(0, 6^4, 0)f$	calc.	4235.61	1.49889	-1.038
	exp.	4236.02	1.49880	-1.038
$(0, 6^6, 0)e$	calc.	4312.18	1.49432	-1.870
	exp.	4312.62	1.49424	-1.871
$(0, 6^6, 0)f$	calc.	4312.18	1.49432	-1.870
	exp.	4312.62	1.49424	-1.871
$(1, 2^0, 0)e$	calc.	4684.59	1.47585	-6.827
	exp.	4684.31	1.47580	-6.830
$(1, 2^2, 0)e$	calc.	4699.50	1.47511	0.754
	exp.	4699.21	1.47506	0.754
$(1, 2^2, 0)f$	calc.	4699.50	1.47507	-3.013
	exp.	4699.21	1.47502	-3.014
$(0, 7^1, 0)e$	calc.	4856.39	1.49012	-9.190
	exp.	4856.70	1.48999	-9.177
$(0, 7^1, 0)f$	calc.	4856.37	1.52364	-14.574
	exp.	4856.68	1.52352	-14.561
$(0, 1^1, 2)e$	calc.	4878.78	1.45763	-2.938
	exp.	4878.29	1.45759	-2.943
$(0, 1^1, 2)f$	calc.	4878.78	1.46510	-3.027
	exp.	4878.29	1.46506	-3.029
$(0, 7^3, 0)e$	calc.	4887.26	1.50530	-0.821
	exp.	4887.58	1.50520	-0.825

To be continued on next page

Table A.10: *Continued from previous page*

State	Method	G_v	B_v	$10^6 D_v$
$(0,7^3,0)f$	calc.	4887.29	1.50449	4.238
	exp.	4887.61	1.50438	4.242
$(0,4^0,1)e$	calc.	4887.85	1.48300	-13.514
	exp.	4888.05	1.48292	-13.517
$(0,4^2,1)e$	calc.	4902.75	1.48288	5.638
	exp.	4902.93	1.48282	5.635
$(0,4^2,1)f$	calc.	4902.76	1.48251	-4.528
	exp.	4902.94	1.48244	-4.539
$(0,4^4,1)e$	calc.	4947.47	1.47992	-1.722
	exp.	4947.60	1.47985	-1.725
$(0,4^4,1)f$	calc.	4947.47	1.47992	-1.750
	exp.	4947.60	1.47986	-1.753
$(0,7^5,0)e$	calc.	4948.96	1.50116	-1.278
	exp.	4949.31	1.50105	-1.273
$(0,7^5,0)f$	calc.	4948.96	1.50115	-1.271
	exp.	4949.31	1.50105	-1.266
$(0,7^7,0)e$	calc.	5041.24	1.49555	-1.871
	exp.	5041.65	1.49547	-1.875
$(0,7^7,0)f$	calc.	5041.24	1.49555	-1.871
	exp.	5041.65	1.49547	-1.875
$(1,3^1,0)e$	calc.	5367.16	1.47200	-4.348
	exp.	5366.88	1.47194	-4.350
$(1,3^1,0)f$	calc.	5367.15	1.48778	-5.051
	exp.	5366.87	1.48772	-5.051
$(1,0^0,1)e$	calc.	5394.35	1.45797	-2.891
	exp.	5393.70	1.45793	-2.892
$(1,3^3,0)e$	calc.	5396.97	1.47821	-1.743
	exp.	5396.70	1.47816	-1.744
$(1,3^3,0)f$	calc.	5396.98	1.47813	-1.235
	exp.	5396.71	1.47808	-1.236
$(0,8^0,0)e$	calc.	5525.83	1.50886	-31.593
	exp.	5525.87	1.50878	-31.598
$(0,8^2,0)e$	calc.	5541.19	1.51397	16.748
	exp.	5541.29	1.51385	16.747

To be continued on next page

Table A.10: *Continued from previous page*

State	Method	G_v	B_v	$10^6 D_v$
$(0, 8^2, 0)f$	calc.	5541.29	1.51079	-10.086
	exp.	5541.38	1.51068	-10.094
$(0, 2^0, 2)e$	calc.	5572.05	1.46511	-6.796
	exp.	5571.74	1.46506	-6.813
$(0, 5^1, 1)e$	calc.	5577.18	1.47525	-6.426
	exp.	5577.45	1.47516	-6.421
$(0, 5^1, 1)f$	calc.	5577.17	1.49915	-8.499
	exp.	5577.44	1.49913	-8.656
$(0, 2^2, 2)e$	calc.	5586.43	1.46442	0.688
	exp.	5586.06	1.46437	0.697
$(0, 2^2, 2)f$	calc.	5586.43	1.46445	-3.211
	exp.	5586.07	1.46432	-3.030
$(0, 8^4, 0)e$	calc.	5587.89	1.50776	0.473
	exp.	5588.03	1.50764	0.466
$(0, 8^4, 0)f$	calc.	5587.89	1.50787	-0.008
	exp.	5588.03	1.50775	-0.016
$(0, 5^3, 1)e$	calc.	5607.16	1.48559	-1.268
	exp.	5607.41	1.48552	-1.284
$(0, 5^3, 1)f$	calc.	5607.17	1.48527	0.724
	exp.	5607.42	1.48520	0.709
$(0, 8^6, 0)e$	calc.	5665.40	1.50307	-1.613
	exp.	5665.64	1.50269	-1.133
$(0, 8^6, 0)f$	calc.	5665.40	1.50307	-1.613
	exp.	5665.64	1.50269	-1.133
$(0, 5^5, 1)e$	calc.	5667.05	1.48184	-1.669
	exp.	5667.27	1.48187	-1.836
$(0, 5^5, 1)f$	calc.	5667.05	1.48184	-1.668
	exp.	5667.27	1.48187	-1.835
$(0, 8^8, 0)e$	calc.	5773.58	1.49628	-1.845
	exp.	5773.90	1.49618	-1.846
$(0, 8^8, 0)f$	calc.	5773.58	1.49628	-1.845
	exp.	5773.90	1.49618	-1.846
$(1, 4^0, 0)e$	calc.	6037.31	1.48403	-13.936
	exp.	6036.97	1.48397	-13.941

To be continued on next page

Table A.10: *Continued from previous page*

State	Method	G_v	B_v	$10^6 D_v$
$(1, 4^2, 0)e$	calc.	6052.23	1.48397	5.975
	exp.	6051.90	1.48391	5.975
$(1, 4^2, 0)f$	calc.	6052.25	1.48356	-4.597
	exp.	6051.92	1.48349	-4.598
$(1, 1^1, 1)e$	calc.	6083.95	1.45780	-2.914
	exp.	6083.35	1.45776	-2.917
$(1, 1^1, 1)f$	calc.	6083.95	1.46547	-3.014
	exp.	6083.35	1.46543	-3.015
$(1, 4^4, 0)e$	calc.	6097.02	1.48091	-1.655
	exp.	6096.73	1.48085	-1.657
$(1, 4^4, 0)f$	calc.	6097.02	1.48092	-1.686
	exp.	6096.73	1.48086	-1.688
$(0, 9^1, 0)e$	calc.	6197.82	1.49451	-12.563
	exp.	6197.36	1.49441	-12.544
$(0, 9^1, 0)f$	calc.	6197.79	1.53825	-23.238
	exp.	6197.32	1.53826	-23.242
$(0, 9^3, 0)e$	calc.	6228.97	1.51507	-0.606
	exp.	6228.68	1.51493	-0.586
$(0, 9^3, 0)f$	calc.	6229.02	1.51347	9.717
	exp.	6228.73	1.51333	9.714
$(0, 0^0, 3)e$	calc.	6229.48	1.44785	-2.925
	exp.	6228.60	1.44781	-2.928
$(0, 6^0, 1)e$	calc.	6254.15	1.49042	-22.093
	exp.	6254.43	1.49038	-22.200
$(0, 3^1, 2)e$	calc.	6267.82	1.46100	-4.292
	exp.	6267.66	1.46099	-4.397
$(0, 3^1, 2)f$	calc.	6267.81	1.47633	-4.997
	exp.	6267.66	1.47630	-5.026
$(0, 6^2, 1)e$	calc.	6269.17	1.49211	11.356
	exp.	6269.44	1.49225	10.905
$(0, 6^2, 1)f$	calc.	6269.21	1.49077	-6.847
	exp.	6269.48	1.49093	-6.926
$(0, 9^5, 0)e$	calc.	6291.48	1.51028	-0.457
	exp.	6291.33	1.51018	-0.492

To be continued on next page

Table A.10: *Continued from previous page*

State	Method	G_v	B_v	$10^6 D_v$
$(0, 9^5, 0)f$	calc.	6291.48	1.51028	-0.430
	exp.	6291.33	1.51017	-0.465
$(0, 3^3, 2)e$	calc.	6296.73	1.46707	-1.785
	exp.	6296.51	1.46702	-1.802
$(0, 3^3, 2)f$	calc.	6296.74	1.46699	-1.289
	exp.	6296.52	1.46694	-1.303
$(0, 6^4, 1)e$	calc.	6314.44	1.48799	-0.860
	exp.	6314.73	1.48790	-0.863
$(0, 6^4, 1)f$	calc.	6314.44	1.48802	-1.012
	exp.	6314.73	1.48793	-1.012
$(0, 9^7, 0)e$	calc.	6385.03	1.50433	-1.344
	exp.	6385.04	1.50416	-1.488
$(0, 9^7, 0)f$	calc.	6385.03	1.50433	-1.344
	exp.	6385.04	1.50416	-1.488
$(0, 6^6, 1)e$	calc.	6389.70	1.48351	-2.104
	exp.	6389.96	1.48343	-1.867
$(0, 6^6, 1)f$	calc.	6389.70	1.48351	-2.104
	exp.	6389.96	1.48343	-1.867
$(0, 9^9, 0)e$	calc.	6509.31	1.49646	-1.797
	exp.	6509.47	1.49636	-1.791
$(0, 9^9, 0)f$	calc.	6509.31	1.49646	-1.792
	exp.	6509.47	1.49636	-1.791
$(2, 0^0, 0)e$	calc.	6520.39	1.45710	-2.858
	exp.	6519.61	1.45707	-2.859

[a] Calculated results are obtained from least-squares fits of variational rovibrational term energies up to $J_{\max} = 20$ using the Comp I adiabatic composite PEF (Table A.4).

[b] Experimental results are obtained from least-squares fits of rovibrational term energies up to $J_{\max} = 20$ obtained by Mellau [17].

Appendix B

Supplemental material for tricarbon C_3

Table B.1: Basic (F12bs), core-valence correlation (CV) and scalar relativisitic (SR) contributions to the composite potential energy function (PEF) of C_3.[a]

			$C_{ijk}^{(\alpha)}$		
i	j	k	F12bs[b]	CV[c]	SR[d]
1	0	0	-0.0028875	0.0043655	0.0002307
2	0	0	0.3357898	-0.0032620	-0.0004915
3	0	0	-0.3510619	0.0016107	0.0003300
4	0	0	0.2271546	-0.0007214	-0.0001359
5	0	0	-0.1186061	0.0003230	0.0000740
6	0	0	0.0534505	-0.0002632	-0.0000958
7	0	0	-0.0283396		
8	0	0	0.0200149		
0	1	0	-0.0028875	0.0043655	0.0002307
0	2	0	0.3357898	-0.0032620	-0.0004915
0	3	0	-0.3510619	0.0016107	0.0003300
0	4	0	0.2271546	-0.0007214	-0.0001359
0	5	0	-0.1186061	0.0003230	0.0000740
0	6	0	0.0534505	-0.0002632	-0.0000958
0	7	0	-0.0283396		
0	8	0	0.0200149		
0	0	2	0.0001519	0.0001133	-0.0000335
0	0	4	0.0005108	-0.0000376	0.0000077
0	0	6	0.0001849	0.0000034	-0.0000003

To be continued on next page

Table B.1: *Continued from previous page*

i	j	k	F12bs[b]	CV[c]	SR[d]
0	0	8	-0.0000446	-0.0000043	0.0000018
0	0	10	0.0001077	-0.0000002	-0.0000003
0	0	12	-0.0000425		
0	0	14	0.0000064		
1	1	0	-0.0053392	0.0003523	-0.0000801
2	1	0	-0.0072080	-0.0001697	-0.0000095
1	2	0	-0.0072080	-0.0001697	-0.0000095
3	1	0	-0.0020469	0.0000764	0.0000126
2	2	0	-0.0016429	0.0002075	0.0000588
1	3	0	-0.0020469	0.0000764	0.0000126
4	1	0	-0.0006525	0.0000468	0.0000385
3	2	0	0.0066329	0.0000742	0.0000285
2	3	0	0.0066329	0.0000742	0.0000285
1	4	0	-0.0006525	0.0000468	0.0000385
5	1	0	-0.0285676		
4	2	0	0.0017669		
3	3	0	0.0139377		
2	4	0	0.0017669		
1	5	0	-0.0285676		
1	0	2	-0.0039282	-0.0001100	-0.0000084
2	0	2	-0.0005903	0.0001519	0.0000561
3	0	2	0.0014869	0.0000855	0.0000266
4	0	2	0.0157070		
0	1	2	-0.0039282	-0.0001100	-0.0000084
0	2	2	-0.0005903	0.0001519	0.0000561
0	3	2	0.0014869	0.0000855	0.0000266
0	4	2	0.0157070		
1	0	4	-0.0007876	0.0000306	-0.0000028
2	0	4	0.0031384	-0.0009064	-0.0001983
3	0	4	-0.0029060	-0.0003173	-0.0001859
4	0	4	-0.0655003		
0	1	4	-0.0007876	0.0000306	-0.0000028
0	2	4	0.0031384	-0.0009064	-0.0001983
0	3	4	-0.0029060	-0.0003173	-0.0001859
0	4	4	-0.0655003		

To be continued on next page

Table B.1: *Continued from previous page*

i	j	k	F12bs[b]	CV[c]	SR[d]
1	0	6	0.0003513	0.0001074	-0.0000192
2	0	6	-0.0029532	0.0021190	0.0003979
3	0	6	0.0043157	0.0007170	0.0005250
4	0	6	0.0631468		
0	1	6	0.0003513	0.0001074	-0.0000192
0	2	6	-0.0029532	0.0021190	0.0003979
0	3	6	0.0043157	0.0007170	0.0005250
0	4	6	0.0631468		
1	0	8	-0.0001258	-0.0001003	0.0000147
2	0	8	0.0003646	-0.0016881	-0.0002633
3	0	8	-0.0011589	-0.0005697	-0.0005116
4	0	8	-0.0093522		
0	1	8	-0.0001258	-0.0001003	0.0000147
0	2	8	0.0003646	-0.0016881	-0.0002633
0	3	8	-0.0011589	-0.0005697	-0.0005116
0	4	8	-0.0093522		
1	1	2	-0.0120698	-0.0000628	0.0000700
1	1	4	-0.0010039	0.0002671	-0.0000042
1	1	6	0.0016727	-0.0007474	0.0000127
1	1	8	0.0000442	0.0006512	-0.0000141
2	1	2	0.0139168	0.0000558	0.0000033
1	2	2	0.0139168	0.0000558	0.0000033
2	1	4	0.0028004	-0.0002731	-0.0001524
1	2	4	0.0028004	-0.0002731	-0.0001524
2	1	6	-0.0041475	0.0009738	0.0004150
1	2	6	-0.0041475	0.0009738	0.0004150
2	1	8	0.0009567	-0.0010832	-0.0003794
1	2	8	0.0009567	-0.0010832	-0.0003794
3	1	2	-0.0194853		
2	2	2	0.0057677		
1	3	2	-0.0194853		
3	1	4	0.0696818		
2	2	4	-0.0575769		
1	3	4	0.0696818		
3	1	6	-0.0669321		

To be continued on next page

Table B.1: *Continued from previous page*

i	j	k	F12bs[b]	CV[c]	SR[d]
2	2	6	0.0170508		
1	3	6	-0.0669321		
3	1	8	0.0010702		
2	2	8	0.0452248		
1	3	8	0.0010702		

[a] PEF coefficients are quoted in atomic units; see Equation (3.10) for their definition. Expanded around $R_{\text{ref}} = 1.2945$ Å.

[b] F12bs: fc-CCSD(T*)-F12b/AV5Z.

[c] CV: [ae-CCSD(T) − fc-CCSD(T)]/ACV5Z.

[d] SR: DKH2-fc-CCSD(T)/AVQZ-DK − fc-CCSD(T)/AVQZ.

Table B.2: Higher-order correlation (HC) contributions to the composite potential energy function (PEF) of C_3.[a]

			$C_{ijk}^{(\alpha)}$		
i	j	k	(Q)-(T)[b]	Q-(Q)[c]	P-Q[d]
1	0	0	-0.0012793	0.0003587	-0.0001271
2	0	0	-0.0016191	0.0007631	0.0001700
3	0	0	-0.0015734	0.0009553	0.0000457
4	0	0	-0.0010091	0.0011411	-0.0001958
5	0	0	-0.0008052	0.0011922	-0.0001718
6	0	0	-0.0001866	0.0003032	0.0008097
0	1	0	-0.0012793	0.0003587	-0.0001271
0	2	0	-0.0016191	0.0007631	0.0001700
0	3	0	-0.0015734	0.0009553	0.0000457
0	4	0	-0.0010091	0.0011411	-0.0001958
0	5	0	-0.0008052	0.0011922	-0.0001718
0	6	0	-0.0001866	0.0003032	0.0008097
0	0	2	-0.0000921	0.0002634	0.0000018
0	0	4	0.0004139	-0.0002808	0.0000317
0	0	6	-0.0000758	0.0000694	-0.0000153
0	0	8	-0.0000045	0.0000012	0.0000015
0	0	10	0.0000001	-0.0000013	
1	1	0	0.0023443	-0.0001146	-0.0007504
2	1	0	0.0017886	-0.0001996	-0.0003582
1	2	0	0.0017886	-0.0001996	-0.0003582
3	1	0	0.0023813	-0.0010748	
2	2	0	-0.0012834	0.0024423	
1	3	0	0.0023813	-0.0010748	
4	1	0	0.0025877		
3	2	0	-0.0012377		
2	3	0	-0.0012377		
1	4	0	0.0025877		
1	0	2	-0.0009057	0.0004465	
2	0	2	-0.0013219	0.0006921	
0	1	2	-0.0009057	0.0004465	
0	2	2	-0.0013219	0.0006921	
1	0	4	0.0003350		

To be continued on next page

Table B.2: *Continued from previous page*

i	j	k	(Q)-(T)[b]	Q-(Q)[c]	P-Q[d]
2	0	4	0.0012310		
0	1	4	0.0003350		
0	2	4	0.0012310		
1	0	6	0.0000161		
2	0	6	-0.0002979		
0	1	6	0.0000161		
0	2	6	-0.0002979		
1	1	2	-0.0001548	0.0000549	
1	1	4	-0.0018988		
1	1	6	0.0006759		
2	1	2	0.0005795		
1	2	2	0.0005795		
2	1	4	-0.0023265		
1	2	4	-0.0023265		
2	1	6	0.0008621		
1	2	6	0.0008621		

[a] PEF coefficients are quoted in atomic units; see Equation (3.10) for their definition. Expanded around $R_{\text{ref}} = 1.2945$ Å.
[b] (Q)-(T): [CCSDT(Q) − CCSD(T)]/VQZ.
[c] Q-(Q): [CCSDTQ − CCSDT(Q)]/VTZ(*spd*).
[d] P-Q: [CCSDTQP − CCSDTQ]/VDZ.

Table B.3: Non-redundant coefficients of the composite potential energy function for C_3.[a]

i	j	k	C_{ijk}	i	j	k	C_{ijk}
2	0	0	0.33240693	4	0	2	0.01570702
3	0	0	-0.35060064	3	1	2	-0.01948533
4	0	0	0.22690209	2	2	2	0.00576765
5	0	0	-0.11822982	1	0	4	-0.00042866
6	0	0	0.05358855	2	0	4	0.00327471
7	0	0	-0.02849987	1	1	4	-0.00263969
8	0	0	0.02001495	3	0	4	-0.00321668
0	0	2	0.00041387	2	1	4	-0.00004568
0	0	4	0.00064654	4	0	4	-0.06550030
0	0	6	0.00016547	3	1	4	0.06968179
0	0	8	-0.00004851	2	2	4	-0.05757693
0	0	10	0.00010604	1	0	6	0.00045529
0	0	12	-0.00004245	2	0	6	-0.00074881
0	0	14	0.00000644	1	1	6	0.00162108
1	1	0	-0.00355710	3	0	6	0.00537182
2	1	0	-0.00614366	2	1	6	-0.00172969
3	1	0	-0.00075277	4	0	6	0.06314677
2	2	0	0.00039680	3	1	6	-0.06693212
4	1	0	0.00215995	2	2	6	0.01705080
3	2	0	0.00544895	1	0	8	-0.00020893
5	1	0	-0.02856759	2	0	8	-0.00157956
4	2	0	0.00176688	1	1	8	0.00068353
3	3	0	0.01393769	3	0	8	-0.00220384
1	0	2	-0.00449159	2	1	8	-0.00059965
2	0	2	-0.00103148	4	0	8	-0.00935219
1	1	2	-0.01222084	3	1	8	0.00107021
3	0	2	0.00155557	2	2	8	0.04522482
2	1	2	0.01460243	1	3	8	0.00107021

[a] PEF coefficients are quoted in atomic units; see Equation (3.10) for their definition. Equilibrium geometry: $R_e = 1.29397$ Å.

Table B.4: Composite electric dipole moment function for HCN.[a]

$\mu_\parallel$				$\mu_\perp$			
i	j	k	$D^{\parallel}_{ijk}$	i	j	k	$D^{\perp}_{ijk}$
0	1	0	-1.741218	0	0	1	-0.491612
0	3	0	-0.010408	0	0	3	0.198205
0	5	0	-0.233818	0	0	5	-0.084483
0	7	0	0.373720	0	0	7	0.014691
1	1	0	0.602984	0	0	9	-0.003926
2	1	0	0.188517	0	0	11	0.000908
3	1	0	-0.003804	0	0	13	-0.000053
1	3	0	0.142400	1	0	1	0.484434
2	3	0	-0.003239	1	0	3	-0.146079
3	3	0	-0.077812	1	0	5	0.087463
1	5	0	0.066664	1	0	7	-0.020468
0	1	2	0.484160	2	0	1	-0.012485
0	1	4	-0.233765	2	0	3	-0.049476
0	1	6	0.098495	2	0	5	0.020932
0	1	8	-0.013023	3	0	1	-0.086571
0	3	2	0.088176	3	0	3	0.009446
0	3	4	-0.092395	4	0	1	0.010684
0	5	2	0.222388	0	2	1	-0.228093
1	1	2	-0.179100	0	2	3	0.256229
1	1	4	0.219666	0	2	5	-0.161277
1	1	6	-0.188606	0	2	7	0.047227
1	1	8	0.032524	0	4	1	-0.117837
2	1	2	-0.059962	0	4	3	0.148244
2	1	4	0.053437	0	4	5	-0.067480
2	1	6	0.045937	0	6	1	0.040903
3	1	2	-0.045672	1	2	1	0.038507
3	1	4	-0.080090	1	2	3	-0.191834
1	3	2	0.176341	1	2	5	0.214740
1	3	4	-0.118169	1	2	7	-0.089206
2	3	2	0.109405	2	2	1	-0.029806
				2	2	3	0.067138
				3	2	1	-0.019096
				1	4	1	0.034292

[a] EDMF coefficients are quoted in atomic units; see Equation (3.11) and (3.12) for their definitions. Expanded around $R_e = 1.29397$ Å.

Appendix C

Supplemental material for propynylidynium l-C_3H^+

Table C.1: Basic contribution[a] to the composite potential energy function (PEF) of l-C_3H^+.[b]

i	j	k	l	m	n	$C_{ijk}^{(\alpha)}$	i	j	k	l	m	n	$C_{ijk}^{(\alpha)}$
1	0	0	0	0	0	-0.00098249	1	1	3	0	0	0	-0.00049978
2	0	0	0	0	0	0.18743885	1	1	4	0	0	0	0.00000954
3	0	0	0	0	0	-0.18885997	1	2	1	0	0	0	-0.00100314
4	0	0	0	0	0	0.12801934	1	2	2	0	0	0	0.00091998
5	0	0	0	0	0	-0.07391227	1	2	3	0	0	0	-0.00003533
6	0	0	0	0	0	0.03902163	1	3	1	0	0	0	0.00034593
7	0	0	0	0	0	-0.01900879	1	3	2	0	0	0	0.00032821
8	0	0	0	0	0	0.00950084	1	4	1	0	0	0	-0.00016070
9	0	0	0	0	0	-0.00532379	2	1	1	0	0	0	0.00035228
10	0	0	0	0	0	0.00189872	2	1	2	0	0	0	-0.00020656
0	1	0	0	0	0	-0.00346423	2	1	3	0	0	0	-0.00013604
0	2	0	0	0	0	0.44636346	2	2	1	0	0	0	-0.00040566
0	3	0	0	0	0	-0.46574790	2	2	2	0	0	0	-0.00024220
0	4	0	0	0	0	0.29947767	2	3	1	0	0	0	0.00023487
0	5	0	0	0	0	-0.15894938	3	1	1	0	0	0	-0.00024704
0	6	0	0	0	0	0.07379974	3	1	2	0	0	0	0.00032533
0	7	0	0	0	0	-0.03060395	3	2	1	0	0	0	0.00027526
0	8	0	0	0	0	0.00965334	4	1	1	0	0	0	0.00016022
0	0	1	0	0	0	-0.00332752	1	1	0	2	0	0	0.01179665

To be continued on next page

Table C.1: *Continued from previous page*

i	j	k	l	m	n	$C_{ijk}^{(\alpha)}$	i	j	k	l	m	n	$C_{ijk}^{(\alpha)}$
0	0	2	0	0	0	0.27616446	2	1	0	2	0	0	0.00244742
0	0	3	0	0	0	-0.28057671	1	2	0	2	0	0	-0.00400316
0	0	4	0	0	0	0.18242127	3	1	0	2	0	0	0.00454354
0	0	5	0	0	0	-0.09491890	2	2	0	2	0	0	0.01349126
0	0	6	0	0	0	0.04400772	1	3	0	2	0	0	-0.00001544
0	0	7	0	0	0	-0.01898566	1	0	1	2	0	0	0.00130424
0	0	8	0	0	0	0.00575521	2	0	1	2	0	0	0.00112793
0	0	0	2	0	0	0.03804410	1	0	2	2	0	0	-0.00091805
0	0	0	4	0	0	-0.00019261	3	0	1	2	0	0	0.00060819
0	0	0	6	0	0	0.00059808	2	0	2	2	0	0	0.01381179
0	0	0	8	0	0	-0.00043214	1	0	3	2	0	0	0.00137130
0	0	0	10	0	0	0.00027386	0	1	1	2	0	0	-0.00404108
0	0	0	12	0	0	-0.00018318	0	2	1	2	0	0	0.00529045
0	0	0	14	0	0	0.00008238	0	1	2	2	0	0	-0.00013600
0	0	0	16	0	0	-0.00001565	0	3	1	2	0	0	0.00185593
0	0	0	0	2	0	0.00403306	0	2	2	2	0	0	0.00342656
0	0	0	0	4	0	-0.00018498	0	1	3	2	0	0	0.00036065
0	0	0	0	6	0	0.00013263	1	1	0	4	0	0	0.00767870
0	0	0	0	8	0	-0.00024314	1	0	1	4	0	0	0.00040782
0	0	0	0	10	0	0.00041954	0	1	1	4	0	0	-0.00034512
0	0	0	0	12	0	-0.00029958	1	1	0	0	2	0	0.00072412
0	0	0	0	14	0	0.00012171	2	1	0	0	2	0	0.00015864
0	0	0	0	16	0	-0.00002644	1	2	0	0	2	0	0.00076714
0	0	0	0	18	0	0.00000244	3	1	0	0	2	0	0.00047706
1	1	0	0	0	0	-0.01329228	2	2	0	0	2	0	-0.01455038
2	1	0	0	0	0	0.00236236	1	3	0	0	2	0	0.00335464
1	2	0	0	0	0	0.00077668	1	0	1	0	2	0	-0.00035367
3	1	0	0	0	0	-0.00294012	2	0	1	0	2	0	0.00015385
2	2	0	0	0	0	-0.00461540	1	0	2	0	2	0	0.00092631
1	3	0	0	0	0	-0.00086321	3	0	1	0	2	0	-0.00144150
4	1	0	0	0	0	0.00268955	2	0	2	0	2	0	-0.01682393
3	2	0	0	0	0	0.00385732	1	0	3	0	2	0	-0.00313611
2	3	0	0	0	0	0.00251883	0	1	1	0	2	0	-0.01735139
1	4	0	0	0	0	0.00131308	0	2	1	0	2	0	0.01739003
5	1	0	0	0	0	-0.00122371	0	1	2	0	2	0	0.00700185

To be continued on next page

Table C.1: *Continued from previous page*

i	j	k	l	m	n	$C_{ijk}^{(\alpha)}$	i	j	k	l	m	n	$C_{ijk}^{(\alpha)}$
4	2	0	0	0	0	-0.00232862	0	3	1	0	2	0	0.00439940
3	3	0	0	0	0	-0.00179371	0	2	2	0	2	0	-0.03645257
2	4	0	0	0	0	-0.00174415	0	1	3	0	2	0	0.01369046
1	5	0	0	0	0	-0.00025716	1	1	0	0	4	0	0.00192881
1	0	1	0	0	0	0.00490167	1	0	1	0	4	0	-0.00478273
2	0	1	0	0	0	-0.00026435	0	1	1	0	4	0	0.00033225
1	0	2	0	0	0	-0.00240709	1	0	0	1	1	1	-0.00048528
3	0	1	0	0	0	0.00033883	2	0	0	1	1	1	-0.00069255
2	0	2	0	0	0	0.00012267	3	0	0	1	1	1	-0.00009932
1	0	3	0	0	0	0.00047115	4	0	0	1	1	1	0.01067593
4	0	1	0	0	0	-0.00033762	0	1	0	1	1	1	0.00423786
3	0	2	0	0	0	-0.00018906	0	2	0	1	1	1	-0.00799769
2	0	3	0	0	0	-0.00014494	0	3	0	1	1	1	-0.00427906
1	0	4	0	0	0	-0.00024738	0	4	0	1	1	1	0.00664445
5	0	1	0	0	0	0.00003222	0	0	1	1	1	1	0.01635910
4	0	2	0	0	0	-0.00018672	0	0	2	1	1	1	-0.00999281
3	0	3	0	0	0	0.00007668	0	0	3	1	1	1	0.00420788
2	0	4	0	0	0	0.00006346	0	0	4	1	1	1	0.00688904
1	0	5	0	0	0	0.00020993	1	0	0	3	1	1	0.00067369
0	1	1	0	0	0	0.00753095	2	0	0	3	1	1	0.00650387
0	2	1	0	0	0	-0.01180174	0	1	0	3	1	1	-0.00466069
0	1	2	0	0	0	-0.00678852	0	2	0	3	1	1	-0.00901044
0	3	1	0	0	0	0.00334001	0	0	1	3	1	1	0.00015304
0	2	2	0	0	0	-0.00931401	0	0	2	3	1	1	0.00409368
0	1	3	0	0	0	-0.00406745	1	0	0	2	2	0	-0.00050621
0	4	1	0	0	0	-0.00286668	2	0	0	2	2	0	0.01294572
0	3	2	0	0	0	0.00886821	0	1	0	2	2	0	0.00118961
0	2	3	0	0	0	0.00279688	0	2	0	2	2	0	0.01079344
0	1	4	0	0	0	0.00067524	0	0	1	2	2	0	0.00143455
0	5	1	0	0	0	0.00372334	0	0	2	2	2	0	0.01816487
0	4	2	0	0	0	-0.00420891	1	0	0	2	2	2	0.00010867
0	3	3	0	0	0	-0.00118173	2	0	0	2	2	2	-0.00367626
0	2	4	0	0	0	-0.00436835	0	1	0	2	2	2	-0.00316732
0	1	5	0	0	0	0.00184341	0	2	0	2	2	2	-0.01025613
1	0	0	2	0	0	-0.00929267	0	0	1	2	2	2	0.00255286

To be continued on next page

Table C.1: *Continued from previous page*

i	j	k	l	m	n	$C_{ijk}^{(\alpha)}$	i	j	k	l	m	n	$C_{ijk}^{(\alpha)}$
2	0	0	2	0	0	-0.00258418	0	0	2	2	2	2	-0.00716006
3	0	0	2	0	0	0.00122436	1	0	0	1	3	1	0.00085873
4	0	0	2	0	0	0.00741127	2	0	0	1	3	1	0.00749245
0	1	0	2	0	0	-0.03875616	0	1	0	1	3	1	0.00030175
0	2	0	2	0	0	-0.00189932	0	2	0	1	3	1	0.01414570
0	3	0	2	0	0	-0.00430929	0	0	1	1	3	1	-0.00487030
0	4	0	2	0	0	0.01043487	0	0	2	1	3	1	0.01070791
0	0	1	2	0	0	-0.00702436	1	1	1	2	0	0	-0.00131618
0	0	2	2	0	0	0.00141736	1	1	2	2	0	0	0.00712249
0	0	3	2	0	0	-0.00080444	1	2	1	2	0	0	-0.00415296
0	0	4	2	0	0	0.00927163	2	1	1	2	0	0	-0.00400242
1	0	0	4	0	0	-0.00113290	1	1	1	0	2	0	-0.00066854
2	0	0	4	0	0	0.00421952	1	1	2	0	2	0	0.00109165
0	1	0	4	0	0	0.00269623	1	2	1	0	2	0	-0.00167744
0	2	0	4	0	0	0.00881127	2	1	1	0	2	0	0.00670916
0	0	1	4	0	0	0.00029574	1	1	0	1	1	1	-0.00143185
0	0	2	4	0	0	0.00467583	2	1	0	1	1	1	-0.00079187
1	0	0	0	2	0	-0.00067714	1	2	0	1	1	1	0.00142293
2	0	0	0	2	0	0.00033767	3	1	0	1	1	1	-0.00067463
3	0	0	0	2	0	0.00018734	2	2	0	1	1	1	0.01891353
4	0	0	0	2	0	-0.01034093	1	3	0	1	1	1	-0.00317190
0	1	0	0	2	0	-0.01472522	1	0	1	1	1	1	-0.00131140
0	2	0	0	2	0	0.00390884	2	0	1	1	1	1	-0.00124648
0	3	0	0	2	0	-0.00464768	1	0	2	1	1	1	0.00167741
0	4	0	0	2	0	-0.00620064	3	0	1	1	1	1	0.00056768
0	0	1	0	2	0	0.00328796	2	0	2	1	1	1	0.01881086
0	0	2	0	2	0	-0.00561882	1	0	3	1	1	1	-0.00384161
0	0	3	0	2	0	0.00546401	0	1	1	1	1	1	0.01275368
0	0	4	0	2	0	-0.01182640	0	2	1	1	1	1	0.01243315
1	0	0	0	4	0	-0.00002296	0	1	2	1	1	1	-0.01544964
2	0	0	0	4	0	-0.00325209	0	3	1	1	1	1	0.01100483
0	1	0	0	4	0	0.00267857	0	2	2	1	1	1	-0.00622110
0	2	0	0	4	0	-0.00065643	0	1	3	1	1	1	0.01486193
0	0	1	0	4	0	-0.00305842	1	1	0	3	1	1	-0.00338753
0	0	2	0	4	0	0.01113482	1	0	1	3	1	1	-0.00334327

To be continued on next page

Table C.1: *Continued from previous page*

i	j	k	l	m	n	$C_{ijk}^{(\alpha)}$	i	j	k	l	m	n	$C_{ijk}^{(\alpha)}$
0	0	0	1	1	1	0.00123853	0	1	1	3	1	1	0.00085985
0	0	0	3	1	1	-0.00229301	1	1	0	2	2	0	-0.00032638
0	0	0	2	2	0	0.00118956	1	0	1	2	2	0	-0.00421174
0	0	0	2	2	2	-0.00024762	0	1	1	2	2	0	0.00085966
0	0	0	1	3	1	-0.00017294	1	1	0	2	2	2	-0.00060169
0	0	0	5	1	1	-0.00030631	1	0	1	2	2	2	-0.00176789
0	0	0	4	2	0	-0.00024010	0	1	1	2	2	2	0.00603540
0	0	0	4	2	2	-0.00000723	1	1	0	1	3	1	-0.00911274
0	0	0	3	3	1	0.00047186	1	0	1	1	3	1	-0.00198495
0	0	0	3	3	3	0.00003515	0	1	1	1	3	1	-0.01038817
0	0	0	2	4	0	0.00055012	1	1	1	1	1	1	0.00097111
0	0	0	2	4	2	0.00058868	1	1	2	1	1	1	0.00325780
0	0	0	1	5	1	-0.00064639	1	2	1	1	1	1	0.00369857
1	1	1	0	0	0	-0.00075973	2	1	1	1	1	1	0.00112922
1	1	2	0	0	0	-0.00040499							

[a] F12b: fc-CCSD(T)-F12b/VQZ-F12.

[b] PEF coefficients are quoted in atomic units; see Equation (5.1) for their definition. Expanded around $r^{\text{ref}} = 1.079$ Å, $R_1^{\text{ref}} = 1.236$ Å and $R_2^{\text{ref}} = 1.340$ Å

Table C.2: Core-valence (CV), scalar relativistic (SR), higher-order correlation (HC) and diagonal Born-Oppenheimer correction (DBOC) contributions to the composite potential energy function (PEF) of l-C_3H^+.[a]

						$C_{ijk}^{(\alpha)}$				
i	j	k	l	m	n	CV[b]	SR[c]	(Q)-(T)[d]	Q-(Q)[e]	DBOC[f]
1	0	0	0	0	0	0.00088213	0.00009911	0.00014070	0.00001244	-0.00014691
2	0	0	0	0	0	-0.00077402	-0.00013841	-0.00008890	0.00002630	0.00010392
3	0	0	0	0	0	0.00048081	0.00010116	-0.00004432	-0.00001386	-0.00004851
4	0	0	0	0	0	-0.00020215	-0.00004691	-0.00001143	-0.00001010	0.00002341
5	0	0	0	0	0	-0.00000445	-0.00000068	0.00003775	0.00002267	-0.00001275
6	0	0	0	0	0	-0.00003045	-0.00000514	-0.00002254	0.00002749	0.00000439
7	0	0	0	0	0	0.00023211	0.00003567	-0.00001864	-0.00007073	
8	0	0	0	0	0	-0.00017082	-0.00002106	0.00002255	0.00003407	
0	1	0	0	0	0	0.00506436	0.00040983	-0.00165046	0.00068107	-0.00004958
0	2	0	0	0	0	-0.00387652	-0.00058733	-0.00005179	0.00085015	0.00008914
0	3	0	0	0	0	0.00211116	0.00035334	0.00003924	0.00045284	-0.00002946
0	4	0	0	0	0	-0.00085134	-0.00027025	0.00050215	-0.00026666	0.00003499
0	5	0	0	0	0	0.00034363	0.00037262	0.00024886	-0.00010085	-0.00001050
0	6	0	0	0	0	-0.00020177	-0.00033980	-0.00031336	0.00058594	0.00000418
0	7	0	0	0	0			-0.00046037	-0.00035959	
0	0	1	0	0	0	0.00374236	0.00016105	-0.00185967	0.00052225	-0.00004255
0	0	2	0	0	0	-0.00291738	-0.00037959	-0.00315411	0.00122546	0.00005650
0	0	3	0	0	0	0.00142450	0.00029569	-0.00259810	0.00150918	-0.00004360
0	0	4	0	0	0	-0.00063591	-0.00010387	-0.00169234	0.00115450	0.00004027
0	0	5	0	0	0	0.00025078	0.00003937	-0.00108489	0.00110967	-0.00004324
0	0	6	0	0	0	-0.00006279	-0.00006116	-0.00043781	0.00071943	0.00002716
0	0	7	0	0	0			0.00051901	-0.00036384	
0	0	8	0	0	0			-0.00130458	0.00093057	
0	0	0	2	0	0	-0.00003541	-0.00001556	-0.00032887	0.00010133	0.00003158
0	0	0	4	0	0	0.00000633	-0.00000779	-0.00025791	0.00006313	0.00000322
0	0	0	6	0	0	-0.00000088	0.00000217	-0.00021008	0.00002082	-0.00000972
0	0	0	8	0	0			0.00009761	-0.00000146	0.00000313
0	0	0	10	0	0			0.00008914	0.00003587	
0	0	0	12	0	0			-0.00004749	-0.00006212	
0	0	0	14	0	0			-0.00000734	0.00003589	
0	0	0	16	0	0			0.00000519	-0.00000720	
0	0	0	0	2	0	0.00012149	-0.00002669	0.00015007	0.00006406	-0.00000585
0	0	0	0	4	0	-0.00000680	-0.00001039	0.00018828	-0.00006054	0.00000134
0	0	0	0	6	0	-0.00000464	0.00001000	0.00001374	-0.00003444	-0.00000101
0	0	0	0	8	0	-0.00000229	-0.00000275	-0.00003290	0.00003184	0.00000048
0	0	0	0	10	0	-0.00000052	0.00000051	0.00000912	-0.00000907	
0	0	0	0	12	0			-0.00000114	0.00000104	
1	1	0	0	0	0	0.00011611	-0.00003094	0.00028777	-0.00008927	-0.00002600
2	1	0	0	0	0	-0.00002966	-0.00001885	-0.00004245	0.00008626	0.00002005
1	2	0	0	0	0	-0.00000161	-0.00002302	0.00001176	-0.00017459	0.00000125

To be continued on next page

Table C.2: *Continued from previous page*

i	j	k	l	m	n	CV[b]	SR[c]	(Q)-(T)[d]	Q-(Q)[e]	DBOC[f]
3	1	0	0	0	0	0.00001166	0.00001928	-0.00005672	0.00001763	-0.00001780
2	2	0	0	0	0	0.00002510	0.00001153	-0.00002284	0.00001469	0.00000046
1	3	0	0	0	0	-0.00000899	-0.00002074	-0.00023363	-0.00012540	-0.00001378
4	1	0	0	0	0	-0.00000775	0.00001250			
3	2	0	0	0	0	0.00005712	0.00001910			
2	3	0	0	0	0	-0.00008664	0.00003773			
1	4	0	0	0	0	0.00003634	0.00006834			
1	0	1	0	0	0	0.00002284	0.00000012	-0.00003405	0.00005654	0.00001383
2	0	1	0	0	0	0.00000210	-0.00000067	0.00002177	-0.00002056	-0.00000737
1	0	2	0	0	0	-0.00001189	-0.00000491	-0.00006055	0.00003743	-0.00000644
3	0	1	0	0	0	-0.00000286	0.00000095	0.00000903	-0.00002841	0.00000442
2	0	2	0	0	0	-0.00000338	0.00001748	0.00000847	-0.00004959	0.00000555
1	0	3	0	0	0	0.00000329	0.00000086	-0.00021037	0.00018014	0.00000459
4	0	1	0	0	0	0.00011143	-0.00000120			
3	0	2	0	0	0	0.00012447	-0.00000182			
2	0	3	0	0	0	0.00016677	0.00001759			
1	0	4	0	0	0	0.00005169	0.00000242			
0	1	1	0	0	0	0.00034247	-0.00007256	0.00021599	0.00006531	0.00000371
0	2	1	0	0	0	-0.00010616	-0.00001134	0.00196827	0.00037791	-0.00000664
0	1	2	0	0	0	-0.00018437	-0.00002363	-0.00156557	0.00025629	0.00002027
0	3	1	0	0	0	0.00008798	-0.00000083	-0.00104798	0.00146467	-0.00001978
0	2	2	0	0	0	0.00013645	0.00002389	0.00346775	-0.00180208	0.00005566
0	1	3	0	0	0	0.00006753	0.00000307	-0.00229728	0.00168967	-0.00004453
0	4	1	0	0	0	0.00008778	0.00002412			
0	3	2	0	0	0	-0.00012251	0.00004415			
0	2	3	0	0	0	0.00012533	-0.00001087			
0	1	4	0	0	0	-0.00001319	-0.00003264			
1	0	0	2	0	0	0.00004021	-0.00001004	-0.00004460	-0.00001254	-0.00000645
2	0	0	2	0	0	0.00002887	0.00013683	-0.00004509	0.00007886	-0.00003432
3	0	0	2	0	0	0.00014143	-0.00005840			
0	1	0	2	0	0	0.00015606	-0.00004447	-0.00035689	0.00036140	0.00008124
0	2	0	2	0	0	0.00009201	0.00009657	-0.00038966	0.00049077	0.00013741
0	3	0	2	0	0	0.00006757	0.00005084			
0	0	1	2	0	0	0.00002715	-0.00001047	0.00000622	-0.00001862	-0.00000221
0	0	2	2	0	0	0.00009103	0.00006273	-0.00009525	0.00007168	0.00000866
0	0	3	2	0	0	0.00009392	0.00019619			
1	0	0	4	0	0	0.00011229	-0.00001629			
0	1	0	4	0	0	-0.00010792	-0.00004747			
0	0	1	4	0	0	0.00018040	0.00014850			
1	0	0	0	2	0	0.00000228	-0.00000453	-0.00002040	-0.00000299	-0.00000107
2	0	0	0	2	0	-0.00003344	0.00001236	-0.00001706	-0.00032112	-0.00000669
3	0	0	0	2	0	0.00015954	-0.00005956			
0	1	0	0	2	0	-0.00004570	-0.00002503	-0.00112748	0.00051774	0.00002579
0	2	0	0	2	0	-0.00001052	0.00002007	-0.00204526	0.00047098	0.00001385
0	3	0	0	2	0	-0.00003406	0.00005861			

To be continued on next page

Table C.2: *Continued from previous page*

i	j	k	l	m	n	CV[b]	SR[c]	(Q)-(T)[d]	Q-(Q)[e]	DBOC[f]
0	0	1	0	2	0	-0.00010507	-0.00000789	0.00051963	-0.00036454	0.00003102
0	0	2	0	2	0	0.00009265	-0.00000333	-0.00020366	-0.00046008	-0.00001211
0	0	3	0	2	0	0.00005128	0.00020320			
1	0	0	0	4	0	0.00011998	-0.00001724			
0	1	0	0	4	0	-0.00000765	-0.00002850			
0	0	1	0	4	0	0.00017631	0.00012945			
0	0	0	1	1	1	-0.00001705	0.00001694	-0.00005317	0.00017554	-0.00001065
0	0	0	3	1	1	0.00004452	0.00001499	0.00019620	-0.00007712	-0.00000035
0	0	0	2	2	0	0.00000666	0.00000120	-0.00017980	-0.00005587	0.00005325
0	0	0	2	2	2	0.00000860	-0.00000484	0.00014605	0.00005846	0.00001394
0	0	0	1	3	1	-0.00000825	0.00001779	-0.00023191	-0.00008717	-0.00000096
1	1	1	0	0	0	0.00000237	0.00000325	0.00022120	0.00006856	0.00000462
1	1	2	0	0	0	0.00000198	-0.00000327	0.00035141	-0.00019857	-0.00000102
1	1	3	0	0	0	-0.00006888	-0.00000047			
1	2	1	0	0	0	0.00001518	0.00000065	0.00021381	0.00011296	0.00001658
1	2	2	0	0	0	0.00006928	0.00000565			
1	3	1	0	0	0	-0.00002108	-0.00001542			
2	1	1	0	0	0	0.00000925	0.00000395	0.00000019	-0.00002805	-0.00001455
2	1	2	0	0	0	0.00001538	-0.00000314			
2	2	1	0	0	0	0.00011696	-0.00000876			
3	1	1	0	0	0	-0.00000514	-0.00000877			
1	1	0	2	0	0	0.00000195	0.00000612	-0.00008267	-0.00000276	-0.00007543
2	1	0	2	0	0	-0.00001682	-0.00002871			
1	2	0	2	0	0	0.00013956	-0.00008892			
1	0	1	2	0	0	-0.00000359	-0.00000626	-0.00003337	0.00006488	0.00000232
2	0	1	2	0	0	0.00034013	0.00003331			
1	0	2	2	0	0	0.00006022	0.00002857			
0	1	1	2	0	0	-0.00004561	0.00002239	0.00024964	-0.00011195	0.00000177
0	2	1	2	0	0	0.00024471	0.00002712			
0	1	2	2	0	0	0.00021411	-0.00007810			
1	1	0	0	2	0	0.00000048	-0.00000742	-0.00001181	-0.00000896	-0.00000483
2	1	0	0	2	0	-0.00014388	-0.00003211			
1	2	0	0	2	0	0.00013273	-0.00004014			
1	0	1	0	2	0	0.00002003	0.00000358	-0.00002020	0.00000325	-0.00000356
2	0	1	0	2	0	0.00031901	0.00003970			
1	0	2	0	2	0	0.00015730	0.00003224			
0	1	1	0	2	0	0.00002420	0.00004656	0.00168903	-0.00053150	-0.00001588
0	2	1	0	2	0	-0.00003585	-0.00003672			
0	1	2	0	2	0	0.00033508	-0.00004703			
1	0	0	1	1	1	0.00000352	-0.00000066	-0.00007619	0.00002247	0.00000437
2	0	0	1	1	1	0.00000188	-0.00011643	-0.00003691	0.00000317	-0.00000241
3	0	0	1	1	1	0.00003323	0.00000310			
0	1	0	1	1	1	0.00010966	-0.00002137	-0.00030091	0.00059431	-0.00001751
0	2	0	1	1	1	0.00008294	-0.00013133	-0.00093413	0.00106675	-0.00002289
0	3	0	1	1	1	0.00014782	0.00005334			

To be continued on next page

Table C.2: *Continued from previous page*

i	j	k	l	m	n	CV[b]	SR[c]	(Q)-(T)[d]	Q-(Q)[e]	DBOC[f]
0	0	1	1	1	1	-0.00016527	0.00001769	0.00010125	-0.00004412	-0.00000361
0	0	2	1	1	1	0.00014098	-0.00013678	-0.00091105	0.00040318	0.00000413
0	0	3	1	1	1	-0.00010086	0.00007235			
1	0	0	3	1	1	0.00000582	-0.00001928			
0	1	0	3	1	1	0.00017534	0.00003675			
0	0	1	3	1	1	-0.00010612	0.00020601			
1	0	0	2	2	0	0.00020955	-0.00004060			
0	1	0	2	2	0	-0.00013834	-0.00003697			
0	0	1	2	2	0	0.00043338	0.00048025			
1	0	0	2	2	2	0.00005852	0.00001652			
0	1	0	2	2	2	0.00013797	-0.00000254			
0	0	1	2	2	2	-0.00005047	-0.00008149			
1	0	0	1	3	1	0.00004138	-0.00002922			
0	1	0	1	3	1	0.00007053	0.00007954			
0	0	1	1	3	1	-0.00018286	0.00018235			
1	1	1	2	0	0	-0.00002263	-0.00003595			
1	1	1	0	2	0	0.00006737	-0.00005305			
1	1	0	1	1	1	-0.00000242	-0.00000176	-0.00020407	0.00014616	0.00001177
2	1	0	1	1	1	0.00007373	0.00001942			
1	2	0	1	1	1	0.00013957	0.00005334			
1	0	1	1	1	1	0.00000133	0.00001482	0.00006997	-0.00000723	0.00000883
2	0	1	1	1	1	0.00004992	0.00001066			
1	0	2	1	1	1	0.00010140	-0.00002949			
0	1	1	1	1	1	-0.00013370	0.00003100	0.00201523	-0.00064717	-0.00005883
0	2	1	1	1	1	-0.00016232	0.00005726			
0	1	2	1	1	1	0.00044867	-0.00001151			
1	1	1	1	1	1	-0.00017642	0.00001555			

[a] PEF coefficients are quoted in atomic units; see Equation (5.1) for their definition.

Expanded around $r^{\text{ref}} = 1.079$ Å, $R_1^{\text{ref}} = 1.236$ Å and $R_2^{\text{ref}} = 1.340$ Å

[b] CV: [ae-CCSD(T) − fc-CCSD(T)]/CV6Z.

[c] SR: DKH2-fc-CCSD(T)/VQZ-DK − fc-CCSD(T)/VQZ.

[d] (Q)-(T): [CCSDT(Q) − CCSD(T)]/VTZ.

[e] Q-(Q): [CCSDTQ − CCSDT(Q)]/VDZ.

[f] DBOC (l-$^{12}C_3H^+$): ae-CCSD/CVQZ.

Table C.3: Adiabatic composite potential energy functions for l-$^{12}C_3H^+$.[a]

i	j	k	l	m	n	C_{ijk}	i	j	k	l	m	n	C_{ijk}
2	0	0	0	0	0	0.18660581	1	1	4	0	0	0	0.00000954
3	0	0	0	0	0	-0.18841809	1	2	1	0	0	0	-0.00064198
4	0	0	0	0	0	0.12779567	1	2	2	0	0	0	0.00099367
5	0	0	0	0	0	-0.07388536	1	2	3	0	0	0	-0.00003533
6	0	0	0	0	0	0.03900499	1	3	1	0	0	0	0.00031112
7	0	0	0	0	0	-0.01883585	1	3	2	0	0	0	0.00032821
8	0	0	0	0	0	0.00936906	1	4	1	0	0	0	-0.00016070
9	0	0	0	0	0	-0.00532518	2	1	1	0	0	0	0.00032321
10	0	0	0	0	0	0.00189872	2	1	2	0	0	0	-0.00019446
0	2	0	0	0	0	0.44434645	2	1	3	0	0	0	-0.00013604
0	3	0	0	0	0	-0.46416893	2	2	1	0	0	0	-0.00029905
0	4	0	0	0	0	0.29951839	2	2	2	0	0	0	-0.00024220
0	5	0	0	0	0	-0.15859023	2	3	1	0	0	0	0.00023487
0	6	0	0	0	0	0.07378424	3	1	1	0	0	0	-0.00026064
0	7	0	0	0	0	-0.03151133	3	1	2	0	0	0	0.00032533
0	8	0	0	0	0	0.00965334	3	2	1	0	0	0	0.00027526
0	0	2	0	0	0	0.26974355	4	1	1	0	0	0	0.00016022
0	0	3	0	0	0	-0.27889552	1	1	0	2	0	0	0.01165042
0	0	4	0	0	0	0.18047266	2	1	0	2	0	0	0.00236433
0	0	5	0	0	0	-0.09425125	1	2	0	2	0	0	-0.00396069
0	0	6	0	0	0	0.04399458	3	1	0	2	0	0	0.00454354
0	0	7	0	0	0	-0.01876572	2	2	0	2	0	0	0.01349126
0	0	8	0	0	0	0.00538120	1	3	0	2	0	0	-0.00001544
0	0	0	2	0	0	0.03783093	1	0	1	2	0	0	0.00132704
0	0	0	4	0	0	-0.00038748	2	0	1	2	0	0	0.00154733
0	0	0	6	0	0	0.00040039	1	0	2	2	0	0	-0.00083315
0	0	0	8	0	0	-0.00033287	3	0	1	2	0	0	0.00060819
0	0	0	10	0	0	0.00039887	2	0	2	2	0	0	0.01381179
0	0	0	12	0	0	-0.00029280	1	0	3	2	0	0	0.00137130
0	0	0	14	0	0	0.00011093	0	1	1	2	0	0	-0.00393735
0	0	0	16	0	0	-0.00001767	0	2	1	2	0	0	0.00556659
0	0	0	0	2	0	0.00435867	0	1	2	2	0	0	-0.00000663
0	0	0	0	4	0	-0.00008020	0	3	1	2	0	0	0.00185593
0	0	0	0	6	0	0.00011629	0	2	2	2	0	0	0.00342656

To be continued on next page

Table C.3: *Continued from previous page*

i	j	k	l	m	n	C_{ijk}	i	j	k	l	m	n	C_{ijk}
0	0	0	0	8	0	-0.00024876	0	1	3	2	0	0	0.00036065
0	0	0	0	10	0	0.00041958	1	1	0	4	0	0	0.00767870
0	0	0	0	12	0	-0.00029968	1	0	1	4	0	0	0.00040782
0	0	0	0	14	0	0.00012171	0	1	1	4	0	0	-0.00034512
0	0	0	0	16	0	-0.00002644	1	1	0	0	2	0	0.00068868
0	0	0	0	18	0	0.00000244	2	1	0	0	2	0	0.00002557
1	1	0	0	0	0	-0.01303699	1	2	0	0	2	0	0.00084793
2	1	0	0	0	0	0.00238924	3	1	0	0	2	0	0.00047706
1	2	0	0	0	0	0.00059449	2	2	0	0	2	0	-0.01455038
3	1	0	0	0	0	-0.00297616	1	3	0	0	2	0	0.00335464
2	2	0	0	0	0	-0.00459616	1	0	1	0	2	0	-0.00034657
1	3	0	0	0	0	-0.00127206	2	0	1	0	2	0	0.00045465
4	1	0	0	0	0	0.00270025	1	0	2	0	2	0	0.00110291
3	2	0	0	0	0	0.00394073	3	0	1	0	2	0	-0.00144150
2	3	0	0	0	0	0.00247856	2	0	2	0	2	0	-0.01682393
1	4	0	0	0	0	0.00141923	1	0	3	0	2	0	-0.00313611
5	1	0	0	0	0	-0.00122371	0	1	1	0	2	0	-0.01615583
4	2	0	0	0	0	-0.00232862	0	2	1	0	2	0	0.01719294
3	3	0	0	0	0	-0.00179371	0	1	2	0	2	0	0.00743413
2	4	0	0	0	0	-0.00174415	0	3	1	0	2	0	0.00439940
1	5	0	0	0	0	-0.00025716	0	2	2	0	2	0	-0.03645257
1	0	1	0	0	0	0.00495414	0	1	3	0	2	0	0.01369046
2	0	1	0	0	0	-0.00026922	1	1	0	0	4	0	0.00192881
1	0	2	0	0	0	-0.00245115	1	0	1	0	4	0	-0.00478273
3	0	1	0	0	0	0.00032211	0	1	1	0	4	0	0.00033225
2	0	2	0	0	0	0.00010162	1	0	0	1	1	1	-0.00053182
1	0	3	0	0	0	0.00044913	2	0	0	1	1	1	-0.00084417
4	0	1	0	0	0	-0.00022814	3	0	0	1	1	1	-0.00006448
3	0	2	0	0	0	-0.00006638	4	0	0	1	1	1	0.01067593
2	0	3	0	0	0	0.00003994	0	1	0	1	1	1	0.00464102
1	0	4	0	0	0	-0.00019171	0	2	0	1	1	1	-0.00790410
5	0	1	0	0	0	0.00003222	0	3	0	1	1	1	-0.00409120
4	0	2	0	0	0	-0.00018672	0	4	0	1	1	1	0.00664445
3	0	3	0	0	0	0.00007668	0	0	1	1	1	1	0.01621785
2	0	4	0	0	0	0.00006346	0	0	2	1	1	1	-0.01045660

To be continued on next page

Table C.3: *Continued from previous page*

i	j	k	l	m	n	C_{ijk}	i	j	k	l	m	n	C_{ijk}
1	0	5	0	0	0	0.00020993	0	0	3	1	1	1	0.00420429
0	1	1	0	0	0	0.00808269	0	0	4	1	1	1	0.00688904
0	2	1	0	0	0	-0.00961510	1	0	0	3	1	1	0.00065809
0	1	2	0	0	0	-0.00828965	2	0	0	3	1	1	0.00650387
0	3	1	0	0	0	0.00386307	0	1	0	3	1	1	-0.00442667
0	2	2	0	0	0	-0.00744918	0	2	0	3	1	1	-0.00901044
0	1	3	0	0	0	-0.00465165	0	0	1	3	1	1	0.00026452
0	4	1	0	0	0	-0.00278851	0	0	2	3	1	1	0.00409368
0	3	2	0	0	0	0.00880355	1	0	0	2	2	0	-0.00034511
0	2	3	0	0	0	0.00288906	2	0	0	2	2	0	0.01294572
0	1	4	0	0	0	0.00065317	0	1	0	2	2	0	0.00099117
0	5	1	0	0	0	0.00372334	0	2	0	2	2	0	0.01079344
0	4	2	0	0	0	-0.00420891	0	0	1	2	2	0	0.00240217
0	3	3	0	0	0	-0.00118173	0	0	2	2	2	0	0.01816487
0	2	4	0	0	0	-0.00436835	1	0	0	2	2	2	0.00018227
0	1	5	0	0	0	0.00184341	2	0	0	2	2	2	-0.00367626
1	0	0	2	0	0	-0.00933692	0	1	0	2	2	2	-0.00299955
2	0	0	2	0	0	-0.00241971	0	2	0	2	2	2	-0.01025613
3	0	0	2	0	0	0.00130100	0	0	1	2	2	2	0.00239265
4	0	0	2	0	0	0.00741127	0	0	2	2	2	2	-0.00716006
0	1	0	2	0	0	-0.03856228	1	0	0	1	3	1	0.00087713
0	2	0	2	0	0	-0.00144926	2	0	0	1	3	1	0.00749245
0	3	0	2	0	0	-0.00423533	0	1	0	1	3	1	0.00040483
0	4	0	2	0	0	0.01043487	0	2	0	1	3	1	0.01414570
0	0	1	2	0	0	-0.00701326	0	0	1	1	3	1	-0.00482668
0	0	2	2	0	0	0.00155408	0	0	2	1	3	1	0.01070791
0	0	3	2	0	0	-0.00045904	1	1	1	2	0	0	-0.00134335
0	0	4	2	0	0	0.00927163	1	1	2	2	0	0	0.00712249
1	0	0	4	0	0	-0.00104559	1	2	1	2	0	0	-0.00415296
2	0	0	4	0	0	0.00421952	2	1	1	2	0	0	-0.00400242
0	1	0	4	0	0	0.00251981	1	1	1	0	2	0	-0.00064812
0	2	0	4	0	0	0.00881127	1	1	2	0	2	0	0.00109165
0	0	1	4	0	0	0.00063907	1	2	1	0	2	0	-0.00167744
0	0	2	4	0	0	0.00467583	2	1	1	0	2	0	0.00670916
1	0	0	0	2	0	-0.00070515	1	1	0	1	1	1	-0.00148453

To be continued on next page

Table C.3: *Continued from previous page*

i	j	k	l	m	n	C_{ijk}	i	j	k	l	m	n	C_{ijk}
2	0	0	0	2	0	-0.00002762	2	1	0	1	1	1	-0.00073969
3	0	0	0	2	0	0.00028762	1	2	0	1	1	1	0.00162942
4	0	0	0	2	0	-0.01034093	3	1	0	1	1	1	-0.00067463
0	1	0	0	2	0	-0.01540963	2	2	0	1	1	1	0.01891353
0	2	0	0	2	0	0.00239950	1	3	0	1	1	1	-0.00317190
0	3	0	0	2	0	-0.00458868	1	0	1	1	1	1	-0.00121921
0	4	0	0	2	0	-0.00620064	2	0	1	1	1	1	-0.00113070
0	0	1	0	2	0	0.00336075	1	0	2	1	1	1	0.00172556
0	0	2	0	2	0	-0.00618815	3	0	1	1	1	1	0.00056768
0	0	3	0	2	0	0.00563204	2	0	2	1	1	1	0.01881086
0	0	4	0	2	0	-0.01182640	1	0	3	1	1	1	-0.00384161
1	0	0	0	4	0	0.00007088	0	1	1	1	1	1	0.01388724
2	0	0	0	4	0	-0.00325209	0	2	1	1	1	1	0.01227173
0	1	0	0	4	0	0.00264426	0	1	2	1	1	1	-0.01493154
0	2	0	0	4	0	-0.00065643	0	3	1	1	1	1	0.01100483
0	0	1	0	4	0	-0.00271919	0	2	2	1	1	1	-0.00622110
0	0	2	0	4	0	0.01113482	0	1	3	1	1	1	0.01486193
0	0	0	1	1	1	0.00136939	1	1	0	3	1	1	-0.00338753
0	0	0	3	1	1	-0.00210941	1	0	1	3	1	1	-0.00334327
0	0	0	2	2	0	0.00101746	0	1	1	3	1	1	0.00085985
0	0	0	2	2	2	-0.00001840	1	1	0	2	2	0	-0.00032638
0	0	0	1	3	1	-0.00049128	1	0	1	2	2	0	-0.00421174
0	0	0	5	1	1	-0.00030631	0	1	1	2	2	0	0.00085966
0	0	0	4	2	0	-0.00024010	1	1	0	2	2	2	-0.00060169
0	0	0	4	2	2	-0.00000723	1	0	1	2	2	2	-0.00176789
0	0	0	3	3	1	0.00047186	0	1	1	2	2	2	0.00603540
0	0	0	3	3	3	0.00003515	1	1	0	1	3	1	-0.00911274
0	0	0	2	4	0	0.00055012	1	0	1	1	3	1	-0.00198495
0	0	0	2	4	2	0.00058868	0	1	1	1	3	1	-0.01038817
0	0	0	1	5	1	-0.00064639	1	1	1	1	1	1	0.00081151
1	1	1	0	0	0	-0.00045909	1	1	2	1	1	1	0.00325780
1	1	2	0	0	0	-0.00025926	1	2	1	1	1	1	0.00369857
1	1	3	0	0	0	-0.00056898	2	1	1	1	1	1	0.00112922

[a] PEF coefficients are quoted in atomic units; see Equation (5.1) for their definition. Equilibrium geometry: $r^{\mathrm{e}} = 1.07896$ Å, $R_1^{\mathrm{e}} = 1.23540$ Å and $R_2^{\mathrm{e}} = 1.34080$ Å.